Republic of Iraq
Ministry of Higher Education
and Scientific Research
University of Babylon
College of Engineering
Department of Mechanical Engineering

The Energy and Exergy Analysis of Different Kalina Cycle Configurations

A Thesis

Submitted to the College of Engineering / University of Babylon in Partial Fulfillment of the Requirements for the Degree of Doctor of Philosophy in Engineering/Mechanical Engineering /Power

By

Abdulkhudhur Kadhim Naser Hussien

Supervised By

Prof. Dr. Haroun A.K. Shahad

2023 A.D **1445 A.H**

بسم الله الرحمن الرحيم

شَهِدَ اللَّهُ أَنَّهُ لا إِلَهَ إِلَّا هُوَ وَالْمَلائِكَةُ وَ أُولُو الْعِلْمِ قَائِماً بِالْقِسْطِ

صدق الله ألعلي العظيم

سورة ال عمران /الايه 18

Dedicated To

To my first teacher who gave me strength

My father.

To her who planted love in my heart

My mother.

To the symbols of love and fait fullness

My brothers and sisters

To my dear life partner s

My family.

With Love and Respect

Abdulkhudhur 2023

Supervisor Certification

I certify that this thesis entitled "**Energy and Exergy Analysis of Different Kalina Cycle Configurations**" is being carried out by **Abdulkhudhur Kadhim Naser** under my supervision at the Mechanical Engineering Department, College of Engineering, University of Babylon, as a partial fulfilment of the requirements for the degree of Doctor of Philosophy in Mechanical Engineering (Power Engineering).

Signature:

Name: Prof. Dr. Haroun A.K. Shahad

Department of Mechanical Engineering / College of Engineering/ University of Babylon

Date: / / 2023

ACKNOWLEDGEMENTS

Praise be to ***ALLAH***, Most Gracious, Most Merciful, who gave me the ability and desire to complete this research work.

I wish to express my cordial thanks and deepest gratitude to my supervisor ***Prof. Dr. Haroun A. K. Shahad*** for his generous guidance, and valuable and active interest in this work.

My great appreciation is expressed to the Dean of the College of Engineering ***Prof. Dr. Hatem Hadi Obeid*** and to the head of Mechanical Engineering Department **Assist. *Prof. Dr. Samer Abdul hleem***.

My special thanks for my wife, my daughter Farah and my sons Ahmed, Ali and Jaafer for their help. My special thanks and deepest and warmest gratitude are due to my family with special gratitude to them, love, support and encouragement during the period of preparing this work.

Furthermore, deepest thanks to my friends for their help to accomplish this study. Finally, I would like to express my deepest thanks and gratitude to all those who have helped me in one way or another in carrying out this research.

Abdulkhudhur 2023

Abstract

In the present work, a theoretical and experimental study was conducted to analyze the available energy from combustion gases of boiler to be used for power generation using Kalina cycle. The Kalina cycle is a thermodynamic cycle used to produce electrical power or cooling. The working fluid was a mixture of ammonia and water. The external source of energy is the combustion gases from a steam boiler located in the University of Babylon / College of Mechanical Engineering / Fluid Laboratory. The temperature of the combustion gases was measured by a thermocouple and the mass discharge was calculated by the standard combustion equation to be 175 °C and 122.3 kg/hr respectively.

In the theoretical part of this study simple Kalina cycle system (SKCS) was modified by adding one and the cycle is known as the first modified Kalina cycle system (MKCS1) and two heat exchangers and the cycle is known as the second modified Kalina cycle system (MKCS2), to recover part of the heat rejected, while in the experimental part a power plant is constructed based on the theoretical cycle (MKCS1) and given the symbol (MKCSE).

In the results of the theoretical part the studied operating conditions include the cycle maximum pressure (P_{max}), the cycle minimum pressure (P_{min}), the ammonia concentration (x), and the dryness fraction at separator entrance (DF), while the studied performance parameters include the cycle thermal efficiency, the cycle net power generation, the cycle exergy efficiency, and the exergy destruction. The maximum pressure (P_{max}) is varied from 20 bar to 40 bar for every 5 bar step. The minimum pressure (P_{min}) is 2 bar, 3 bar, and 4 bar, and the ammonia concentration (x) varied from 0.85 to 0.89 for each step of 0.01, as well as the dryness fraction (DF) was 0.2, 0.3, and 0.4.

In the beginning, the effect of dryness fraction was studied theoretically on the performance of the three cycles, and the behavior was similar in the three cases. It is found that the highest thermal efficiency was at dryness fraction (DF) =0.3.The thermal efficiency for (SKCS), (MKCS1) and (MKCS) was 9.44%, 14.23%, and 23.53%, respectively. Then the effect of the dryness fraction on the net power was studied, and the result was 0.26 kW, 0.29 kW, and 0.38 kW for (SKCS), (MKCS1) and (MKCS2) respectively. Exergy efficiency was 24.2%, 30.2%, and 59.06% for SKCS, MKCS1 and MKCS2 respectively.

The results of the ammonia concentration effect show that when the ammonia concentration increases the cycle thermal efficiency decrease for all cycles. For example the thermal efficiency for MKCS2 at ammonia mass fractions of 0.85 and 0.89 are 23.53% and 21.7% respectively.

The effect of the maximum pressure on the performance of the three cycles was also studied. For MKCS1, the net power at a pressure of 20 bar and 25 bar at x=0.89 is 0.394 kW and 0.391 kW respectively.

The impact of the minimum pressure (P_{min}) on the performance of the three cycles was also investigated. It is found from the theoretical study of the three cycles that the MKCS2 is the best cycle because it has the highest thermal efficiency of 23.5% at ammonia mass fraction (x) =0.85 and P_{max}=35 bar, the highest net power of 0.59 kW at x=0.89 and P_{max}=20 bar and the highest exergy efficiency of 60% at x=0.85 and maximum pressure (P_{max}) =35 bar as well.

The optimum operating conditions for SKCS were found at P_{max}=30.8 bar and x=0.88, where the optimum thermal efficiency and the optimum net power were 8.8% and 0.33 kW respectively. However the optimum conditions for MKCS1 was at x=0.88 and P_{max}=33.5 bar. Moreover, the optimum value of the thermal efficiency and the net power were 13.5% and

0.354 kW respectively. Additionally it is found that the values of the optimum P_{max} and (x) were 34 bar and 0.88 respectively for MKCS2 where the of the optimum thermal efficiency and net power were 21.8% and 0.462 kW respectively.

The results for MKCSE cycle were taken at maximum pressure =35 bar, minimum pressure=2 bar, ammonia mass fraction=0.85, and dryness fraction=0.3. It is noticed that when the ammonia concentration is increased the thermal efficiency is decreased, the net power is increased, and the exergy efficiency is decreased. The highest thermal efficiency is 12.9% at P_{max}=35 bar, P_{min}=2 bar, DF=0.3 and x=0.85. The highest value of the net power was 0.367 kW at x=0.89 at turbine inlet, P_{max}=20 bar and DF=0.3. The highest value of exergy efficiency was 28.5% at P_{max}=35 bar, P_{min}=2 bar and DF=0.3. It is seen when P_{max} is increased the thermal efficiency increased sharply till P_{max}=35 bar. The values of the net power at 2 bar, 3 bar and 4 bar were 0.37 kW, 0.33 kW and 0.295 kW respectively. The exergy efficiency was 28.4%, 27.35% and 25.4% at 2 bar, 3 bar and 4 bar respectively. It is seen the thermal efficiency dropped because as the minimum pressure is increased. The value of the net power was 0.364 kW at x=0.89 and P_{min}=2 bar. It is found that the highest exergy efficiency is obtained at low pressure 2 bar, high pressure 35 bar at x=0.85, which is 28.5%.

A comparison of the theoretical and experimental results is carried out at the conditions of P_{max}= 35 bar, P_{min} = 2 bar, x= 0.85 and DF= 0.3. The theoretical thermal efficiency was 14.23%, while in the experimental work it was 13.09%, and the error rate between them was 8.01%. As for the theoretical net power, it was 0.289 kW, whereas in the experimental net power it was 0.272 kW and the error rate between them was 5.88%. The exergy efficiency in a theoretical work was 30.24%, in however experimental work was 28.43%, and the error rate between them was 5.99%.

As for the theoretical losses, it was 0.5239 kW, but the experimental losses were greater than 0.581 kW, and the error rate was 10.899%.

An economic feasibility study was done by calculating the net power obtained under the same conditions in which the comparison was made. It was found that to obtain a net power of 0.272 kW, 858 kg of fuel must be annually burned and thus the use of the first improved Kalina cycle annually reduced carbon dioxide emissions by 2672 kg. Finally, the net power for MKCS2 was 0.585 kW at the same conditions and 1844.9 kg of fuel must be annually burned and practically reduced carbon dioxide emissions by 5820.5 kg annually.

NOMENCLATURE

Symbol	Description	Unit
A	Cross-sectional area	m^2
A_s /v	Surface area to volume ratio	m^2/m^3
c_p	Specific heat of the fluid mixture	kJ/kg.°K
C_d	Discharge coefficient	------
c_w	Specific heat of water.	kJ/kg K
D	Diameter	m
d	Exergy destroyed	kJ
DF	Dryness fraction	kg_v/kg_{mixtu}
d_s	Diameter of the cylinder	m
d_{to}	Tube outlet diameter	m
d_{ti}	Tube internal diameter	m
d_H	Hydraulic diameter	m
dT/dx	Temperature gradient	K/m
E	Exergy	kJ
$\dot{E}$	The rate of exergy	kW
h_{fg}	the evaporation heat	kJ/kg
h	Convective heat transfer coefficient	kw/m^2 K
h_l^m	Specific liquid enthalpy of the mixture	kJ/kg
h_a^l	Specific enthalpy of ammonia liquid	kJ/kg
h_w^l	Specific enthalpy of water liquid	kJ/kg
h_v^m	Specific enthalpy for mixture at vapor phase	kJ/kg
h_a^v	Specific enthalpy of ammonia vapor	kJ/kg
h_w^v	Specific enthalpy of water vapor	kJ/kg

I	Electrical Current	Amber
k	Thermal conductivity	kW/m.K
k_m	Thermal conductivity of mixture	kW/m.K
k_w	Water thermal conductivity	kW/m.K
L	Distance	m
LS	The stroke	m
len	Length	cm
LCV	Lower calorific value	kJ/kg
$\dot{m}$	Mass flow rate	kg/s
Nu	Nusselt number	-----
n_c	Number of turns of the condenser tube.	-----
N	Number of the motor rotation	-----
n	Number pump cylinders	-----
Pr	Prandtl No.	-----
P	Power	kW
p	Pressure	bar
Q	Heat transfer	kJ
$\dot{Q}$	The rate of heat transfer	kW
Re	Reynold No	-----
r	Radius	cm
s	Specific entropy	kJ/kg.°K
s_a^v	Specific entropy of ammonia vapor	kJ/kg.°K
s_w^v	Specific entropy of water vapor	kJ/kg.°K
s_v^m	Specific entropy of the mixture in the vapor phase	kJ/kg.°K
s_l^m	Specific entropy of the mixture in the liquid phase	kJ/kg.°K
s_a^l	Specific entropy of ammonia liquid	kJ/kg.°K

s_w^l	Specific entropy of water liquid	kJ/kg.°K
t_{Ave}	Mean temperature for Inner pipe fluid stream	℃
T	Temperature	°C
U	Overall heat transfer coefficient	kW/m^2K
$\dot{V}$	Volume flow rate	m^3/s
V	Velocity.	m/s
V_o	Volume of one cylinder	m^3
Vo	Voltage	Volt
v_m^v	Specific volume of mixture vapor phase	m^3/kg
v_a^v	Specific volume of ammonia vapor	m^3/kg
v_w^v	Specific volume of water vapor	m^3/kg
v_m^l	Specific volume of mixture liquid phase	m^3/kg
v_a^l	Specific volume of ammonia liquid	m^3/kg
v_w^l	Specific volume of water liquid	m^3/kg
WF	Wetness fraction	kg_l/kg_{mixtur}
$\dot{W}$	Net power	kW
x	Ammonia mass fraction	kg_{NH3}/kg_{mi}

Greek Symbols

Symbol	Description	Units
η	The efficiency	------
δ	Transition ratio	------
μ	Viscosity	N s/m^2
μ_w	Viscosity of fluid at wall temperature	N s/m^2
ρ	Density	kg/m^3
α_t	Heat transfer coefficient in tube side	kW/m^2 K
α_s	Heat transfer coefficient in shell side	kW/m^2 K
Cos θ	Power factor	-------
$\emptyset$	Angle of the needle	Degree
ϵ	Effectiveness of the heat exchanger	-------

Subscripts

Symbol	Meaning
a	Ammonia
ave	Average
act	Actual
bp	Bubble point
CAES	Compressed air energy storage
ci	Cold stream inlet
co	Cold stream outlet
conv	Conversation
coup	coupling
d	Destruction
dp	Dew point
e	Equivalent

ex	Exergy
exh	Exhaust
elect	Electrical
fuel	Fuel
f	Saturated liquid
g	Saturated vapor
gen	Generator
H	High
hi	Hot stream inlet
ho	Hot stream outlet
hx	Heat exchanger
i	Inlet
in	Inlet
isen	Isentropic
inner	Inner
l	Liquid
L	Low
m	Mixture
max	Maximum
min	Minimum
mix	Mixer
net	Net power
o	Surrounding
out	Outlet
outer	Outer
P	Pump
v	Vapor

t	Tube
th	Thermal
tot	Total
T	Turbine
s	Shell
sa	Saturated vapor
sep	Separator
sw	Saturated liquid (water)
w	Water
win	Water inlet

Abbreviations

Symbol	Description
AP	Approach point
AWKRC	Ammonia Water Kalina Rankine Cycle
AWRC	Ammonia Water Rankine Cycle
ARC	Absorption refrigeration cycle
T_{bp}	Boiling point temperature
CAES	Compressed air energy storage
COSQC	Central Orga for Standardization and Quality Control
DF	Dryness fraction
T_{dp}	Dew point temperature
ed	Energy donor
ea	Energy acceptor
HRVG	Heat recovery vapor generator
SKCS	Simple Kalina cycle system
MKCS1	First modified of Kalina cycle

MKCS2	Second modified of Kalina cycle
MKCSE	Experimental of Kalina cycle
HTR	High temperature regenerative
HP	Horse power
K^	Number of processes in the subsystem
KCPC	Kalina cycle power cooling
KLPCC	Kalina cycle power cooling vapor absorption cycle
$LiBr/H_2O$	Lithium Bromide-water
LMTD	Logarithmic Mean Temperature Difference
LCV	Lower calorific value
LTHS	Low-temperature heat source
NH_3-H_2O	Ammonia-water
Ni	Total number of measurements
ORC	Organic Rankine Cycle
OTEC	Ocean thermal energy cycle
RC	Rankine Cycle
RKCC	Rankine-Kalina Combined cycle
PPRKC	Parallel cogeneration power and refrigeration
PP	Pinch point
SD	The standard uncertainty
TTD	Terminal temperature difference
$X_{average}$	The average readings of temperature

TABLE OF CONTENTS

Chapter One

Introduction

Introduction

1.1 General

Simple Kalina cycle system (SKCS) was invented by Alexander Kalina (Russian engineer) in 1967 and firstly was demonstrated in Paratunka, Russia. Then in the 1980 this cycle has been completely tested in USA. The industry was not ready to use this type of the technology because this technology uses low temperature sources to produce power. During the decade 1980-1990 the technology development of the energy production was focused mainly on the improvement of high temperature technologies effectiveness that is of large power stations operated on conventional fuels. There is a big need to generate power with lower emissions to the atmosphere and to develop new effective technologies of energy production. One of these technologies is the Kalina cycle system. Simple Kalina cycle system (SKCS) is modification of Rankine cycle. It is suitable to produce power from low temperature, intermediate temperature and high temperature heat sources. The range of the low temperature is from 100℃ to 200℃, the range of the intermediate temperature is from 250℃ to 300℃ and the range of the high temperature is from 400℃ to 600℃ **[1]**. Kalina Cycle System which is working with low temperature consists basically of vapor generator, separator, mixer (absorber), condenser, turbine and pump as shown in fig (1.1). The SKCS which operates with intermediate temperature is more complicated than SKCS which works with low temperature as it has no throttling. It consists of seven heat exchangers, two pumps, two mixers (absorbers), separator, condenser and turbine. This cycle operates with two pressures level with one condenser as shown in fig (1.2) **[2]**.

Kalina Cycle System which is working with high temperature is most complicated of them (simple Kalina and KCS works with intermediate temperature). It consists of seven heat exchangers, two pumps, throttling

valve, two condensers, separator and turbine. It is noticed that this cycle operated with three pressure levels with two condensers as shown in fig (1.3) **[2]**. In many developing countries, especially Iraq, there exit two major problems namely, electrical power shortage and environmental pollution. In Iraq the electrical power demand exceeds the power production by more than 100%. Also all power generation stations in Iraq burns fossil fuel, which is considered as a major source of pollution. The present work is a step to improve electrical power generation capacity from the existing power station, mainly gas turbine units, by installing Kalina cycle as a bottoming cycle and make use of energy available in combustion gases as a heat source for Kalina cycle by improving the power production capacity the fossil fuel consumption will be reduced and hence reducing pollutants emission especially carbon dioxide which is the main cause of greenhouse warming.

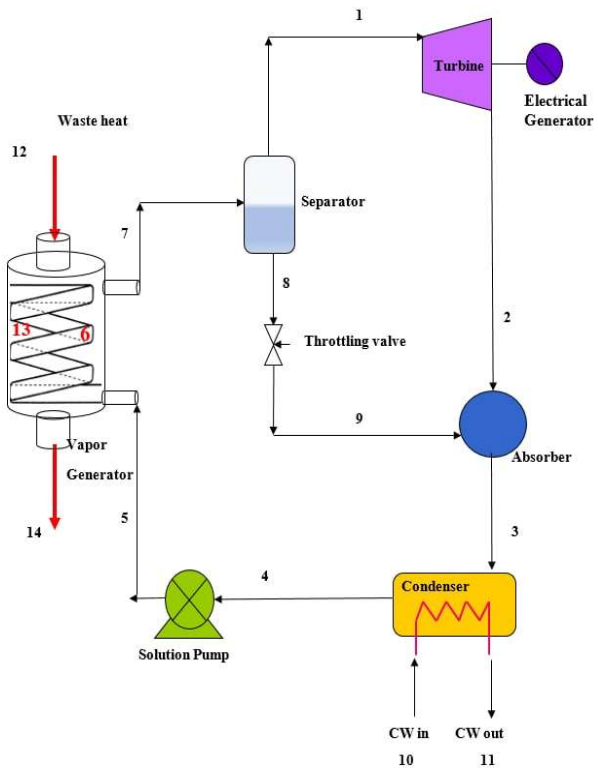

Figure (1-1) Simple Kalina Cycle System Works with Low Temperature [2].

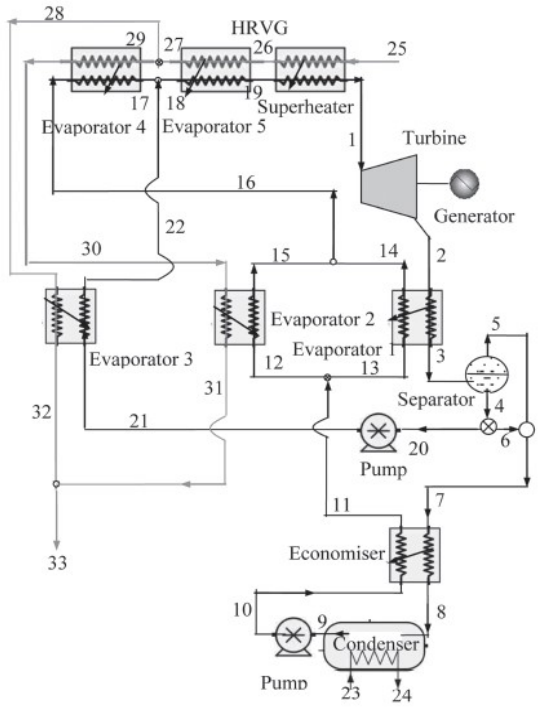

Figure (1-2) KCS Works with Intermediate Temperature [2].

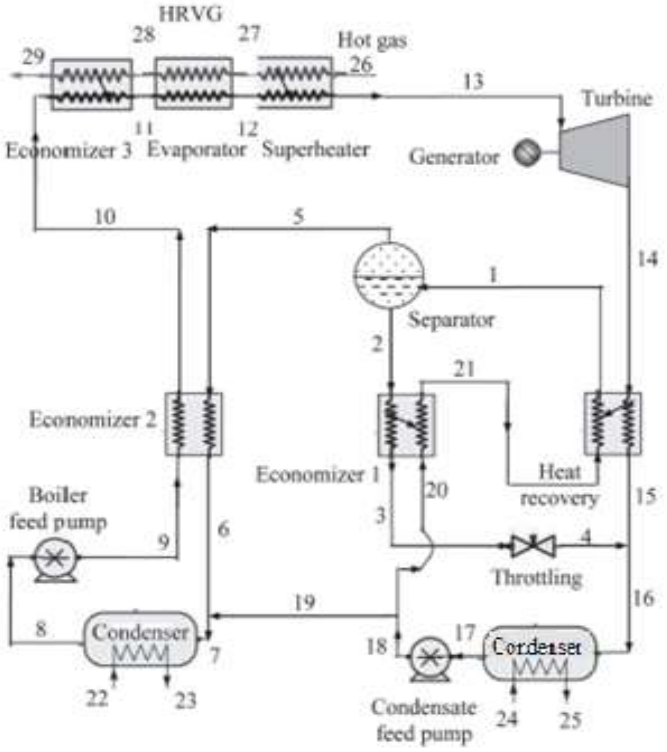

Figure (1-3) KCS Works with High Temperature [2].

1.2 Existing Installations

Many Kalina cycle system are installed in few countries. There are two Kalina power plants in Japan and one Kalina power plant in Iceland, Italy, USA and Germany. The capacity of Kalina cycle was (3-6 MW) in Canoga Park (California) in USA in 1991-1997. The capacity of Kalina cycle power plants in Japan (1999), one of them 5MW in Fukuoka city and the second 3.1 MW plant with waste heat recovery from the steel plant, in Sumitomo. In 2000 another plant was built with (2 MW) in Iceland, Husavik. Germany installed a power plant of (3.4MW) in 2007. After that Kalina cycle was developed and used widely in hundreds of plants in China, India, USA and everywhere **[3]**. Kalina cycle is used with wide range of power generation and heat as shown in fig (1-4).

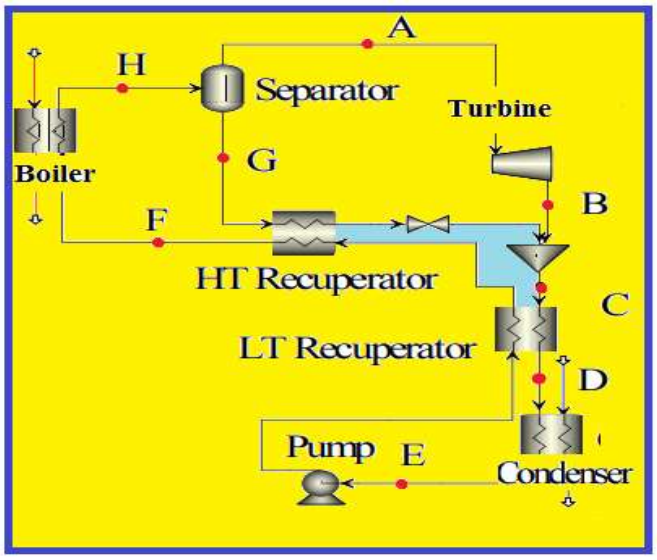

Figure (1-4) Kalina Cycle to Generate Power [3].

1.3 Description of Kalina Cycle.

The Kalina cycle is a principle modification Rankine cycle. It uses a working fluid comprised of at least two different components for example aqua-ammonia (water and ammonia), Lithium-Bromide-water (LeBr-H_2O), Methanol-water and Ethanol-Hexanol. The binary working fluid consists of

two components (absorbent and refrigerant). Kalina cycle system can be operated by different types of energy sources such as geothermal energy, biomass energy and waste heat (exhaust from a gas turbine or a gas from boiler). Kalina cycle replaces the previously used Rankine Cycle as a bottoming cycle for a combined cycle energy system for generation electricity using low-temperature heat resources, Alexander I. Kalina designed a new power cycle in which ammonia-water is used as a working fluid **[3]**. In this cycle there are many varieties. The heat transfers from the hot gases to the working fluid (aqua-ammonia) in the heat exchange known as heat recovery vapor generator (HRVG). Then the working fluid passes through the separator and separates it into two parts. First part (strong solution is saturated vapor of ammonia and water) goes to the turbine with high ammonia concentration around (0.85 to 0.95). The second part is weak solution passes to the mixer through the expansion valve with low ammonia concentration around (0.20 to 0.40). After the expansion valve the weak solution at low pressure mixes with strong solution which comes from the turbine. Then the working fluid with different ammonia mass fraction around (0.25-0.5) passes through the condenser to leave it as saturated liquid and then passes through the pump to leave it as sub-cool to the HRVG [**4**].

1.3.1 Why Kalina Cycle?

Kalina cycle has the following advantages compared with Rankine cycle **[3]**:

1- Generate 10%-20% more power than conventional steam power generation technologies (simple Rankine cycle).

2- Have lower capital costs due to smaller heat exchangers.

3-The demands of cooling water and infrastructure are low.

4- The maintenance is easy and doesn’t take long time.

5- Kalina cycle use binary working fluid.

6- It works with low temperature (100°C-200°C).

7- It uses waste heat as a heat resource, also it works with different source of energy such as (geothermal, solar energy).

8- It can use different concentration ratio, providing a good deal of flexibility.

9- Effect of Kalina cycle on the environment is a very small such as Global warming (near zero), smog and depletion of ozone layer (zero).

1.4 Working Fluid-Mixture and its Thermodynamic Properties

The working fluid in Kalina cycle consists of two substances, absorbent and refrigerant such as ammonia-water. The working fluid mixture should have the following thermodynamic properties:

1- They should have different boiling point and dew point temperatures.
2- They should have good miscibility.
3- The refrigerant should have high latent heat of evaporation.
4- They should be save and non-toxic.
5- The heat of mixing should be low.
6- No solid formation during the operation condition.

1.5 Temperature-Mass Fraction (T-x) Chart for Binary Fluid.

The T-x diagram for any binary fluid consists of two intersecting curves at any pressure. The upper curve represents the saturated vapor curve of the binary fluid while the lower curve represents the saturated liquid curve at same pressure. Fig (1.5) shows the T-x diagram for the ammonia-water binary fluid. At point (1) the working fluid is pure water (x=0), which means a single component fluid, while at point (2) the working fluid is pure ammonia (x=1) which is also a single component fluid. For $0<x<1$ the working fluid is a binary fluid. In this region the temperature of the saturated

vapor differs from that of the saturated liquid at same ammonia mass fraction (x). For example at x=0.7 the temperature of saturated liquid is -8.5 ℃ (point3) and the temperature of saturated vapor is 88℃ (point 7), see fig (1.5). It must be mentioned here that for single component fluid the saturated liquid temperature is the same as the saturated vapor temperature. Fig (1.5) shows also that for same temperature the ammonia mass fraction in the saturated liquid is different than that in the saturated vapor as shown in points 6 and 5. The advantage of that is producing a binary vapor mixture at wide range of temperatures and dryness fractions with same refrigerant fraction, or it is possible to produce a binary vapor mixture with different refrigerant mass fraction and dryness fraction for same temperature.

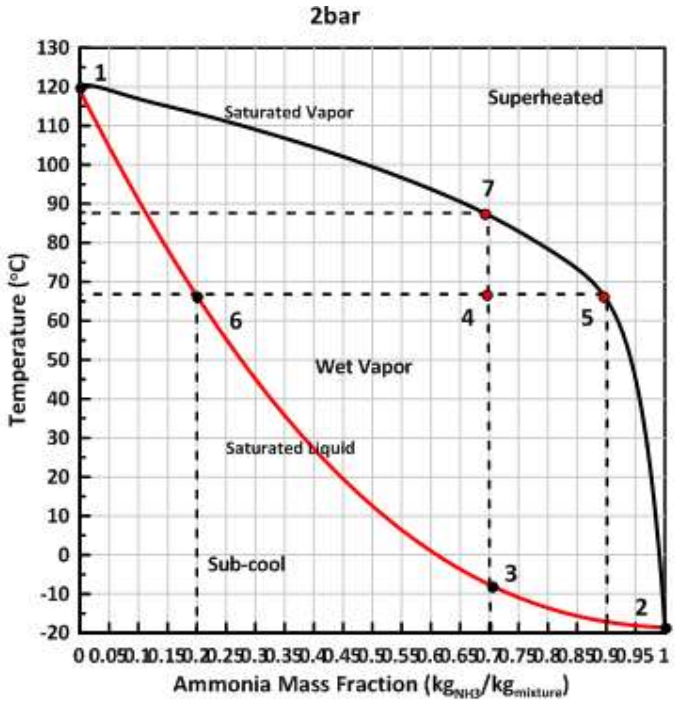

Figure (1-5) Temperature and Ammonia Mass Fraction (T-x)

The working fluid which is used in our work is aqua-ammonia (NH_3-H_2O). The temperature of the saturated liquid water (T_{sw}), as shown in fig (1.6), represents the temperature of pure water at x=0. The temperature of saturated vapor (T_{Sa}) represents the temperature of pure ammonia at x=1. If the

temperature is located between the (temperatures of saturation liquid (T_{sw}) and dew point temperature (T_{dp})) at any x the state of this region is assumed at considered pressure is a meta-stable vapor saturation. Same in the liquid zone, it is also assumed a meta-stable liquid state for ammonia between the saturation temperature of pure ammonia (T_{sa}) and the bubble point of the mixture (T_{bp}).The ammonia mass fraction on the saturated liquid curve is x_f while on the saturated vapor curve it is x_g. For the range of temperature $T_{bp} < T < T_{dp}$ the vapor is a wet vapor. In the liquid zone below the bubble point T_{bp} the liquid is a sub-cooled liquid. Kalina has a good flexibility to suit wide range of many heat source temperatures. The type of potential sources are direct burning (fuel), solar energy, hot water from another plant and waste heat recovery. Many of waste heat sources such as engine exhaust may be used as a source with Kalina cycle system. In this work the boiler hot combustion gases is used to produce vapor.

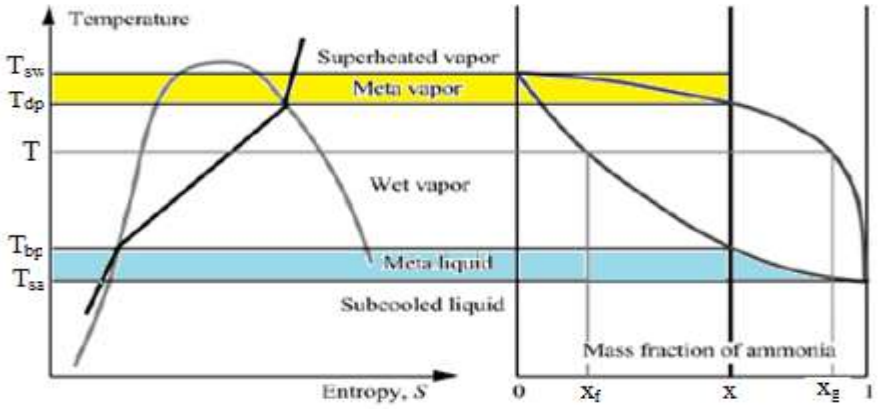

Figure (1-6) the Various States on T-S and T-X Diagrams [4]

1.6 Low Grade Heat

Many low grade energy sources are shown in table (1.1), which are available at different temperature ranges. There are many energy sources, such as solar energy, geothermal energy and waste heat or low grade heat, are promising

energy sources. Organic Rankine Cycle (ORC) and Kalina cycle system are the main cycles were developed to convert low-grade heat into power.

Table (1.1) Temperature Range of Various Types of Low-Grade Sources [2]

Temperature Range (°C)	Sources Temperature
70-800	Solar thermal
149-370	Geothermal
80-400	Industrial waste thermal

1.7 Objective of the Present Work

The objectives of the present work are summarized below:-

1- Study and analysis theoretically the simple case of Kalina cycle system, first modified of Kalina cycle system (MKCS1) and second modified of Kalina cycle system (MKCS2) with ammonia-water mixture as working fluid and the waste heat recovery from the hot gases of boiler. The study includes the energy and exergy analysis.

A- The first modification is the addition of a heat exchanger between the separator and expansion valve (economizer 1).

B- Second modification is adding another heat exchanger (economizer 2) to heat the high pressure liquid (after the pump) by the wet vapor coming from the turbine.

2. Study and analysis experimentally the modified Kalina cycle system (MKCSE).

3. Test the cycle performance with different values of maximum pressure from 10 bar to 40 bar with step of 5 bar and different value of minimum pressure from 2 bar, 3 bar and 4 bar. Also the ammonia mass fraction at turbine entrance from 0.85-0.89 with step of 0.1. Also

different dryness fraction at separator inlet from 0.2-0.4 with step is 0.1.

4. Test the cycle performance at different values of ammonia mass fraction at turbine inlet and different dryness fraction at separator inlet.
5. Design and build modified Kalina cycle system (MKCSE).

1.8 Layout of the Dissertation

This dissertation consists of six chapters are:

- The introduction and general overview are introduced in chapter one.
- Chapter two gives a systematic and comprehensive review of the literature related to the research problem.
- Chapter three is devoted to the experimental construction and measuring instrumentations.
- Chapter four studied and analyzed theoretically the Kalina cycle system and the modification modal of Kalina cycle system with different maximum and minimum pressure.
- Results of the study are presented and discussed in chapter five.
- The conclusions and suggestions for further studies are summarized in chapter six.

Chapter Two

Literature Review

Literature Review

2.1 Introduction:

The demand for power is in rising with the increasing population and advancement of civilization, while the conventional resources such as fossil fuel are insufficient and decreasing. Therefore, it is important to look for other sources of energy to meet population needs. Other types of energy resources are wind, geothermal, solar, waste heat and so on, but some of these energies are of low grade. Low grade energy (solar energy, geothermal energy, biomass energy and waste heat (industrial thermal) means that heat is extracted from low and medium temperature sources whose energy density is small and can't be converted to work using available technologies. Special technologies are needed to convert low-grade energy sources into useful power. Temperatures of low grade energy sources range from atmosphere temperature to about 400°C **Nihaj and Uddin [4].** The first technology used was Organic Rankine Cycle (ORC), which uses low boiling temperature organic working fluids to recover heat from low temperature heat sources. Another technology was suggested by Alexander I. Kalina in 1980. It involved a new cycle using aqua ammonia (NH_3-H_2O) as a working fluid and this type of cycle was called Kalina cycle system **Ibrahim, Kalina and Kalina [5, 6** and **7]. Kumar et al [8]** reported that KCS 1 is important , which consisted of eight parts: two heat exchangers, throttling valve, pump, absorber, turbine and separator. In this cycle the working fluid (NH_3-H_2O) was heated in heat exchanger and then passed into the separator. It is similar to Rankine Cycle (RC), both of them have vapor generator, turbine, condenser and pump. The difference is the heat source, separator and the mixer. It is preferable for small units(less than 20 MW) and used as a bottoming cycle. The cycle is shown in fig (2.1).The working fluid is a solution consists of two fluids with different boiling point. As a binary

mixture, the aqua ammonia mixture is very important in Kalina cycle system. The concentration of the working fluid changes throughout the cycle. The working fluid which is used in Kalina cycle system consists of at least two or three different constituents for example ammonia and water. The binary working fluid consists of two components (absorbent and refrigerant). Aqua ammonia mixture improved system thermodynamic efficiency and provided more flexibility of numerous operating situations. It is working in low temperature range (100°C-200°C) to generate power, cooling and heating. It is the best bottoming cycle for the combined cycle, it has better thermodynamic performance than the RC and ORC. The impact of Kalina cycle on the environment is very small. It Generates 10%-20% more power than conventional steam power generation technologies (simple Rankine cycle). The capital cost is low because KCS uses small heat exchangers and lower plant auxiliary loads. Kalina cycle uses binary working fluid such as ammonia-water or lithium Bromide-water and it can work with different concentration ratios. It uses a waste heat or renewable energy as a resource such as (geothermal, solar energy) to produce power. It needs a short time for maintenance.

2.2 Kalina Cycle System for Power Generation:

Chen et al [9] studied experimentally the effect of inlet temperatures of both cooling water and heat resource on the system efficiencies such as exergy efficiency and thermal efficiency. The model used in this study was ammonia-water Kalina-Rankine Cycle (AWKRC) and ammonia-water Rankine cycle (AWRC). The results revealed that the thermal efficiency and the exergy efficiency of KCS were 18.2% and 41.9% respectively, while the thermal efficiency and exergy efficiency of AWRC were 21.1% and 43% respectively. **Zhang et al [10]** analyzed the performance of heating and power generation of integrated system of aqua ammonia Kalina cycle-

Rankine cycle. The integrated system (ammonia-water Kalina-Rankine cycle (AWKRC)) was based on the KC and converted to the RC with a set of valves. The RC could achieve extra heating by around 55.3% of the heating load which was absorbed in the evaporator and its efficiency was 23.7% higher than that of Kalina cycle system. **Deepak and Gupta [11]** studied the effect of the turbine inlet concentration, strong solution concentration and separator temperature on the cycle efficiency and specific power. The results showed 11.77% cycle efficiency at a separator temperature of 125°C and 95% vapor concentration. **Congcong et al [12]** developed a pinch-based mathematical model and optimization of Kalina cycle. The mathematical model improves heat integration with variable heat capacities and enables the modifications of KC simultaneously. The study leads to a 15.8% increase in net power output and a 4.13% decrease in the efficiency. **Ulirk et al [13]** compared the Kalina cycle system and Kalina Split cycle. The Kalina split-cycle and Kalina cycle is based on the same principles, the difference between of SC and KCS is the SC has two evaporators but the KCS has one evaporator. Two streams of different ammonia mass fraction enter the boiler. Both of them use the same working fluid (ammonia-water). The changing of ammonia concentration is the main difference between them. Five different concentrations was tested in the Kalina split-cycle. The results showed that the power for the split cycle (SC) with reheat is higher than the power for KCS without reheating by around 5.1%. The power of the SC without reheat is higher by about 2.5% than the reference KCS. Also the Split-cycle with reheat is able to produce around 11.4% more power for the same heat source conditions. **Eller et al [14]** studied and analyzed techno-economic evaluation of the Kalina cycle system (KCS) and the Organic Rankine Cycle, with the temperatures of the heat source are 200°C, 300°C and 400°C. Also they analyzed the pressure and the temperature of the heat source, the capacity of the heat exchanger, parameter

size and the output power. When increasing the temperature of the heat source the costs will decrease. For ORC with hexane/toluene at 300°C and 400°C heat source temperature the cost amount 49.7% and 39.8% of the costs for 200°C respectively. The output power of the Kalina cycle (KC) with ethanol/hexanol shows up to 3 MW higher gross and 3.5 MW higher net power compared to Kalina cycle (KC) with aqua ammonia (NH_3-H_2O). The heat exchanger capacity for the Organic Rankine cycle (ORC) with ethanol/hexanol was 66.7% lower than heat exchanger capacity compared to Kalina cycle system with aqua ammonia. **Modi et al [15]** analyzed and optimized thermo economically the Kalina cycle for a central receiver concentrating solar plant. This work used a high temperature KC for central receiver concentrating solar plant with direct vapor generation and without storage. The Kalina cycle system consists of two recuperator, three mixers, two pumps, throttling valve, two condensers, separator and turbine. The results showed that, the specific investment cost for KC is still within the ranges. **Knudsen et al [16]** analyzed the energy and exergy of Kalina cycle system used in concentrated power plants with direct steam generation. The results showed that Kalina cycle system has no benefit to generate power from the solar energy directly. The efficiency of KC was less than that of RC by about 5%. The RC was preferable when using just heat from the solar receiver directly. **Revz and Engelhard [17]** studied the Kalina cycle version KSGa2. It is very complicated cycle. It consists of six heat exchangers, three separators, three pumps, four mixers, two expansion valves and turbine. This cycle has the highest output of electricity as shown in Fig (2.2). **Zhao et al [18]** studied and analyzed a Kalina cycle system (KCS 6) integrated with compressed air energy storage (CAES) system. They performed thermodynamic analysis (energy and exergy analysis) and the parametric analysis. The suggested system consisted of two parts or two cycles: CAES and KCS 6. The exergy efficiency can be improved about 4%, and it can be

further improved after parameters optimization. Another version of Kalina cycle system is called KCS6 as shown fig (2.3). The overall efficiency of the cycle with out and with KCS6 was 42.68% and 46.42% respectively. **Long et al [19]** studied the effect of the evaporation pressure (P_{max}) and ammonia mass fraction (x) of ammonia-water mixture (NH_3-H_2O) on the performance of Kalina cycle system 11(KCS11). The optimal case results showed that all efficiencies increased with the increasing of the inlet temperature (waste heat). The results showed that, there is an increase in the exergy efficiency from58.88% to 72.75% and the optimum evaporation pressure was 2100kPa. **Ahmed and Karimi [20]** studied the effect of inlet temperature with fixed pressure on the performance of Kalina cycle system 11 (KCS11). The range of the temperature was taken from 130°C to 200°C and the range of the pressure was chosen from 2MPa to 5 MPa with a step of 0.5 MPa. The results showed that when the inlet temperature increased the thermal efficiency increased too. At pressure of 2MPa with the range of input temperature (130-160°C) the efficiency increased from 1.64% to 8.91 %. **Adi et al [21]** adopted and studied Kalina cycle system as a bottoming cycle in Wayang Windu. A geothermal sources was used as a main heat source to produce power. Kalina cycle system (KCS 11) which consisted of ten parts, five heat exchangers, turbine, two pumps and two mixers. The system can produce 1660.3 kW of power from 48 kg/s of used brine with 13.20% energy efficiency. The results also showed that for different pinch temperatures (5, 10, 15, 20°C), the best performance was found at 5°C. Another version of Kalina cycle (KCS5) studied by **Sayed and Tribus [22]**. It is a direct fired plants and it has a refinement arrangement, which is KCS5n similar to KCS5. KCS5n is used with low temperature, but KCS5 is used with the hot gases are mostly used to superheat rather than boil**.** It is used for large unit and proposed for the gas turbine-based bottoming cycle. **Milenko et al [23]** analyzed another type of Kalina cycle (KCDCS) used in biomass plants. The

results showed that it has advantages and a feasible alternative to initial KCS11. **Gaosheng et al. [24]** analyzed the performance on Kalina cycle works on a dry hot rock geothermal source power production. In this system used two condensers high and low pressure was used to condensate the working fluid (aqua ammonia) mixture. Water was used to cool the condensers. The results showed that, when the temperature of the heat source increases the energy efficiency and power recovery increases too. The range of the thermal efficiency was between 8.5%-18%, at the range of the heat resource temperature of 150 °C-220 °C as shown Fig (2.4). **Nasruddin et al. [25]** studied and analyzed the energy and exergy of Kalina cycle system 34 (KCS 34) with different ammonia mass fraction of aqua ammonia (NH_3-H_2O). The heat source was low temperature geothermal resources. The working fluid used in Kalina cycle system 34 was ammonia-water. They used four concentrations of aqua ammonia (78% ammonia and 22% water), (81% ammonia and 19% water), (84% ammonia and 16% water) and (85.5% ammonia and 14.5% water). For mass fraction 85.5% the highest exergy efficiency is 69%, mass fraction 84% is 68.6%, mass fraction 81% is 67.1%, mass fraction 78% is 66.9% as shown in fig (2.5). **Modi and Haglind [26]** studied Kalina cycle system (KCS) in high temperature (500°C) and high pressure over than 100 bar. They studied and compared among four types of Kalina cycle system. The types are KCS12, KCS234, KCS123 and KCS1234. The types of Kalina cycle depend on the number and location of the recuperators. It is named as KCS12 because it used two (first one and the second one) recuperators, also KCS 234 used three (second, third and fourth) recuperators and so on for the others (KCS123 and KCS 1234) as shown fig (2.6). The comparison was based on the cycle efficiency and the amount of water requirement for cooling. When the turbine inlets ammonia mass fraction (x) increases the cycle efficiency increases for all Kalina cycle, except KCS234 where the cycle efficiency decreased when mass fraction (x)

increases. When the mass fraction increases the amount of cooling water decreases for all the KCS, except with the KCS234 the amount of cooling increases. The KCS 1234 has the highest efficiency of 31.47%, at inlet turbine pressure of 140 bar, x=0.8. The KCS 123 has the second highest efficiency of 31.46%, at inlet turbine pressure 140 bar, x=0.8. While the lowest efficiency was for the KCS 234 which was 27.35% with the inlet turbine pressure (100 bar), x=0.8. **Parvathy and Varghese [27]** studied the effect of two turbines on the performance of Kalina cycle system. The aim of this work was improving the power output and improve the efficiency of Kalina cycle system with used two turbine expansion. In this work MKCS was proposed with two turbines and reheat between of them. The modification of Kalina cycle system (MKCS) was tested with different intermediate pressure. In this modification Kalina cycle system (MKCS) with two turbines and intermediate heating the vapor after expanding in the high pressure turbine is separated, reheated and expanded again in the low pressure turbine. The results showed that, the efficiency of MKCS was improved up 4.04% compared to simple kalian cycle system. The maximum efficiency was obtained was 28.7% for intermediate pressure of 35 bar. **Diniz and Raul [28]** studied and improved the generation of electricity with this cycle can reach around 2.725 MW, with energy efficiency of 21.8% and exergy efficiency of 55.2% and the cost of the generation was 278.03$/MWh. **Ishida and Kawammura [29]** studied and analyzed thermodynamically and economically on the Kalina cycle system 1-2 (kcs1-2). It consists of six heat exchanger, two pumps, separator, expansion valve and turbine. It was used for waste heat recovery from a cement factory as shown in fig (2.7). The result was a reduction in the cost of electricity and the cost of the generation was 240.00$/MWh. **Qu et al [30]** studied and analyzed the Kalina cycle system with solar energy as heat source. It consists of three parts concentrator, photovoltaic subsystem and the Kalina cycle

subsystem with an absorption as shown in fig (2.8). Photovoltaic can work in low-temperature conditions. When use absorption chiller, if the pressure at turbine outlet decreased the power increased by 4.2%. The results showed that the waste heat with very low temperature around 60℃ and 70℃ can be used for producing power with efficiency between 4-5%. **Hoon et al [31]** compared between the Kalina flash cycles (KFC) and simple Kalina (KCS). The main reason to add flash vessel is to protect the blades of the turbine. If the flash pressure increased the exergy efficiency increased. The results showed that the enthalpy which exits from the separator was 1732.60 kJ/kg. Also the exergy efficiency decreased with the increasing of ammonia concentration with constant of flash pressure as shown fig (2.9). **Lee et al [32]** compared the exergy analysis, thermodynamic performance and optimization of Organic Flash Cycle and Organic Rankine Cycle. The results showed that the thermal efficiency was improved by flash from 10% to 20%**.** **Gharde et al [33]** designed and studied basic kalian cycle system (KCS) operated with the waste heat from the exhaust of the gasoline engine. The engine was a four cylinder, four stroke, water cooled, S.I engine with a capacity of 1196 cc and a power 73 HP at 6000 rpm. The overall thermal efficiency increased from 40% to 60% with the use of Kalina cycle. Kalina cycle system was also developed for the conversion of ocean thermal energy (OTEC) to electricity. The used working fluid was aqua-ammonia **Uehara et al [34]**, gasoil engine works combined cycle **Jonsson [35]** the cycle works by coal (solid)-fired.

2.3 Kalina Cycle for Power Generation and Cooling

Dhahad et al [36] analyzed a new integrated system thermodynamically and thermo economically. The new integrated system consisted of a modified Kalina cycle (MKC) and an absorption refrigeration cycle (ARC) used for producing power and cooling together. It was driven

by a low-temperature heat source (LTHS). The results showed that, the suggested power generation and cooling system can produce 158.3 kW as a net power output and 1084 kW as cooling capacity**. Lui et al [37]** studied the coupled system which consists of two cycles, the first cycle is an absorption chiller, while the second cycle is a Kalina cycle system 34 (KCS 34). The waste heat source is divided into two parts: the first part is high-temperature used to generate power, the second part is low-temperature used to produce cooling effect. Fig (2.10) displays the schematic diagram of the integrated coupled cycles LiBr/H_2O and NH_3-H_2O. The net power output increases with the increase of the ammonia concentration. **Zhang et al [38]** studied and analyzed the parallel cogeneration power and refrigeration of Kalina cycle (PPR-KC). The parallel means that the working solution which passed through the mid-pressure absorber was splited into two branches. The first one goes to the turbine via preheat, boiler and throttling valve then to turbine to produce power, while the second branch goes to evaporator via pump, preheat, rectifier/generator then to the evaporator to produce cooling. The results showed that, when the dew point in the boiler was 255°C and the working fluid concentration was 0.5, the minimum split fraction was 0.57 and the corresponding optimized basic concentration was 0.34. **Demirkaya et al [39]** studied theoretically the effect of different boiler pressures, ammonia concentrations, rectifier temperature and expander isentropic efficiency on the output power, cooling production and efficiencies. They also experimentally studied the effect of the evaporation pressure on the production of vapor at the separator, which was responsible for providing the mass flow circulating through the expander. The results showed that the maximum theoretical effective first law and exergy efficiencies were 7.2% and 45% respectively. **Abam et al [40]** used a modified Kalina power-cooling cycle (KCPC) as a topping cycle while the vapor absorption cycle as a bottoming cycle. This system was called modified Kalina power-cooling

vapor absorption cycle (KLPCC). The energy efficiency and COP were increased from 13.82% to 16.39% and 0.59 to 0.75 respectively. **Shanker and Srinivas [41]** proposed a new cooling cogeneration cycle to generate cooling and power from one source of heat. They used two types of working fluids i.e. aqua ammonia and LiBr-water mixture. The cycle power efficiency of the LiBr-water was higher than aqua-ammonia. The efficiency of cooling cycle cogeneration was as high as 3-13% it was 1-1.65% for ammonia-water cooling cogeneration cycle.

2.4 Choice of Working Fluid and Its Thermodynamic Properties

Fig (2.11) shows (T-s and T-x) diagrams for the fluid used in the KCS. The T-s diagram shows that the heat is added at variable temperature in KCS in the mixed phase region due to the use of binary fluid, while in RC the heat is added at constant temperature. The T-x diagram shows that the boiling temperature of the binary fluid decreases as the volume fraction of the refrigerant increases. The selection of the working fluid is based on their environmental characteristics such as low boiling temperature, non-toxicity and zero ozone depletion according to **Kumer et al [42]**. These working fluids are classified into four groups based on the component with low boiling temperature, which are, R32 group, propylene group, propane group and CO_2 group as shown in **table(2.1) Hettiarachchi [43].**The most suitable for KCS is a mixture of aqua ammonia (NH_3-H_2O). Ammonia-water (NH_3-H_2O) mixture have properties different from the properties of just water or just ammonia **Khankari et al [44]**. Pure ammonia and pure water, both of them have constant and steady temperatures of condensing and boiling, but the mixture of aqua ammonia has varying temperature to condense and boil. The thermo physical properties for just water or just ammonia are constant, but the thermo physical properties of the mixture of ammonia-water are varying by changing the ammonia concentration **Ogriseck et al [45]. Table**

(2.2) shows the type of cycle with working fluid and their efficiencies from **[46- 49]**. **Nasruddin et al [50]** analyzed and optimized Kalina cycle and absorption cycle to produce power and cooling. In this work the main heat source was Lahendong geothermal source. Ammonia-water (NH_3-H_2O) mixture was used as the working fluid, with a concentration ratio of 70% ammonia and 30% water. With Kalina cycle (KC) the exergy efficiency and exergoeconomic is better than that with Rankine cycle (RC). The thermal efficiency of Kalina cycle is around 40%-60%. The properties of the working fluid pair depends on the thermodynamic properties of the pure substances. The properties of the working fluid which are important to be considered are as follows **[51]**. The range of the boiling point of the mixture can be provided by low waste heat. There should be a high miscibility between the components of the mixture. The process of changing the liquid saturation to vapor saturation is none isothermal (none zoetropic). There should be a low heat of mixing, no solid formation, low cost and availability. It is very important for low boiling point and high latent heat of vaporization for the refrigerant, but is not important for the absorbent. There should be a low viscosity for both of them. No toxic and environment friendly **[52].**

2.5 Working Fluid Circulation in Kalina Cycle.

Kalina cycle is similar, in principle to, Rankine Cycle (RC). Both of them have vapor generator, turbine, condenser and pump. The difference is the heat source, separator and the mixer. It consists of six items: turbine, condenser, mixer, pump, generator and separator as shown in fig (2.1). It is preferable for small units(less than 20 MW) of total output used as a bottoming cycle. The working fluid enters the generator as sub-cooled liquid and leave the generator as wet vapor. The working fluid will be separated totally into saturated liquid and saturated vapor in the separator. The saturated vapor expanded in turbine and leaves as a wet mixture and mix

with the weak solution that comes from the separator in the mixer. Then it leaves the mixer as wet vapor and enters the condenser. At condenser exit it is a saturated liquid which is then pumped by pump to the generator as sub-cooled liquid, **Eller et al and Park [53 and 54]**.

2.6 Types of working fluids is used in Kalina Cycle System

There are many pairs of working fluids used in Kalina cycle system, such as H_2O-NH_3, LiBr-H_2O, Methanol-H_2O and Ethanol-H_2O. Every pair consists of refrigerant and absorbent.

2.6.1 Aqua-Ammonia

It is very important and used in many applications. It is used as working fluid since the mid of 19^{th} century and it was extended for commercial and residential cooling, heating purposes and used it with Kalina cycle system. Water (R718) is the absorbent, while the ammonia (R717) is the refrigerant, they have same molecular weight. The boiling point of water and ammonia in atomic sphere are 100℃ and -33℃ respectively. The freezing point for water and ammonia 0℃ and -78℃ respectively.

2.6.2 Lithium-Bromide-Water (LiBr-H_2O)

Lithium- Bromide is a salt represents the absorbent in Kalina cycle system and the water represents the refrigerant. The lithium bromide is sold salt; its density is 3464 g/cm^3. It is soluble in water and not flammable. It is not toxic but it can cause eye damage/irritation and itching the skin. It is a highly corrosive brine and concerns crystallization problem. It is used in many applications such as cooling, heating and in Kalina cycle system to produce power.

2.6.3 Methanol-Water

Methanol (ethyl alcohol) is a clear, colorless liquid highly flammable, and it is used to dissolve other chemical substance. It has a good solubility

in the water. The density of CH_3OH is 0.981 g/ml. Methanol represents the refrigerant and the water represents the absorber. Also it is used in Kalina cycle system to produce power. Methanol and water nearly have the same properties, both are of comparable size, and hydrogen bonding. Consequently, they are fully miscible in each other and have high boiling temperature, but the density of water is higher than the density of ethanol

2.6.4 Ethanol-Hexanol

The boiling point of the ethanol (C_2H_5OH) is 78℃, while the boiling point of hexanol ($C_6H_{13}OH$) is 157℃. In this pair the ethanol represents the refrigerant, while the hexanol represents the absorbent. This pair is used in Kalian cycle system to produce power, but with higher cost compared to aqua-ammonia **[14]**. Generally, this pair produces more power than aqua-ammonia by a factor of by 1.5.

2.7 Thermodynamic Analysis of Kalina Cycle

The thermodynamic analysis includes both energy and exergy analysis. This analysis is performed for a typical Kalina cycle system 1 (KCS 1), shown in fig (2.1). This cycle consists of six components: turbine, condenser, mixer, pump, generator and separator. The analysis is performed for each component as explained below.

2.7.1 Energy and Mass Analysis

The governing equations to be solved are the continuity equation and the first law of thermodynamic (energy equation) applied for each component of the cycle.

$$\sum \dot{m}_i = \sum \dot{m}_0 \tag{2.1}$$

$$\sum (m_i x_i)_i = \sum (m_i x_i)_e \tag{2.2}$$

$$\sum \dot{Q} + \sum \dot{m}_i h_i = \sum \dot{W} + \sum \dot{m}_o h_o \quad (2.3)$$

The analysis is based on the following assumptions: -

1-Steady state and steady flow process.

2- Pressure and heat losses in the connecting pipes are neglected.

3- The heat exchanger's effectiveness is unity.

4-All the process are adiabatic.

5- Change in KE and PE of fluid in each component are neglected.

The above equations are used in the thermodynamic analysis of each component in the cycle with specific assumptions.

2.7.2 Kalina Cycle Efficiency

The cycle thermal efficiency is calculated as follow:

$$\eta_{th} = \frac{W_{net}}{Q_{in}} = \frac{W_T - W_P}{Q_{in}} \quad (2.4)$$

Where Q_{in} is the net heat in the heat recovery vapor generator

Rogdakis [47] suggested the following empirical mathematical formulation to calculate the thermal efficiency of the cycle (KCS) in terms of low pressure (p_L) as

$$\eta_{th} = \frac{A}{P_L} + BP_L + C \quad (2.5)$$

OR

$$\eta_{th} = a_2 + b_2\, T_H + c_2\, T_H^2 \quad (2.6)$$

Where: -

A, B and C are constant

P_L is the low pressure of the cycle

η_{th} is the thermal efficiency

T_H is the maximum temperature of the cycle.

T_L is the minimum temperature of the cycle.

a_2, b_2 and c_2 are constants

$$a_2 = -0.049 - 0.0022T_L \quad (2.7)$$

$$b_2 = 0.0035 * 0.92^{\frac{1}{P_L}} \quad (2.8)$$

$$c_2 = -2.36 * 10^{-6} - 2.19 * 10^{-6} P_L + 3.14 * 10^{-7} P_L^2 \quad (2.9)$$

2.7.3 Exergy Analysis

The exergy analysis is also performed for each component under same general assumptions. The rate of exergy flow of fluid stream is written as: **Hoon et al [31]**:

$$\dot{E}^{\cdot} = \dot{m} * [h - h_o - T_o * (s - s_o)] \quad (2.10)$$

$$\dot{W}_{net} = \dot{W}_t - \dot{W}_p \quad (2.11)$$

The subscript o denotes the state of surroundings **[47]**.

Where $\dot{W}_{net}$ is the net power, $\dot{W}_t$ is rate of work produced by turbine and $\dot{W}_p$is rate of work consumed by pump.

$$\dot{E}_{in} = \dot{E}_1 - \dot{E}_2 \quad (2.12)$$

Where $\dot{E}_{in}$ is the total exergy obtained from the hot fluid (exhaust)

The exergy destruction is

$$\dot{E}_d = \sum \dot{E_{in}} - \sum \dot{E_{out}} + \dot{W}_{net} \quad (2.13)$$

The total exergy destruction in the cycle is

$$(\dot{E}_d)_{cycle} = \sum \dot{E}_{di} \quad (2.14)$$

The exergy efficiency of the cycle is

$$\eta_{ex} = \frac{\dot{W}_{net}}{(\dot{E}_{in} - \dot{E}_{out})_{hot\ gases}} \quad (2.15)$$

Where η_{ex} is the exergy efficiency

The exergy analysis for each component is performed under same assumptions as in the energy analysis.

The exergy flow of fluid stream is also written as, **Wall et al [48]:**

$$\sum \Delta H_K = 0 (K = 1, \ldots., K^{\wedge} \quad (2.16)$$

Where K^ is the number of processes in the subsystem, classified into energy donors and energy acceptors, the above equation becomes

$$\sum \Delta H_K^{ed} + \sum \Delta H_K^{ea} = 0 \quad (2.17)$$

Where the super script ed and ea are the energy donor and energy acceptor, respectively.

According to the second law of the thermodynamics the entropy equation is

$$\sum \Delta S_K = \sum \Delta S_K^{ed} + \sum \Delta S_K^{ea} \geq 0 \quad (2.18)$$

The exergy is

$$\sum \Delta E_K = \sum \Delta H_K - T_0 \sum \Delta S_K \quad (2.19)$$

Wall et al. [48] suggested the following equation for the availability (A).

$$A = \Delta E / \Delta H \quad (2.20)$$

$$A = \frac{\Delta H - T_{\circ} \Delta S}{\Delta H} = 1 - \frac{T_0 \Delta S}{\Delta H} \quad (2.21)$$

If ΔS=0 (reversible process) then the availability A=1

The **aqua. (2.19)** will be:

$$-\sum \Delta E_K = \sum \Delta H_K^{ea} \left(A_K^{ed} - A_K^{ea}\right). \quad (2.22)$$

If k^ goes to infinity the relation becomes:

$$-\int dE = \int (A^{ed} - A^{ea}) dH^{ea} \quad (2.23)$$

Note, by plotting A^{ed} and A^{ea} with H^{ea}, the exergy loss is represented by the area between A^{ed} and A^{ea} this plot is named Energy-Utilization Diagram **[48].**

2.8 Energy-Utilization Diagram

The Energy-Utilization Diagram (EUD) for KCS is presented in fig (2.12) **[48].** This figure shows and illustrates the transfer of energy from the donor (A^{ed}) to the accepter (A^{ea}) and the energy level. Care should be taken about the pinches because the pinches is not easy to find. Fig (2.12) is divided to different regions related to the components of the KCS. The loss of exergy in each component is shown as the area between the energy donated and energy accepted lines (shadowed area). The biggest shaded area in the boiler and the second is turbine, the third is the condenser **Murugan and Subbarao, Wang et al and Rumminger et al [55, 56 and 57]**.

2.9 Comparison between Rankine and Kalina Cycles

1. In a common RC power plant, the working fluid is water, and in ORC the working fluid is a low molecular weight and low boiling temperature fluid.

2. KCS uses binary mixture to improve thermodynamic efficiency.

3. The relative gain of the RC (works in low temperature) is less than the relative gain of KCS.

4.The thermal efficiency of RC is less than the thermal efficiency of Kalina cycle because the average temperature of heat rejection of RC is more than in KCS, and the average temperature of heat addition of RC is less than in KCS as shown in fig (2.13) **Kumar et al [8].**

5. In general, the performance of KCS is better than the performance of both RC and ORC.

6. A family of Kalina cycles are used in different fields such as electricity production from solar energy, waste heat, geothermal and biomass **Kumar et al [8].** A plant operating on Kalian cycle produces 30% to 50% more power than an Organic Rankine Cycle (ORC) plant **Leibowitz [58].**

7. Kalina cycle achieves higher exergy efficiency than RC and ORC **Wang et al [56].**

8. The Kalina Cycle System (KCS 1) has additional degree of freedom, but the RC has not, the working fluid is a binary mixture such as (NH_3-H_2O), LiBr-H_2O, Methanol-H_2O and Ethanol-H_2O **[58-63].**

9. The working fluid selected for ORC is R245fa, while for RC is water and for KCS11 is NH_3 -H_2O mixture **Lin et al [64]**.

2.10 Summary

Kalina Cycle System was designed for using instead of RC or ORC as a bottoming cycle for the combined-cycle energy system as well as for the generation of electricity or cooling using low-temperature heat resources. The review of previous literature has shown many different versions and improvement of Kalina cycle system. Some of researchers added extra components to the cycle such as heat exchangers, separators, turbines and condensers to improve the performance. Other researchers used flash to protect the blade of the turbine. Also they used waste heat, solar energy, geothermal energy and biomass energy as heat sources. Also they used different types of working fluid such as aqua-ammonia, LiBr-water, methanol-water and ethanol-hexanol. There are limited works, how to exploit the heat in the weak solution that come from the separator. Also how to exploit the heat in the strong solution that exit from the turbine and use another heat exchanger before the turbine to superheat the strong solution

before it passes throughout the turbine. Table (2.3) displays the development history of Kalina cycle types.

2.11 Contribution of the Present Work

It is clear from the previews cited survey that most research focused on improving the performance of Kalina Cycle System. They used many working fluids such as LiBr-H_2O and aqua ammonia (NH3-H_2O). The present research aims to develop a new versions of Kalina cycle. This work includes three modifications of simple Kalina cycle system (KCS1). The first modification is the use of heat exchanger between the separator and expansion valve to improve the efficiency of the simple Kalina cycle. This developed version will be tested experimentally and theoretically with different operating conditions such as high pressure, low pressure, ammonia mass fraction at turbine inlet and dryness fraction at separator inlet. The performance of this new version shall be compared with that of KCS1.The second modification is the use of another heat exchanger between the turbine and the pump to reduce the heat rejected. This developed version will be tested theoretically only with the same operating conditions and the results will be compared with the results of first modification and with basic simple Kalina cycle. The third modification is the use of a cooling system to cool the mixer, it is named diabetic process. The waste heat from the combustion gases of a boiler shall be used as a heat source in the heat recovery vapor generator (HRVG).

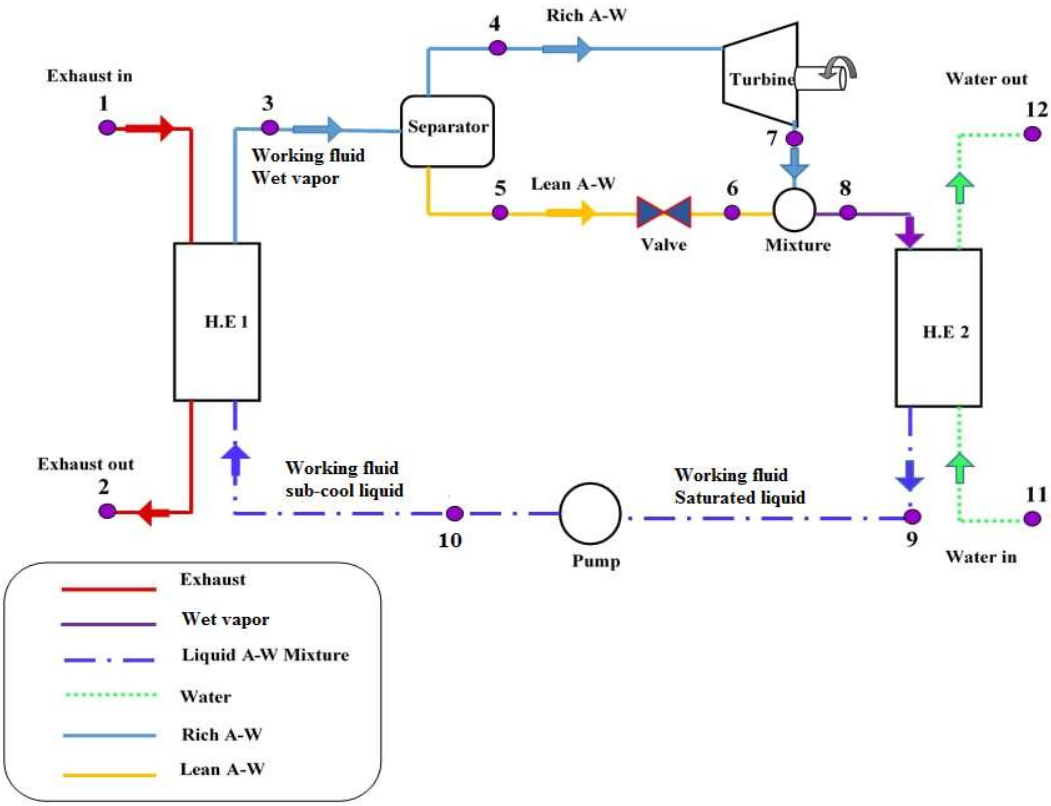

Figure (2-1) Kalina Cycle System 1 (KCS 1) [33]

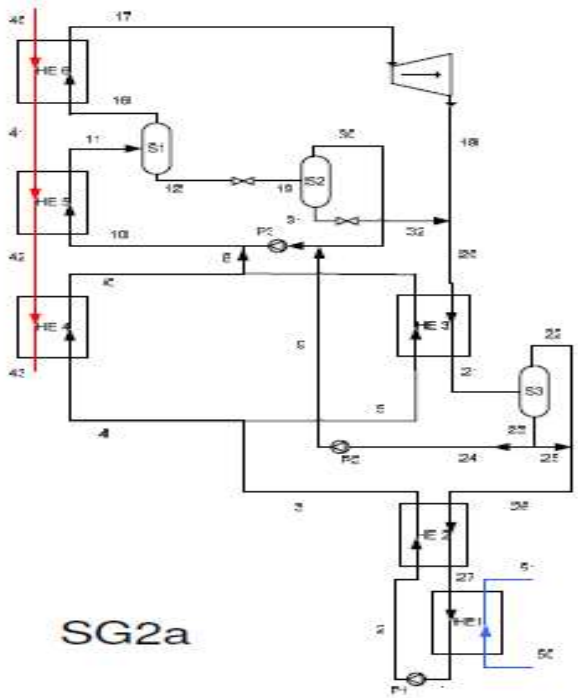

Figure (2-2) Various Kalina Cycle Layout for High Temperature Application [17]

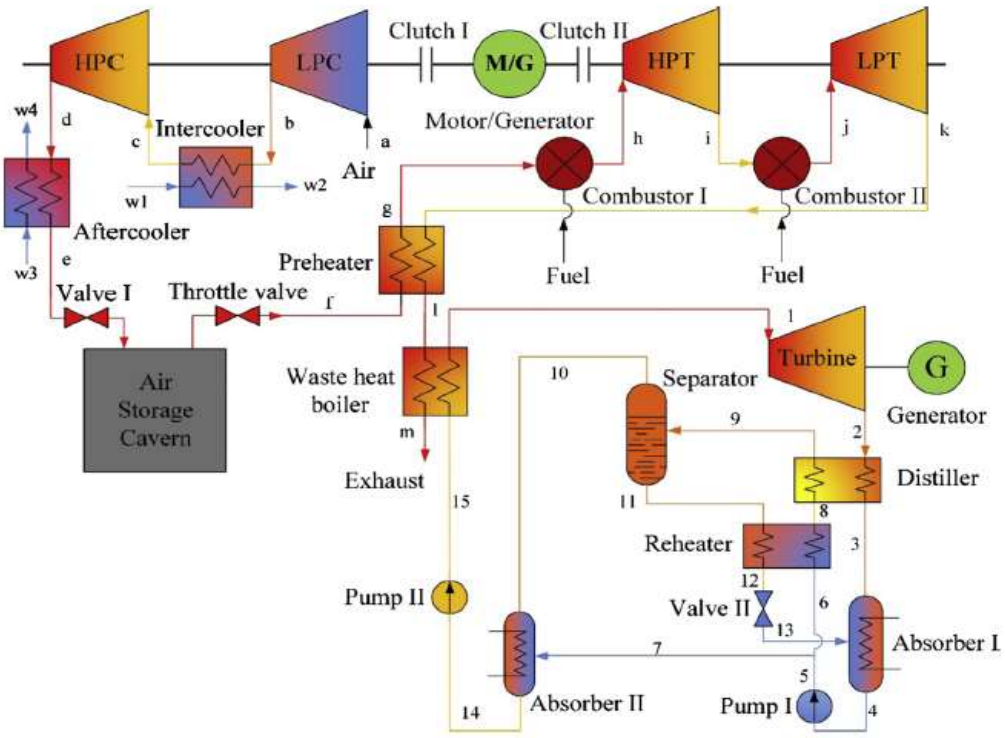

Figure (2-3) Schematic of the Proposed CAES-KCS6 System [18]

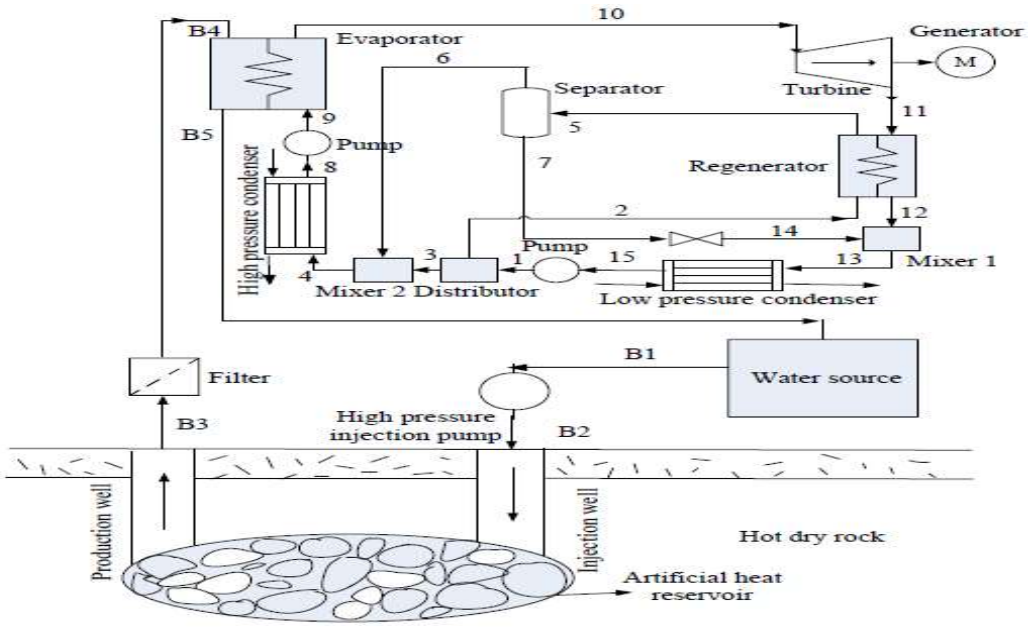

Figure (2-4) Sketch of a Hot Dry Rock Power Generation System Based On Kalina Cycle [24]

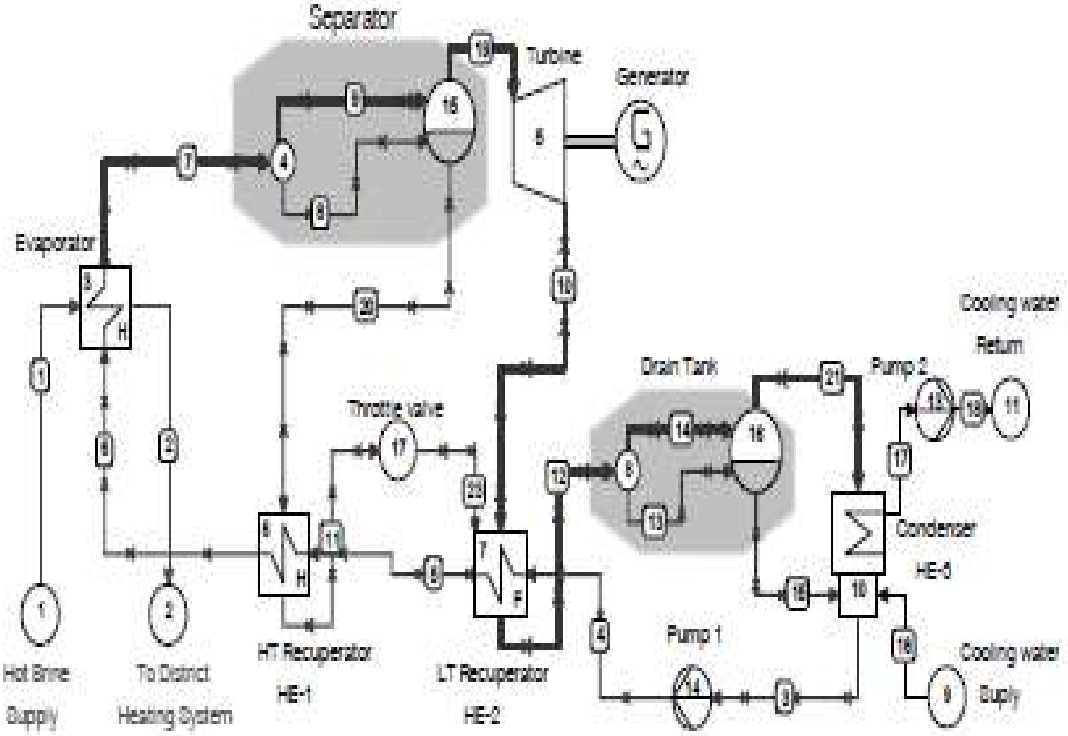

Figure (2-5) Kalina Cycle System 34 (KCS34) [25].

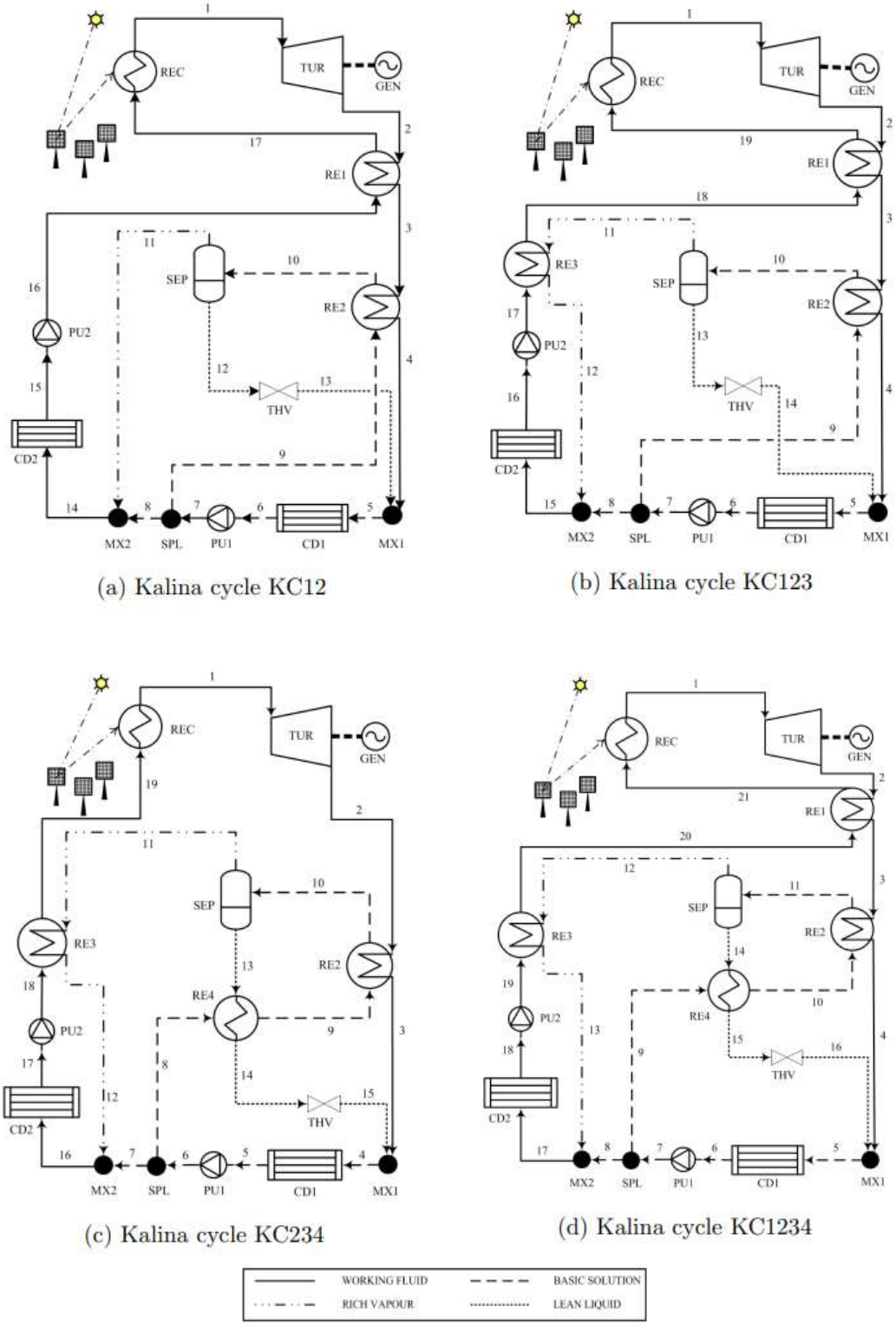

(a) Kalina cycle KC12

(b) Kalina cycle KC123

(c) Kalina cycle KC234

(d) Kalina cycle KC1234

Figure (2-6) Kalina Cycle Systems (a, b, c and d) [26].

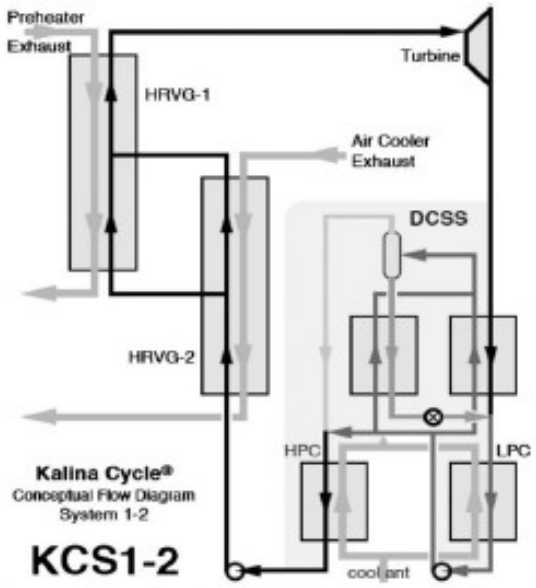

Note: HRVG: Heat Recovery Vapor Generator; LPC: Low Pressure Condenser; HPC: High Pressure Condenser; DCSS: Distillation and Condensation Sub System.

Figure (2-7) Kalina Cycle for a Cement [29].

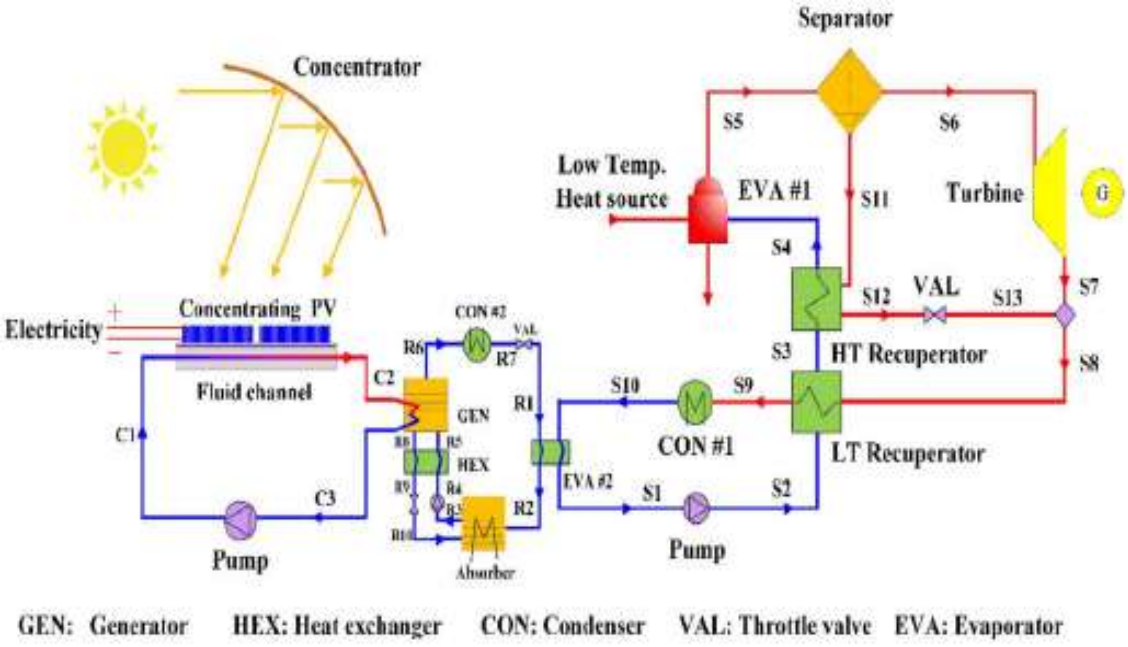

Figure (2-8) Flow Diagram of Concentrating Photovoltaic/Thermal and KC Combined [30].

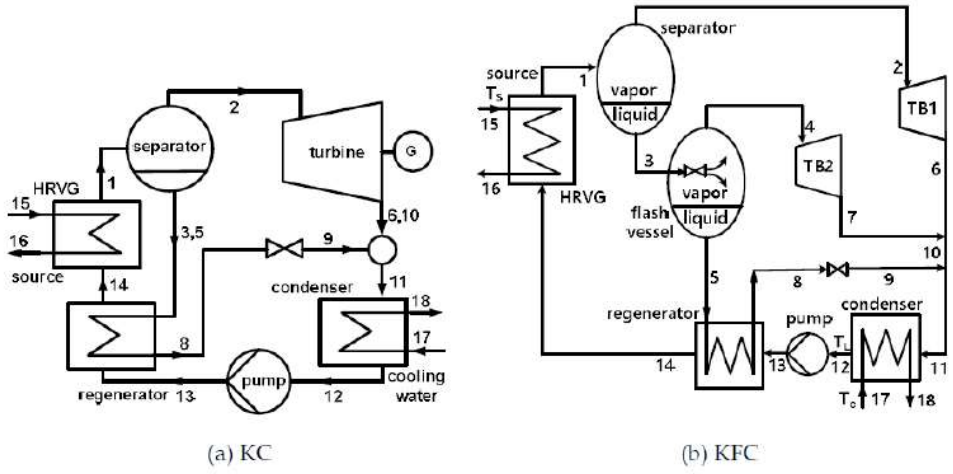

Figure (2-9) (a) Kalina Cycle without Flash (b) Kalina Cycle with Flash [31]

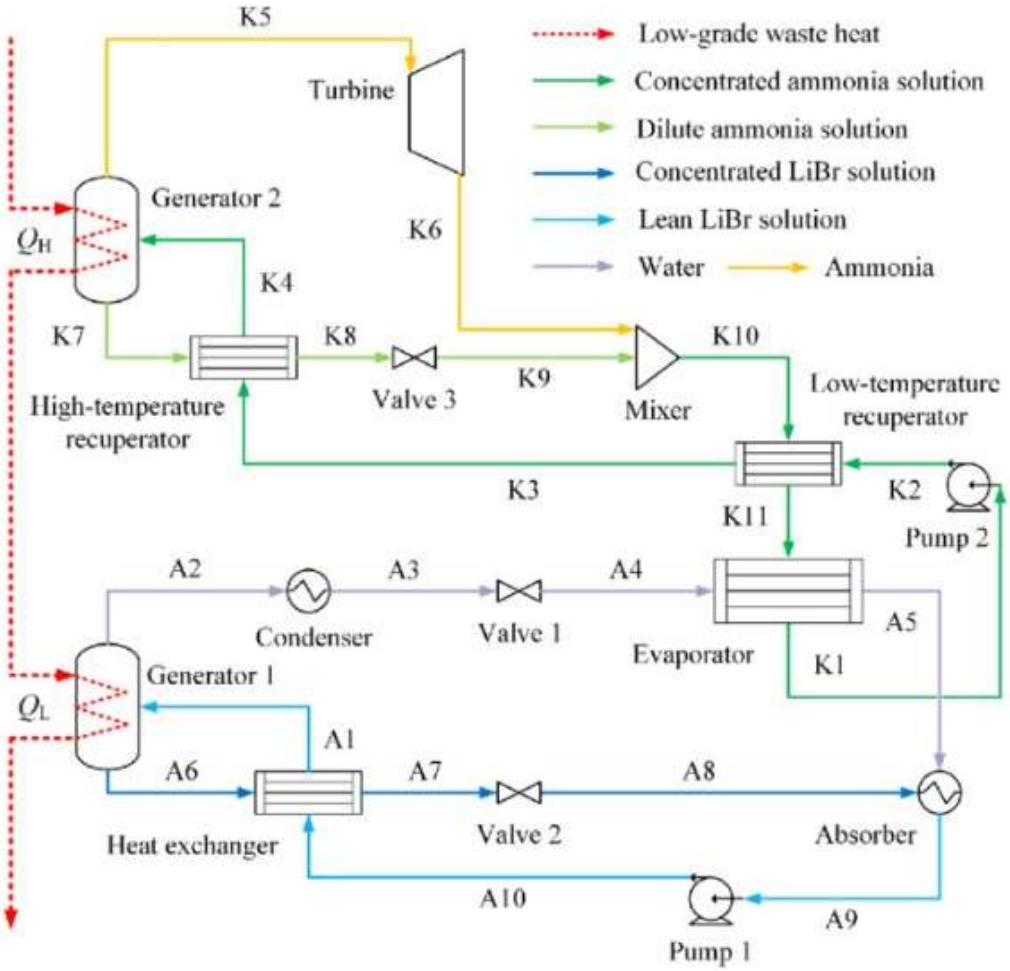

Figure (2-10) Schematic Diagram of the Coupled Libr/H_2O Absorption Chiller/Kalina [37]

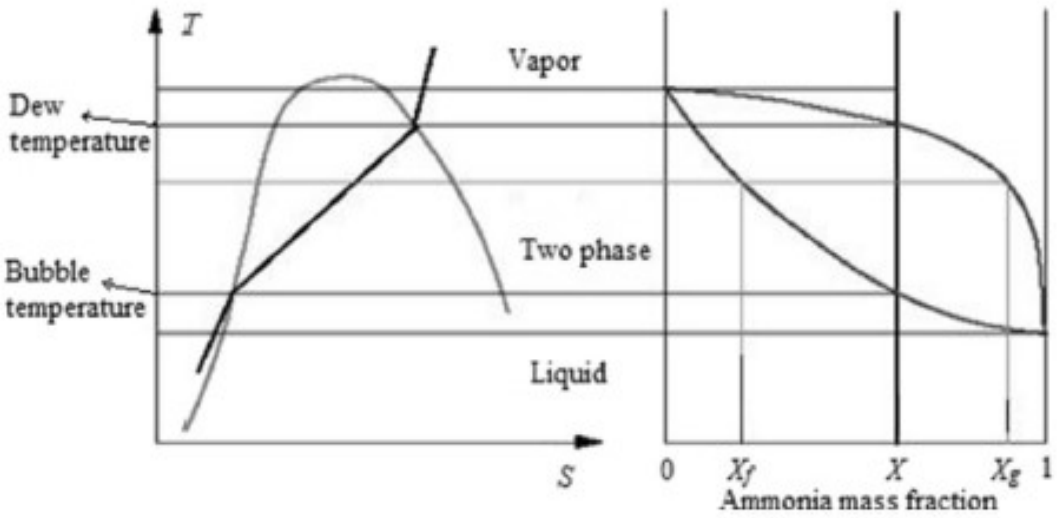

Figure (2-11) The States On T-S And T-X Diagram [48].

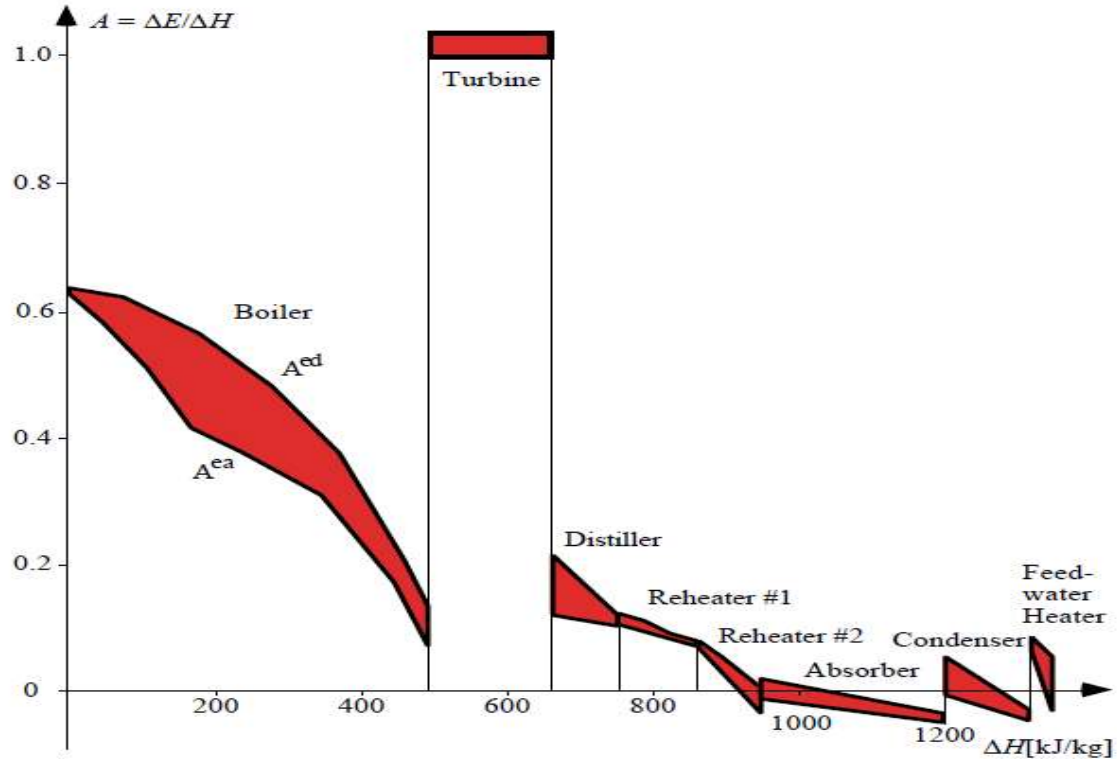

Figure (2.12) Energy-Utilization Diagram for the Kalina Cycle [48]

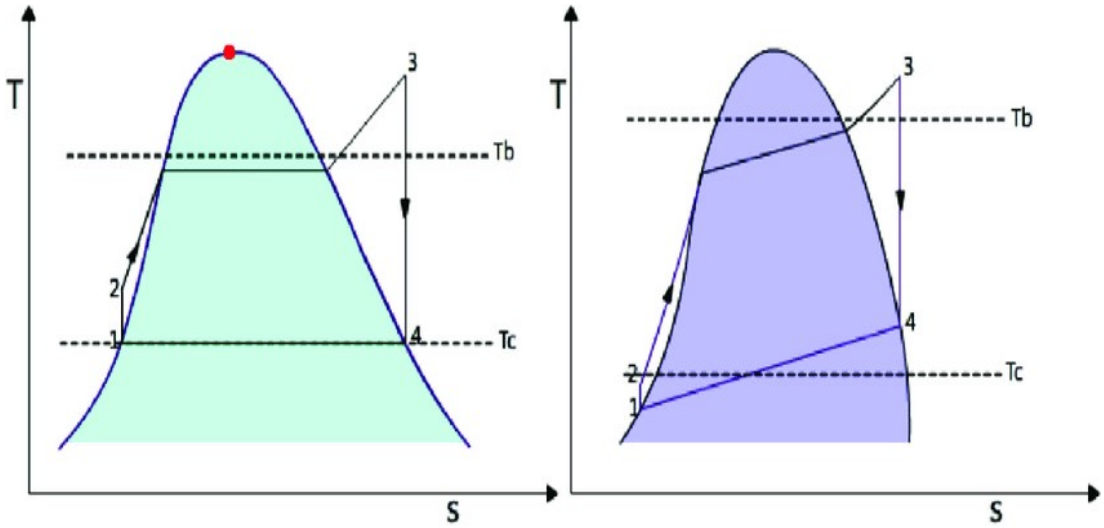

Figure (2.13) On the Left Rankine Cycle, On the Right Kalina Cycle [8]

Table (2.1) Working Fluid for the KCS 11 [42].

Proposed binary mixtures						
CO_2 mixtures	R32 mixtures		Propane mixtures		Propylene mixtures	
CO_2–DME	R32–DME		R290–R601		R1270–R601	
CO_2–R1270	R32–R600		R290–R600		R1270–R600	
CO_2–R290	R32–R600a		R290–R600a		R1270–R600a	
CO_2–R601a	R32–R601a		R290–R601a		R1270–R601a	
CO_2–R601						
CO_2–R600a						
CO_2–R600						
Refrigerant	NPB (°C)	GWP	Hfg (kJ/kg)	Flammability	Toxicity	ASHRAE safety [14]
Ammonia (R717)	−33.34	<1	1370	Yes	Yes	B2
Water (R718)	100	0	2256	No	No	A1
Carbon Dioxide (R744)	−78.46	1	232	No	No	A1
Difluoromethane (R32)	−51.65	650	382	Yes	No	A2
Propylene (R1270)	−47.62	3	438	Yes	No	A3
Propane (R290)	−42.11	3	425	Yes	No	A3
Butane (R600)	−0.49	3	386	Yes	No	A3
Iso-butane (R600a)	−11.749	3	365	Yes	No	A3
Pentane (R601)	36.06	3	357	Yes	No	A3
Iso-pentane (R601a)	27.5	3	343	Yes	No	A3
Dimethylether (DME)	−24.782	2	465	Yes	No	A3

Table (2.2) Combined Ammonia-Water Kalina Cycle from the Literature

Reference	Cycle	Type	Working fluid	Efficiency %	
				Thermal	Exergy
Zheng et al. **[47]**	Kalina	Theoretical	Ammonia-water	24.2	37.3
Amano et al. **[61]**	Kalina	Experimental	Ammonia-water	N.A.	N.A.
Amano et al. **[62]**	Kalina	Theoretical	Ammonia-water	N.A.	N.A.
Takeshita et al. **[49]**	Kalina	Experimental	Ammonia-water	26	N.A.

Table (2.3) Kalina Development Status [4]

System	Application	Development
KCS1	Bottoming cycle small plants	Design completed
KCS2	Low temperature geothermal	Design completed
KCS3	High temperature geothermal and industrial waste	Under development
KCS4	Cogeneration	Planned
KCS5	Direct-fired for coal and other solid fuels	Design completed
KCS5n	High temperature gas-cooled nuclear reactor	Design completed
KCS6	Bottoming for utility combined cycle	Design completed
KCS7	Direct fired, split cycle	Under development
KCS8	Bottoming cycle, split cycle	Under development
KCS9	Retrofit subsystem	Under development
KCS12	Low temperature geothermal	Design completed
KCS34	Cascade utilization of low-grade waste heat	Design completed
KCDCS	Biomass chip plants	Design completed
KCS-11	Bagasse-fired cogeneration plant of sugar industry	Under development

Chapter Three

Experimental Work

Chapter Three: Experimental Work

3.1 Introduction

Kalina cycle is used to recover part of the waste thermal energy which is otherwise rejected to the environment. Therefore, the aim of this research work is to recover part of the heat rejected with the combustion gases of a steam boiler available in the power plant laboratory at the Department of Mechanical Engineering-College of Engineering-University of Babylon. The boiler is fired with diesel fuel which has an assumed average chemical formula of $C_{16}H_{34}$ fuel. The mass flow rate of the combustion gases is calculated, based on the stoichiometric chemical reaction equation, and found to be 120.704kg/hr. The temperature of these gases in the chimney is measured and found to be 175℃. However, in the experimental study, the heat source (combustion gases) was replaced by an electric source supplies the same input heat as combustion gases to ensure the continuity of the cycle work regularly. The work of Kalina cycle system requires a stable and continuous source. Achieving such a complex system requires practical capabilities and a high cost that the University of Babylon lacks. Therefore, this system cannot be built inside the university campus. All these reasons led to the replacement of the external source with an electrical source. Kalina cycle is a closed cycle for electrical generation similar to the Rankine cycle. The design and fabrication of each component of Kalina cycle system is illustrated in this chapter, as shown in fig (3.1). It consists of heat recovery vapor generator (HRVG), separator, turbine, electric generator, heat exchanger (HE), throttling valve, mixer (absorber), condenser and pump as shown in fig (3.2). The construction is carried out in the local markets. The testing of the system is done in the power plant laboratory at the Department of Mechanical Engineering-College of Engineering-University of Babylon. Water and ammonia mixture is chosen as a working pair. The experimentally

constructed cycle is a modification of a simple Kalina cycle and is named as (MKCSE) as seen fig (3.3).

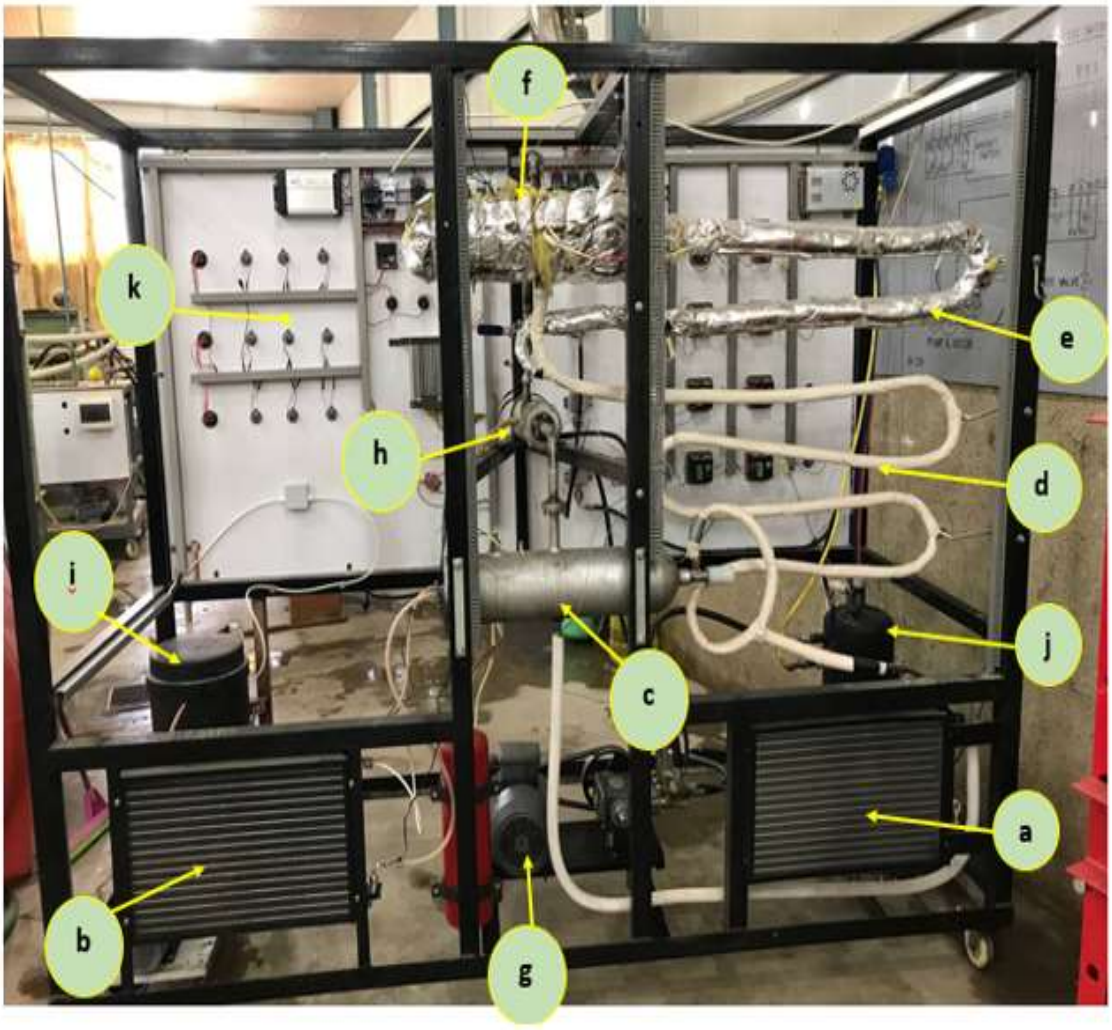

a	condenser	**g**	supply pump
b	cooling system	**h**	turbine with electrical generator
c	mixer	**i**	cooling water tank
d	heat exchanger	**j**	solution tank
e	heat recovery vapor generator	**k**	control panel
f	separator		

Figure (3- 1) Experimental Rig Component

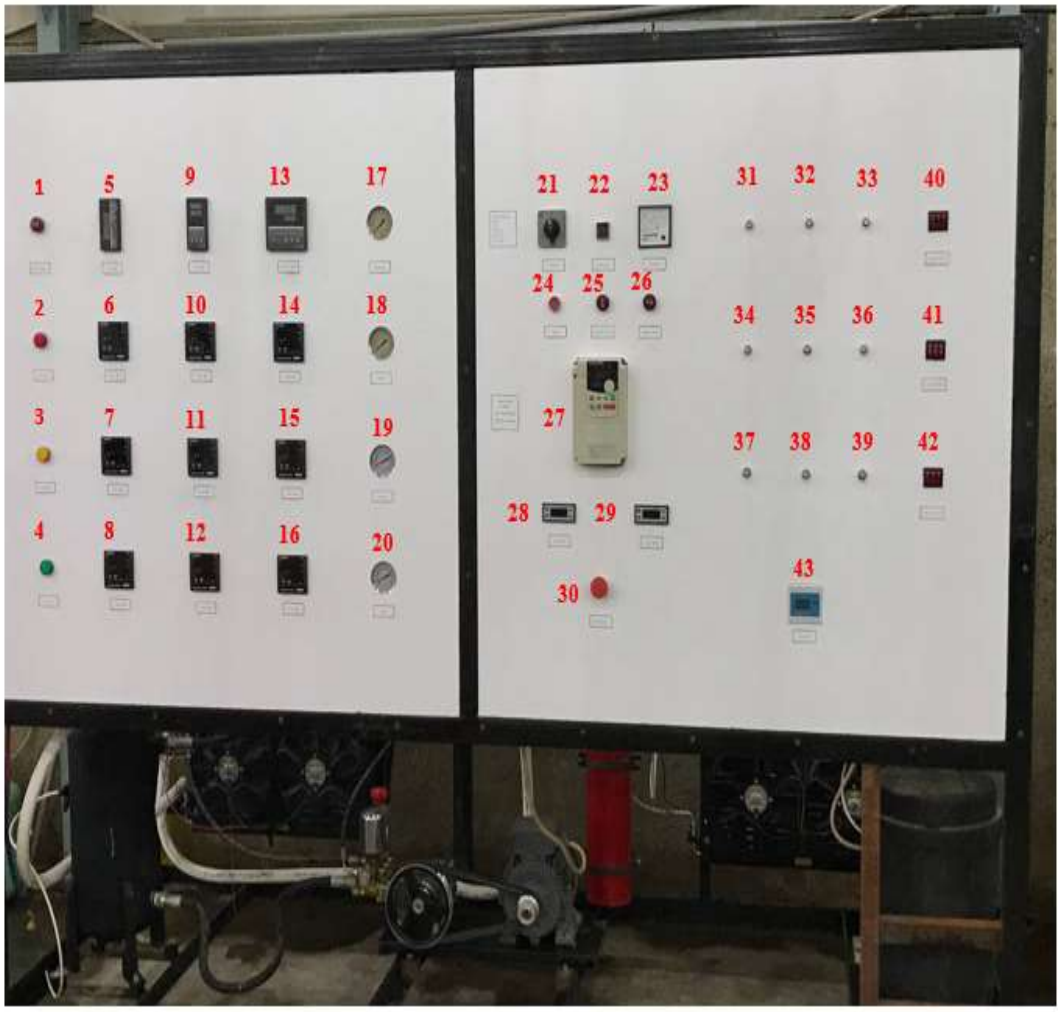

1,2,3, 4	Alarm lamp with whistle	27	The pump speed control
5,6,7,8,9,10,11, 12,13,14,15, 16	Temperature measurement for all points	28, 29	Water inlet and outlet temperature
17,18,19, 20	Pressure gauge	30	Emergency key
21	Main control switch	31,32,33,34,35,36,37 ,38, 39	Thermal resistors for controlling the load on the turbine
22	Voltmeter	40,41,42	Control switches for loads on the turbine
23	Ammeter	43	Cooling water mass flow meter inside the mixer
24,25,26	Warning lamps		

Figure (3- 2) Experimental Cycle Control Board

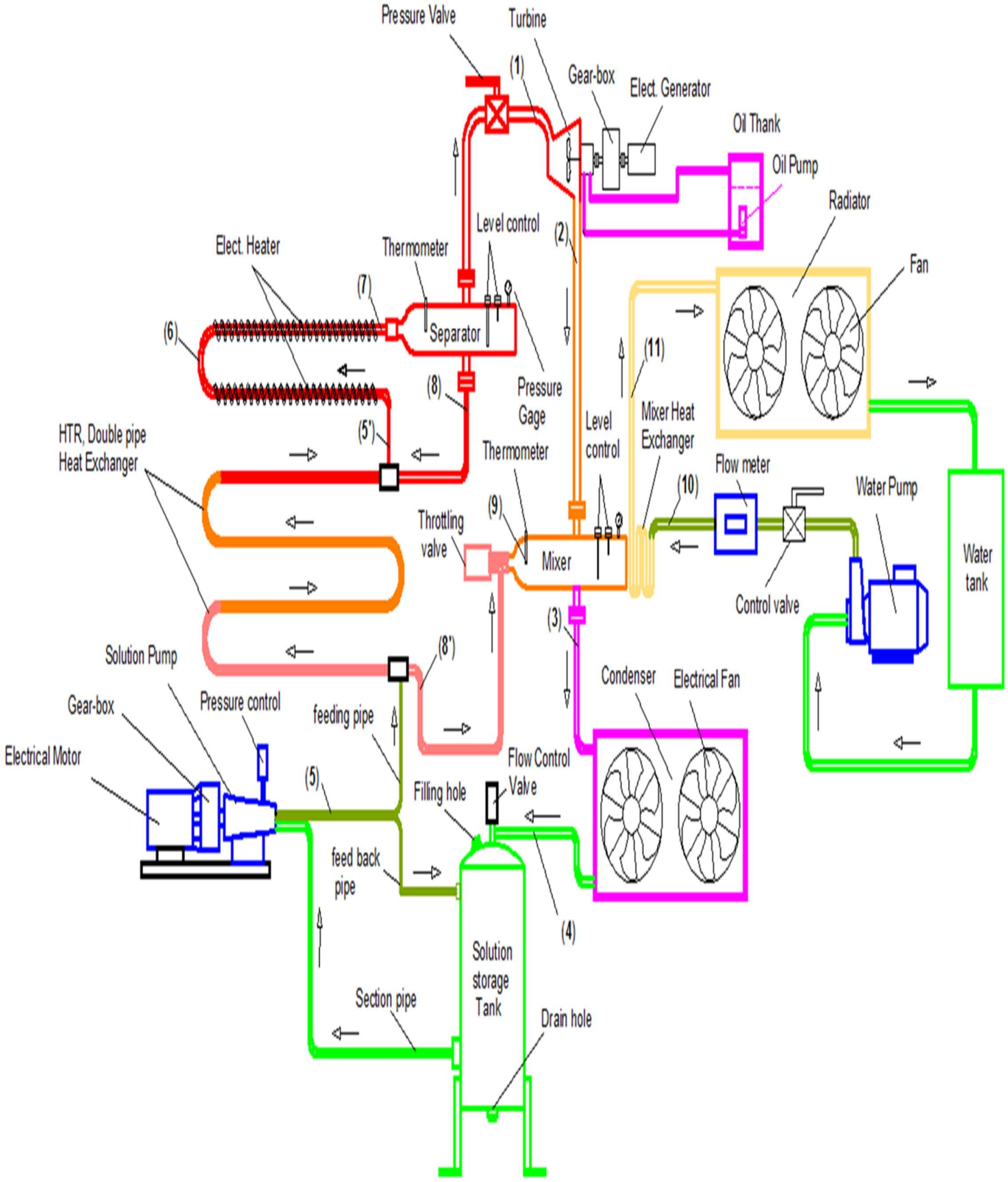

Figure (3- 3) Schematic Diagram of Modification Kalina Cycle System (MKCSE)

3.2 Description of Simple Kalina Cycle

As mentioned earlier, the simple Kalina cycle is the first version of Kalina cycles. It consists of the following components:

1-Heat recovery vapor generation (HRVG)

2-Separator

3-Turbine

4-Mixer (absorber)

5-Condenser

6-Solution Pump

7-Throttling Valve

However, in the present work this simple version is modified by adding a heat exchanger after the separator to recover part of the heat of the weak solution to heat the working fluid coming from the pump. The MKCSE water-ammonia as a working pair, where water is the absorbent and ammonia is the refrigerant. The source of heat for MKCSE heat recovery vapor generator is an electrical heater to ensure continuous operation of the cycle.

3.3 Design of Modified Kalina Cycle System (MKCSE)

The design of the MKCSE includes the following

1- Choosing the proper working pair
2- Calculating the required mass flow rate of working pair
3- Thermodynamic design of the cycle as a whole and each component which is based on mass-energy and exergy balances

The thermodynamic design which depends on the mass, energy and exergy conservation equation.

$$\sum \dot{m}_i = \sum \dot{m}_0 \tag{3.1}$$

$$\sum \dot{Q} + \sum \dot{m}_i h_i = \sum \dot{W} + \sum \dot{m}_o h_o \tag{3.2}$$

$$(\dot{E}_d)_{tot} = \sum \dot{E}_{in} - \sum \dot{E}_{out} \tag{3.3}$$

Where

$(\dot{E}_d)_{tot}$ is the total rate exergy destruction (kW).

$\dot{E}_{in}\ and\ \dot{E}_{out}$ are the rate of exergies input and output respectively (kW).

3.3.1 -Choosing the Pair of Working Fluid Type

The first step in designing Kalina cycle is to choose the proper working pair. In this research the ammonia-water pair is chosen as the working fluid. The selection of the working fluid is based on their environmental characteristics such as low boiling temperature, non-toxicity and zero ozone depletion. The main advantages of ammonia are: it can operate under low evaporating temperatures and no crystallization. Ammonia (NH_3) has better heat transfer properties than most of chemical refrigerants and therefore allow for the use of equipment with a smaller heat transfer area. Thereby plant construction cost will be lower. The ammonia has the advantage of self-alarming leakage, because of its overpowering odor. The disadvantages are corrosion and irritation. Ammonia causes the corrosion particularly with the copper, so the copper metal is excluded because of its rapid corrosion with the solution, which leads to rapid failure. Exposure to high concentrations of ammonia in air causes immediate burning of the eyes, nose, throat and respiratory tract and can result in blindness, lung damage or death. Inhalation of lower concentrations can cause coughing, and nose and throat irritation. Table (3.1) shows the properties of aqua-ammonia for many pressure from 20 bar to 40 bar with step 5 bar. It shows the temperature, specific enthalpy, specific entropy and the specific volume for the saturated liquid and saturated vapor at ammonia

mass fraction x=0.85 at turbine entrance and dryness fraction=0.3 at separator inlet. Also V_m represents the volume of the mixture at separator inlet.

Table (3.1) Properties of NH_3-H_2O

P (bar)	T_f ©	T_g ©	h_f (kJ/kg)	h_g (kJ/kg)	s_f (kJ/kgK)	s_g (kJ/kgK)	v_f*10^{-3} (m^3/kg)	v_g*10^{-3} (m^3/kg)	v_m*10^{-3} (m^3/kg)
20	55.442	135.523	164.147	1670.353	0.831	5.108	1.3549	15.0999	5.4784
25	63.941	143.385	211.264	1676.314	0.957	5.028	1.3837	12.2625	4.6474
30	72.541	149.548	251.106	1677.249	1.083	4.956	1.4115	10.0612	4.0064
35	78.542	155.297	284.607	1677.660	1.183	4.896	1.4401	08.5287	3.5663
40	85.700	160.159	320.450	1678.285	1.283	4.839	1.4667	07.4065	3.2486

3.3.2 Calculation of the Required Mass Flow Rate

The calculation of the mass flow rate should be able to generate the maximum possible power from the available waste heat. So the design of the maximum output power for the cycle depends directly on the mass flow rate. There are three mass flow rates during the cycle, the main mass flow rate, the strong solution mass flow rate and the weak solution mass flow rate. The mass flow rate depends on

- The amount of energy which is available from the thermal source.
- The size of the turbine which should suit the amount of the energy to be converted into work.
- The size of the solution pump.
- Throttle valve (weak solution throttling).

The design of the Kalina cycle depends on the existence of a throttle valve that controls the amount of discharge (weak solution) between the

separator and the mixer (absorber). It represents an important balancing parameters in the cycle. The calculation of the required mass flow rate during the cycle is started from the pump. The displacement pump has three cylinders and the diameter (d_s) and the stroke (LS) are 2.02 cm and 2.15 cm respectively. Firstly calculating the mass per one cycle at P_{max}=35 bar and x=0.47 (the ammonia mass fraction for the working fluid) as shown below:-

$$V_o = A_s * LS \tag{3.4}$$

$$A_s = \frac{\pi d_s^2}{4} \tag{3.5}$$

$$A_s = 3.20474 cm^2$$

$$V_o = \frac{\pi d_s^2}{4} * LS \tag{3.6}$$

$$V_o = 6.8902 cm^3$$

Where

V_o the volume of one cylinder

LS the stroke

d_s the diameter of the cylinder

$$V_{pump} = n * V_o \tag{3.7}$$

$V_{pump} = 20.671 cm^3$ For one cycle

$$\rho_{mix} = x * \rho_{NH3} + (1 - x) * \rho_{H2O} \tag{3.8}$$

$$\rho_{mix} = 0.47 * 686 + 0.53 * 1000 = 852.42 \frac{kg}{m^3}$$

$$m_{pump} = \rho_{mix} * V_{pump} \tag{3.9}$$

$m_{pump} = 0.01762\ kg$ *per one cycle*

For N=10 RPM

$$\dot{V}_{pump} = V_{pump} * \frac{N}{60} \quad (3.10)$$

$$\dot{V}_{pump} = 20.672 * \frac{10}{60} * 10^{-6} = 3.45 * 10^{-6} \ \frac{m^3}{s}$$

$$\dot{m}_{pump} = \rho_{mix} * \dot{V}_{pump} \quad (3.11)$$

$$\dot{m}_{pump} = 0.0029\ kg/s$$

Where

n is the number of cylinder

ρ_{mix} is the density of the mixture (kg/m^3).

m_{pump} is the mass of the working fluid for one cycle (kg).

N is the revolution of the pump

$\dot{V}_{pump}$ is the volume flow rate (m^3/s)

$\dot{m}_{pump}$ is the mass flow rate (kg/s).

Fig (3.4) shows the relationship between the mass flow rate at turbine entrance and the speed of the pump (RPM). This calculation method is used to calculate the mass of the working fluid, the total mass flow rate, the mass flow rate at turbine entrance and the speed of pump.

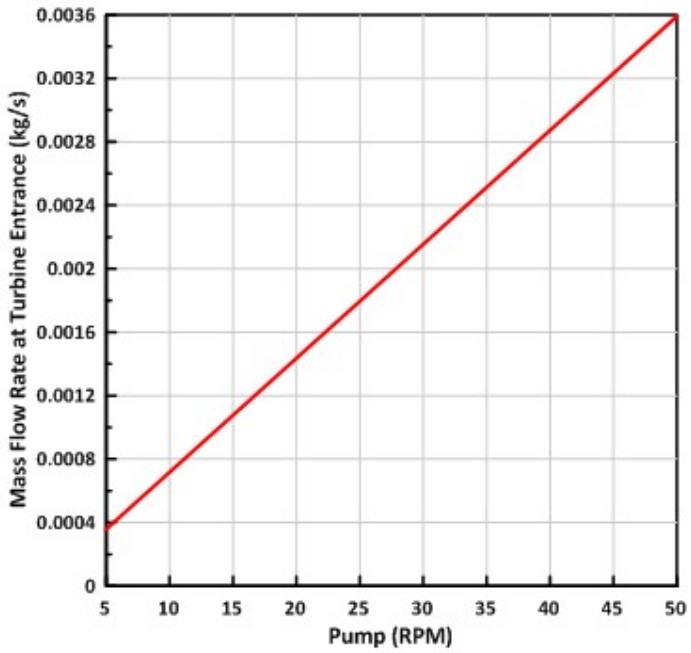

Figure (3.4) Relationship between Strong Solution and Pump Speed (RPM).

3.3.3 - Design of the Different Cycle Components

The design is based on the following general assumptions

1-Steady state operation throughout the cycle.

2-The pressures of the HRVG and condenser are constant. Also the pressure constant at the separator and the mixer (absorber).

3-Throttling process is isenthalpic.

4-The isentropic efficiencies of pump and turbine are 100% and 85% respectively.

5- The coupling efficiency between the turbine and electrical generator is 0.91.

6-Pressue losses, heat losses and friction losses in pipes are neglected.

7-The effectiveness in HRVG and condenser is unity($\epsilon = 1$).

8-All cycle components are adiabatic.

9-The absorption process in the mixer is considered as diabatic. The kinetic and potential energies changes in all components are neglected.

10-The used water and ammonia are pure substances.

11- The inlet temperature of the hot gases is 175℃ . The temperature at the entrance of the turbine equals the saturation temperature at turbine pressure.

12- The pinch point (PP) in the HRVG is 20℃. The terminal temperature difference (TTD) at evaporator part of the heat recovery vapor generator (HRVG) inlet with hot gases is taken at 15℃. Approach point (AP) in the boiler is 2℃.

13-Table (3.2) shows the quality of working fluid at each key point in the cycle presented in fig (3.3).

Table (3- 2) the Situation of the Fluid during the MKSC1

Point	**Situation**
1	Saturated vapor mixture (strong solution)
2	Wet vapor mixture (strong solution)
3	Wet vapor mixture (working fluid)
4	Saturated liquid (working fluid)
5	Sub-cool liquid (working fluid)
5̀	Warm liquid (working fluid)
6	Hot liquid (working fluid)
7	Wet vapor (working fluid)
8	Saturated liquid mixture (hot weak solution)
8̀	Saturated liquid mixture (warm weak solution)
9	Saturated liquid mixture (warm weak solution)

3.3.3.1 Heat Recovery Vapor Generator (HRVG)

The design is based on the specific assumption in addition to the general assumption mentioned in section 3.3.3, where

1- Constant wall temperature which equal 175^0C.

2- Nusselt number equals 3.66 for fully developed and laminar flow.

3- One dimensional heat transfer (along tube radius).

The HRVG is an aluminum pipe wrapped with an electrical heater. The length of the heater is 3m, the power of the heater is 2000W with voltage 220V. Mass and energy balances are bused in the design. The design of HRVG consists of two stages

A- First stage (sensible heating)

Mass balance

$$\dot{m}_{5} = \dot{m}_{6} = \dot{m}_{T} \tag{3.12}$$

Where the $\dot{m}_{5}$ is the mass flow rate at the entrance of HRVG, $\dot{m}_{6}$ is the mass flow rate at point6 and $\dot{m}_{T}$ is the total mass flow rate during the HRVG.

The energy ($\dot{Q}_{out}$)which loses from the source is equal to the energy ($\dot{Q}_{in}$) that gains by the working fluid.

$$(\dot{Q}_{out}) = (\dot{Q}_{in}) \tag{3.13}$$

$$h_a * A * (T_w - T_b) = \dot{m}_{5} * c_p * (T_6 - T_{5}) \tag{3.14}$$

Where h_a the heat is transfer coefficient and c_p is the specific heat of the fluid mixture. Cp=3251.2 J/kg K of NH_3 - H_2O mixture as pointed by **[66]**

$$Nu = \frac{h_a * D}{k_m} \tag{3.15}$$

$$h_a = \frac{Nu * k_m}{D} \tag{3.16}$$

$$A = \pi * D * L_1 \tag{3.17}$$

$$T_b = \frac{T_6 + T_{5}}{2} \tag{3.18}$$

$$L_1 = \frac{\dot{m}_T * c_p * (T_6 - T_{5})}{\pi * Nu * k_m * (T_w - T_b)} \tag{3.19}$$

Where T_b is the bulk temperature, Nu=3.66 for internal flow with constant wall temperature. k_m =0.45 kW/m K is thermal conductivity of NH_3-H_2O mixture pointed by **[66]**

B- Second stage (Boiling stage)

Same mass balance of first stage

$$\dot{m}_7 = \dot{m}_6 = \dot{m}_T \tag{3.20}$$

Energy balance

$$h_b * A * (T_w - T_b) = \dot{m}_T * DF * h_{fg} \tag{3.21}$$

$$A = \pi * D * L_2 \tag{3.22}$$

$$T_b = \frac{T_7 + T_6}{2} \tag{3.23}$$

There two equations for h_b is the boiling heat transfer coefficient, T_w is the temperature of the wall, T_{sat} is the saturation temperature.

If $(\dot{Q}_{in}/A) < 16 \quad use\ this\ equ.(3.24)$**[73]**

$$h_b = 1042 * (T_w - T_{sat})^{\frac{1}{3}} \tag{3.24}$$

$$If\ 240 > (\dot{Q}_{in}/A) > 16\ use\ equ.(3.25)$$

$$h_b = 5.56 * (T_w - T_{sat})^3 \tag{3.25}$$

$\dot{Q}_{in}/A < 16\ then\ equ.(3.24)\ is\ used\ in\ the\ design.$ Where A is the surface area of the tube.

$$L_2 = \frac{\dot{m}_T * DF * h_{fg}}{\pi * D * 1042 * (T_w - T_{sat})^{\frac{1}{3}} * (T_w - T_b)} \tag{3.26}$$

$$L_T = L_1 + L_2 \tag{3.27}$$

The tube is made from aluminum. It is designed with thickness 1 mm, length 2 m, outer diameter 16 mm, inner diameter 14 mm. With assuming the fully developed, the properties are constant. Figs (3.5) and (3.6) represent the photograph and schematic diagram of HRVG.

Figure (3- 5) the Heat Recovery Vapor Regenerator (HRVG)

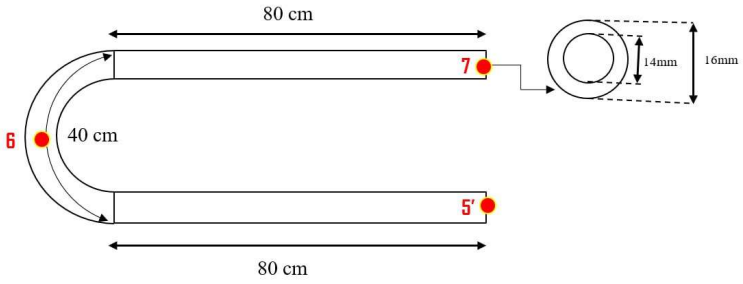

Figure (3- 6) Schematic diagram of HRVG Tube Dimensions.

3.3.3.2 Separator

The separator is a horizontal cylindrical vessel made of stainless steel and used to separate the liquid by gravity from the liquid-vapor mixture see fig (3.7). The vapor is tapped from the top of the cylinder. The state of the working fluid entering the separator is wet vapor with 0.3 dryness fraction. Fig (3.8) shows the separation process on T-x diagram (1-7-8). It is assumed that wet vapor enters the separator, saturated vapor leaves the separator and enters the turbine, and saturated liquid leaves the separator and enters the

heat exchanger. It is also assumed that the separation processes happen at constant pressure. The separator volume calculation based on the mass per one cycle which is calculated from the pump equals 0.01762kg per one cycle as following:

$$V_{sep} = v_{sep} * m_{pump} \quad (3.27)$$

$$v_{sep} = (1 - DF) * v_f + DF * v_g \quad (3.28)$$

$$v_f = x * v_{fNH3} + (1 - x) * v_{fH2O} \quad (3.29)$$

$$v_g = x v_{gNH} + (1 - x) v_{gH2O} \quad (3.30)$$

$$m_{pump} = 0.01762 kg\ per\ one\ cycle$$

From the steam tables of the water and ammonia at P_{max}=35 bar, the specific volume of water and ammonia ($v_{gH2O}, v_{gNH3,} v_{fNH3}, v_{fH2O}$) can be found. The dimensions of the separator are the length of the cylinder of 60cm, the inner diameter of 13.8cm, outer diameter of 15cm and the thickness of 0.6cm. Real size of the separator=8974.3cm^3

$$V_{sep} = 288\ cm^3 < real\ size\ of\ the\ separator$$

Where

V_{sep} is the volume of the separator

v_{gNH3} and v_{fNH3} are the specific volume of ammonia saturated vapor and ammonia saturated liquid.

v_{fH2O} and v_{gH2O} are the specific volume of saturated water liquid and specific volume of saturated vapor.

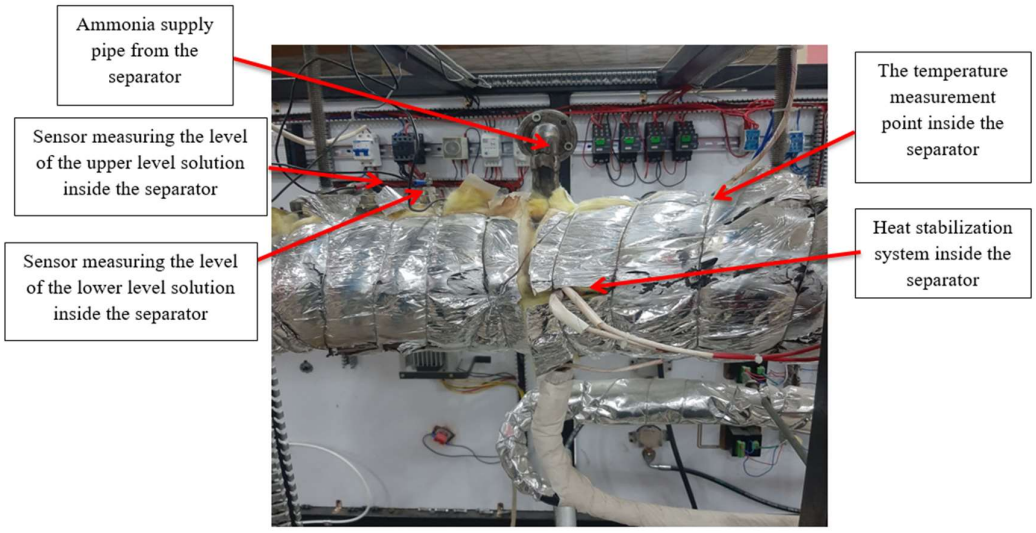

Figure (3- 7) the Separator

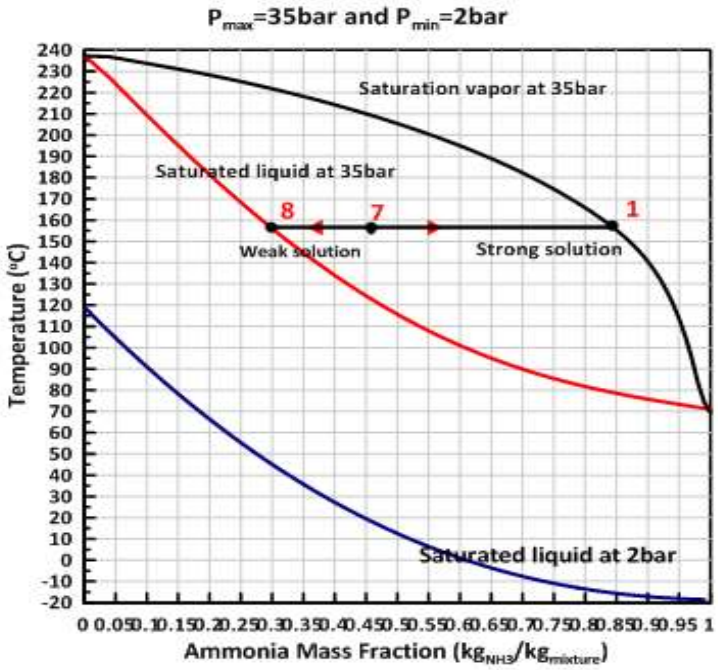

Figure (3- 8) the Separation Process on T-x diagram.

3.3.3.3 Turbine and Electrical Generator

The design point of the turbine includes each of power output, mass flow rate, and rotor speed. The turbine parts are illustrated in fig (3.9A and B). The type of turbine used is radial impulse turbine, single stage and has

12 blades. Fig (3.9C) shows all the dimensions of the turbine which is used in this work. The maximum and minimum speed are 9000RPM and 6000RPM respectively. The maximum power of this turbine is 1500W and the maximum temperature bears it around 400℃. The isentropic efficiency of the turbine is 85% and the coupling efficiency between the turbine and electrical generator is 91%. There is a nozzle connected to the turbine in order to push the strong solution that comes from the separator. The nozzle is connected with turbine by a tangent angle of 10° see fig (3.9D). The diameter of the nozzle is 2 mm and the ratted pressure is 30-40 bar and its maximum pressure is 50 bar. Also there is a gear box between the turbine and the electrical generator as shown fig (3.9B), the type of the gear box is epicycle gear box with change ratio of 1/5. The benefit of the epicycle gear box is to reduce the speed to be suitable with the electrical generator. The electrical generator as shown in fig (3.9E) produces on DC current with voltage of 12 volt. Its capacity is 1000 W and the range of the speed is 1200 RPM to 1800 RPM. Moreover the turbine is sported by lubrication system to cool it and remain it for long time. The lubrication system consists of tank, electrical oil pump and tubes. The capacity of the tank is 4liters see fig (3.9F), the electrical oil pump operates with DC current as shown in fig (3.9 G), voltage 12 volt, maximum pressure 10 bar and rated pressure is 6 bar. The discharge of the electric oil pump is 10 cm^3/s and the type of the oil is light oil SNSW20, its maximum temperature is 100 ℃ and the rated temperature is 70℃.

$$(\dot{W}_T)_{act} = \dot{m}_1(h_1 - h_{\acute{2}}) \tag{3.31}$$

$$(\dot{W}_T)_{isent} = \dot{m}_1(h_1 - h_2) \tag{3.32}$$

$$\dot{m}_1 = \dot{m}_2 \tag{3.33}$$

$$(\eta_t h)_{isent} = \frac{h_1 - h_{\acute{2}}}{h_1 - h_2} \quad (3.34)$$

$$\eta_{coup} = \frac{\dot{W}_{Elect}}{\dot{W}_{Tact}} \quad (3.35)$$

$$\dot{W}_{Elect} = \eta_{coup} * (\dot{W}_T)_{act} \quad (3.36)$$

$$\dot{W}_{Elect} = \eta_{coup} * (\eta_t)_{isent} * (\dot{W}_T)_{isent} \quad (3.37)$$

Where

$\dot{W}_{Elect}$ is the net power (kW)

$(\dot{W}_T)_{act}$ is the actual power (kW)

$(\dot{W}_T)_{isent}$is the isentropic power (kW)

η_{coup} is the coupling efficiency (%)

$(\eta_{th})_{isent}$ is the isentropic efficiency (%)

$\dot{m_1}, \dot{m_2}$ are the mass flow rate at inlet and outlet of the turbine

h_1, h_2 are the enthalpy at inlet and outlet of the turbine

$h_{\acute{2}}$ is the actual enthalpy at turbine exit

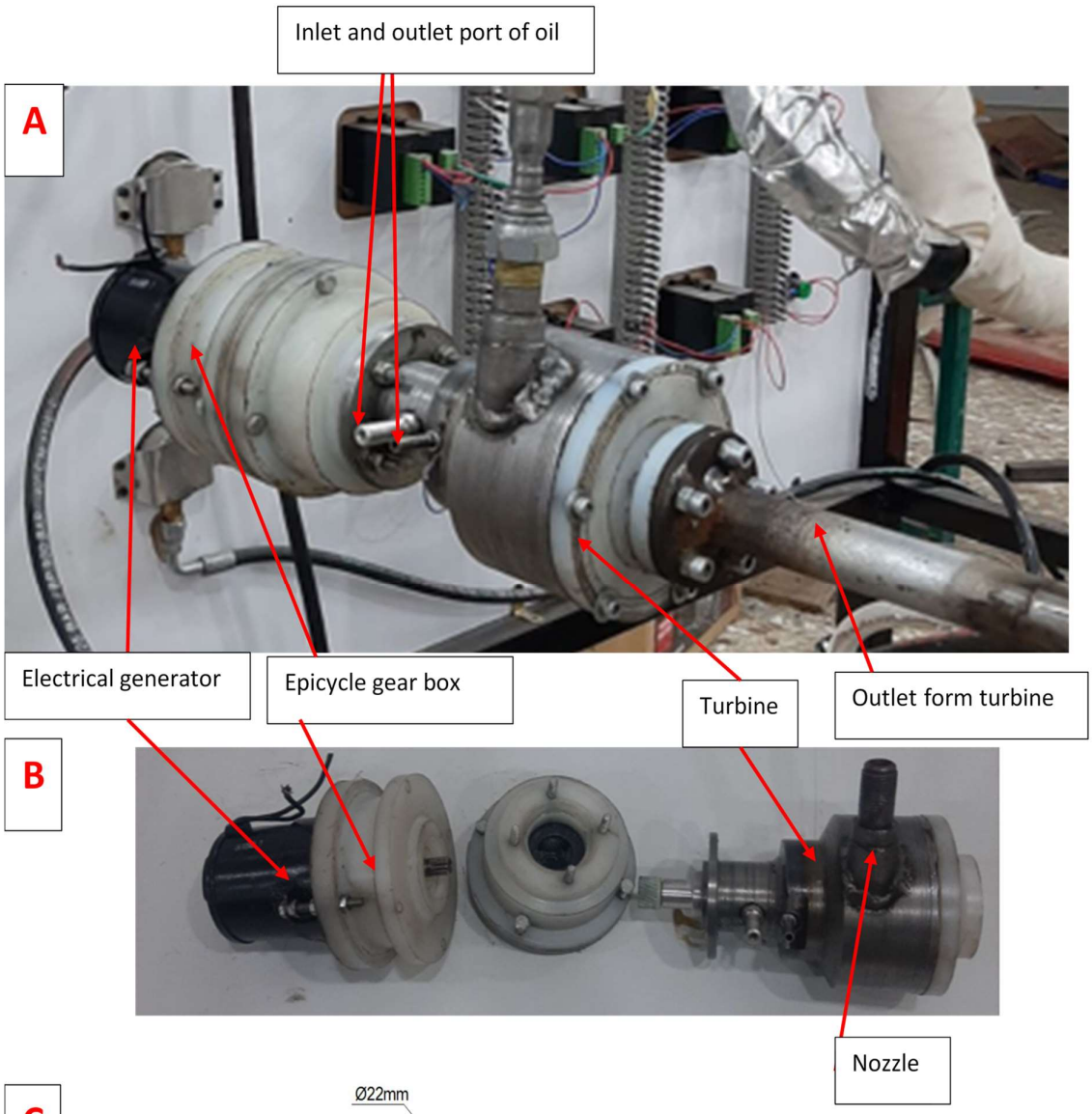
Inlet and outlet port of oil
A
Electrical generator
Epicycle gear box
Turbine
Outlet form turbine
B
Nozzle
C
Ø22mm
Ø26mm
Ø25mm
Ø96mm
Ø115mm

Figure (3- 9):(A) Turbine (B) The Connections, (C) Turbine Dimensions, (D) The Nozzle, (E) Electrical Generator, (F) Oil Pump and (G) Tank Of Oil With Oil Pump.

3.3.3.4 Heat Exchanger

The chosen configuration of the heat exchanger is the concentric double pipe as shown in fig (3.10). The hot fluid coming from the separator flows in the inner diameter while the cold fluid coming from the pump flows in the annulus. The presence of the heat exchanger reduces the required heat in the HRVG and reduces the cooling utility required in the mixer (absorber).

The assumptions are the wall temperature (T_{wall}) is the average between the temperature of inlet hot stream and the outlet temperature of cold stream.

Gather the required information:

$$T_{wall} = \frac{T_{hot\_in} + T_{cold\_out}}{2} \tag{3.39}$$

Inlet and outlet temperatures of the hot and cold fluids (T_{hot_in}, T_{hot_out}, T_{cold_in}, T_{cold_out} and T_{wall}) are known.

Fluid properties (density, specific heat and thermal conductivity) for both hot and cold fluids are also known and inner and outer pipe diameters (D_{inner} and D_{outer}) are known as well.

To find heat transfer coefficients (h_i and h_o) for Laminar Flow (Re <= 2300), Seider Tate equation is used **[75]**. These equations are applicable for laminar flow conditions in both the inner and outer pipes.

$$Re_i = \frac{4\times\dot{m}_\iota}{\pi\times D_i\times\mu_m} \tag{3.40}$$

$$Re_o = \frac{4\times\dot{m}_o}{\pi\times D_h\times\mu_m} \tag{3.41}$$

Where $D_h = 2 \times (r_o - r_i)$

For the inner pipe:

$$h_i = 0.027\ Re_{in}^{4/5}\ Pr^{\frac{1}{3}} \left(\frac{\mu}{\mu_s}\right)^{0.14} \left(\frac{k_{in}}{D_{in}}\right) \tag{3.42}$$

For the outer pipe:

$$h_o = 0.027\ Re_{out}^{4/5}\ Pr^{\frac{1}{3}} \left(\frac{\mu}{\mu_s}\right)^{0.14} \left(\frac{k_{outer}}{D_{outer}}\right) \tag{3.43}$$

Where $G = \frac{\dot{m}}{A_c}$ (area of the mass flow rate (kg/s.m^2)

Calculate the log mean temperature difference (LMTD):

$$LMTD\ =\ (\Delta T_1 -\ \Delta T_2)/ln(\ \Delta T_1/\Delta T_2) \tag{3.44}$$

For Counter-current flow

$$\Delta T_1 = T_{h,i} - T_{c,o} \quad (3.45)$$

$$\Delta T_2 = T_{h,o} - T_{c,i} \quad (3.46)$$

Calculate the overall heat transfer coefficient (U):

$$1/U = D_o/h_i.D_i + D_o.\ln(D_o/D_i)/2k_t + 1/h_o \quad (3.47)$$

$$\dot{Q} = \dot{m}_h \, cp_h\left(T_{h,i} - T_{h,o}\right) \quad (3.48)$$

Determine the required heat transfer area (A) based on the desired heat transfer rate ($\dot{Q}$) and the overall heat transfer coefficient:

$$\dot{Q} = U * A * LMTD \quad (3.49)$$

$$A = \frac{\dot{Q}}{U * LMTD} \quad (3.50)$$

$$A = \pi * D_o * L \quad (3.51)$$

Calculate the length of the double-pipe heat exchanger:

$$L = \frac{\dot{Q}}{\pi * D_{o*} U * LMTD} \quad (3.52)$$

Viscosity is calculated for both streams at wall temperature (Tw).

Where

Ac: Cross sectional area (m^2)

A: Surface area (m^2)

U: Overall heat transfer coefficient ($W/m^2.K$)

LMTD: Logarithmic mean temperature difference

$\dot{m}_h$: Mass flow rate of hot stream (kg/s)

cp_h : Specific heat of hot stream (kJ/kg K)

$T_{h,i}$, $T_{h,o}$: Inlet and outlet temperature of hot stream (^0K)

D_i : Inside pipe inner diameter (mm)

D_o : Inside pipe outer diameter (mm)

L : Length of double pipe exchanger(m)

k_t: Thermal conductivity of the tube material (W/mK)

μ_w : Viscosity of fluid at T_{wall} (Pa.s).

h_i : Convection heat transfer coefficient for inner pipe (W/m^2K)

h_o : Convection heat transfer coefficient for annular pipe(W/m^2K)

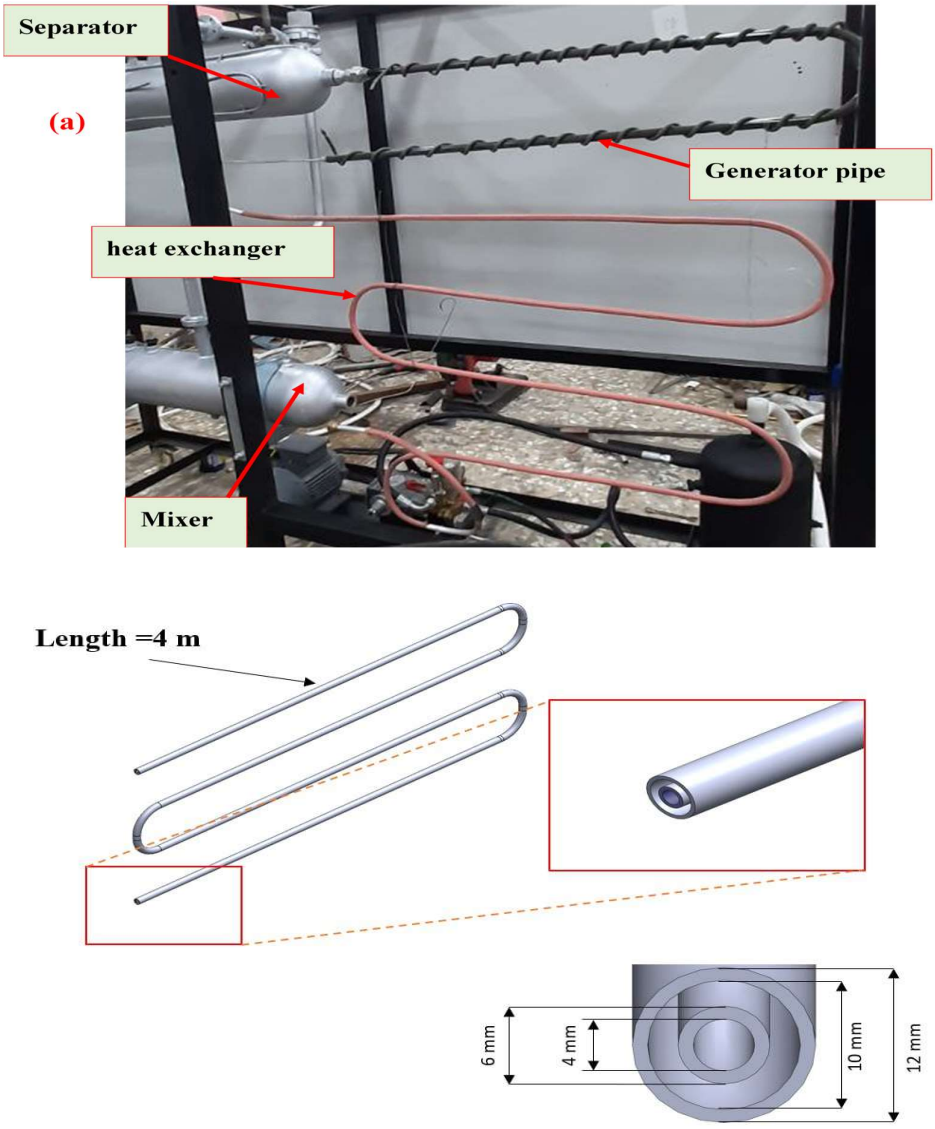

Figure (3- 10) Heat Exchanger

3.3.3.5 Throttling Valve

The throttling valve is located between the heat exchanger and the mixer (absorber) to reduce the pressure of the hot liquid from P_{max} to P_{min}. The throttling process is assumed to be at a constant enthalpy and adiabatic. The throttling valve that is used in this work consists of a body and a needle (tapered needle). The slop (angle) of the needle is 4˚to help slowly change in the mass flow rate. The throttling valve parts are illustrated in fig (3.11).The orifice method is used in this work to measure the mass flow rate due to its low friction losses and high change pressure (ΔP). The calculation is carried out under the following assumptions:

Assumptions

1. Incompressible flow (weak solution is liquid).
2. The flow is subsonic.
3. All the properties are constant such as c_p, μ, ρ

To apply the Bernoulli equation across the orifice fig (3.12) to measure the pressure drop (ΔP) **[70]**

$$\Delta P = \frac{\rho}{2} * (V_2^2 - V_1^2) \tag{3.53}$$

By continuity equation:

$$\dot{Q}_{tho} = A_1 * V_1 = A_2 * V_2 \tag{3.54}$$

$$V_1 = \frac{\dot{Q}_{tho}}{A_1}, V_2 = \frac{\dot{Q}_{tho}}{A_2} \tag{3.55}$$

$$\dot{Q}_{tho} = \sqrt{\frac{2(P_1 - P_2)}{\rho_{mix}} * \frac{A_2}{\sqrt{1 - \left[\frac{A_2}{A_1}\right]^2}}} \tag{3.56}$$

$$\rho_{mix} = x * \rho_{NH3} + (1 - x) * \rho_{H2O} \tag{3.57}$$

x=0.3,$\rho_{NH3} = 680 kg/m^3$, $\rho_{H2O} = 1000 kg/m^3$

The equation (3.56) will be

$$\dot{Q}_{act} = C_d * \sqrt{\frac{2(P_1 - P_2)}{\rho_{mix}} * \frac{A_2}{\sqrt{1-\left[\frac{A_2}{A_1}\right]^2}}} \quad (3.58)$$

$$A_2 = \frac{\pi d_2^2}{4} - \frac{\pi * (2R)^2}{4} \quad (3.59)$$

The discharge coefficient (C_d) is a dimensionless number used to characterize the flow and pressure losses behavior of the orifices in fluid systems.

Where:

C_d is a discharge coefficient (0.65) **[70]**.

A_1 is cross section area before the orifice.

A_2 is cross section area of orifice.

$\dot{Q}_{tho}$ is the theoretical volume flow rate (m^3/s).

$\dot{Q}_{act}$ is the actual volume flow rate (m^3/s).

R is the radius (mm).

Fig (3.13) shows the relationship between the pitch of the throttling valve and the volume flow rate or the mass flow rate at P_{max}=35 bar, P_{min}=2 bar and ammonia mass fraction=0.85. The pitch equals 1.26 mm for one turn of the screw (2π)

Figure (3- 11) Throttling Valve

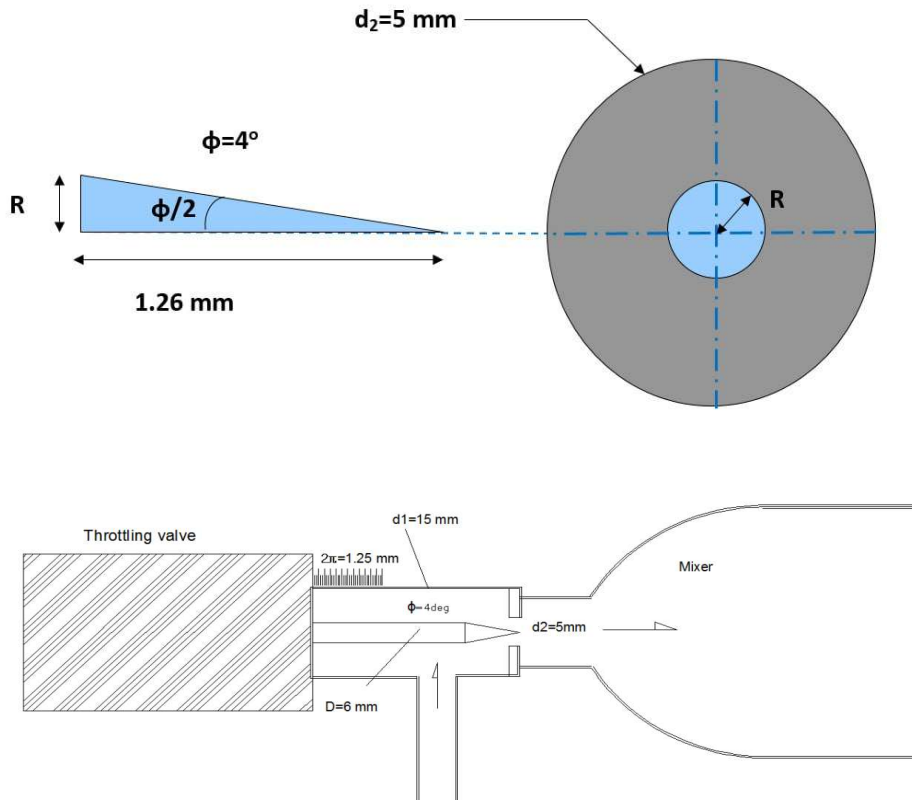

Figure (3- 12) Schematic of Obstruction Orifice Meter

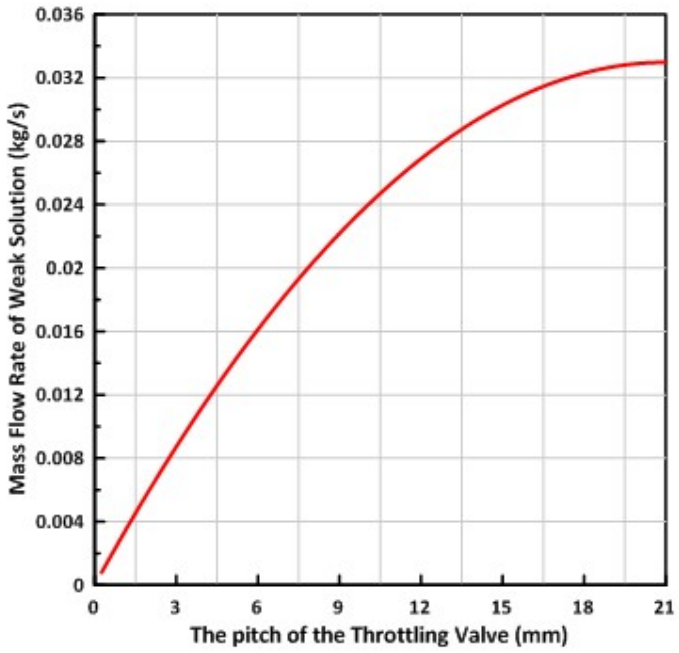

Figure (3- 13) the Relationship between the Mass Flow Rate of weak solution and the Pitch of the Throttling Valve at P_{max}=35 bar and P_{min}=2 bar.

3.3.3.6 Mixer (Absorber) Design

The design of the absorber is the same as that of the separator but at low pressure. The absorber design depends on whether the process is adiabatic or diabetic. There are two important parameters that effect the mixer efficiency which are the temperature of the mixer and the ammonia mass fraction in the weak solution. The mixer is a horizontal cylinder shaped vessel that mixes the weak solution (saturated liquid) coming from the separator with the strong solution (wet vapor) coming from the turbine. It is made of stainless steel as shown in fig (3.14). The mixing process is shown in fig (3.15) on the T-x diagram. The strong solution comes from the turbine (state2) is mixed with weak solution coming from the separator (state 9). The mixture is represented by state 3 which is wet vapor.

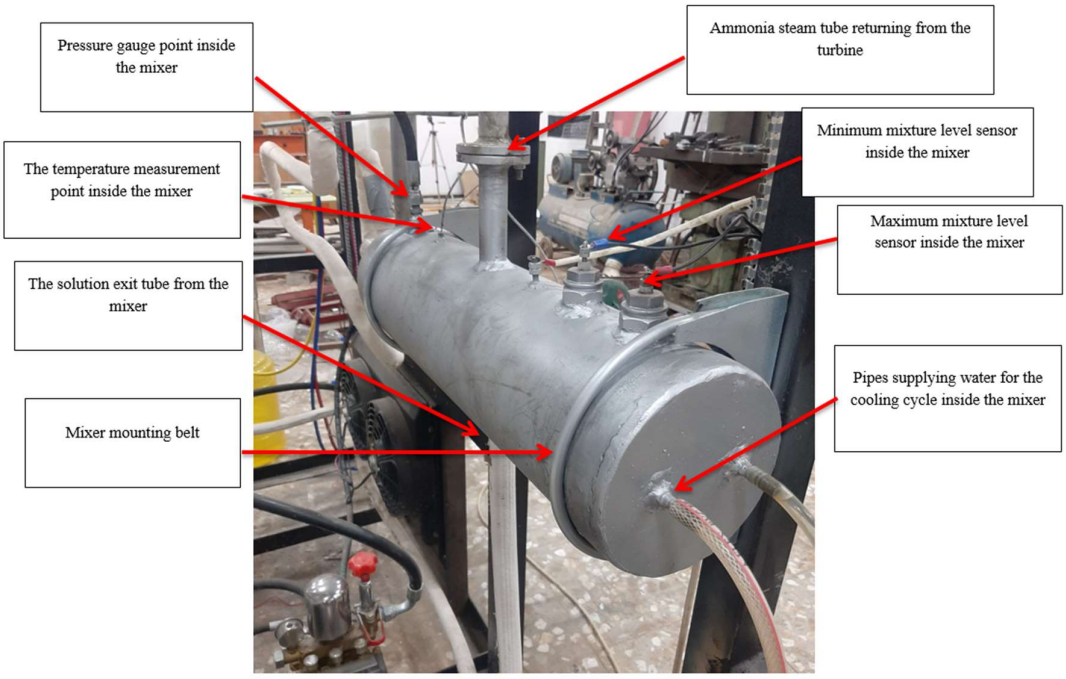

Figure (3- 14) the Mixer (Separator)

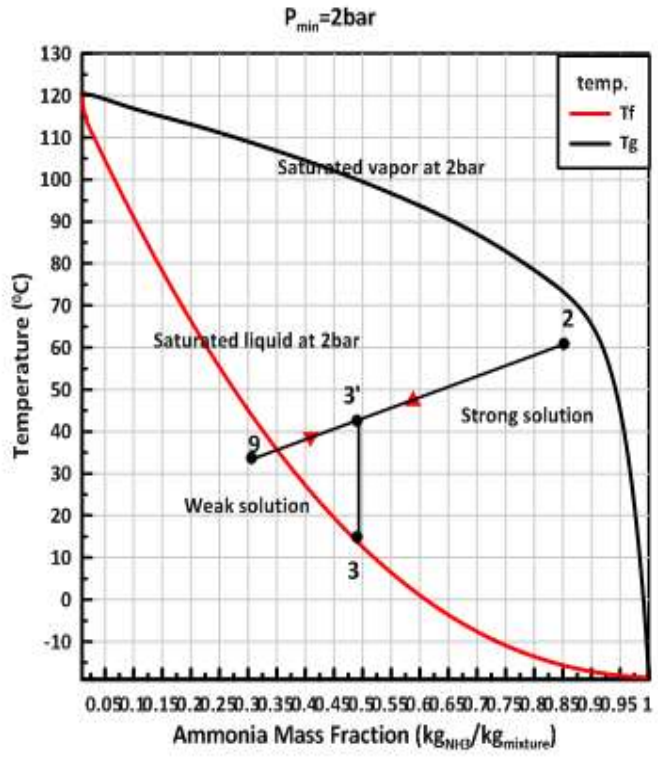

Figure (3- 15) Diabetic Mixing In Absorber to Result A Saturated Liquid Solution

The mixer (absorber) volume calculation based on the mass per one cycle which is calculated see section 3.3.2 as 0.01762kg per one cycle as following:

$$V_{mix} = v_{mix} * m_{pump} \quad (3.60)$$

$$v_{mix} = (1 - DF_3) * v_f + DF_3 * v_g \quad (3.61)$$

$$v_f = x v_{fNH3} + (1 - x) v_{fH2O} \quad (3.62)$$

$$v_g = x v_{gNH3} + (1 - x) v_{gH2O} \quad (3.63)$$

$$m_{pump} = 0.01762kg\ per\ one\ cycle$$

From the steam tables of the water and ammonia at P_{min}=2 bar, the specific volume of water and ammonia ($v_{gH2O}, v_{gNH3,} v_{fNH3}, v_{fH2O}$) can be found.

The dimensions of the mixer are length is 60 cm, inner diameter is 13.8 cm, outer diameter is 15 cm and the thickness is 0.6 cm. Therefore, the real size of the mixer=$8.97*10^3$ cm^3

$$V_{mix} = 3.77 * 10^3\ cm^3 < real\ size\ of\ the\ mixer$$

Where

V_{mix} is the volume of the mixer (absorber)

v_{gNH3} and v_{fNH3} are the specific volume of ammonia saturated vapor and ammonia saturated liquid.

v_{fH2O} and v_{fH2O} are the specific volume of saturated water liquid and specific volume of saturated vapor.

DF_3 is the dryness fraction at mixer exit

3.3.3.7 Condenser

Serpentine Condenser Heat Exchangers are a very simple and given reliable cooling or heating option for smaller spaces with basic climate control needs. Therefore, it is used in the present work as shown in fig (3.16). Serpentine air cooled condenser is designed to allow working fluid with high inside pressure about 42 bar. Volumetric flow rate of air ($\dot{V}$air=0.2 m^3/s) is known. Also the specific heat of air is known Cp_{air}=1.005 kJ/kg K. The density of the air is 1.16kg/m^3. The quality of the working fluid at the condenser inlet is wet vapor (point 3) and at the condenser outlet is saturated liquid. The dimensions of the condenser are indicated on the fig (3.16) as well as the length of the fin is 40m and its width is 0.043 m. The surface area to volume ratio of the condenser is 3285m^2/m^3. Table (3.3) shows all the results regarding the condenser. The design process depicted in **appendix (A)**.

Table (3- 3) Condenser Heat Exchanger Design Results.

Parameter	**Results**
surface area to volume ratio	3285 (m^2/m^3)
A_C (contact area)	6.711 (m^2)
A_{fin} /A_C	0.95
fin thickness	0.0004064 (m)
heat exchanger height	0.3556 (m)
heat exchanger depth	0.06096 (m)
single tube length	0.5588 (m)
working fluid mass flow rate	0.00288 (kg/s)
tube thickness	0.001651 (m)
inlet air temperature	291.2 (K)
outlet air temperature	296.4 (K)
inlet working fluid temperature (T_3)	317.4 (K)
outlet working fluid temperature (T_4)	291.2 (K)

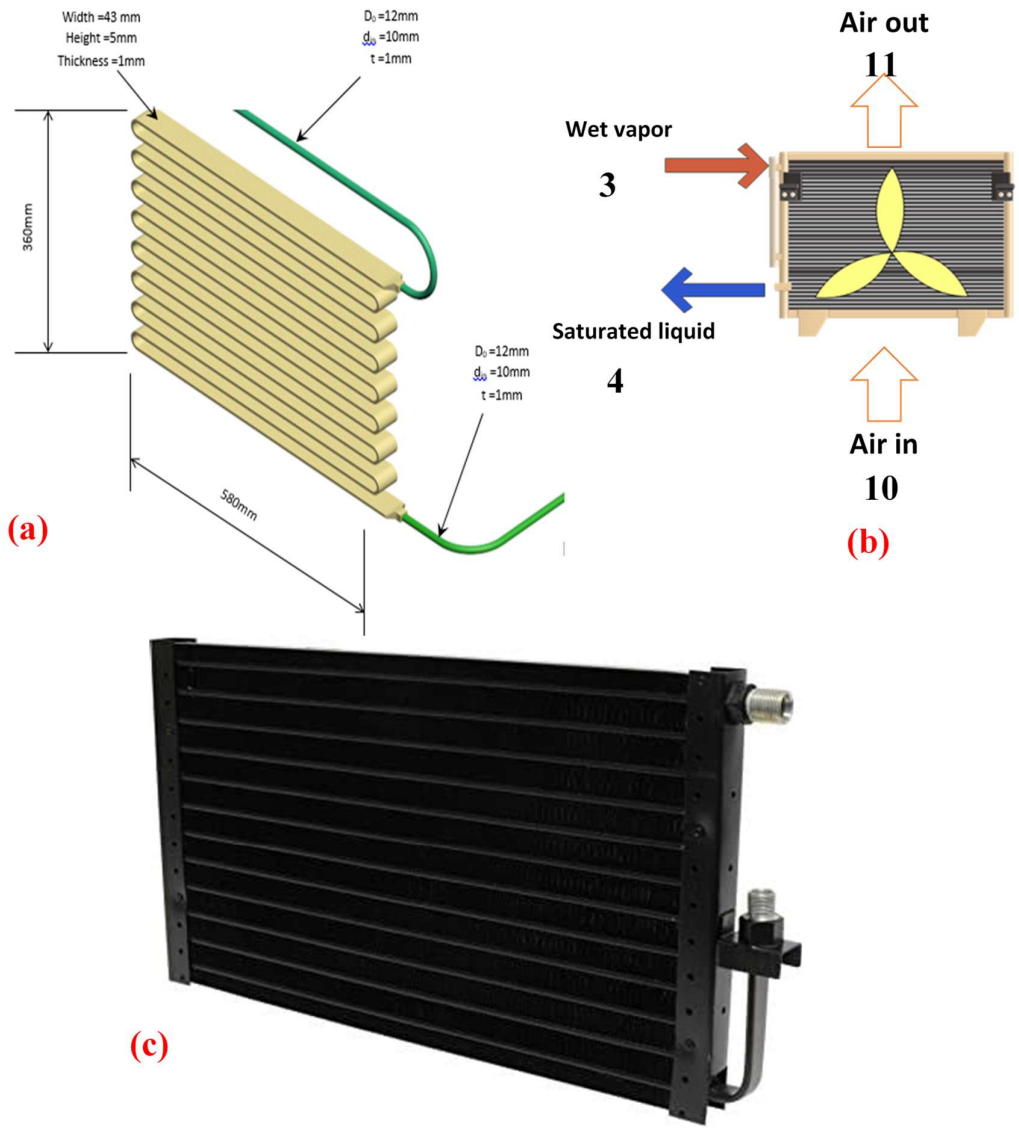

Figure (3-16) Condenser Heat Exchanger

3.3.3.8 Pump

In this work the pump unit consists of four parts the motor, the motor drive control (inverter), the solution pump and the motor/pump speed ratio as shown in fig (3.17). Displacement pump is used in this work which consists of three cylinders. Each cylinder has stroke of 2.15cm and a diameter of 2.02cm. The speed of pump in revolution per minute is around (5rpm-200rpm). The volume flow rate and mass flow rate across the pump depends on the pump RPM. It is found that the mass per one cycle and the

mass flow rate across the pump are as mentioned previously in section 3.3.2. Fig (3.18) shows the relationship between RPM, total mass flow rate and the frequency.

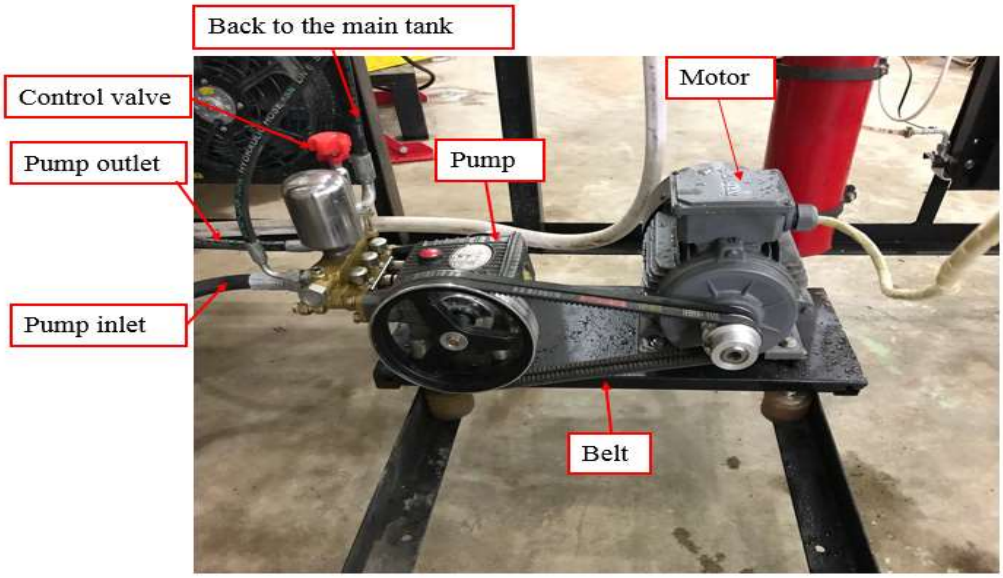

Figure (3-17) the Pump Unit

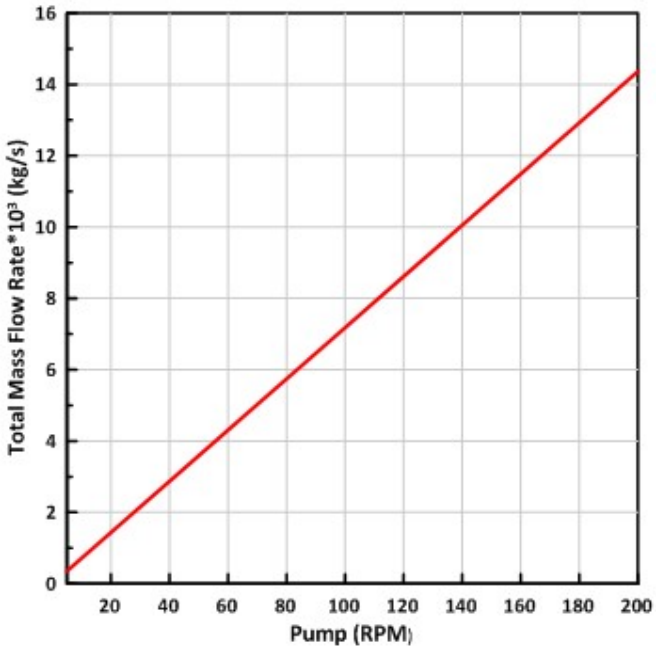

Figure (3-18) Relationship between RPM and Total Mass Flow Rate

3.4 Mixer Cooling Unit

The cooling cycle parts are illustrated in fig (3.19). This cycle is very important to remove the heat from the mixer to increase water absorptivity to ammonia. The quality of the working fluid is wet vapor with low dryness fraction at mixer exit. This cycle is very active and useful for low pressure in the mixer but with the pressure more than 3 bar it is not useful because of the high temperature helps to rise the required pressure. It consists of

- Water tank made of stainless steel with capacity of 50litter.
- The condenser in this cycle is exactly same the main condenser with a discharge of 0.2 L/s. The dimensions of the condenser are 58.5 cm (width), 36.5 cm (height) and 5 cm (thickness) see fig (3-20).
- A digital flow meter is type 8000T with discharge (volume flow meter) of 30 L/min as shown in fig (3-21).
- Center fugal water pump with a power of ½ HP (0.37 kW), a discharge of 35 L/min, the speed 2850 rpm, voltage 220 volt and head 35m as shown fig (3.22) are used to circulate water.
- Control valve helps to control the amount of water.
- Heat exchanger located inside the mixer made of aluminum. The dimension of this heat exchanger are inner diameter of 5 mm, outer diameter of 6.5 mm, thickness of 0.75 mm, the number of turns are 3, the length 3 m and the mass flow rate of water 0.0212 kg/s as shown fig (3.23).

3.4.1 Heat Exchanger of Mixture

A steady-state mathematical model has been developed using the computer software MATLAB based on momentum, heat and energy balances. Heat transfer from the bulk liquid to the cooling water can be calculated using Eq. 3.64 as pointed by **Shi et al [67]**

$$Q = \frac{T_l - T_{win}}{\frac{1}{\alpha_s \pi d_{to}} + \frac{\ln(d_{to}/d_{ti})}{2\pi k_t} + \frac{1}{\alpha_t \pi d_{ti}}} \quad (3.64)$$

Where Q is the heat that must reject per meter (kJ/m), T_l is bulk NH_3H_2O liquid mixture, d_{to} is tube outlet diameter, d_{ti} is tube internal diameter, k_t is tube thermal conductivity, and T_{win} is water inlet temperature. Heat transfer coefficient in tube side (α_t) can be found by using the analytical solutions for the heat transfer of single phase flow in tubes: considering a constant wall temperature (Nu = 3.66) as pointed by **Miyatabe [68]** in the following equation:

$$\alpha_t = \frac{Nu_t * k_w}{d_{ti}} \quad (3.65)$$

Heat transfer coefficient in shell side (α_s)calculated based on **Nefs [69]** empirical equations:

$$\alpha_s = \frac{k_w}{d_H}\sqrt{0.008495^2 + 0.4775^2\left(\dot{m}_s.\frac{c_{p,w}}{k_w.L}\right)^{2/3}} \quad (3.66)$$

Where d_H is the hydraulic diameter (equal to tube diameter d_{to}), k_w is water thermal conductivity, L is tube length, $\dot{m}_s$is mass flow rate in shell side in kg/hr.

Therefore, the mass flow required to cool the mixture of ammonia and water can be calculated by using the energy balance as explained by **Shi et al [67]:**

$$\dot{m}_{w,in} = \dot{m}_{w,out} = \dot{m}_w \quad (3.67)$$

$$\dot{m}_{w,in} * \left(cp_w * T_{w,in}\right) + Q * L = \dot{m}_{wout} * (cp_w * T_{wout}) \quad (3.68)$$

$$\dot{m}_w * cp_w * \left(T_{wout} - T_{w,in}\right) = Q * L \quad (3.69)$$

$$L = \frac{\dot{m}_w * cp_w * (T_{w,out} - T_{w,in})}{Q} \quad (3.70)$$

By using the above equations, the heat exchanger can be designed and the tube length as well as the mass flow of the cooling water can be determined. As shown in Table (3.4) design conditions and material properties.

Table (3-4) Input Parameter to the Code

cooling water thermal conductivity (W/m.K)	0.6
tube inner diameter (m)	0.005
tube outer diameter (m)	0.0065
cooling water inlet temperature (°C)	20
bulk temperature of NH_3H_2O liquid mixture (°C)	44.3
shell side mass flow rate (kg/hr)	10.4
specific heat of cooling water (J/kg.K)	4186

Table (3- 5) Design Results For Cooling Cycle

Cooling water mass flow rate (kg/s)	**Equivalent tube length (m)**
bulk temperature of NH_3H_2O =44.3 °C	
0.01	1.412
0.02	2.824
0.0212	3
0.03	4.236
0.04	5.648
0.05	7.06
0.06	8.472
0.07	9.883
0.08	11.3
0.09	12.71
0.1	14.12

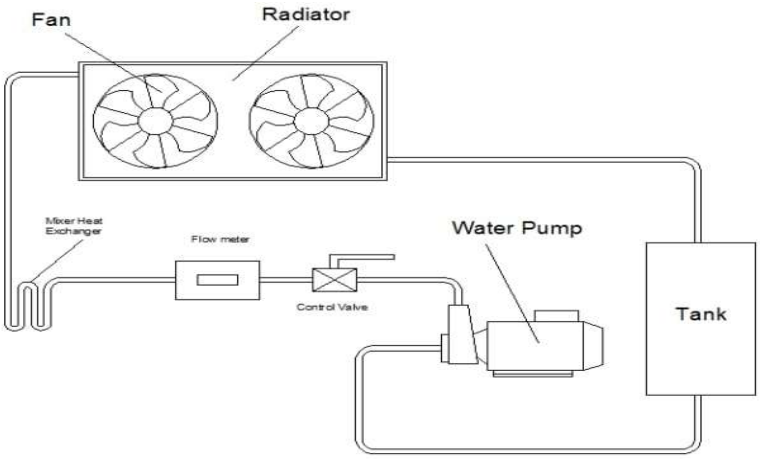

Figure (3-19) ***Schematic Diagram of the Cooling Cycle***

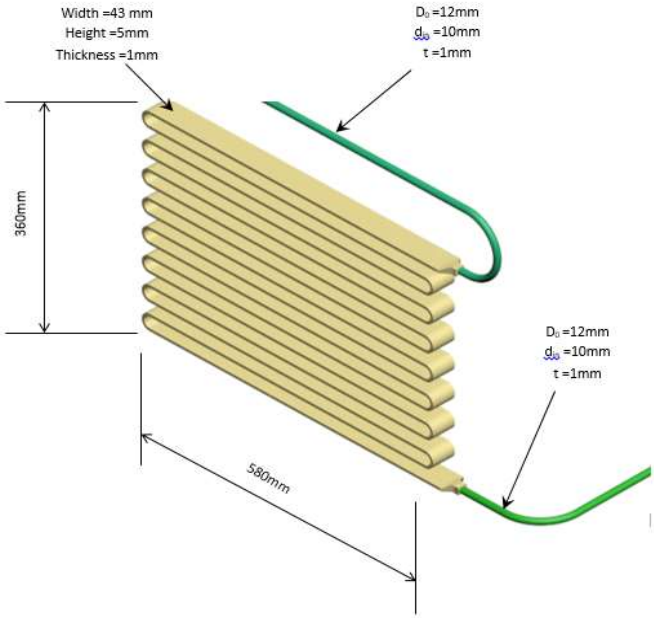

Figure (3- 20) the Condenser

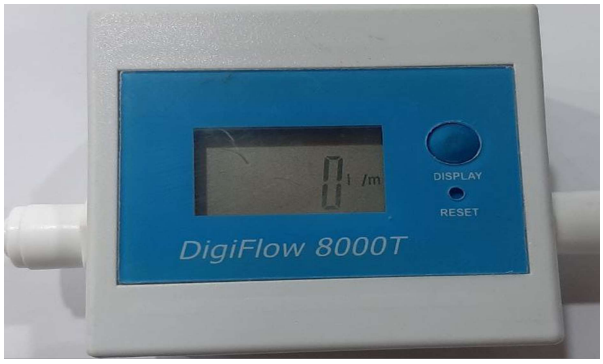

Figure (3- 21) ***Digital Flow Meter Type 8000T***

Figure (3-22) ***pump***

Figure (3- 23) ***Heat Exchanger***

3.5 Calculation of the Required Total Mass (kg)

To calculate the required mass, the size of the pipes, of the mixer, of the separator and of condenser should be found. The capacity of the main tank is 30 litter as shown in fig (3-24). The calculation of mass of working fluid is depicted in **appendix (B)**.

The size of the separator=$\pi * r_{sep}^2 * l_{sep}$ (3.71)

The size of the mixer=$\pi * r_{mix}^2 * l_{mix}$ (3.72)

The size of the condenser=$a_c * b_c * l_c * n_c$ (3.73)

There are many pipes have different lengths and different diameters

The size of pipes which connected the heat exchanger to mixer to the tank =$\pi * r_p^2 * l_p$ (3.74)

The size of the HRVG=$\pi * r_{SG}^2 * l_{SG}$ (3.75)

Other plastic pipes= $\pi * r_1^2 * l_1 + \pi * r_2^2 * l_2$ (3.76)

In this calculation the half size of the mixer and the half size of the separator are taken into account.

Where

r_{sep} radius of the separator

r_{mix} radius of the mixer

l_{sep} length of the separator (cm)

l_{mi} length of the mixer (cm)

a_c, b_c, l_c and n_c are the width, height of the cross section of tube of the condenser, length and number of turns of the condenser tube.

r_p and l_p are the radius and the length of the pipes which connected the heat exchanger and mixer.

r_{SG} and l_{SG} are the radius and length of the steam generator.

r_1, l_1, r_2 and l_2 the radius and the length of the two plastic pipes.

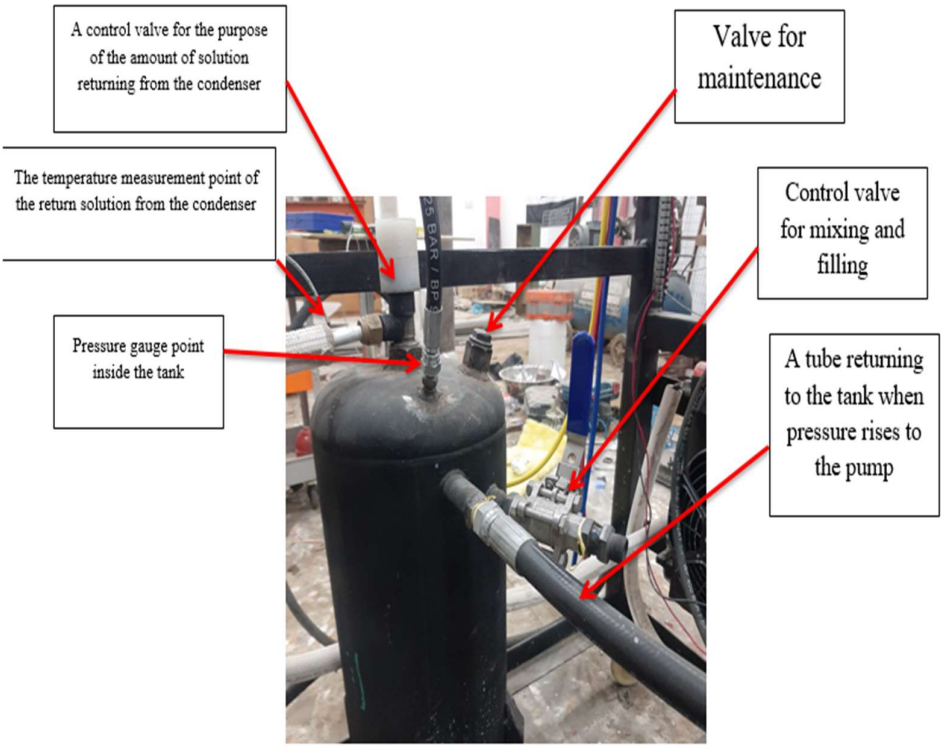

Figure (3- 24) Main Tank

3.6 The Pressure Valves

There are two pressure valves. The first pressure valve is very important to control and keep the maximum pressure of the separator and control the mass flow rate at turbine inlet. It is located between the separator and the turbine. The output power depends on the mass flow rate through the turbine and must be controlled by a valve. The second valve is located between the main tank and the ammonia storage of working fluid to control the ammonia amount in the main tank during the charging see fig (3.25).

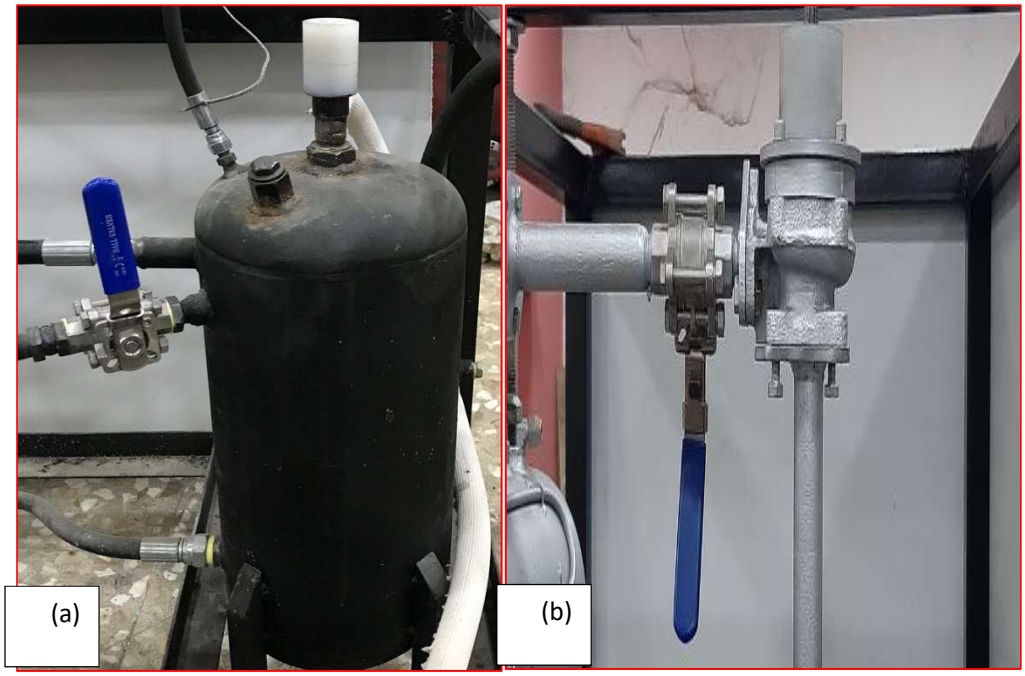

Figure (3- 25) Pressure Valves, (A) Pressure Valve before the Storage Tank, (B) Pressure Valve before the Turbine.

3.7 Measurements Device

3.7.1 Temperature Measurement

The calibration of the K-type thermocouple shown in fig (3.26) was done in Central Organization for Standardization and Quality Control (COSQC), Metrology Department-Physics Section. The calibration of the thermocouple is illustrated in fig (3.27) which shows an error value equal or less than (0.6℃).

Error=0.6 (℃)

$$\text{Percent Error} = \frac{|\text{measured} - \text{real}|}{\text{real}} * 100\% \qquad (3.77)$$

Percent Error=0.0075%.

Uncertainty=∓1℃

Figure (3- 26) Thermocouple, (a) Digital Panel, (b) Thermocouple Type and Connections.

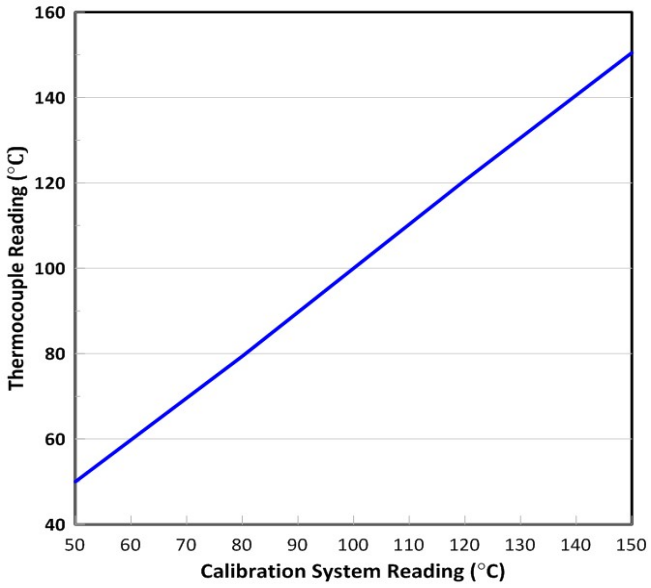

Figure (3- 27) Calibration of the Thermocouple

3.7.2 Pressure Measurement

The type of pressure gauge used is Bourdon Tube as shown fig (3.28). The range of the Bourdon gauge is between (0-60 bar). The calibration of the pressure gauge is done in Central Organization for Standardization and Quality Control (COSQC), Metrology Department/Mass & Pressure Section/Pressure Lab. The calibration of the pressure gauge is illustrated in fig (3.29). The figure shows that the error value is equal or less than (0.8 bar).

Error=0.7 bar

$$\text{Percent Error} = \frac{|\text{measured} - \text{real}|}{\text{real}} * 100\% \quad (3.78)$$

Percent Error=0.02%.

Uncertainty=∓0.15 bar

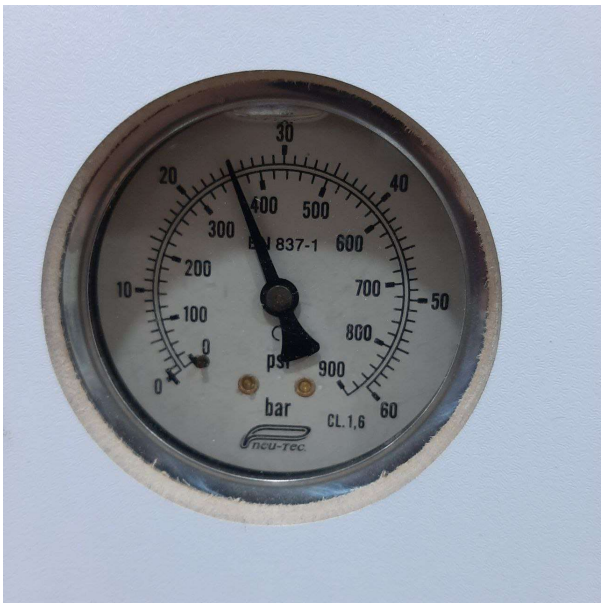

Figure (3- 28) Bourdon Gauge

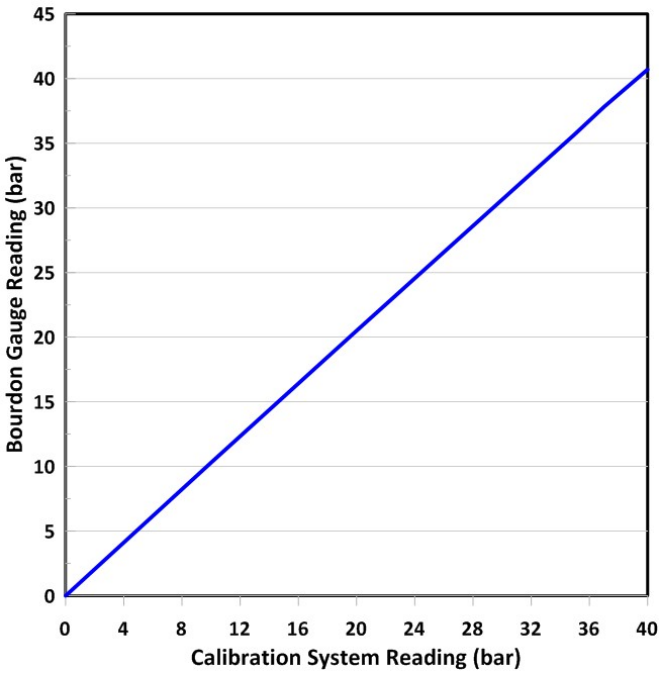

Figure (3- 29) ***Pressure Calibration***

3.7.3 Flow Measurement

There are two flow meters in this work. The first flow meter is an orifice plate installed upstream the mixer to measure the flow rate into mixer. The calibration of this flow meter as shown in fig (3.30). The second flow meter in the cooling cycle. It is located between the pump and the heat exchanger (condenser). The range of this flow meter between (0-10) l/min. The calibration of the second flow meter is illustrated in fig (3.31). Error=0.09 (L/min)

$$\text{Percent Error} = \frac{|\text{measured} - \text{real}|}{\text{real}} * 100\% \qquad (3.79)$$

Percent Error=0.0075%.

Uncertainty=∓0.2 (L/min)

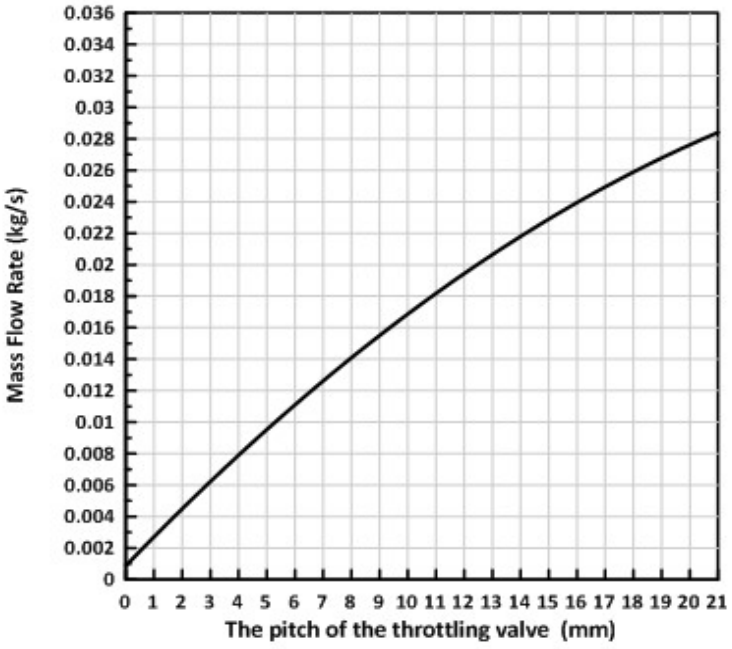

Figure (3- 30) Calibration of the Orifice Flow Meter

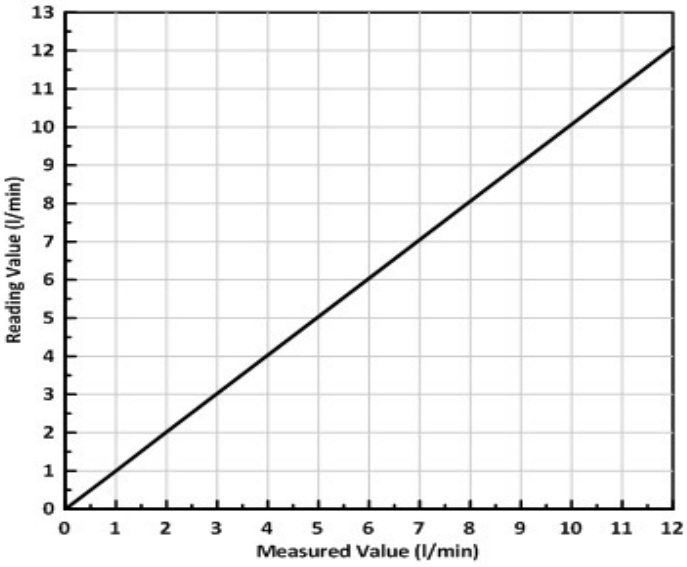

Figure (3- 31) Calibration the Second Flow Meter

3.7.4 Electrical Power Measurement

As stated before the function of this cycle is to generate electrical power by a vapor turbine which rotates the electrical generator. The voltmeter and ammeter explains in fig (3.32).

$$\text{Power (P)} = \text{Voltage (Vo)x Current (I)x COS}\theta \qquad (3.80)$$

Where Cos θ is the power factor equal unity.

P is the electrical power (W).

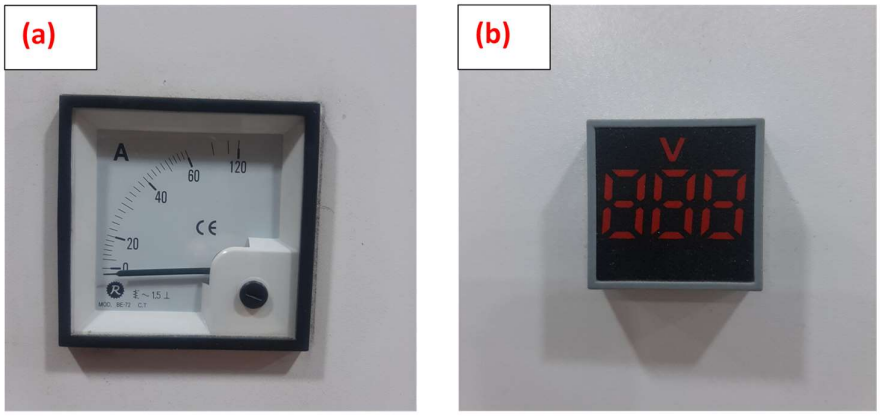

Figure (3- 32) Power Measurement, (a) Ammeter, (b) Voltmeter.

3.8 Preparing Ammonia-Water Mixture (Working Fluid)

The preparation process of the ammonia-water mixture is performed outside the cycle. The required mass of mixture is 20kg as explained in section 3.5. The mass of water is fixed while the mass of ammonia changes.

The preparation procedure is as follows:

1- A clean and dry container is used for the process of mixing ammonia with water with a volume of 20-liter.

2- A sensitive balance type (VALUE VES-50B) with 50 kg maximum weight is used for measuring the mass of fluids. The accuracy of balance is ∓2 g (∓0.05%) see fig (3.33).

Figure (3- 33) Sensitive Balance Type (VALUE VES-50B)

3- Turn on the electronic scale of sensitive balance, then weight the empty container with its connections and record the reading where the weight of the empty container with its connections is 0.5kg.

4- Determine the desired ammonia concentration of the solution. The mixing ratio, and let it be x=0.47 (the ammonia mass fraction in the working fluid). Then ammonia is weighed and injected into the container. The ammonia mass is calculated based on the following equation:

$$x = \frac{m_{NH3}}{m_T} = \frac{m_{NH3}}{m_{NH3} + m_{H2O}} = 1 - \frac{m_{NH3}}{m_{H2O}} \quad (3.81)$$

$$1 - x = \frac{m_{NH}}{m_{H2O}} \quad (3.82)$$

$$m_{NH} = x * m_T \quad (3.83)$$

$$m_T = m_{NH} + m_{H2O} \quad (3.84)$$

$$m_{H2O} = m_T - m_{NH} \quad (3.85)$$

$$m_{NH3} = 0.47 * 20 = 9.4kg$$

$m_{H2O} = 20 - 9.4 = 10.6kg$

5- Add 10.6 kg of water into container, the water is free of impurities (distilled water).

6- The container is connected to a source for the preparation of pure ammonia, using a set of rubber tubes, pressure gauges, and valves controlling the flow of ammonia from the source to the water bottle, and adding 9.4 kg of ammonia. Fig (3.34) shows the connection method.

7- The mixture should be weighed accurately as it does not exceed the total mixing ratio by adjusting the masses of the mixed materials of water and ammonia to achieve a total mass of 20 kg. It is possible to target the total mass less or more than 20 kg according to the requirements of the work.

8- For new concentration the same procedure is repeated.

9- After completing the weighing process, the mixture is left for 60 min for stabilization.

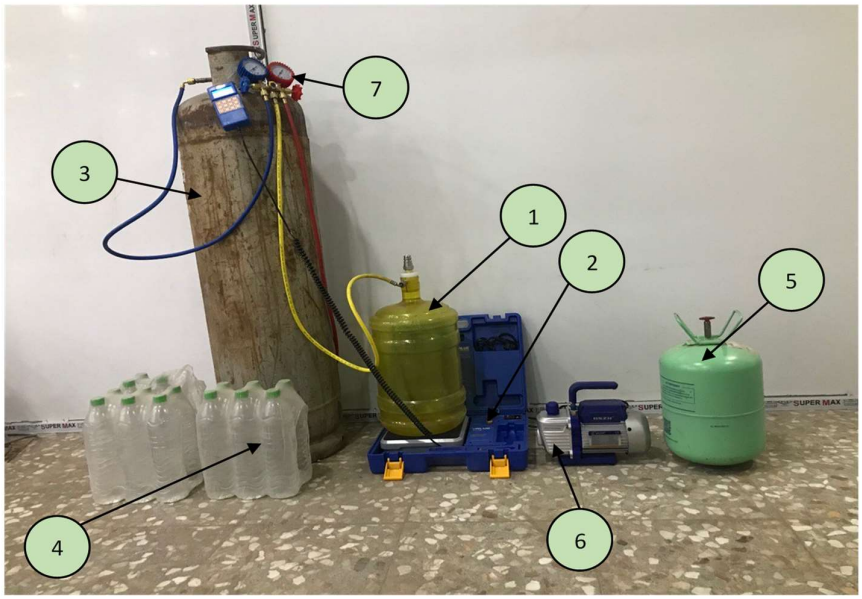

1- Mixing container
2-The sensitive balance
3- Ammonia storage
4- pure water
5- Ammonia storage (small)
6- Vacuum pump
7- Pressure gage

Figure (3- 34) Mixing Process Equipment

3.9 Charging

The charging process is carried out as follows:

1- The pump is used to empty the air from the system by connecting it to a designated point in the separator, which represents the highest point in the system, and it is point 1 in the cycle to ensure the emptying of air. The type of the vacuum pump is WK-115, pumping rate 2 CFM, ultimate vacuum 150 micron and power rate is ¼ HP as shown in fig (3.34).

2- Connect the container with the main system and connect it with the tank designated for preparing the pump, point No. 4 on the cycle, and unload the charge inside the system within a period of 10-15 minutes, and close the valves after completion.

3- For the purpose of increasing the concentration of ammonia within the mixture, we target a new or required mixing ratio and extract the mass of

ammonia that must be injected into the system directly using the following equation

$$x_i = \frac{M_{NH3_i}}{M_{T_i}} \tag{3.86}$$

$$x_i = \frac{M_{NH3_i}}{M_{NH3_i} + M_{H2O_{I-1}}} \tag{3.87}$$

4- An additional ammonia for example x=0.48 (the ammonia mass fraction in the working fluid). The mass of which is added is 9.6 kg. The cycle already has 9.4kg, should be inject 0.2kg of ammonia to the cycle, use another small bottle with weight 5kg ammonia. The electronic scale has the ability to program gravimetrically and calculate the decreasing weight of the small bottle before and after the injection process. The device is programmed to inject an amount of 0.2 kg. The small bottle is connected with the control valve and connected to the electrical power source of 220 volts, then the exit valve is connected to the system (cycle) at point4.

5- Thus, the process is repeated for different concentrations by adding ammonia directly to the system (cycle) the mass of water still constant.

3.10 Expermantal procedure

1. Preparing the mixture, and injecting it into the system, as explained in sections 3.8 and 3.9 according to the test conditions.

2. Connecting the system with electrical source.

3. Making sure the pressure valves are closed and the mixer cooling system is switched off. The main control switch has four grades (1, 2, 3 and 4) as shown in fig (3.35).

Figure (3.35) the Main Switch

4. Put the emergency switch on and turn the main control switch on the number one. The number one represents test all the cycle parts (thermocouples, pressure gages, pump and heat exchangers) before the operation.

5. Put the main control switch on number two to operate the pump. The pump starts to circulate the working fluid from storage tank to the HRVG and then to the separator.

6. Open the throttling valve partially to avoid suffocation and to let the working fluid pass from the separator to the heat exchanger via throttling valve to the mixer, condenser, storage tank and then to the pump to complete this cycle.

7. Open the throttling valve gradually to let mass flow rate passes to the mixer (absorber).

8. Put the main control switch on number three to start the heating system for 30 min and observe the temperature in the separator. The temperature increases and the ammonia starts evaporating and the pressure increases till 80% to 90% from the pre-set maximum pressure.

9. Open the pressure valve which is located before the turbine gradually to let the vapor of the mixture passes through the turbine. The pressure and the temperature in the separator will drop. When the temperature in the separator drops adjust the pump feed.

10. When the pressure increases inside the separator, the opening of the valve increases located before the turbine to let more amount of the vapor passes through the turbine. Also we should control on the speed of the turbine by increasing the load.

11. When the pressure in the separator increases the minimum pressure after the turbine increases also the pump speed is adjusted.

12. For mixer cooling put the main control switch on the number 4 to operate the mixer cooling system.

13. Leave the cycle operating until reaching thermal equilibrium i.e the temperatures remain constant. It takes about 4-5hrs.

14. Record the required data when the system reaches steady state at the required pressures and temperatures. Then record the required data as shown on the data sheet table (3.6).

Table (3.6) Data Sheet

Points	Properties							
	P	T	x	DF	$\dot{m}$	h	s	v
1								
2								
3								
4								
5								
6								
7								
8								
9								

3.11 Data Processing

In this section, data is analyzed according to the first and second law of thermodynamic. The data obtained from the experimental work includes the properties of working fluid which are the temperature and pressure in each point. To find the other properties such as the specific enthalpy, specific entropy and specific volume tables are used. Figs (3.36) and (3.37) show the thermal cycle of MKCSE on the T-x and h-x diagram respectively. The procedure of analysis can be summarized as follows:

1-The mass flow rate is calculated.

2-The ammonia mass fraction at turbine inlet is selected for the working fluid.

3-The dryness fraction at the separator inlet is selected and the dryness fraction at point1 of saturated vapor equals one, the dryness fraction at the separator exit point8 of saturated liquid equals zero.

4- The temperature and pressure in the separator are constant that is mean $T_1=T_7=T_8$. The pressure is known in all points.

5- Go to the charts or tables to intersect the two data of ammonia mass fraction and dryness fraction to get the x_f and x_v at constant pressure and temperature. The dryness fraction equal zero at x_f and dryness fraction equal one at x_v.

6- To find the dryness fraction at point 3, T_3, x_3 and P_3 are known from the tables thus the dryness fraction can be calculated.

7- At the condenser exit, the situation of the solution is saturated liquid, T_4, x_4, DF and P_4 are known from the tables find all the properties at point4.

8- At the pump exit is point 5, the situation of the solution sub-cool liquid. Also T_5, x_5 and P_5 are known from the table to thus all properties can be found at point5. The pump work is neglected.

9- At the exit of heat exchanger, the situation of the solution is warm and $T_{5'}$, $x_{5'}$ and $P_{5'}$ are known from the tables, to find all the properties at point$5'$.

10- At point6 the ($T_6 = T_{boiling}-2^0C$).

11- At point7, the quality of the solution is wet vapor, T_7, DF_7, x_7 and P_7 are known from tables to find all the properties.

12- Applying the first law and second law of thermodynamic to find the performance of KCSME for example, the conditions are used (P_{max}=35 bar, P_{min}=2 bar and x=0.85) to show the performance of KCSME as shown in fig (3.36).and fig (3.37).

$$\dot{W}_T = \dot{m}_1 * (h_1 - h_2) \quad (3.88)$$

$$\dot{W}_P = \dot{m}_4 * (h_5 - h_4) \quad (3.89)$$

$$\dot{W}_{net} = W_T - \dot{W}_P \quad (3.90)$$

$$\dot{E}_{in} = \dot{m}_7 * (h_{5'} - T_o * s_{5'}) \quad (3.91)$$

$$\dot{E}_{out} = \dot{m}_7 * (h_7 - T_o * s_7) \quad (3.92)$$

$$(\dot{E}_d)_{tot} = \sum(\dot{E}_d)_i \quad (3.93)$$

$$\eta_{ex} = \frac{\dot{W}_{net}}{\dot{E}_{in} - \dot{E}_{out}} \quad (3.94)$$

$$\eta_{th} = \frac{\dot{W}_{net}}{\dot{Q}_{in}} = \frac{\dot{W}_T - \dot{W}_P}{\dot{Q}_{in}} \quad (3.95)$$

Where

$\dot{W}_{net}$ is the net power

$\dot{W}_T$ is rate of work produced by turbine.

$\dot{W}_P$ is rate of work consumed by pump (is neglected)

$\dot{E}_{in}$ is the input exergy at inlet of HRVG

$\dot{E}_{out}$ is the exit exergy at exit of HRVG

$(\dot{E}_d)_{tot}$ is total destroyed exergy at the system components

η_{ex} is the exergy efficiency (%).

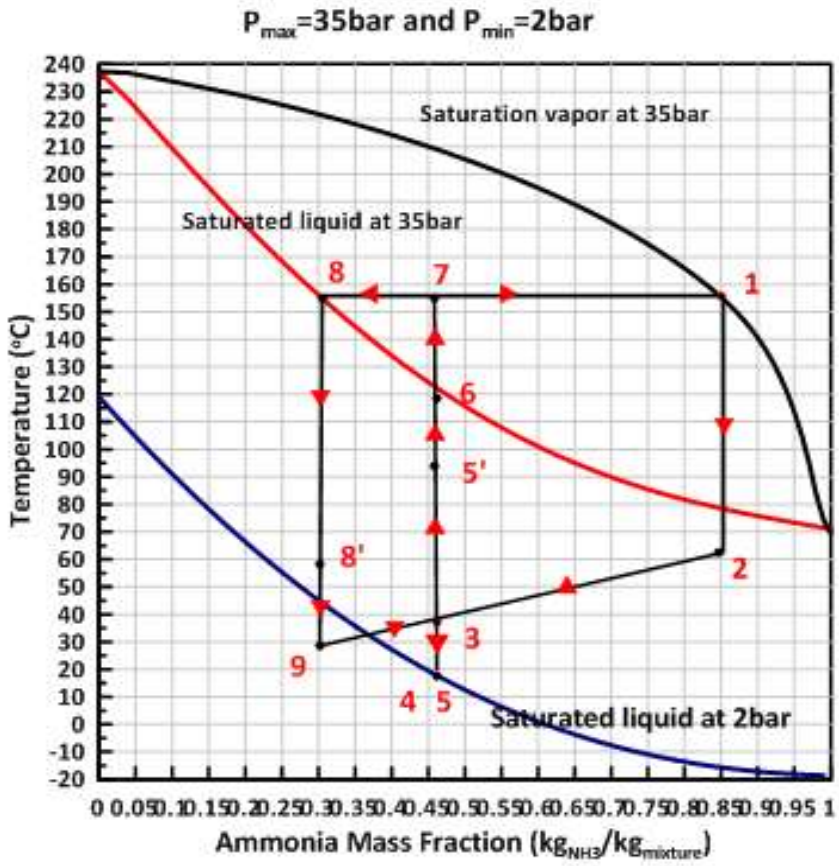

Figure (3.36) MKCSE on the T-x Diagram at P_{max}=35 bar, P_{min}=2 bar and x=0.85

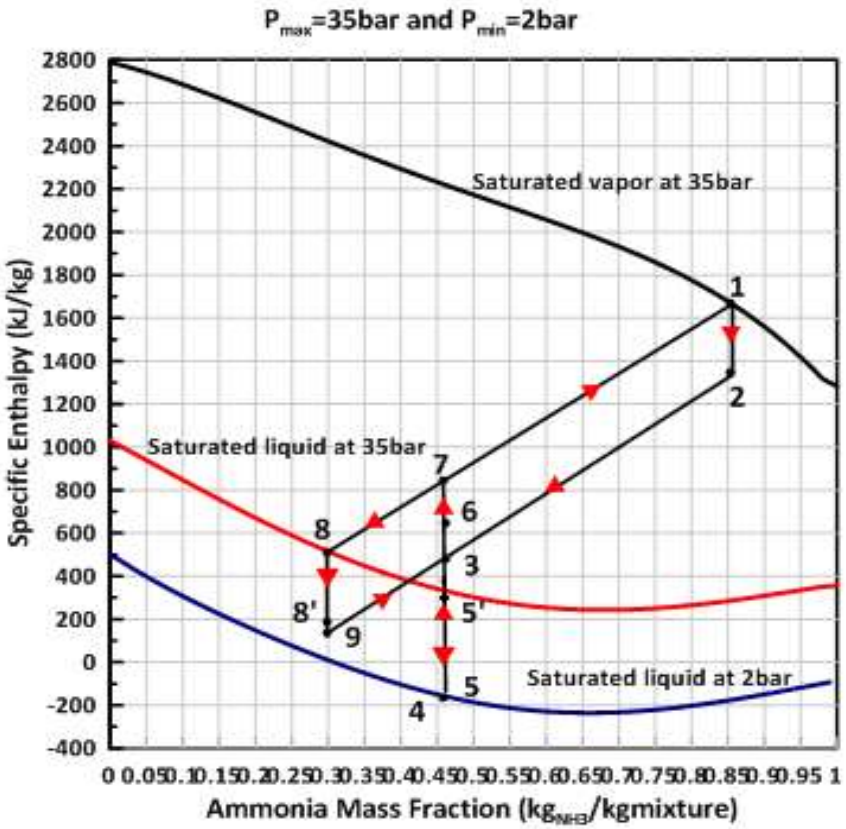

Figure (3.37) MKCSE on the h -x Diagram at P_{max}=35 bar, P_{min}=2 bar and x=0.85

Chapter Four

Theoretical Analysis

Chapter Four: Theoretical Analysis

4.1 Introduction

Theoretical analysis of simple kalian Cycle System (SKCS) and the suggested modifications of Kalina Cycle System (MKCS) are shown in figs (4.1), (4.2) and (4.3). The analysis is required to apply the first and the second laws of thermodynamic on all modifications and simple Kalina. In addition, the state of the working fluid at every point and the thermodynamic properties of the working fluid must be known. The working fluid is aqua-ammonia (NH_3-H_2O) with different concentrations. Generally, the thermodynamic properties of working fluid in a thermal cycle play an important role in its evaluation. Currently, researchers are focusing on the vapor absorption systems in the Kalina cycle system, vapor absorption refrigeration, and cooling cogeneration cycle. Compared to the assessment of thermodynamic properties of pure substance, evaluation of binary mixture properties is complicated due to addition of an extra property that is mixture concentration. Ammonia-water mixture is a well- known and established zeotropic mixture for vapor absorption systems. In this mixture ammonia has low boiling point $(-33℃)$ and the water has high boiling temperature$(100℃)$ at atmospheric pressure. This difference in the boiling point allows the separation and the distillation of the mixture required in the cycles. Unlike pure substance the binary mixture changes its temperature in phase-change heat transfer from bubble point temperature T_{bp} to dew point temperatureT_{dp} .

This chapter includes two parts, first part is the thermodynamic properties of ammonia-water mixture have been generated from the reported correlations, derivations and the iterations using MATLAB programing. The second part is analyzing the simple Kalina cycle system and all the modifications. The temperature-concentration (T-x) and specific enthalpy-

concentration (h-x) graphs for ammonia-water mixtures shall be plotted up to 50 bar pressure. Two modifications are introduced on simple Kalina cycle system. The first modification is the addition of a heat exchanger between the separator and the expansion valve. This modification reduces the heat rejection and improve the thermal efficiency as shown in fig (4.2). The second modification is same as the first modification but with another heat exchanger that is positioned between the turbine and the pump to use the heat that comes from the turbine to reheat the cold working solution that come from the pump as presented by fig (4.3).

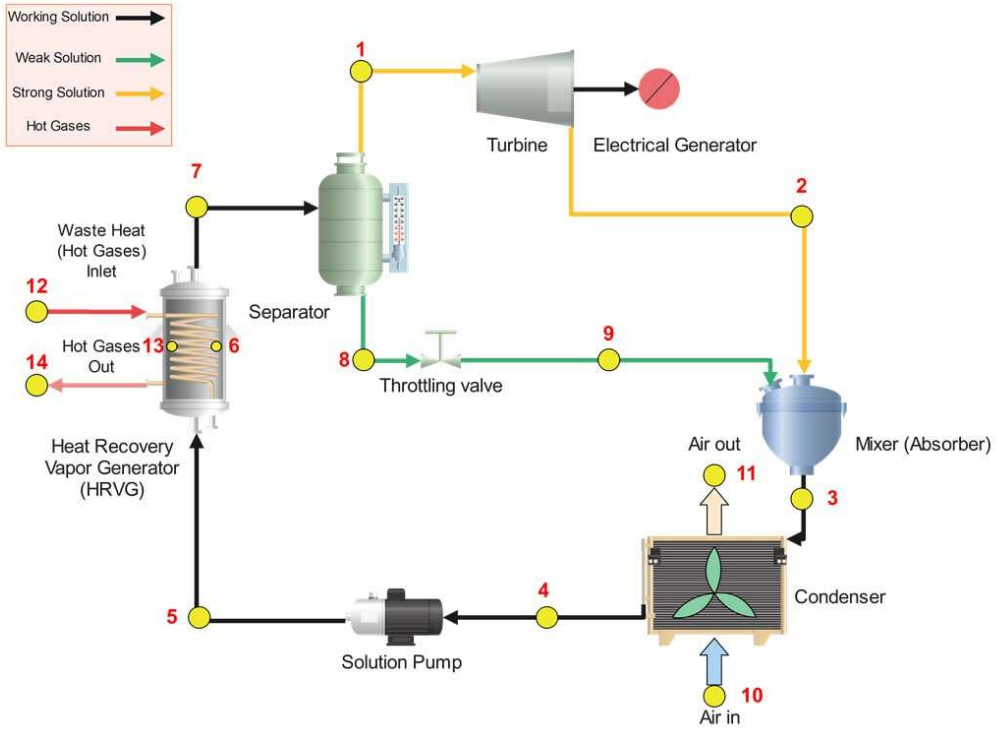

Figure (4.1) Simple Kalina Cycle System (SKSC) [2]

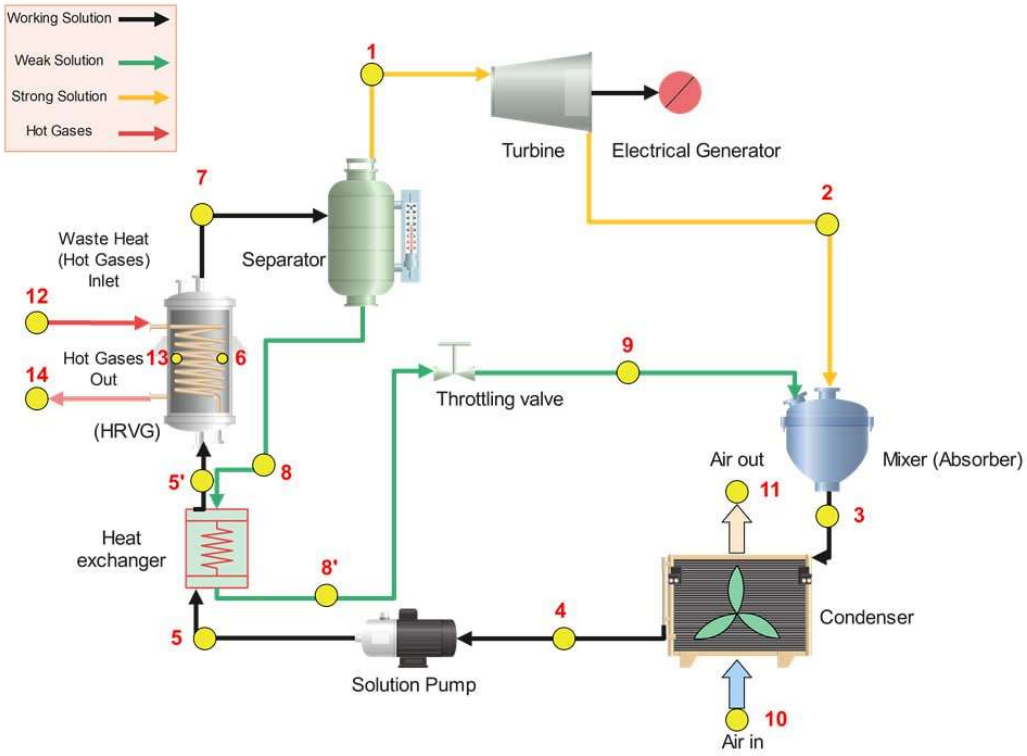

Figure (4.2) Modified Kalina Cycle System (MKCS1).

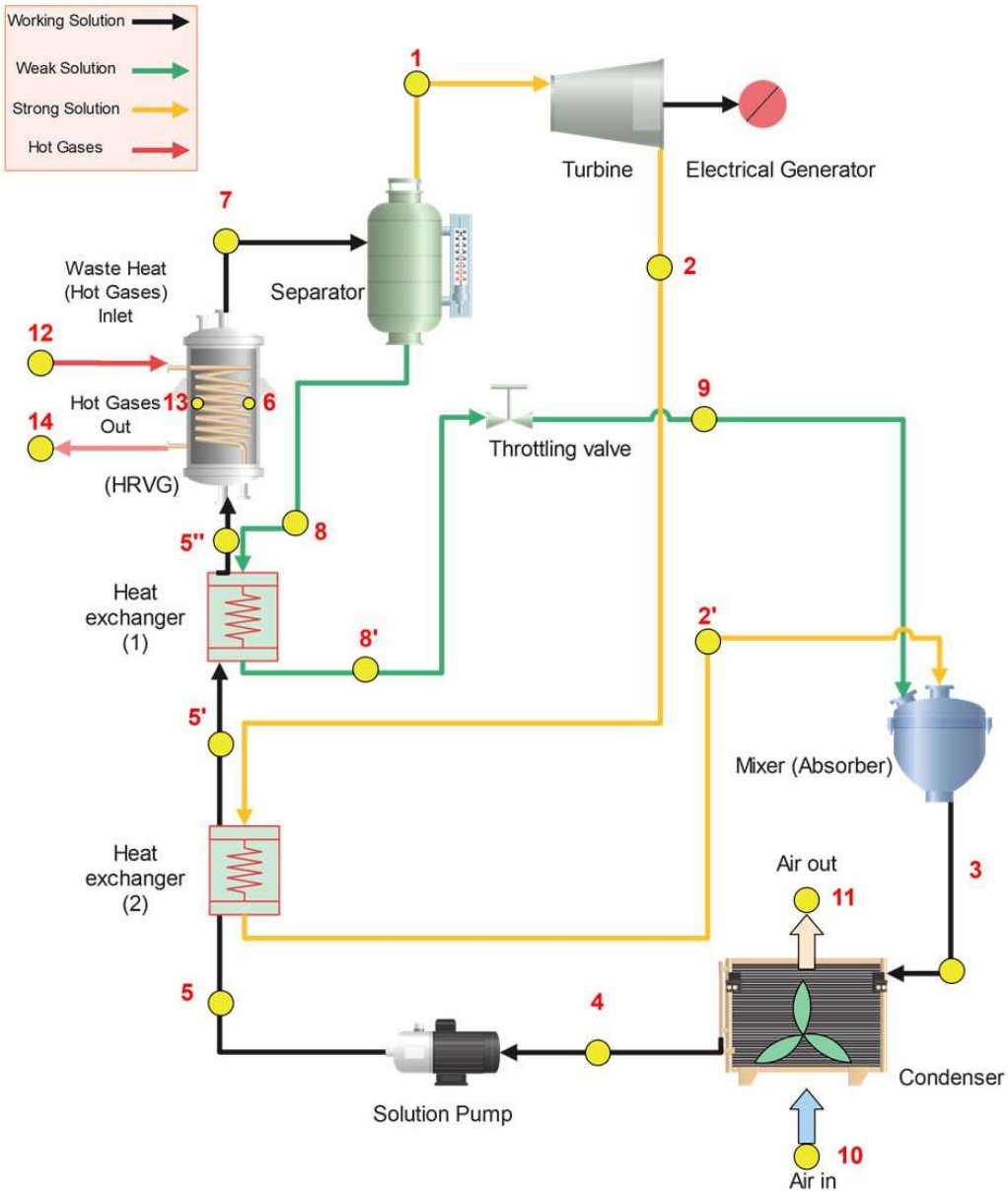

Figure (4.3) Modified Kalina Cycle System (MKCS2)

4.2 Evaluation of Working Fluid Thermodynamic Properties

4.2.1 Bubble Point and Dew Point Temperatures Calculation.

To evaluate other thermodynamic properties of the mixture, the bubble point and dew point temperature are to be calculated at given concentration and pressure. Pressure, concentration and temperature are required to obtain other properties of the mixture without knowing the

quality or phase. The mixture temperature along with the bubble point temperature and the dew point temperature specify the quality of mixture that is liquid mixture (sub-cooled or compressed liquid mixture), saturated liquid, liquid (wet) vapor mixture, saturated vapor or superheated vapor. Fig (4.4) describes the possible quality in binary fluid mixture. The regions are grouped with reference to T_{bp} and T_{dp} and compared to the mixture pressure, temperature, and concentration. The temperature-concentration plot is generated at 40 bar pressure. The T_{bp} curve represents all the starting states of phase change and T_{dp} curve represents the completed states of phase change of the mixture at different concentrations. The bubble point temperature and the dew point temperature curves are also known as saturated liquid curve and saturated vapor curve respectively. Between these two curves the mixture exists in the liquid-vapor mixture. Below the bubble point temperature curve the mixture is completely liquid at sub-cooled state. Above the dew point temperature curve the mixture is vapor in superheated state. The phase change starts from bubble point saturation temperature at fluid pressure at a particular concentration. The zero concentration point represents pure water and 100% concentration point represents pure ammonia with properties of pure substance at respective saturation temperature at the given pressure. The plot shows five regions namely superheated vapor zone, saturated vapor zone, liquid vapor mixture zone, saturated liquid zone and sub-cooled liquid zone. Bubble point temperature and dew point temperature are determined from the curve-fit of the below equations and corresponding coefficients are tabulated in tables 4.1 and 4.2 for T_{bp} and T_{dp} respectively **[71]**.

$$T_{bp}(P,x) = T_o \sum a_i (1-x)^{m_i} \left[\ln\left(\frac{P_o}{P}\right)\right]^{n_i} \tag{4.1}$$

$$T_{dp}(P,DF) = T_o \sum a_i (1-DF)^{m_i} \left[\ln\left(\frac{P_o}{P}\right)\right]^{n_i} \tag{4.2}$$

Where:-

n_i, m_i and a_i are constants

T_{bp} is the bubble point temperature(℃).

T_{dp} is the dew point temperature(℃).

x is the mass fraction of ammonia (kg_{NH3}/kg mixture).

DF is dryness fraction (kg vapor of mixture/kg of mixture).

T_o, P_o are temperature and pressure at reference state.

(P, T, x) are the three properties required to find the other thermodynamic properties of the mixture. The known temperature should be compared with the T_{bp} and T_{dp} to decide the state of working fluid. If the known temperature is less than T_{bp} it is sub-cooled liquid or compressed liquid. When temperature equal to T_{bp} is saturated liquid. Between T_{bp} and T_{dp} it is the mixture of liquid and vapor. When temperature equalsT_{dp}, it is saturated vapor and when temperature exceedsT_{dp}, it is superheated vapor.

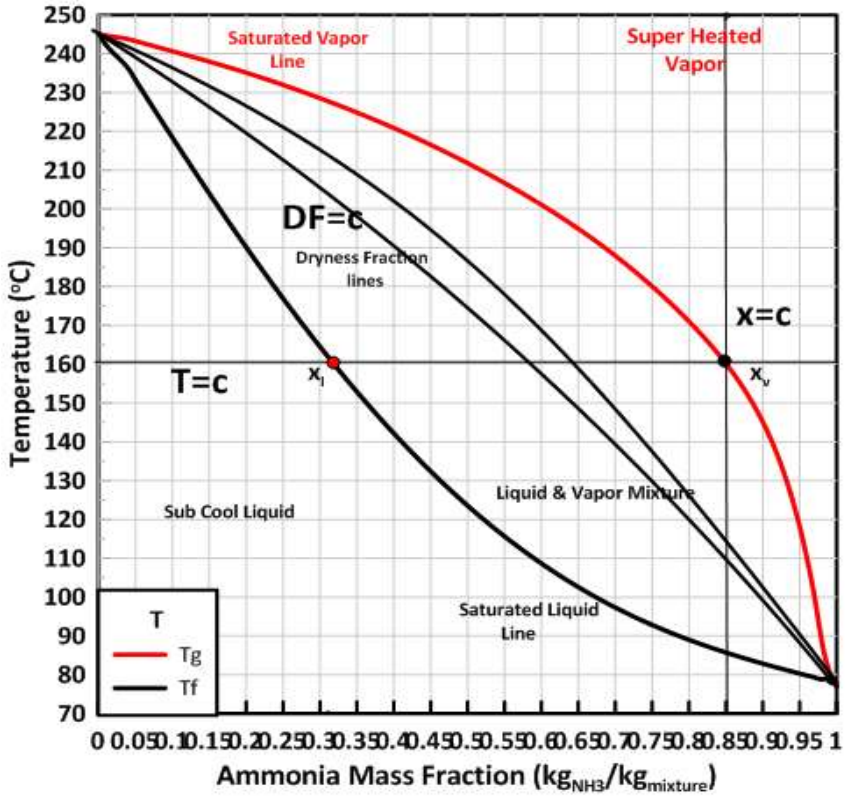

Figure 4.4 Temperature-Concentration Diagram with Five Regions at 40 bar

Table 4.1 Constant for T_{bp} Used in eq. 4.1[2]

i	m_i	n_i	a_i
1	0	0	+00322302
2	0	1	-0.3842060
3	0	2	+0.0460965
4	0	3	$-0.378945*10^{-2}$
5	0	4	$+0.135610*10^{-3}$
6	1	0	$+0.487755*10^{0}$
7	1	1	$-0.120108*10^{0}$
8	1	2	$+0.106154*10^{-1}$
9	2	3	$-0.533589*10^{-3}$
10	4	0	$+0.785041*10^{1}$
11	5	0	$-0.115941*10^{2}$
12	5	1	$-0.523150*10^{-1}$
13	6	0	$+0.489596*10^{1}$
14	13	1	$+0.421059*10^{-1}$

Table 4.2 Constant for T_{bp} Used in eq. 4.2[2]

i	m_i	n_i	a_i
1	0	0	0000324004
2	0	1	0.395920000
3	0	2	0.043562400
4	0	3	$-0.218943*10^{-2}$
5	1	0	$-0.143526*10^{1}$
6	1	1	$+0.105256*10^{1}$
7	1	2	$-0.719281*10^{-1}$
8	2	0	$+0.122362*10^{2}$
9	2	1	$-0.224368*10^{1}$
10	3	0	$-0.201780*10^{2}$
11	3	1	$+0.110843*10^{1}$
12	4	0	$+0.145399*10^{2}$
13	4	2	$+0.644312*10^{0}$
14	5	0	$-0.221246*10^{1}$
15	5	2	$-0.756266*10^{0}$
16	6	0	$-0.135529*10^{1}$
17	7	2	$+0.183541*10^{0}$

4.2.2 Specific Enthalpy of Liquid and Vapor Phase

The specific enthalpy of the liquid mixture is determined from Equ. (4.3) **[2]**.

$$h_l^m = x h_a^l + (1 - x) h_w^l \qquad (4.3)$$

Where:-

h_l^m is the specific liquid enthalpy of the mixture (kJ/kg).

h_a^l is the specific enthalpy of ammonia liquid (kJ/kg).

h_w^l is the specific enthalpy of water liquid (kJ/kg).

x is the mass fraction of ammonia (kg_{NH3}/kg mixture).

The enthalpy of pure component in the vapor phase can be expressed in the following equation**: [2]**

$$h_v^m = xh_a^v + (1-x)h_w^v \quad (4.4)$$

Where:-

h_v^m is the specific enthalpy for mixture at vapor phase(kJ/kg).

h_a^v is the specific enthalpy of ammonia vapor (kJ/kg).

h_w^v is the specific enthalpy of water vapor (kJ/kg).

4.2.3 Specific Entropy of Vapor and Liquid Phases

The specific entropy of the vapor and liquid phases is obtained from eqs. (4.5) and (4.6) **[71]**.

$$s_v^m = xs_a^v + (1-x)s_w^v \quad (4.5)$$

$$s_l^m = xs_a^l + (1-x)s_w^l \quad (4.6)$$

Where:

s_a^v: Specific entropy of ammonia vapor (kJ/kg K).

s_w^v: Specific entropy of water vapor (kJ/kg K).

s_v^m: Specific entropy of the mixture in the vapor phase (kJ/kg K).

s_l^m: Specific entropy of the mixture in the liquid phase (kJ/kg K).

s_a^l: Specific entropy of ammonia liquid (kJ/kg K).

s_w^l: Specific entropy of water liquid (kJ/kg K).

4.2.4 Specific Volume of Vapor and Liquid Phases

The specific volume of the vapor and liquid phases is obtained from eqs (4.7) and (4.8) **[2]**.

$$v_m^v = x v_a^v + (1-x) v_w^v \quad (4.7)$$

$$v_m^l = x v_a^l + (1-x) v_w^l \quad (4.8)$$

Where:

v_m^v: Specific volume of mixture vapor phase (m^3/kg).

v_a^v: Specific volume of ammonia vapor (m^3/kg).

v_w^v: Specific volume of water vapor (m^3/kg).

v_m^l Specific volume of mixture liquid phase (m^3/kg).

v_a^l Specific volume of ammonia liquid (m^3/kg).

v_w^l Specific volume of water liquid (m^3/kg).

4.2.5 Description the Method of Finding Thermodynamic Properties

A special routine is developed in MATLAB to calculate the thermodynamic properties of ammonia-water mixture at varying pressures, temperatures and concentrations. The calculation steps are as follows:

1- Read pure NH_3 liquid and vapor properties for range (P and T).
2- Read pure water liquid and vapor properties for a selected range of pressures and temperatures.
3- Read pressure, temperature and concentration.
4- Calculate the corresponding T_{bp} and T_{dp} for ammonia-water mixture.
5- Calculate other thermodynamic properties for ammonia water mixture including specific enthalpy, specific entropy and specific volume. The flow chart of the routine is shown in fig (4.5).

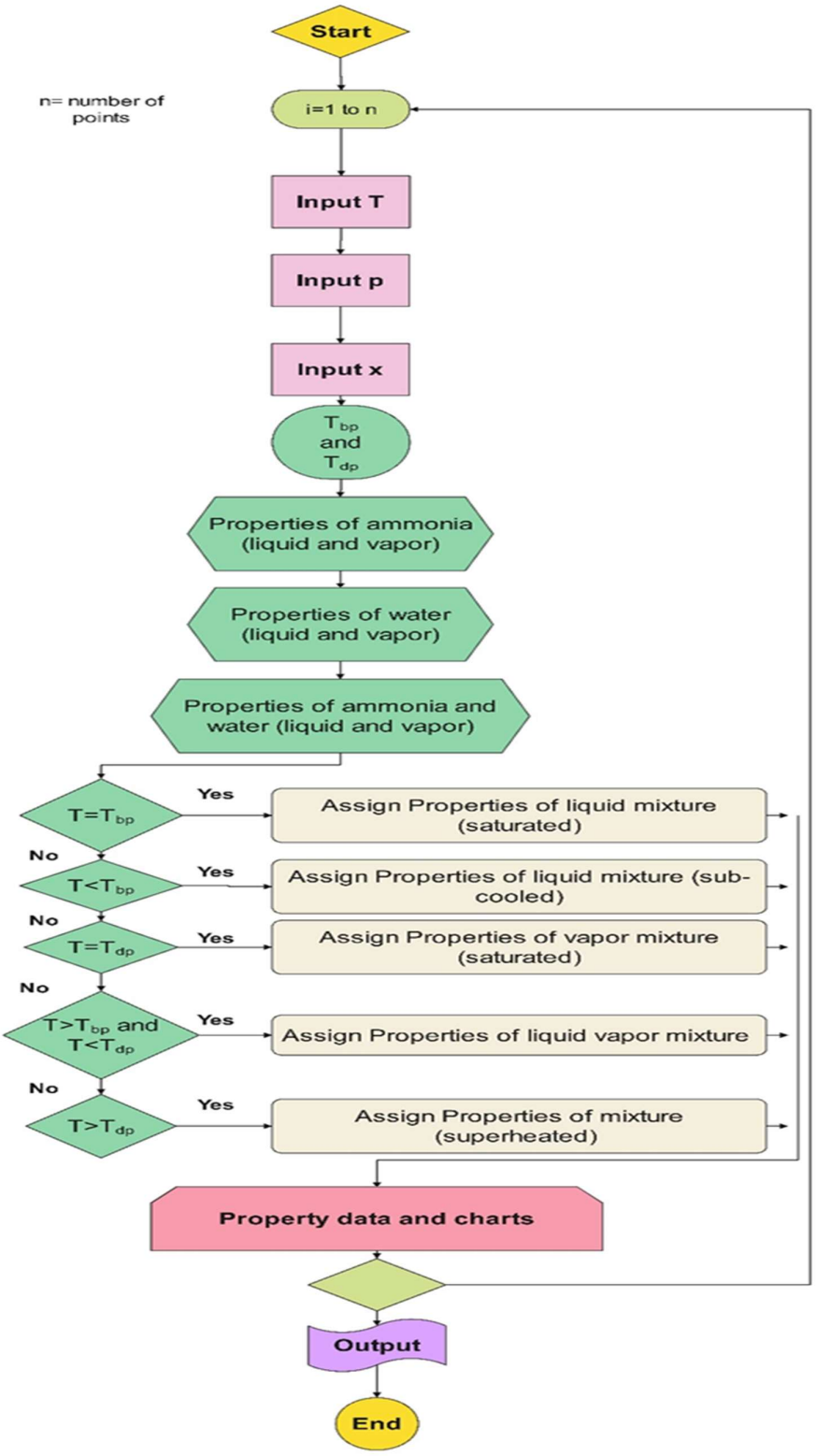

Figure 4.5 Flow Chart to Evaluate the Thermodynamic Properties of Ammonia- Water Mixture.

4.3 Cycle Analysis

4.3.1 Governing Equations

Thermodynamic evaluation of binary fluid system is complicated compared to the single fluid system due to the extra property of concentration. The understanding of process evaluation helps to develop the computer model to obtain the results from the function of properties. The main processes in the vapor absorption cycle (power, cooling and combined power and cooling) are preheating, evaporation, distillation, expansion, throttling, mixing and absorption, cooling and condensation and pumping. These processes are governed by mass, energy and exergy conservation equations (4.9-4.11).

$$\sum \dot{m}_i = \sum \dot{m}_0 \tag{4.9}$$

$$\sum \dot{Q} + \sum \dot{m}_i h_i = \sum \dot{W} + \sum \dot{m}_o h_o \tag{4.10}$$

$$\dot{\mathrm{E}}_{\mathrm{dtot}} = \sum \dot{E}_{in} - \sum \dot{E}_{out} \tag{4.11}$$

The heat transfer processes in Kalina Cycle System happen in the heat recovery vapor generator (HRVG), condenser, solution heat exchanger, and absorber. Also there are other processes in this cycle such as throttling, expansion, pumping, adiabatic mixing and separation. It is used lever rule in some processes such as mixing and separation to get the ammonia mass fraction and other properties.

4.3.2 Assumptions: -

The following assumptions are adopted in developing the computer program used for solving the governing equations.

1-Steady state operation is assumed throughout the cycle.
2-Working fluid at the outlet of condenser is saturated liquid.

3-Working fluid at the inlet of turbine is saturated vapor at turbine pressure (P_{max}).

4-The weak solution before throttling valve is saturated liquid at P_{max}.

5-The pressures of the HRVG and condenser are constant.

6-Throttling process is isenthalpic.

7-Separation process in the separator at constant pressure (vapor and liquid).

8-The isentropic efficiencies of pump and turbine are 100%, 85% respectively.

9-Pressure losses, heat losses and friction losses in pipes are neglected.

10-The effectiveness of HRVG and condenser is unity($\epsilon = 1$).

11-All the devices are adiabatic.

12-The kinetic energy and potential energy changes in the devices are neglected.

13- Neglect the work of the pump.

14-The used water and ammonia are pure substance.

15- The inlet temperature of the hot gases is 175℃.

16- The pinch point (PP) in the boiler is 20℃. The terminal temperature difference (TTD) at evaporator of heat recovery vapor generator (HRVG) inlet with hot gases is taken at 15℃. Approach point (AP) in the HRVG is 2℃. Approach point (AP) in the HRVG is 2℃ to prevent the sudden phase change in the generator [74].

17- The value of T_1, T_6 and T_{13} are

$$T_1 = T_{12} - TTD \quad (4.12)$$

$$T_6 = T_{bp} - AP \quad (4.13)$$

$$T_{13} = T_{bp} + PP \quad (4.14)$$

$$T_{14} \leq T_6 \quad (4.15)$$

4.3.3 Applications of Governing Equations to Each Cycle Component.

4.3.3.1 Separator

It is cylindrical shaped vessel that allows the separation of liquid by gravity from the liquid-vapor mixture. The vapor is tapped from the top of the cylinder. The state of the working fluid which is passed through the separator is wet vapor. The separator is shown schematically in fig (4.6).

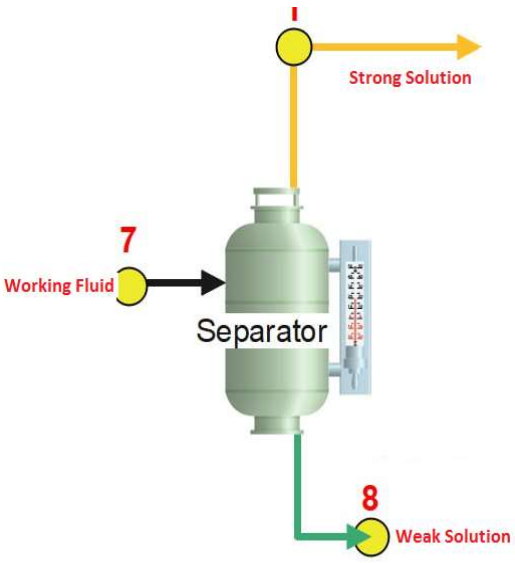

Figure (4.6) Schematic Representation of Separator.

There are three different ammonia concentrations namely inlet mixture concentration (working fluid), weak solution concentration (saturated liquid) and strong solution (saturated vapor) concentration. It is assumed that the separation processes happen at constant pressure. The total mass balance is

$$\dot{m}_7 = \dot{m}_8 + \dot{m}_1 \qquad (4.16)$$

The total ammonia balance is,

$$\dot{m}_7 x_7 = \dot{m}_8 x_8 + \dot{m}_1 x_1 \qquad (4.17)$$

$$\dot{m}_7 x_7 = (\dot{m}_7 - \dot{m}_1)x_8 + \dot{m}_1 x_1 \quad (4.18)$$

$$\dot{m}_7 x_7 = \dot{m}_7 x_8 - \dot{m}_1 x_8 + \dot{m}_1 x_1 \quad (4.19)$$

$$\dot{m}_7 (x_7 - x_8) = \dot{m}_1 (x_1 - x_8) \quad (4.20)$$

$$DF = \frac{\dot{m}_1}{\dot{m}_7} = \frac{x_7 - x_8}{x_1 - x_8} \quad (4.21)$$

Dryness fraction (DF) at separator inlet is defined from the simplification:

The wetness fraction (WF) or liquid fraction:

$$WF = \frac{\dot{m}_8}{\dot{m}_7} == \frac{x_1 - x_7}{x_1 - x_8} \quad (4.22)$$

Similar to ammonia balance the energy before separation is equal to the total energy after the separation neglecting the heat losses from the process (adiabatic process).

$$\dot{m}_7 h_7 = \dot{m}_1 h_1 + \dot{m}_8 h_8 \quad (4.23)$$

$$\dot{m}_7 h_7 = (\dot{m}_7 - \dot{m}_8)h_5 + \dot{m}_8 h_8 \quad (4.24)$$

$$\dot{m}_7 h_7 = \dot{m}_7 h_1 - \dot{m}_8 h_1 + \dot{m}_8 h_8 \quad (4.25)$$

$$\dot{m}_7 (h_7 - h_1) = \dot{m}_8 (h_8 - h_1) \quad (4.26)$$

The dryness fraction also can be written as a function of enthalpies. After the simplification of the above equations

$$DF = \frac{\dot{m}_1}{\dot{m}_7} == \frac{h_7 - h_8}{h_1 - h_8} \quad (4.27)$$

The wetness fraction or liquid fraction will be

$$WF = \frac{\dot{m}_8}{\dot{m}_7} == \frac{h_1 - h_7}{h_1 - h_8} \quad (4.28)$$

Concentration at separator inlet

$$x_7 = x_8 + DF(x_1 - x_8) \tag{4.29}$$

The exergy balance is

$$\dot{E}_7 = \dot{E}_1 + \dot{E}_8 + (\dot{E}_d)_{sep} \tag{4.30}$$

$(\dot{E}_d)_{sep}$ is the exergy destruction in the separator.

4.3.3.2 Adiabatic Mixing –Absorption Processes

The mixing-absorption process is an exothermic process where heat is liberated. This heat affects the efficiency of the mixing-absorption process. Therefore, this heat must be removed by some sort of cooling process. The mixing-absorption process with cooling is known as diabetic process. However, during this analysis, the heat generation is neglected and the process is assumed to be adiabatic at constant pressure. Fig (4.7) shows the adiabatic mixing of two fluids into a single fluid.

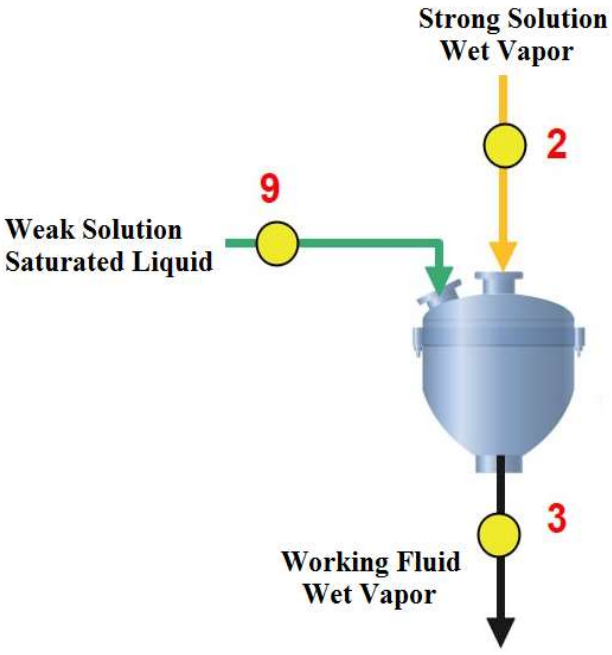

Figure (4.7) Adiabatic Mixing.

The mass and energy balances for the mixer are outlined below: -

Total mass balance

$$\dot{m}_9 + \dot{m}_2 = \dot{m}_3 \tag{4.31}$$

Ammonia mass balance

$$\dot{m}_9 x_9 + \dot{m}_2 x_2 = \dot{m}_3 x_3 \tag{4.32}$$

Energy balance

$$\dot{m}_9 h_9 + \dot{m}_2 h_2 = \dot{m}_3 h_3 \tag{4.33}$$

The mixture concentration (x) and mixture enthalpy (h) could be calculated from the following equations.

$$\dot{m}_2 = \dot{m}_3 - \dot{m}_9 \tag{4.34}$$

$$x_3 = \frac{\dot{m}_2 x_2 + \dot{m}_9 x_9}{\dot{m}_3} = \frac{\dot{m}_3 x_2 - \dot{m}_9 x_2 + \dot{m}_9 x_9}{\dot{m}_3} \tag{4.35}$$

$$x_3 = x_2 + \frac{\dot{m}_9}{\dot{m}_3}(x_9 - x_2) \tag{4.36}$$

$$\frac{\dot{m}_9}{\dot{m}_3} = \frac{x_3 - x_2}{x_9 - x_2} \tag{4.37}$$

Similarly

$$h_3 = h_2 + \frac{\dot{m}_9}{\dot{m}_3}(h_9 - h_2) \tag{4.38}$$

$$\frac{\dot{m}_9}{\dot{m}_3} = \frac{h_3 - h_2}{h_9 - h_2} \tag{4.39}$$

The exergy balance equation is

$$(\dot{E}_d)_{mix} = \left(\dot{E}_2 + \dot{E}_9\right) - \dot{E}_3 \tag{4.40}$$

Where the $(\dot{E}_d)_{mix}$is exergy destruction in the absorber in the adiabatic process.

4.3.3.3 Throttling process

The throttling valve separates the high pressure lines and low pressure lines. It is assumed that the work and heat transfer in throttling are neglected. The throttling process is an isenthalpic process as shown in fig (4.8).

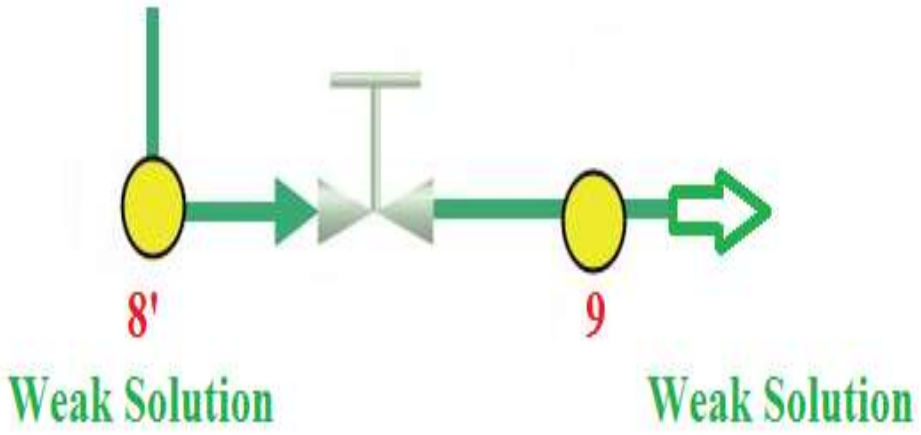

Figure 4.8 Throttling Process

$$\dot{m}_{8'} = \dot{m}_9 \quad (4.41)$$

$$h_{8'} = h_9 \quad (4.42)$$

$$x_{8'} = x_9 \quad (4.43)$$

The exergy equation is

$$(\dot{E}_d)_{thr} = \dot{E}_{8'} - \dot{E}_9 \quad (4.44)$$

Where $(\dot{E}_d)_{thr}$ is the rate of exergy destruction (kW) in the throttling valve.

4.3.3.4 Heat Exchangers

A- The Generator (Heat Recovery Vapor Generator)

Heat recovery vapor generator (HRVG) is a heat exchanger as shown in fig (4.9). It takes the heat from the hot exhaust of a boiler available in the Mechanical Engineering Department laboratories. It is used to generate

steam, at a pressure of 5 bar. The maximum power is 213 kW with consumption 18 kg/hr; while the minimum power is 90 kW with fuel consumption 7.6kg/hr. The fuel used is gasoil with an assumed average chemical formula of ($C_{16}H_{34}$). The minimum case which is 90 kW and 7.6 kg/hr is used in this work. The mass of air required to complete combustion of 1 kg fuel is obtained from the chemically balanced stoichiometric equation.

$C_{16}H_{34}+24.5(O_2+3.76N_2) \rightarrow 16\ CO_2+ 17\ H_2O+ 92.12\ N_2$

The mass flow rate of required air is required

$$\dot{m}_{air} = 113.104 kg/hr$$

The mass flow rate of combustion gases is

$$\dot{m}_{exh} = \dot{m}_{fuel} + \dot{m}_{air} \qquad (4.45)$$

$$\dot{m}_{exh} = 7.6 + 113.104 = 120.704\ kg/hr$$

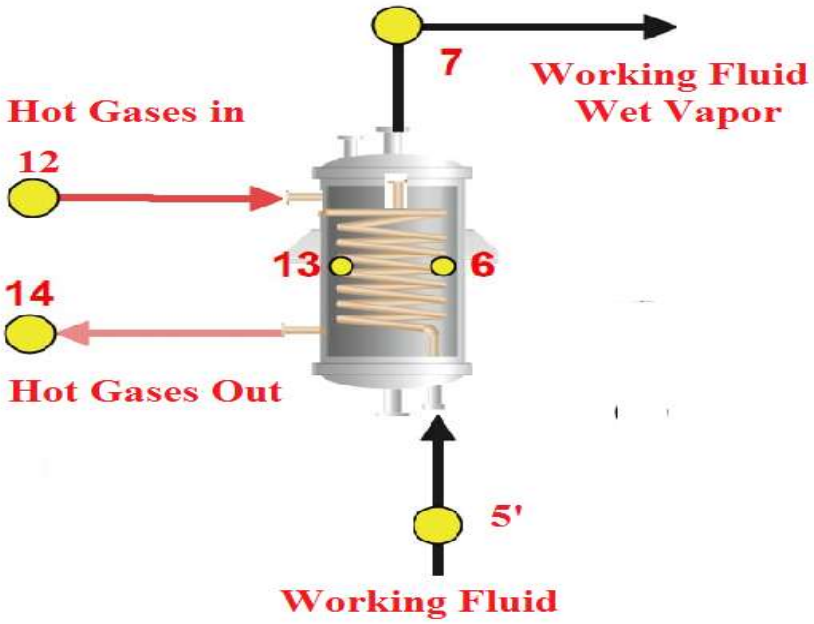

Figure (4.9) the Heat Recovery Vapor Generator

The mass and energy balances on the HRVG are as follows:

$$\dot{m}_{12} = \dot{m}_{14} \tag{4.46}$$

$$\dot{m}_{5'} = \dot{m}_7 \tag{4.47}$$

$$x_{5'} = x_7 \tag{4.48}$$

$$\dot{Q}_{in} = \dot{m}_{exh} cp_{exh} (T_{12} - T_{14}) \tag{4.49}$$

$$\dot{Q}_{in} = \dot{m}_{tot} (h_7 - h_{5'}) \tag{4.50}$$

Where

$\dot{Q}_{in}$ is heat addition from the hot gases.

cp_{exh} is the specific heat of combustion gas and its value 1.109

kJ/kg K **[33]**. The exergy balance equation is

$$(\dot{E}_d)_{HRVG} = (\dot{E}_{12} - \dot{E}_{14}) - (\dot{E}_7 - \dot{E}_{5'}) \tag{4.51}$$

Where

$(\dot{E}_d)_{HRVG}$ is the exergy destruction in the HRVG.

B- Condenser

The condenser is used to condense the working fluid (wet vapor point 3) that comes from the mixer as shown schematically in fig (4.10). It is assumed that saturated liquid condensate leaves the condenser point4.

$$\dot{Q}_c = \dot{m}_3 (h_3 - h_4) \tag{4.52}$$

$$\dot{m}_3 = \dot{m}_4 \tag{4.53}$$

$$x_3 = x_4 \tag{4.54}$$

$$\dot{Q}_c = \dot{m}_a c_a (T_{out} - T_{in}) \tag{4.55}$$

Where $\dot{Q}_c$ the reject heat in the condenser is, $\dot{m}_a$ is the mass flow rate of air, c_a is the specific heat of air.

The exergy equation is:

$$(\dot{E}_d)_{con} = (\dot{E}_3 - \dot{E}_4) - (\dot{E}_{11} - \dot{E}_{10}) \quad (4.56)$$

$(\dot{E}_d)_{con}$ is the exergy destruction in the condenser.

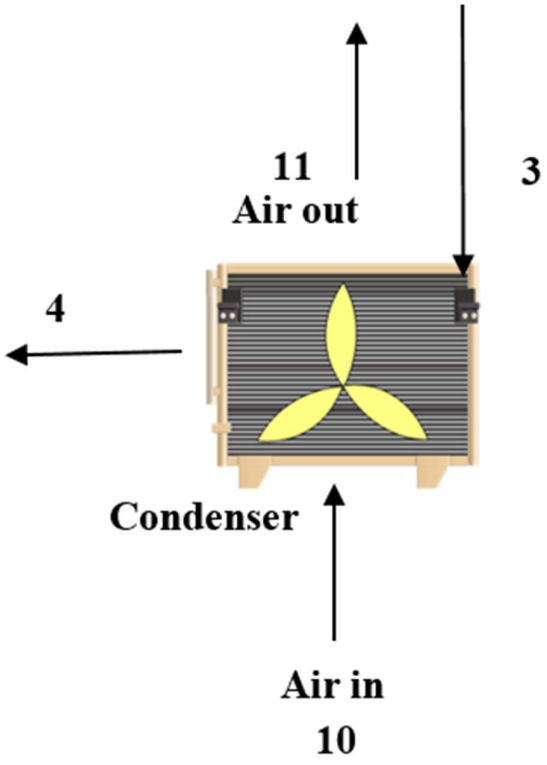

Figure (4.10) Condenser

C- Heat Exchanger (HEi)

There are two heat exchangers in this work. The main function of the heat exchanger is heating or cooling the working fluid. All heat exchangers have the same analysis as shown in fig (4.11). The mass, energy and exergy balances on this heat exchangers are as follows:

$$\dot{m}_{heat\ in} = \dot{m}_{heat\ out} \quad (4.57)$$

$$\dot{m}_{cold\ in} = \dot{m}_{cold\ out} \quad (4.58)$$

$$(\dot{m}h)_{heat\ in} - (\dot{m}h)_{heat\ out} = (\dot{m}h)_{cold\ out} - (\dot{m}h)_{cold\ in} \quad (4.59)$$

The exergy equation is

$$(\dot{E}_d)_{HX} = (\dot{E}_{heat\ in} - \dot{E}_{heat\ out}) - (\dot{E}_{cold\ out} - \dot{E}_{cold\ in}) \quad (4.60)$$

Where $(\dot{E}_d)_{HX}$ is the rate of the exergy destruction in the heat exchanger.

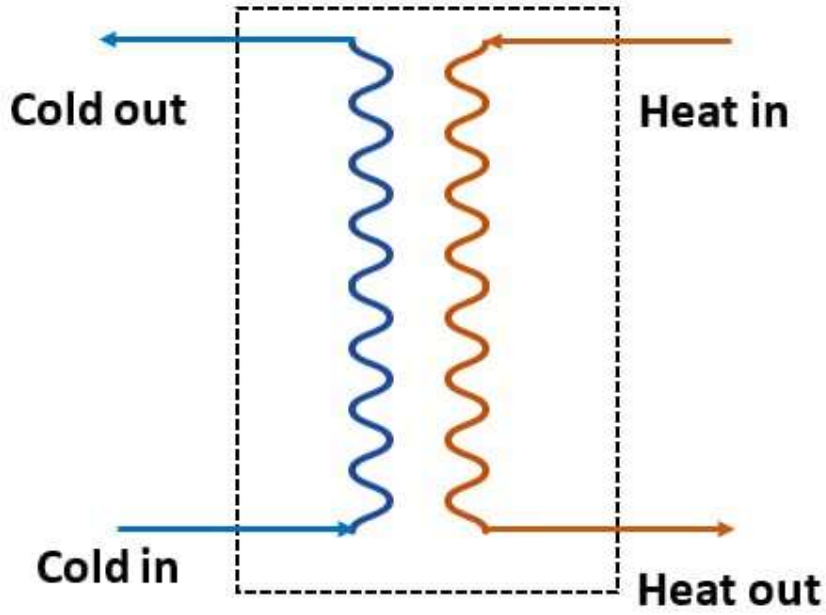

Figure (4.11) the heat exchanger.

4.3.3.5 Expansion process in Turbine.

The expansion process occurs in the turbine is shown in fig (4.12). The mass and energy balances are as follows:

$$\dot{m}_1 = \dot{m}_{\acute{2}} \quad (4.61)$$

$$x_1 = x_{\acute{2}} \quad (4.62)$$

$$(\dot{W}_T)_{act} = \dot{m}(h_1 - h_{\acute{2}}) \quad (4.63)$$

$$(\eta_t)_{isent} = \frac{h_1 - h_{\acute{2}}}{h_1 - h_2} \quad (4.64)$$

$$(\dot{E}_d)_{tur} = (\dot{E}_1 - \dot{E}_{\acute{2}}) - (\dot{W}_T)_{act} \quad (4.65)$$

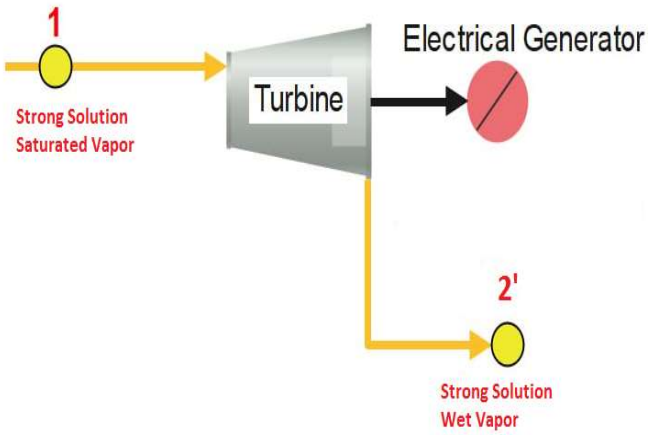

Figure (4.12) the turbine.

Where $h_{\dot{2}}$ is the actual enthalpy at turbine outlet as shown in fig (4.13).

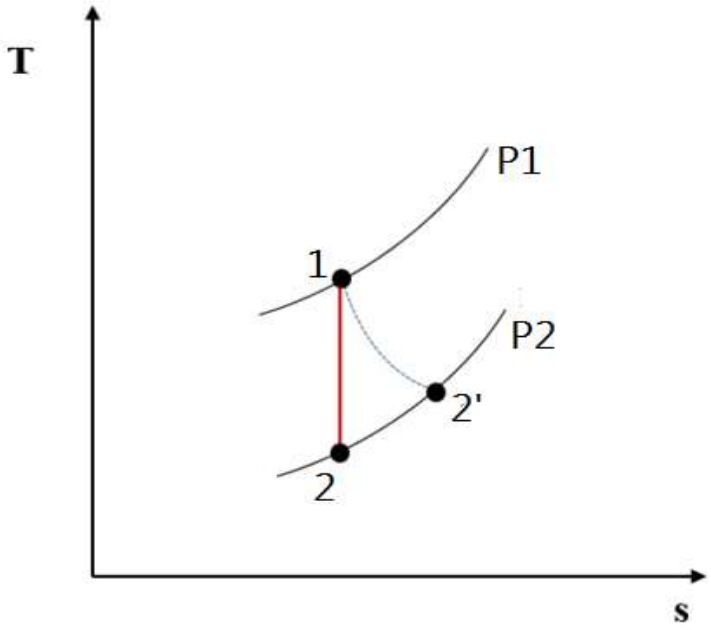

Figure (4.13) turbine expansion on the T-s diagram.

4.3.3.6 Solution Pump

In this studying the work of the pump is neglected. The mass and energy balance are on follows:

$$\dot{m}_4 = \dot{m}_5 \qquad (4.66)$$

$$x_4 = x_5 \tag{4.67}$$

$$h_5 = h_4 \tag{4.68}$$

$$\dot{W}_p = \dot{v}_f * (P_5 - P_4) \tag{4.69}$$

The rate of exergy destruction in the pump is obtained from exergy balance on the pump on follows:

$$(\dot{E}_d)_{pump} = (\dot{E}_4 - \dot{E}_5) + \dot{W}_P \tag{4.70}$$

Where

v_f is the specific volume of the working solution assumed to be sub-cool liquid at HRVG pressure. $\dot{W}_P$ is neglected.

$(\dot{E}_d)_{pump}$ is the rate of the exergy destruction in the pump.

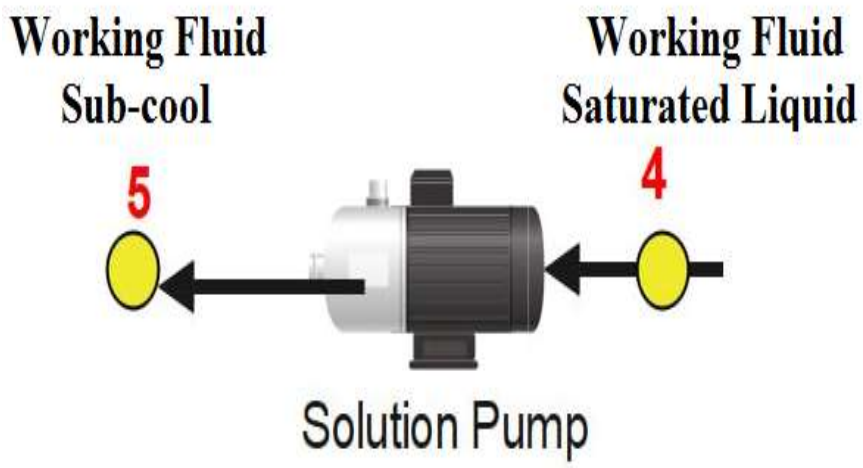

Figure (4.14) the Solution Pump.

4.4 The Specific Exergy, Exergy destruction and Exergy Efficiency

The specific exergy is the maximum possible useful work obtained from any process. Equation (4.71) is used to calculate the specific exergy of a flow process. Exergy destruction is the energy losses during the components, the equation (4.73) is used to calculate the exergy destruction in each

components. Exergy efficiency is the ratio between the network and net of the exergy, the equation (4.77) is used to calculate the exergy efficiency.

$$e = h - T_0 s \tag{4.71}$$

$$\dot{E}^{\cdot} = \dot{m}[h - h_o - T_o(s - s_o)] \tag{4.72}$$

$$\dot{E}_d = \dot{E}_{in} - \dot{E}_{out} \tag{4.73}$$

The total exergy destruction in the cycle is

$$(\dot{E}_d)_{total} = \sum \dot{E}_{di} \tag{4.74}$$

4.5 Cycle Exergy Efficiency

The net power obtained from equation (4.63).

$$\dot{E}_{in} = \dot{E}_{12} - \dot{E}_{14} \tag{4.75}$$

Where $\dot{E}_{in}$ is the total exergy obtained from the hot gases.

$$\dot{E}_{in} = \dot{W}_{net} + (\dot{E}_d)_{total} \tag{4.76}$$

After that calculate the exergy efficiency η_{ex} .

$$\eta_{ex} = \frac{\dot{W}_{net}}{(\dot{E}_{in} - \dot{E}_{out})_{hot\ gases}} \tag{4.77}$$

Where η_{ex} is the exergy efficiency (%).

4.6 Algorithm Program to Find the Thermodynamic Properties of Working Fluid (Ammonia–Water Mixture)

The algorithm has been prepared to identify the region for thermodynamic properties generation using MATLAB codes

```
%DIFFERENT PHASES OF AMMONIA-WATER MIXTURE
if(((T-Tbp)> =-0.05)&&((T-Tbp))< =0.05))||(T==Tbp)
%1. saturated liquid mixture
df=0
```

```
RGN=1
elseif (T<Tbp&&T<Tdp)
%2. Sub-cooled liquid mixture
df=0
RGN=2
Elseif(((T-Tdp)> =-0.05)&&((T-Tdp)< =0.05))||(T==Tdp)
%3. Saturated vapor mixture
df=1
RGN=3
elseif (T>Tbp&&T<Tdp)
%4. Liquid-vapor mixture
RGN=4
Elseif(T>Tdp)
%5. Superheated mixture
df=1
RGN=5
end
switch(RGN)
case1
hm=(1-df)*hf+df*hg2;
sm=(1-df)*sf+df*sg2;
vm=(1-df)*vf+df*vg2;
Tdp=Tdp-273.15;
Tbp=Tbp-273.15;
case2
if(((Tbp-Tdp)> =-1)&&((Tbp-Tdp))< =1))
df=1
end
hm=(1-df)*hf+df*hg2;
sm=(1-df)*sf+df*sg2;
vm=(1-df)*vf+df*vg2;
Tdp=Tdp-273.15;
Tbp=Tbp-273.15;
hg1=0;
hg2=0;
case3
hm=(1-df)*hf+df*hg2;
```

```
sm=(1-df)*sf+df*sg2;
vm=(1-df)*vf+df*vg2;
Tdp=Tdp-273.15;
Tbp=Tbp-273.15;

case4
%AMMONIA-WATER LIQUID MIXTURE
hm=(1-df)*hf+df*hg2;
sm=(1-df)*sf+df*sg2;
vm=(1-df)*vf+df*vg2;
Tdp=Tdp-273.15;
Tbp=Tbp-273.15;

case5
hm=(1-df)*hf+df*hg2;
sm=(1-df)*sf+df*sg2;
vm=(1-df)*vf+df*vg2;
Tdp=Tdp-273.15;
Tbp=Tbp-273.15;
End
```

Chapter Five

Results and Discussions

Chapter Five: Results and Discussions

5.1 Introduction

In this chapter the results are presented and discussed. The results are divided into two parts theoretical and experimental. The theoretical part includes studying the effect of the operating conditions on the performance of different Kalina cycles (SKCS, MKCS1 and MKCS2). The operating conditions are maximum pressure, minimum pressure, ammonia mass fraction and dryness fraction. The performance parameters of the cycles are thermal efficiency, net power, exergy efficiency and exergy destruction. The experimental part includes the results of an experimentally modified version of Kalina cycle corresponds to the theoretical cycle MKCS1. It is named as MKCSE. Then the results include the effect of the operating conditions on the performance of MKCSE. The experimental and the theoretical results are compared.

5.2 Validation of the Theoretical Results

To ensure the validity of theoretical results of the present code developed using MATLAB Multiphasic software, the outcomes of the present code were compared with the results of other researchers. The validation was against the results of **Srinivas et al [2].** The theoretical MATLAB code was applied for simple Kalina using same operating conditions used by ref **[2]**. The operating conditions are the temperature of the hot gases, the inlet temperature of the turbine, ammonia mass fraction at turbine inlet and the dryness fraction at separator inlet which are: 175℃, 160℃, 0.85 and 0.1569 respectively. Also the high pressure and low pressure are 37.67 bar and 2.58 bar respectively. All the results of the present work and that of ref **[2]** using present code are shown in tables (5.1) and (5.2).

There is a good agreement with the previous works. The deviation in thermal efficiency and net power is 4.445% and 4.841% respectively.

Table (5-1) Comparison of Performance Parameters Obtained From Present Work (P) and Srinivas Et Al. Work (R)

Case	Srinivas et al.	Present work	Deviation (%)
$\dot{Q}_{in}$ (kW)	1366.358	1360.698	0.414239
$\dot{Q}_{rej}$ (kW)	1254.551	1248.433	0.48761
$\dot{W}_{net}$ (kW)	86.6457	82.45098	4.841231
Cycle/Eff % η_{th}	6.341361	6.059462	4.445399

Table (5-2) Comparison of Present results (P) with Srinivas et al. Results (R) for Each Point in The Cycle.

Point	P (bar)	X	T (℃)			h (kJ/kg)			S (kJ/kg K)			M (kg/s)			DF		
			R	P	D%	R	P	D%	R	P	D%	R	P	D%	R	P	D%
1	37.67	0.85	160	159.9894	0.0066165	1707.4	1707.565	0.009658	4.9	4.885	0.1007	0.27	0.25962	3.84346	1	1	0
2	2.58	0.85	64.37	65.12469	1.17242591	1386.13	1389.985	0.2781	5.2	5.077	2.3537	0.27	0.25962	3.84346	0.86621	0.86838	0.25052
3	37.67	0.4	76.09	74.97865	1.46057301	663.47	654.3049	1.381394	2.6	2.420	7.9634	1.72	1.72	0	0.32248	0.318459	1.24695
4	37.67	0.4	35	35.32076	0.91646171	-72.57	-71.5286	-1.43509	0.4	0.391	0.3841	1.72	1.72	0	0	0	0
5	37.67	0.4	35.82	35.32076	1.39374204	-65.92	-71.5286	-8.50812	0.4	0.391	2.125	1.72	1.72	0	0	0	0
6	37.67	0.4	141.31	140.1648	0.81042347	424.79	421.717	0.723411	1.76	1.753	0.3644	1.72	1.72	0	0	0	0
7	37.67	0.4	160	159.9894	0.0066165	737.82	719.5749	2.472833	2.5	2.395	4.1851	1.72	1.72	0	0.1569	0.1569	0
8	37.67	0.32	160	159.9894	0.0066165	530.71	523.5173	1.355295	1.99	1.753	11.880	1.45	1.46037	0.71568	0	0	0
9	2.58	0.32	78.9	77.786547	1.2855693	533.15	523.5173	1.806749	2.16	2.009	6.9764	1.45	1.46037	0.71568	0.22474	0.220538	1.87074

5.3 -Repeatability

To ensure the repeatability of experimental results, many tests are repeated under same operation conditions for MKCSE at P_{min}=2 bar, x=0.85 and DF=0.3. The tests are repeated five times every day along five days. Fig (5.1) shows the repeatability test, some differences between these tests are noticed. The maximum deviation is 2.7%. Same trend is shown for all tests

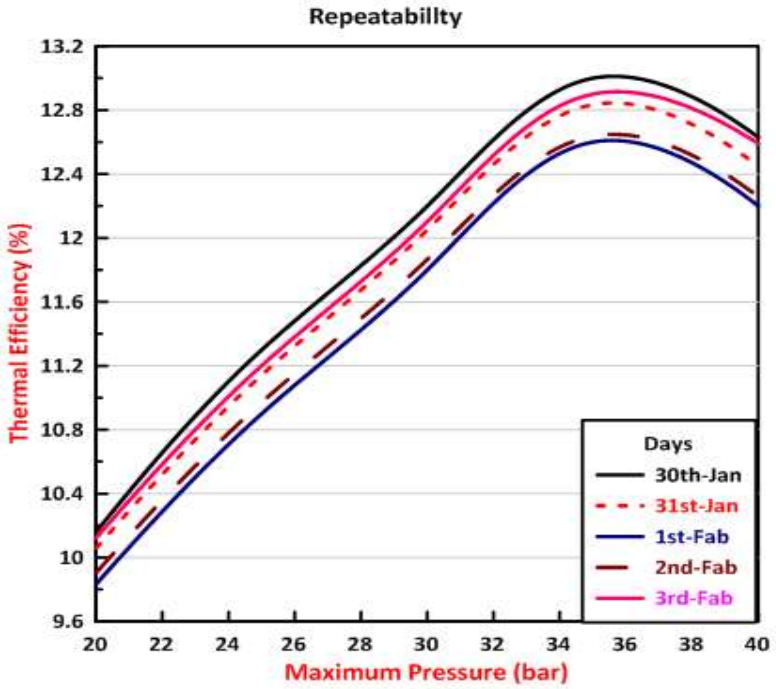

Figure (5.1) Repeatability for MKCSE

5.4 -Uncertainty and Error Analysis

Uncertainty is a measure of the lack of knowledge or precision in a measurement or calculation. It refers to the degree of doubt or the range of values within which the true value of a quantity could lie. In other words, it is the amount by which a measurement or calculation might deviate from the true value. The standard uncertainty (S.U) can be calculated by equation (5.1) suggested by Bell **[72]** as:

$$SU = \frac{SD}{\sqrt{Ni}} \qquad (5.1)$$

Where,

Ni is the total number of measurements

S.D is the standard deviation which is calculated as:

$$S.D = \sqrt{\frac{\sum_{i=1}^{N}\left(X_i - X_{average}\right)^2}{\left(N-1\right)}} \qquad (5.2)$$

$X_{average}$ is the average readings of temperature. The average experimental values of readings in each pipe which were repeated N times. The value of average readings is calculated as:

$$X_{average} = \frac{1}{N}\sum_{i=1}^{N} X_i \ldots\ldots \qquad (5.3)$$

Where X_i is represented the values for measurements data of temperature or any function measured in each pipe. Then, all experimental analysis depending on measuring values are uncertain. Tables (5-4) and (5-5) show the uncertainty tests.

Table (5-4) Uncertainty of Temperature Measurement Point.

Temperature measurement point (°C)	S.U Value	Temperature measurement point (°C)	S.U Value
T_1	0.354859	T_6	0.305012
T_2	0.295101	T_7	0.452306
T_3	0.154573	T_8	0.65321
T_4	0.127331	$T_{8'}$	0.339914
T_5	0.198375	T_9	0.295528
$T_{5'}$	0.270039		

Table (5-5) Uncertainty of Calculated Variables

Variable	S.U Value
η_{th} (%)	0.066002331
$\dot{W}_{net}$(kW)	0.001371431
η_{ex} (%)	0.143281116

5.5 - T-s Diagrams of Analyzed Kalina Cycles

Simple Kalina Cycle System (SKCS) is modified to MKCS1 by addition of a heat exchanger after the separator to recover part of heat of the weak solution, which is otherwise rejected to the environment, to heat the working fluid before entering the HRVG. Then MKCS1 is modified to MKCS2 by adding other heat exchanger to recover the heat from hot strong solution which comes from turbine to heat the cold working fluid which comes from the pump. The experimental cycle MKCSE corresponds to the MKCS1.

Figs (5.2-5.4) illustrate simple Kalina cycle system on the T-x diagram, T-s diagram and schematic of SKCS respectively. The SKCS consists of heat recovery vapor generator, separator, turbine, throttling valve, mixer, condenser and pump. The state of the working fluid during SKCS, at the separator inlet (point7) is wet vapor. The wet vapor separates into two parts in the separator, strong solution (saturated vapor) and weak solution (saturated liquid). The strong solution inters the turbine (point1). At the turbine entrance the quality of the vapor is saturated vapor at maximum pressure. Then the saturated vapor expands in the turbine and it leaves as a wet vapor (point2).The weak solution inters the throttling valve (point8) as saturated liquid and leaves it as a saturated liquid (point9). The strong solution (point2) and the weak solution (point9) will mix with each other in the mixer (absorber) and the solution leaves the mixer (absorber) as wet vapor at minimum pressure (point3). After that the solution enters the condenser and leaves it as a saturated liquid (point4). The solution is pumped

back to the HRVG as sub-cool liquid at maximum pressure to enter the HRVG, (point5) and heated to (point6) which is less than the boiling temperature of the working fluid at maximum pressure. The solution leaves the HRVG as wet vapor at maximum pressure point7 to complete the cycle.

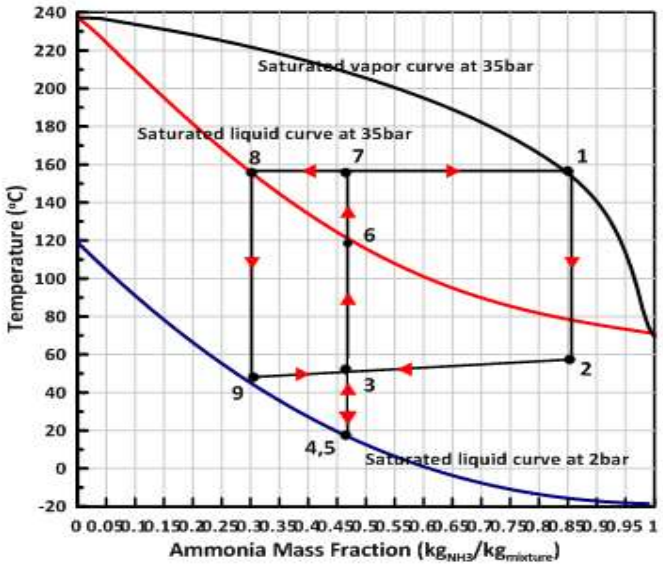

Figure (5.2) T-x Diagram of SKCS at P_{max}=35 bar, P_{min}=2 bar, X=0.85 and DF=0.3

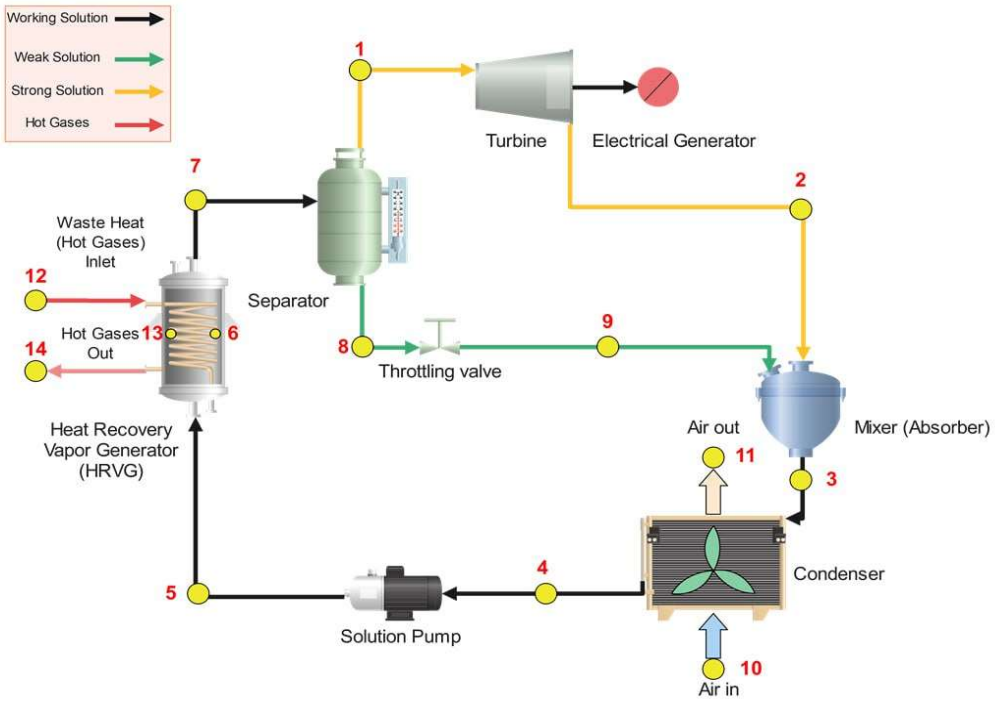

Figure (5.3) Simple Kalina Cycle System (SKSC) [2]

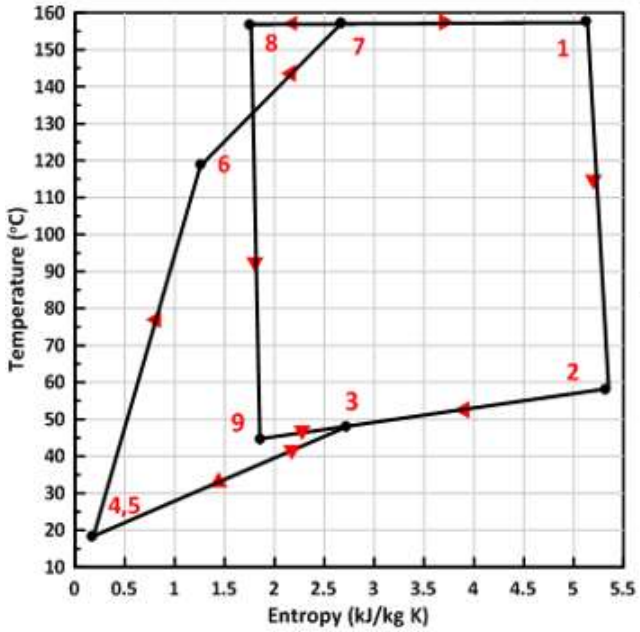

Process	Type
1-2	Irreversible expansion
2-3-9	Adiabatic Mixing
3-4	Condensing
4-5	Pumping
5-6-7	Heat Addition in HRVG
1-7-8	Separation
8-9	Throttling

Figure (5.4) T-s Diagram for SKCS at P_{max}=35 bar, P_{min}=2 bar, x=0.85 and DF=0.3

Fig (5.5) shows a schematic diagram for MKCS1 and MKCSE while figs (5.6 and 5.7) show T-s diagram for the MKCS1 and MKCSE respectively. MKCS1 and MKCSE consist of same components as SKCS except a heat exchanger between the separator and the throttling valve to recover heat from the weak solution which comes from the separator to heat the working fluid which comes from the pump before entering the HRVG. The weak solution enters the heat exchanger as saturated liquid at maximum pressure (point8) and leaves the heat exchanger at (point8̀). The working fluid enters the heat exchanger at point5 as sub-cool with maximum pressure and it leaves from point5̀. The main difference between the SKCS and MKCS1 is the amount of the rejected heat and heat addition in the HRVG. The rejected heat in SKCS is more than the heat rejected in MKCS1 because the MKCS1 has a heat exchanger to recover some of rejected heat. Also the addition heat in MKCS1 is less than the addition heat in SKCS for the same reason. That's lead to improve to the performance of Kalina cycle.

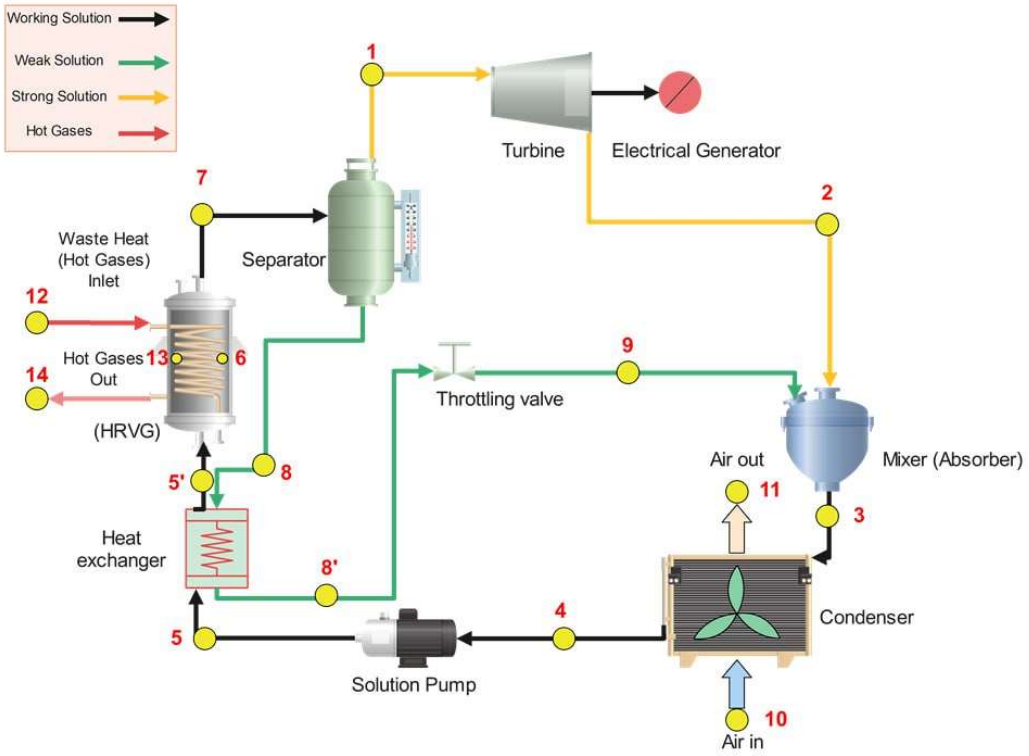

Figure (5.5) Modified Kalina Cycle System (MKCS1)

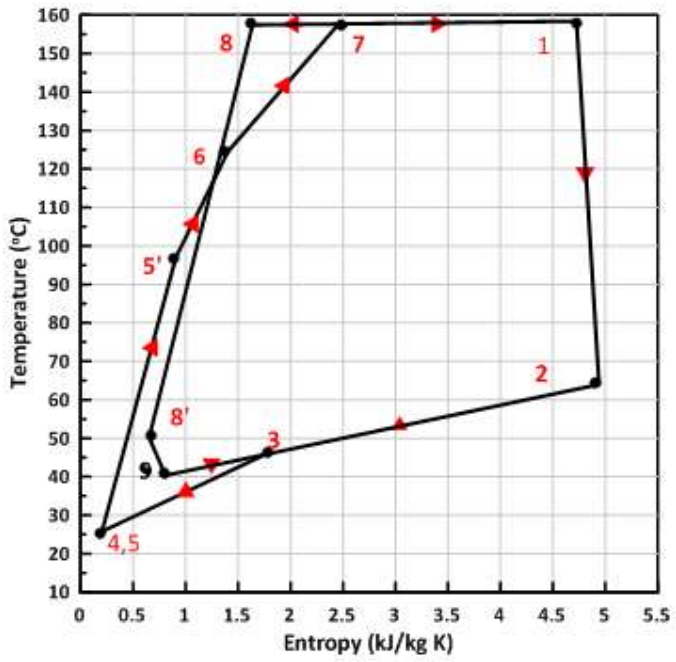

Figure (5.6) T-s Diagram for MKCS1 at P_{max}=35 bar, P_{min}=2 bar, x=0.85 and DF=0.3

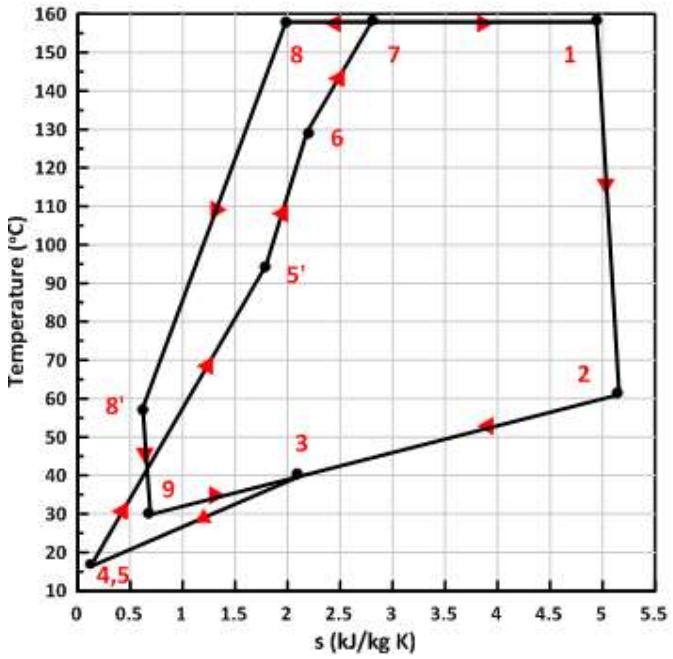

Figure (5.7) T-s Diagram for MKCSE at P_{max}=35 bar, P_{min}=2 bar, x=0.85 and DF=0.3

Figs (5.8) and (5.9) show the MKCS2 on the T-s diagram and the schematic. It consists of the same components as the SKCS1 except a second heat exchanger is added between the turbine and the pump to recover part of heat of the wet vapor coming from the turbine to heat the working fluid before entering the first heat exchanger. At the second heat exchanger the strong solution which comes from the turbine enters at point2 and it leaves from point$\grave{2}$. The working fluid which comes from the pump enters at point5 and it leaves from point$\grave{5}$. At first heat exchanger the weak solution which comes from separator enters at point 8 and it leaves from point$\grave{8}$, the working fluid enters the first heat exchanger at point$\grave{5}$ and it leaves from point$\grave{\grave{5}}$. The second heat exchanger helps to reduce the heat rejected (process 3-4) and decrease the heat addition (process$(5-\grave{5})$, $(\grave{\grave{5}}-7)$ as shown in the fig (5.9).

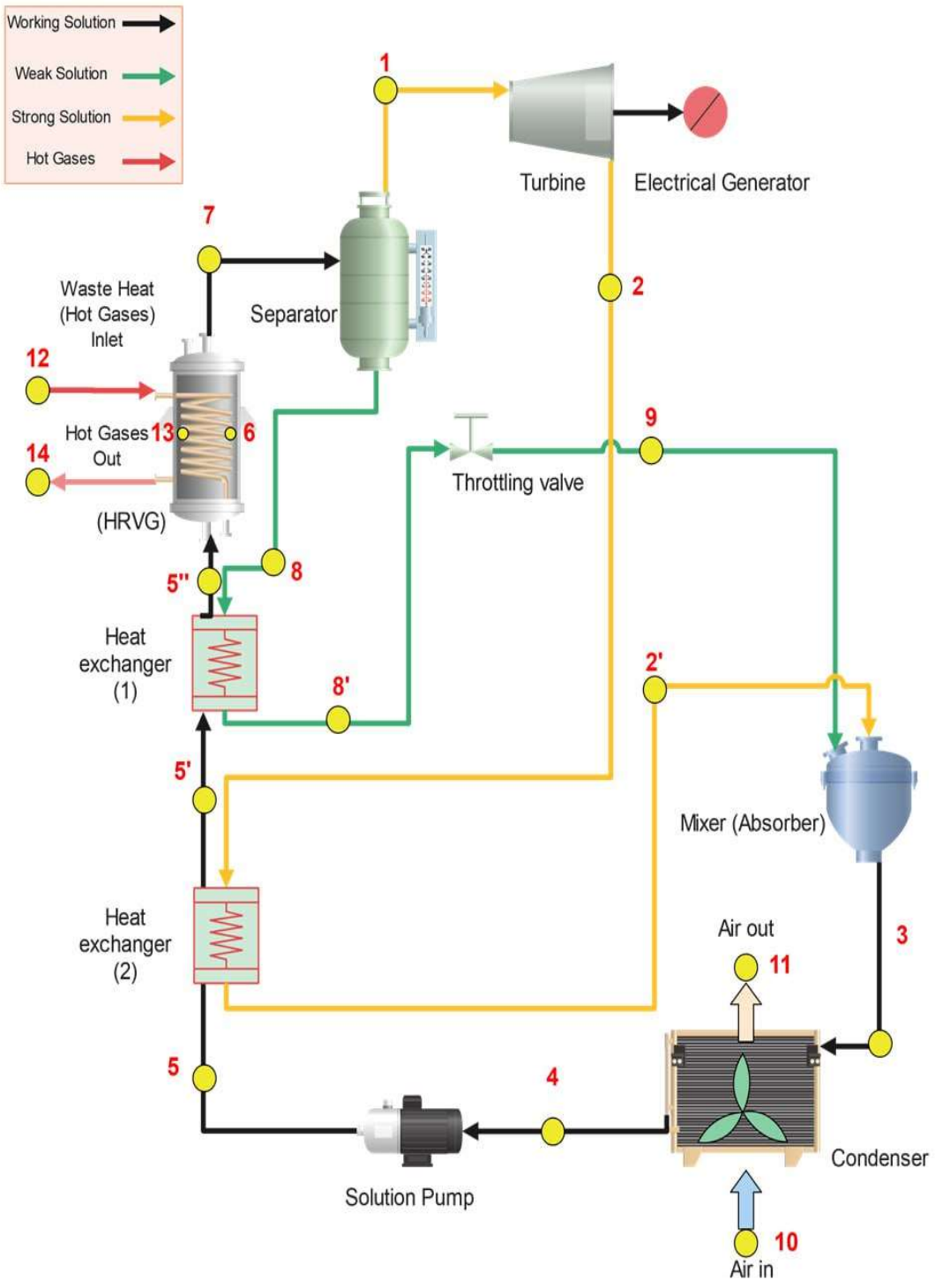

Figure (5.8) Modified Kalina Cycle System (MKCS2)

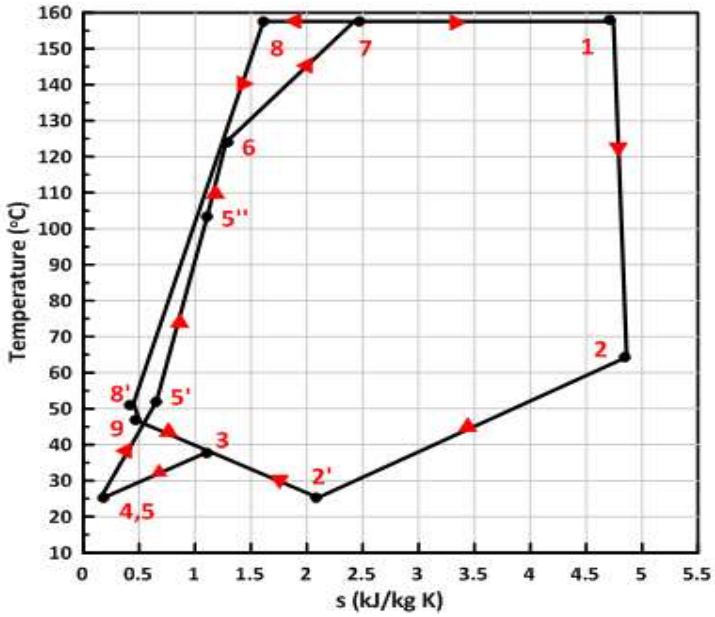

Figure (5.9) T-s Diagram for MKCS2 at P_{max}=35 bar, P_{min}=2 bar, x=0.85 and DF=0.3

5.6 Theoretical Results

A mathematical algorithm and a computer program, developed by (MATLAB) are used to solve the equations to predict all operating and performance parameters of the cycle. The predicted results are compared with measured results to validate its correctness. The effect of dryness fraction, ammonia mass fraction, maximum pressure and minimum pressure on the performance of simple Kalina cycle (SKCS), first modified of Kalina cycle system (MKCS1) and second modified of Kalina cycle system (MKCS2) are presented in the following sections.

5.6.1 -The Relationship between the Ammonia Mass Fraction and Mass Flow Rate

Fig. (5.10) shows the relationship between ammonia mass fraction and the mass flow rate with different maximum pressures at constant minimum pressure of 2 bar and a dryness fraction of 0.3. The working fluid consists of ammonia and water. Due to experimental difficulties in changing the ammonia mass fraction working fluid for each test, the ammonia mass fraction is changed by adding the amount of ammonia required and keeping

the mass of water constant. This leads to increase the mass flow rate of the working fluid when the ammonia mass fraction is changed after each maximum pressure. The high ammonia mass fraction in the mixture means low enthalpy of the working fluid and low the temperature of evaporation of the mixture. Therefore, the increase in the mass flow rate means increasing the working fluid flow rate for same high pressure. But as the P_{max} increases the mass flow rate must be reduced as shown in fig (5.11).

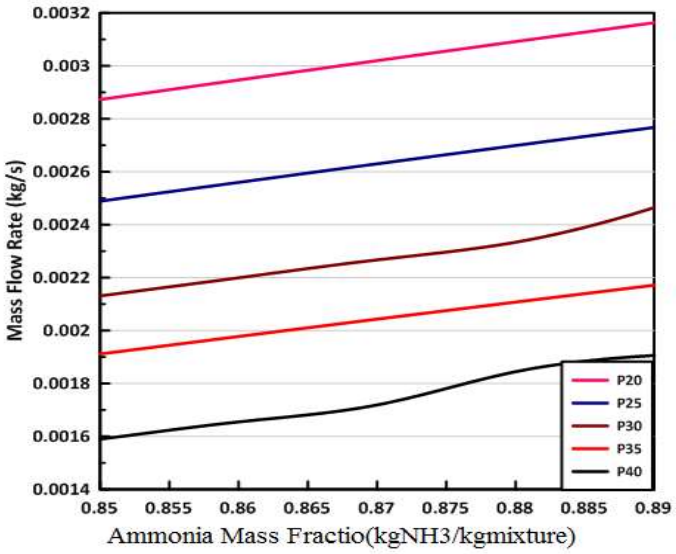

Figure (5.10) the Effect of the Ammonia Mass Fraction on the Mass Flow Rate

5.6.2 -The Relationship between the Maximum Pressure and Mass Flow Rate

Fig. (5.11) displays the effect of the maximum pressure on the mass flow rate with different ammonia mass fraction at constant minimum pressure of 2 bar and dryness fraction 0.3. When the mass flow rate decreases the maximum pressure increases. As the pressure in the HRVG increases the saturation temperature of this working fluid at this pressure increases. Therefore the mass flow rate must be reduced for same heat input to attain that pressure. Therefore the retention time of the fluid is in the HRVG is

increased and more heat is transferred to the working fluid. This is clear in fig (5.11).

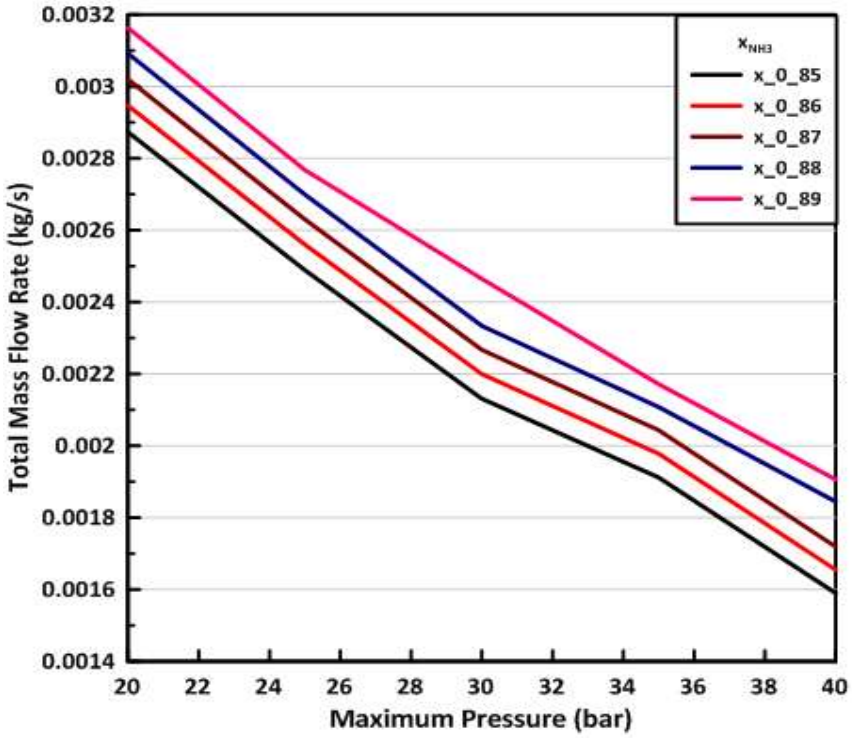

Figure (5.11) the Effect of the Maximum Pressure on the Mass Flow Rate

5.6.3 -The Effect of Dryness Fraction on the performance

5.6.3.1 Thermal Efficiency

Figs (5.12-5.17) show influence of dryness fraction (DF) at separator inlet on thermal efficiency for different ammonia mass fractions in SKCS, MKCS1 and MKCS2 at constant maximum pressure and minimum pressure. All figures show same behavior. It is noticed that there is an inflection point at DF=0.3 where the efficiency reaches maximum value and then decreases with further increase in DF. The same behavior is shown for all ammonia mass fraction. It is noticed that as the DF increases the cycle efficiency increases and reaches the maximum value at DF equal 0.3 for all ammonia concentration. This is due to the combined effect of the net power generated and the required heat input for values less than 0.3 the effect of the net power

is dominant which for values larger than 0.3 the effect of heat input is dominant. The same behavior is shown for the three cycles but the highest efficiency is obtained with MKCS2 which is 23.88% at DF=0.3, P_{max}=35 bar and P_{min}=2 bar which is due to adding the two heat exchangers. For same operating conditions $\eta_{SKCS} < \eta_{MKCS1} < \eta_{MKCS2}$.

Figure (5.12) Effect of Dryness Fraction on Thermal Efficiency for SKCS at P_{max}=35 bar and P_{min}=2 bar

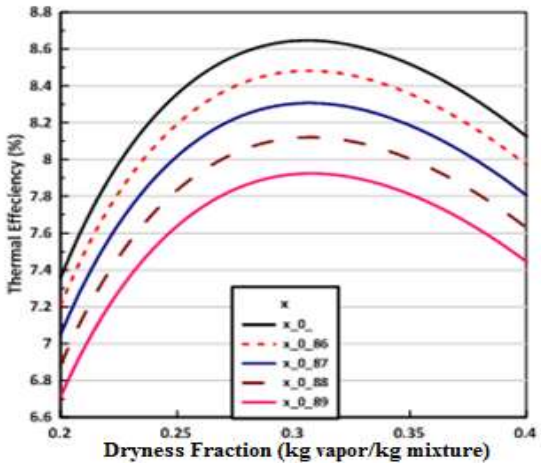

Figure (5.13) Effect of Dryness Fraction on Thermal Efficiency for SKCS at P_{max}=35 bar and P_{min}=3 bar

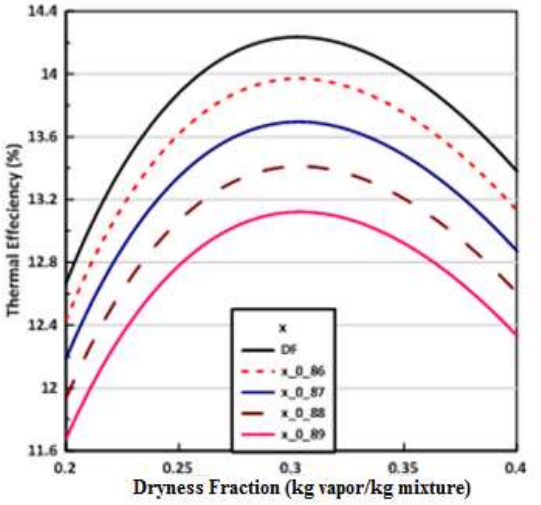

Figure (5.14) Effect of Dryness Fraction on Thermal Efficiency for MKCS1 At P_{max}=35 bar and P_{min}=2 bar

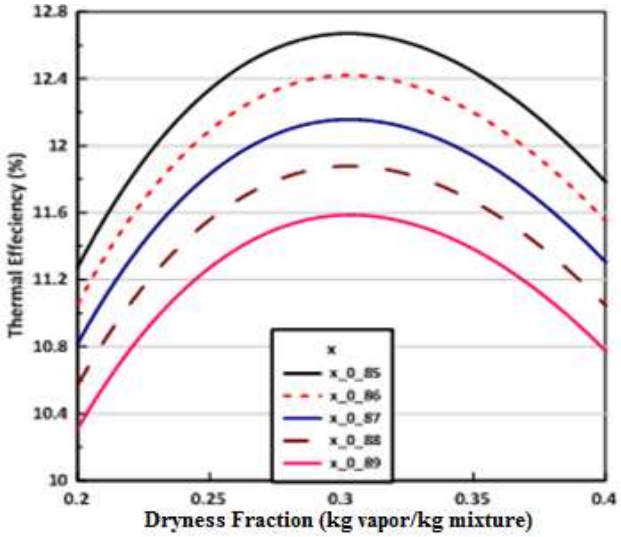

Figure (5.15) Effect of Dryness Fraction on Thermal Efficiency for MKCS1 At P_{max}=35 bar and P_{min}=3 bar

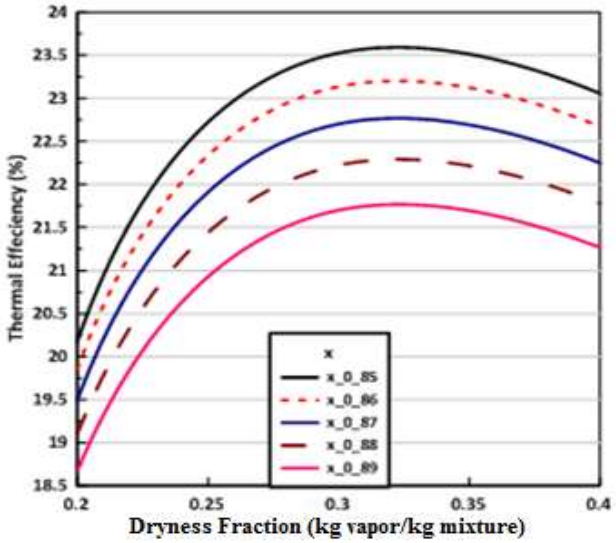

Figure (5.16) Effect of Dryness Fraction on Thermal Efficiency for MKCS2 at P_{max}=35 bar and P_{min}=2 bar

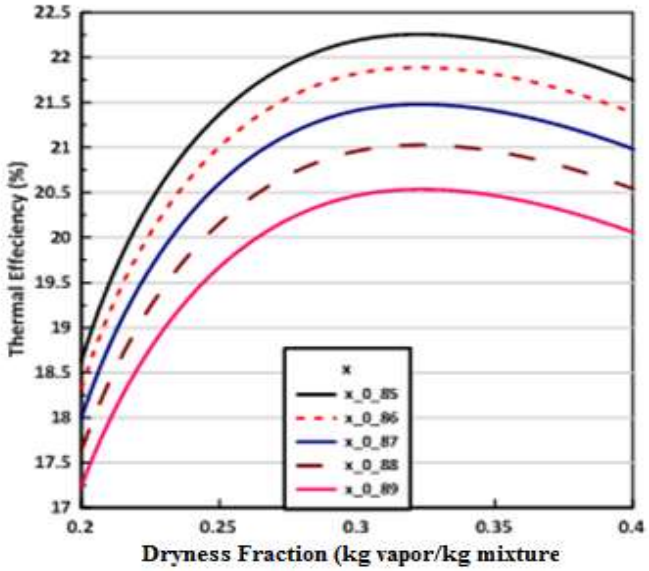

Figure (5.17) Effect of Dryness Fraction on Thermal Efficiency for MKCS2 at P_{max}=35bar and P_{min}=3 bar

5.6.3.2 Net Power

Figs (5.18-5.20) display the effect of the dryness fraction at separator inlet on the net power for different ammonia mass fraction at constant maximum pressure and minimum pressure. When the dryness fraction increases the net power increases due to the increase in mass flow rate of vapor at turbine inlet. As the ammonia mass fraction increases the evaporated mass increases since ammonia evaporates faster than water. Therefore, the vapor contains more ammonia. This reduces the enthalpy of the vapor at turbine inlet which should reduce the power output. The net combined effect of mass flow rate increase and the drop in enthalpy is to increase the power output. The highest value of the net power is 0.58 kW with MKCS2 at DF=0.4. The ratio of the increase of the net power between SKCS and MKCS1 is 27.3% and the ratio of the increase of the net power between SKCS and MKCS2 is 63.6% at conditions P_{min}=2 bar, P_{max}=35 bar and DF=0.3.

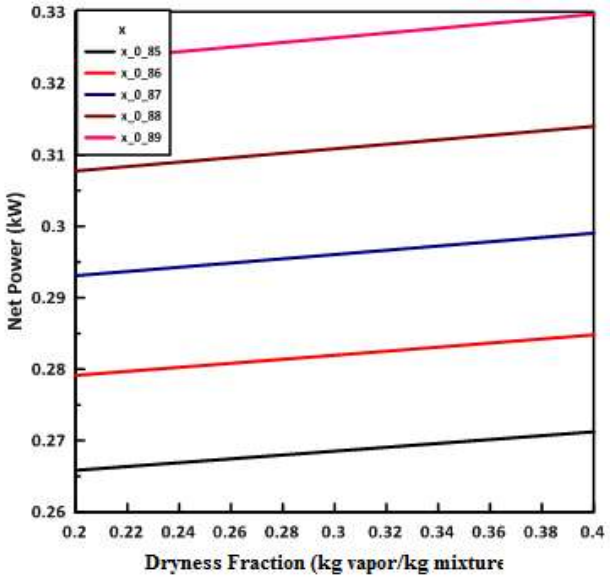

Figure (5.18) Effect of Dryness Fraction on Net Power for SKCS at P_{max}=35 bar and P_{min}=2 bar

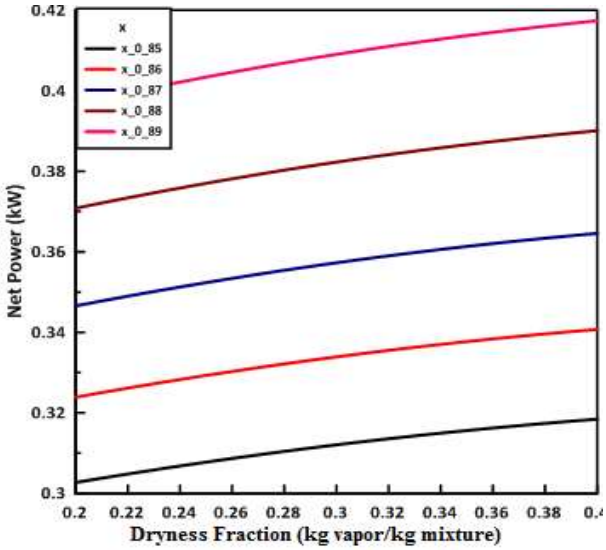

Figure (5.19) Effect of Dryness Fraction on Net Power for MKCS1 at P_{max}=35 bar and P_{min}=2 bar

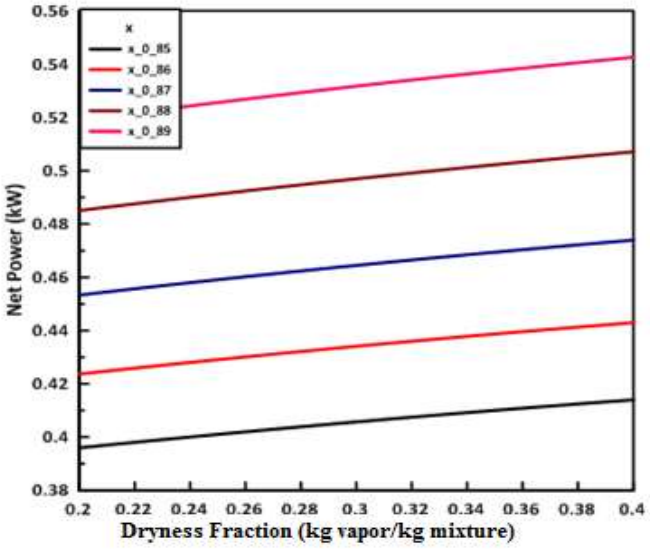

Figure (5.20) Effect of Dryness Fraction on Net Power for MKCS2 at P_{max}=35 bar and P_{min}=2b ar

5.6.3.3 Exergy Efficiency

Figs (5.21-5.23) illustrate the influence of dryness fraction at separator inlet on the exergy efficiency with different ammonia mass fraction at constant maximum pressure and minimum pressure. When the dryness fraction increases the exergy efficiency decreases since more heat is required to increase the amount of vapor that leads to more exergy change across the separator. The highest exergy efficiency with MKCS2 because it has two heat exchangers which means less exergy destruction. It is also shown that the exergy efficiency decreases as ammonia mass fraction increases for all dryness fraction since more heat require and more exergy is destructed. The values of the exergy efficiency for SKCS, MKCS1 and MKCS2 are 26.65%, 33.3% and 66.2% respectively at P_{max}=35 bar and P_{min}=2 bar.

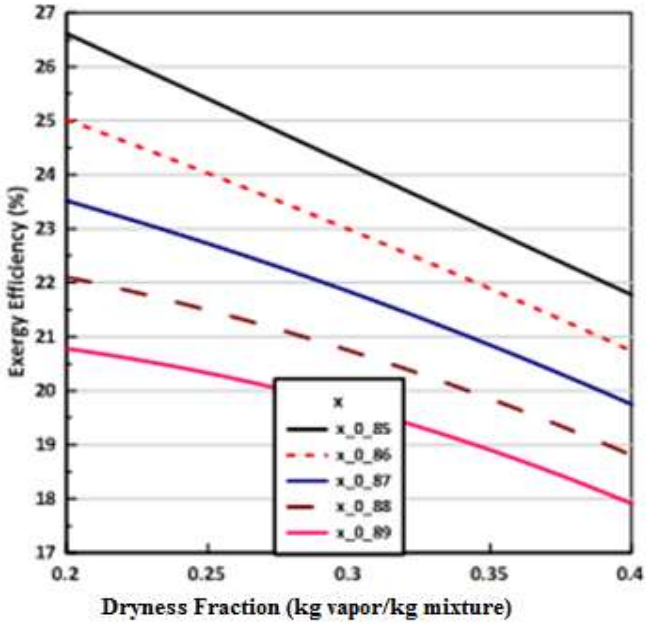

Figure (5-21) Effect of Dryness Fraction on Exergy Efficiency for SKCS at P_{max}=35 bar and P_{min}=2 bar

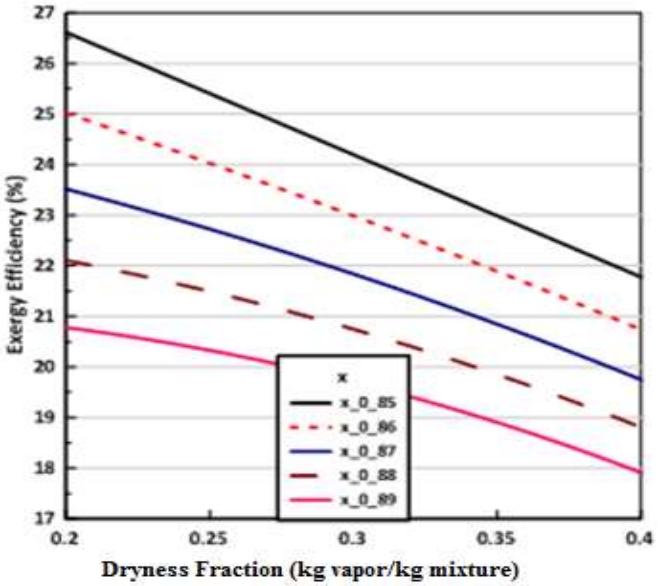

Figure (5-22) Effect of Dryness Fraction on Exergy Efficiency for MKCS1 at P_{max}=35 bar and P_{min}=2 bar

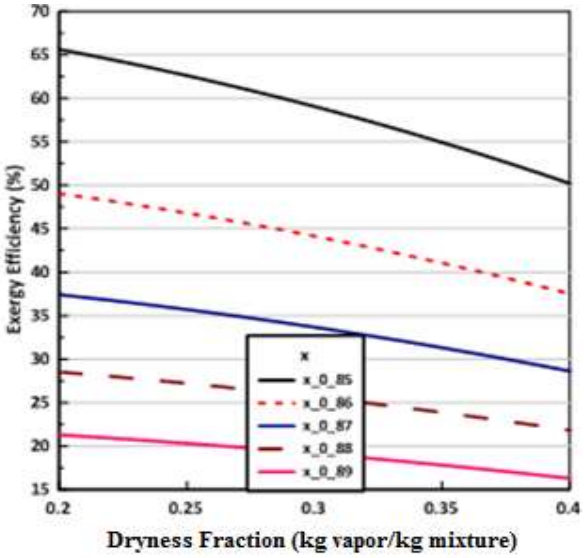

Figure (5-23) Effect of Dryness Fraction on Exergy Efficiency for MKCS2 at P_{max}=35 bar and P_{min}=2 bar

5.6.4 The Effect of ammonia mass fraction on the performance

5.6.4.1- Thermal Efficiency and Net Power

The effect of the ammonia mass fraction at turbine inlet on the thermal efficiency and net power is seen very clearly in figs (5.24-5.26). The trend of the effect of the ammonia mass fraction on the thermal efficiency and net power is same for the three cycles. As ammonia mass fraction at turbine inlet increases the cycle thermal efficiency decreases while the net power increases. This increase in net power is due to the increase in the vapor mass flow rate. However, this increase in vapor mass flow rate is assonated with increase in heat input in the HRVG which causes the reduction in the cycle thermal efficiency. It is found the highest thermal efficiency occurs at x=0.85 and the lowest value occurs at x=0.89. The highest thermal efficiency for SKCS, MKCS1 and MKCS2 is 9.44%, 14.4% and 23.53% respectively. After these modifications is found the thermal efficiency is improved about 52.4% to 149.25%. The highest net power is found at x=0.89 and the lowest net power is found at x=0.85. The net power for SKCS, MKCS1 and MKCS2

is 0.388 kW, 0.45 kW and 0.57 kW respectively. The net power is improved by about 15.98% to 46.91%. It is clear from these figs that the highest net power is found at P_{max}=20 bar, P_{min}=2 bar and x=0.89. The points of intersection for thermal efficiency curve and net power curve represent the optimum operating conditions under the mentioned parameters.

Fig (5.24) shows the optimum operating conditions for SKCS at 35 bar, 30 bar and 25 bar are (x=0.89, thermal efficiency=8.7% and net power=0.35 kW), (x=0.873, thermal efficiency=8.62% and net power=0.32 kW) and (x=0.856, thermal efficiency=8.55% and net power=0.32 kW) respectively.

Fig (5.25) shows the optimum conditions for MKCS1when the curve of the thermal efficiency intersected with the curve of the net power. The optimum operating conditions for 25 bar are x=0.855, thermal efficiency=12.25% and net power=0.314 kW. The optimum conditions for 30 bar are x=0.87, thermal efficiency=12.7% and net power=0.327 kW. The optimum conditions for 35 bar are x=0.883, thermal efficiency=13.3% and net power=0.35 kW.

Fig (5.26) shows the optimum operating conditions for MKCS2. The intersection points as shown in the figure represent the optimum conditions at 25 bar, 30 bar and 35 bar. The optimum operating conditions are at 25 bar are x=0.85, thermal efficiency=19.7% and net power=0.404 kW, at 30 bar are x=0.87, thermal efficiency=21% and net power=0.41 kW, at 35 bar are x=0.883, thermal efficiency=22% and net power=0.455 kW. It is noticed that the range of the optimum pressure from 25 bar to 35 bar and also the optimum ammonia mass fraction is from 0.85 to 0.89. In this work, the conditions chosen are P_{max}=35 bar, x=0.85, P_{min}=2 bar and DF=0.3 as the best parameters are chosen.

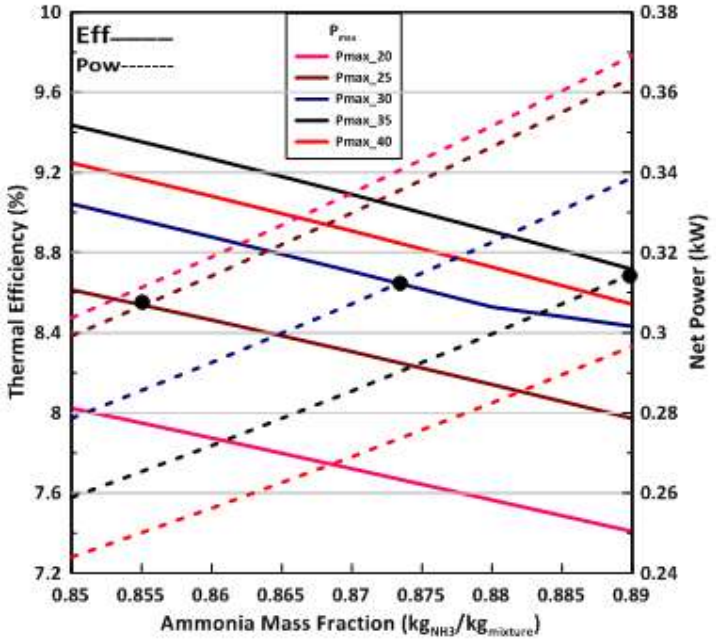

Figure (5.24) Effect of Ammonia Mass Fraction on Thermal Efficiency and Net Power for SKCS with Different Maximum Pressure at P_{min}=2 bar and DF=0.3

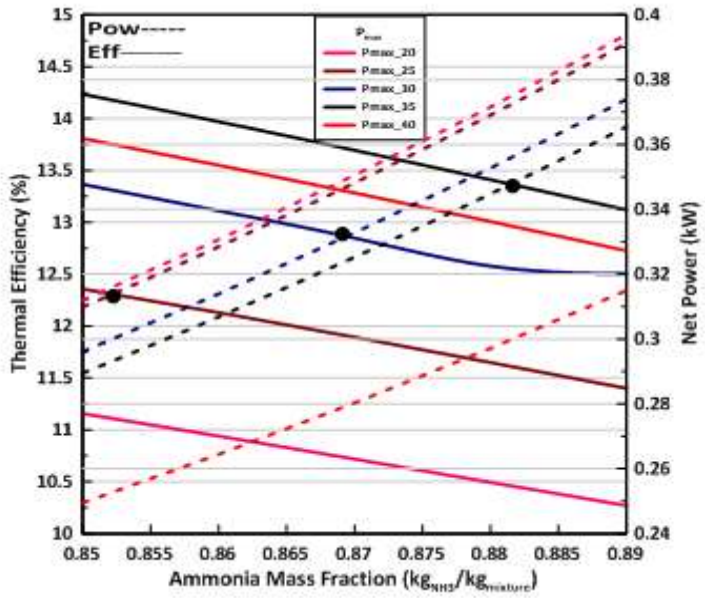

Figure (5.25) Effect of Ammonia Mass Fraction on Thermal Efficiency and Net Power for MKCS1 at P_{min}=2 bar and DF=0.3

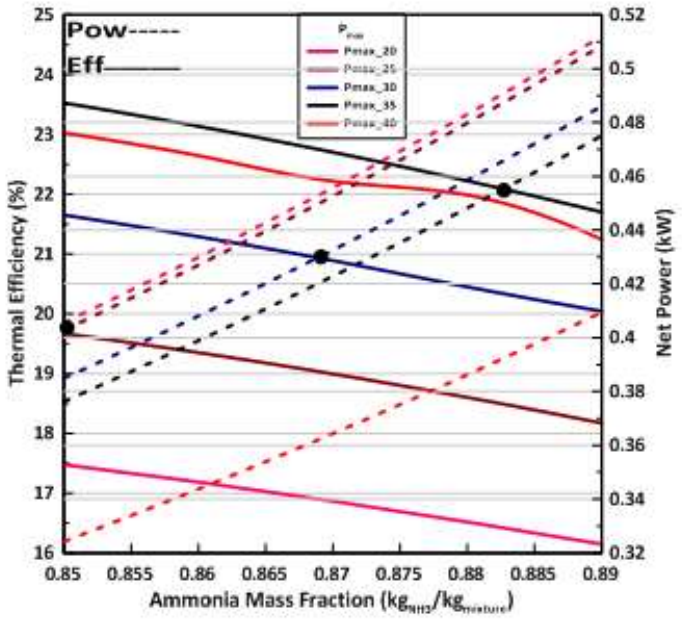

Figure (5.26) Effect of Ammonia Mass Fraction on Thermal Efficiency and Net Power for MKCS2 at P_{min}=2 bar and DF=0.3

5.6.4.2- Exergy Efficiency

The effect of ammonia mass fraction on cycle exergy efficiency with different maximum pressures at constant minimum pressure is shown in figs (5.27-5.29). The trend of variation is the same for all P_{max} and the same for the three cycles. When ammonia mass fraction increases the exergy efficiency decreases because the vapor mass flow rate increases which means the working fluid is fast and it does not gain heat enough that means more exergy destruction. It is clear that the highest exergy efficiency is found at x=0.85 and the lowest at x=0.89. The values of the exergy efficiency for SKCS, MKCS1 and MKCS2 are 24.3%, 30.1% and 59% respectively at P_{max}=35 bar, P_{min}=2 bar, DF=0.3 and x=0.85. The exergy efficiency is improved by about 23.87% to 142.8% compared to SKCS. It is noticed that the highest exergy efficiency is obtained with MKCS2 since more heat is recovered by adding two heat exchangers to the SKCS.

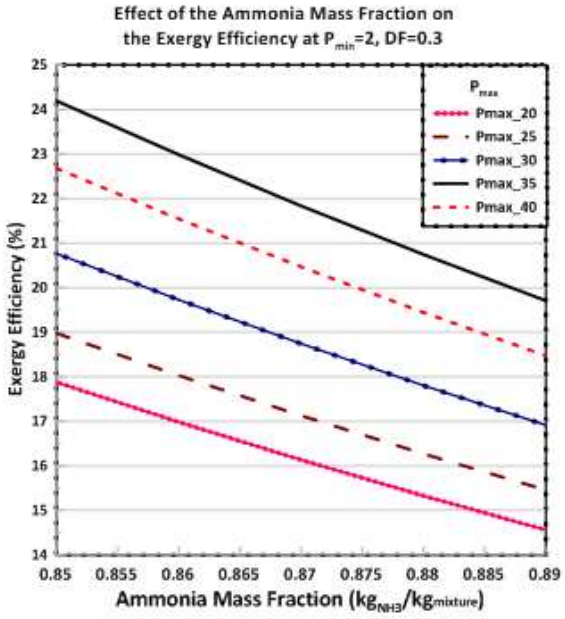

Figure (5.27) Effect of Ammonia Mass Fraction on Exergy Efficiency for SKCS

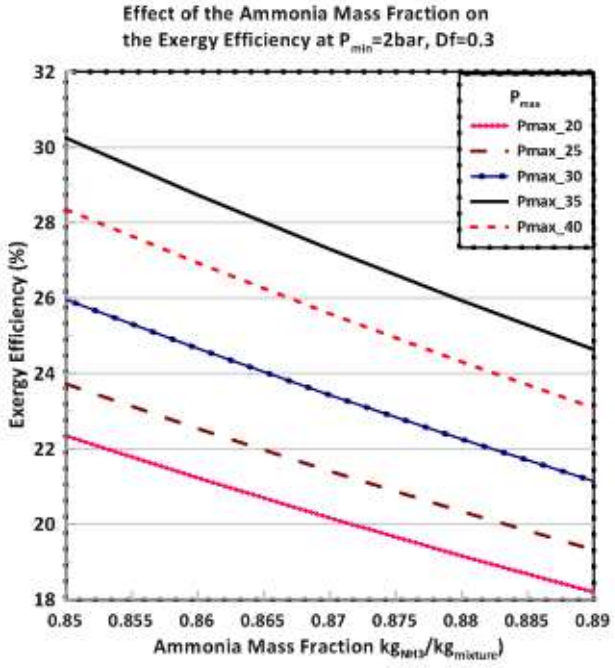

Figure (5.28) Effect of Ammonia Mass Fraction on Exergy Efficiency for MKCS1

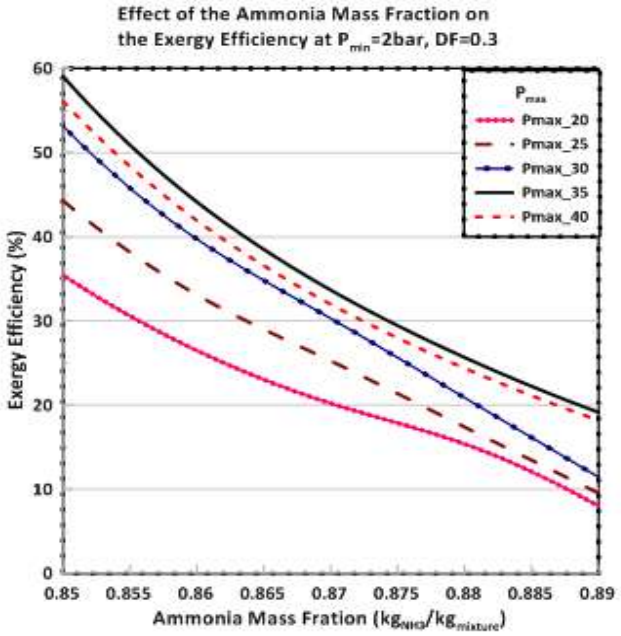

Figure (5.29) Effect of Ammonia Mass Fraction on Exergy Efficiency for MKCS2

5.6.5 The Effect of the maximum pressure on the performance

5.6.5.1 Thermal Efficiency and Net Power

Figs (5.30-5.32) show the effect of maximum pressure on the thermal efficiency and net power for different ammonia mass fraction at constant minimum pressure. The trend of the effect of maximum pressure on the thermal efficiency and net power is same in the three cycles. When the maximum pressure increases the thermal efficiency increases due to the decreasing of the mass flow rate through the HRVG and the increase of vapor enthalpy at turbine inlet. The highest thermal efficiency is found at P_{max}=35 bar and x=0.85for all ammonia mass fraction. After P_{max}=35 bar the thermal efficiency decreases with increase of the maximum pressure. Since the net power decreases faster than the heat input as P_{max} rises, as shown in table (5.6). The highest net power at P_{max}=20 bar and x=0.89. The points of intersection denote the optimum working conditions.

Fig (5.30) shows the optimum operating conditions for SKCS. Which is found at P_{max}=30.8 bar and x=0.88. The optimum thermal efficiency and optimum net power are 8.8% and 0.33 kW respectively.

Fig (5.31) shows the optimum operating conditions for MKCS1. It is noticed that the optimum operating conditions at x=0.88 and P_{max}=33.5 bar. The optimum value of the thermal efficiency is 13.5% and the value of the optimum net power is 0.354 kW.

Fig (5.32) shows the optimum operating conditions for MKCS2. It is found that the value of the optimum maximum pressure and ammonia mass fraction are 34 bar and 0.88 respectively. The value of the optimum thermal efficiency and net power are 21.8% and 0.462 kW respectively.

Table (5.6) shows sample of calculation for thermal efficiency. When the maximum pressure increases the thermal efficiency increases, but it drops at maximum pressure 40 bar because the net power and input heat decrease due to the decrease of the mass flow rate during the cycle. All the information is tabled in table (5.6) at conditions P_{min}=2 bar, x=0.85 and DF=0.3.

Table (5.6) Properties of Aqua-Ammonia at P_{min}=2 bar, x=0.85 and DF=0.3

P1 (bar)	h1(kJ/kg)	h2(kJ/kg)	h5(kJ/kg)	h7(kJ/kg)	$\dot{m}_T$(kg/s)	$\dot{m}_1$(kg/s)	$\dot{W}_{T\,(kW)}$	$\dot{Q}_{in}$(Kw)	Thr-Eff %
20	1690.413	1423.98	-141.139	832.1934	0.002873	0.000842	0.224351	2.796272	8.023202
25	1696.985	1405.976	-149.529	858.0384	0.002489	0.000742	0.216006	2.507615	8.614006
30	1698.014	1388.247	-157.554	882.3115	0.002131	0.000647	0.200379	2.215816	9.043137
35	1698.708	1373.892	-165.207	898.7533	0.001911	0.000591	0.191899	2.033643	9.436223
40	1699.76	1360.531	-165.207	926.9057	0.00159	0.000471	0.159796	1.736259	9.203479

$$\dot{W}_T = \dot{m}_1 * (h_1 - h_2) \quad (5.4)$$

$$\dot{Q}_{in} = \dot{m}_{Total} * (h_7 - h_5) \quad (5.5)$$

$$\eta_{th} = \frac{\dot{W}_T}{\dot{Q}_{in}} \quad (5.6)$$

Where

$\dot{W}_T$ is the power from turbine

$\dot{Q}_{in}$ is the heat input in HRVG

$\dot{m}_{Total}$ is the total mass flow rate during the cycle

$\dot{m}_1$ is the mass flow rate at the turbine entrance

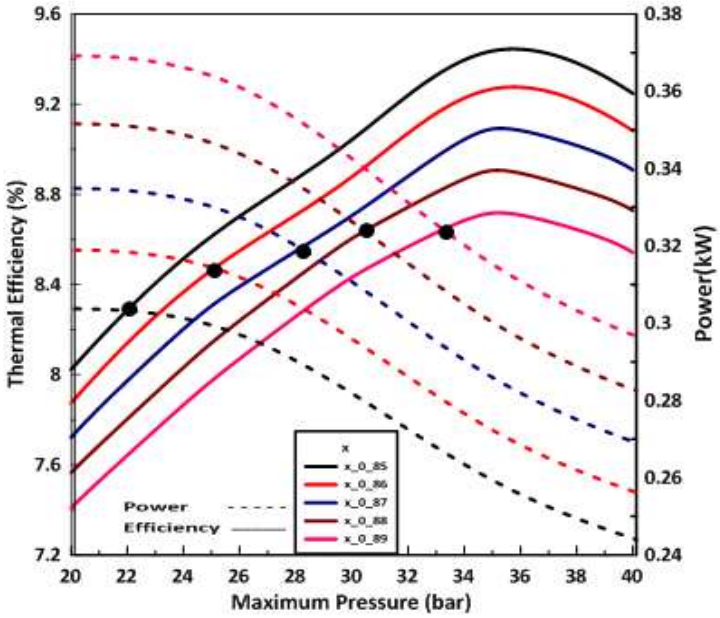

Figure (5.30) Effect of Maximum Pressure on Thermal Efficiency and Net Power for SKCS at P_{min}=2 bar and DF=0.3

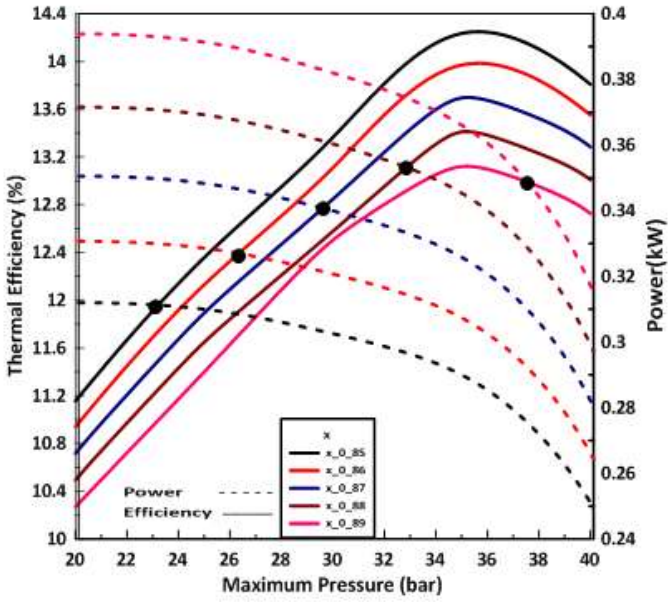

Figure (5.31) Effect of Maximum Pressure on Thermal Efficiency and Net Power for MKCS1 at P_{min}=2 bar and DF=0.3

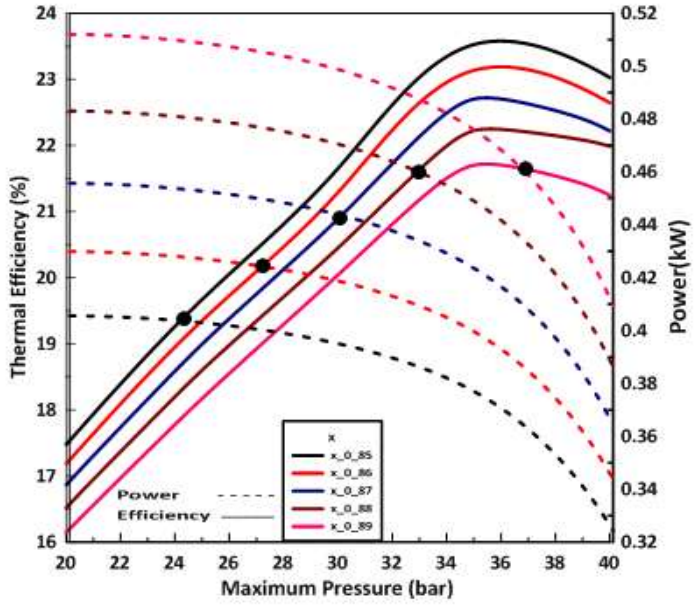

Figure (5.32) Effect of Maximum Pressure on Thermal Efficiency and Net Power for MKCS2 at P_{min}=2 bar and DF=0.3

5.6.5.2 Exergy Efficiency

Figs (5.33-5.35) show the effect of the maximum pressure on the exergy efficiency for SKCS, MKCS1 and MKCS2. When the maximum pressure increases the exergy efficiency increases and reaches maximum value at P_{max} 35 bar. With further increase of P_{max} the exergy efficiency decreases. The increase in the exergy efficiency is due to decrease in exergy difference across the HRVG caused by less flow rate. The highest exergy efficiency at x=0.85 is found with MKCS2 59% because it has lower loses than other cycles. The lowest value of the exergy efficiency with SKCS is 24.3% because it has more loses than other cycles. It is very clear from the figures when the maximum pressure increases the exergy efficiency increases till P_{max}=35 bar after that the exergy efficiency decreases because the net power decreases that leads to reduce the exergy efficiency as mention

before. It is seen the highest exergy efficiency is found at x=0.85 and maximum pressure 35 bar.

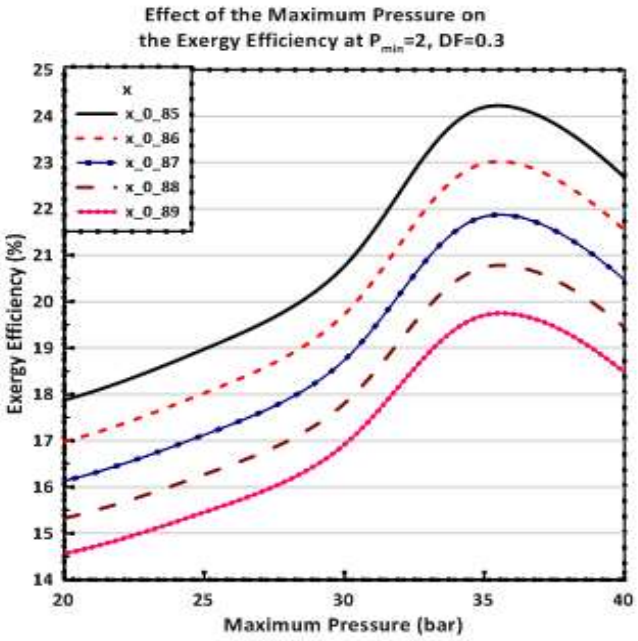

Figure (5-36) Effect of Maximum Pressure on Exergy Efficiency for SKCS

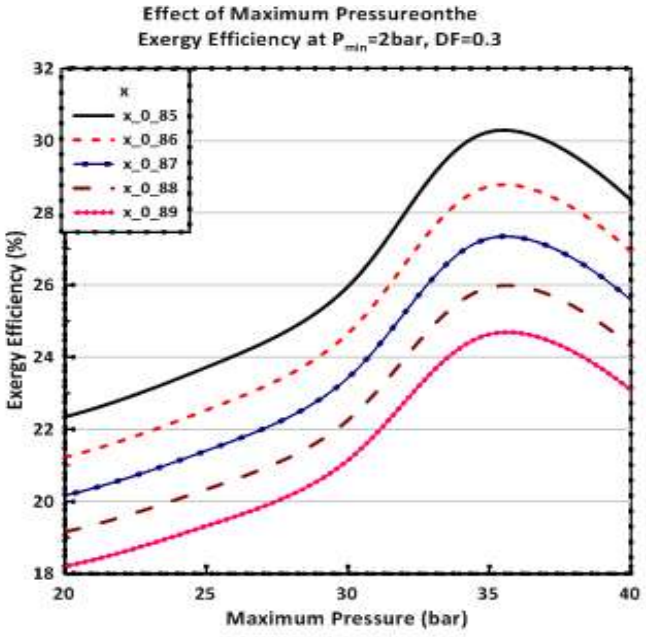

Figure (5-37) Effect of Maximum Pressure on Exergy Efficiency for MKCS1

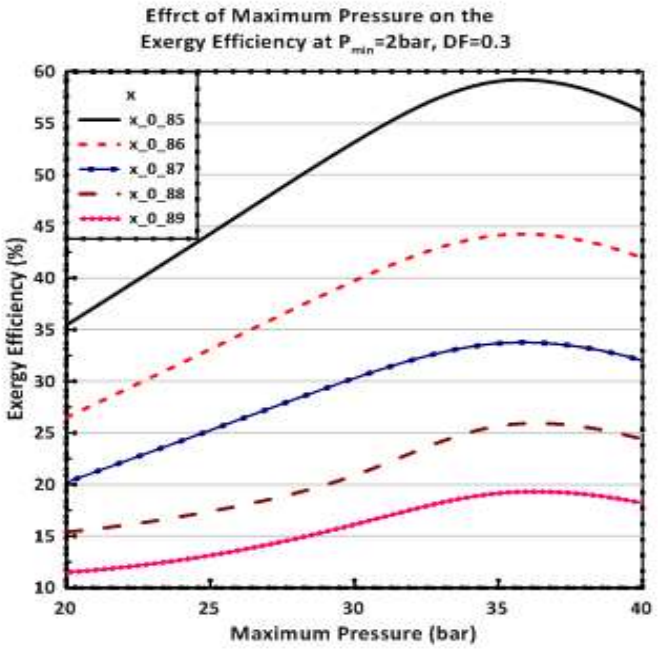

Figure (5-38) Effect of Maximum Pressure on Exergy Efficiency for MKCS2

5.6.6 The Effect of the Minimum Pressure on the performance

5.6.6.1- Thermal Efficiency

Figs (5.39-5.41) illustrate the effect of cycle minimum pressure on thermal efficiency for different ammonia mass fractions at constant maximum pressure. The minimum pressure is very important factor especially in the mixer. When the temperature of the mixer increases the minimum pressure increases that leads to reduce the thermal efficiency. Therefore, it is important to control the mixture temperature to keep the minimum pressure constant. This is done by cooling the mixer up to the required temperature. It is noticed when the minimum pressure decreases the cycle efficiency increases because the difference of enthalpy across the turbine increases. The trend of the effect of the minimum pressure on the thermal efficiency is same for the three cycles. It is clear that the maximum efficiency is obtained at minimum pressure 2 bar and ammonia mass fraction

is =0.85 with constant of the maximum Pressure ($P_{max)}$ is 35 bar and dryness fraction equal 0.3.

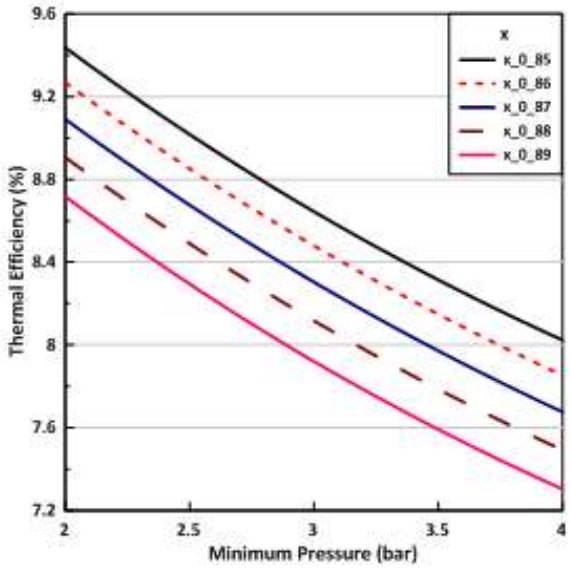

Figure (5.39) Effect of Minimum Pressure on Thermal Efficiency for SKCS at P_{max}=35 bar and DF=0.3

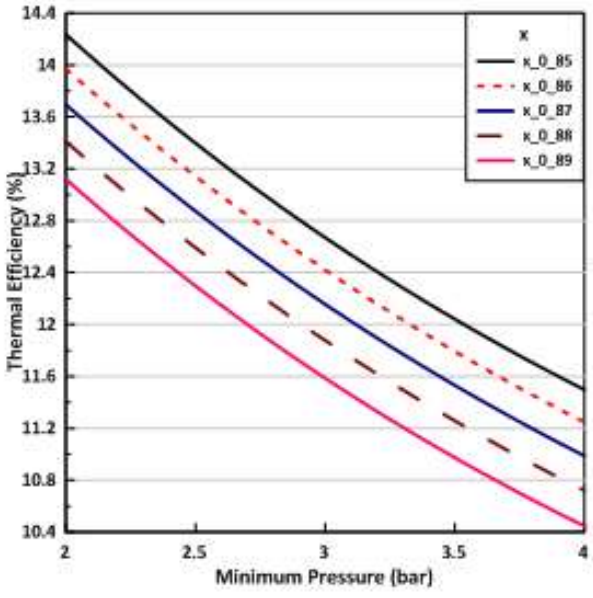

8

Figure (5.40) Effect of Minimum Pressure on Thermal Efficiency for MKCS1 at P_{max}=35 bar and DF=0.3

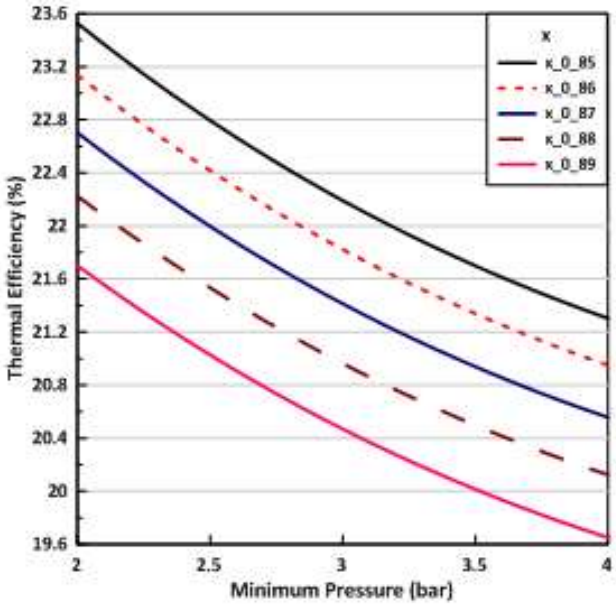

Figure (5.41) Effect of Minimum Pressure on Thermal Efficiency for MKCS2 at P_{max}=35 bar and DF=0.3

5.6.6.2 Net power

Figs (5.42-5.44) display the effect of cycle minimum pressure on net power for different ammonia mass fraction at constant maximum pressure and constant dryness fraction at separator inlet. The net power is found in MKCS2, MKCS1 and SKCS at P_{max}=35 bar, DF=0.3 and x=0.89 is 0.475 kW, 0.365 kW and 0.315 kW respectively. It is noticed when the minimum pressure decreases the net power increases due to the increase in enthalpy drop across the turbine. It is clear that the best conditions is found at low pressure is 2 bar.

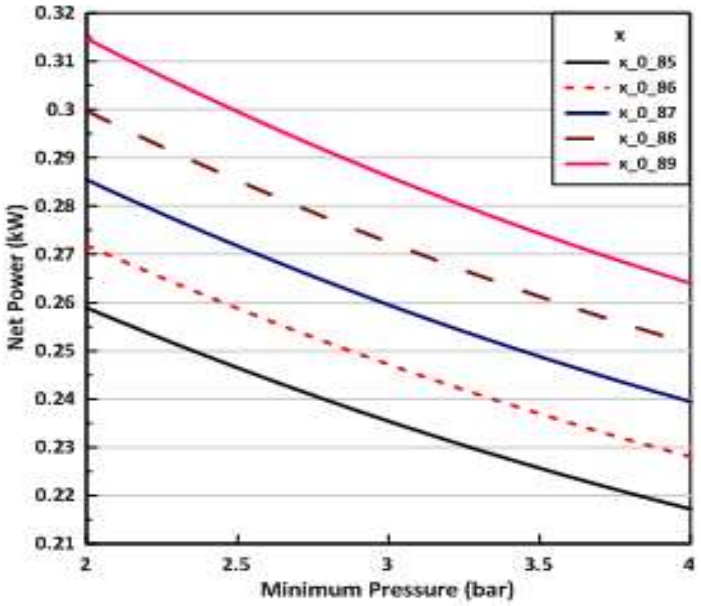

Figure (5.42) Effect of Minimum Pressure on Net Power for SKCS at P_{max}=35 bar and DF=0.3

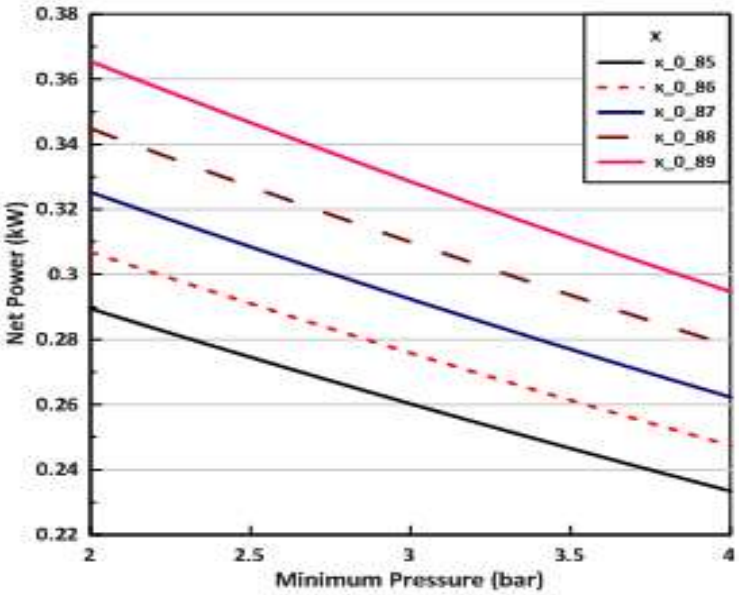

Figure (5.43) Effect of Minimum Pressure on Net Power for MKCS1 at P_{max}=35 bar and DF=0.3

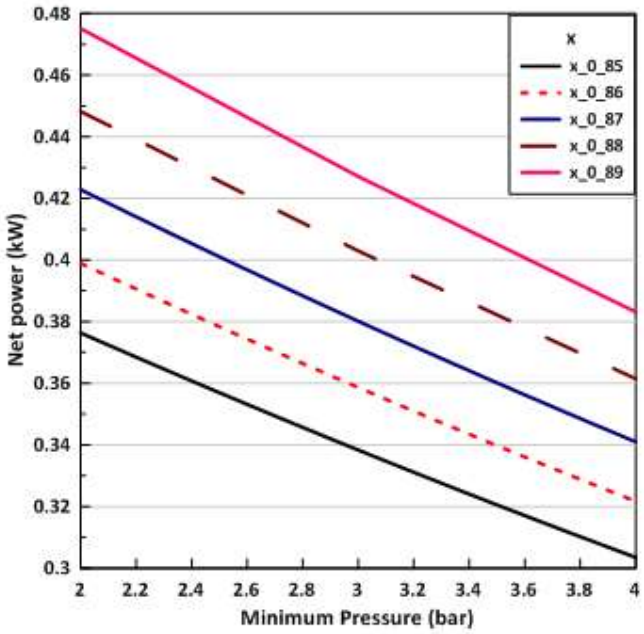

Figure (5.44) Effect of Minimum Pressure on Net Power for MKCS2 at P_{max}=35 bar and DF=0.3

5.6.6.3 - Exergy Efficiency

The effect of the minimum pressure on the exergy efficiency is illustrated in figs (5.45-5.47). The trend of the effect of the minimum pressure on the exergy efficiency is same for the three cycles. When the minimum pressure increases the exergy efficiency decreases since less useful work is done and more energy is destructed. It has same behavior of thermal efficiency. It is clear that the best low pressure is 2 bar with constant of the maximum Pressure (P_{max}=35 bar) and dryness fraction (DF=0.3). The value of the exergy efficiency for SKCS, MKCS1 and MKCS2 is 24.2%, 30.24% and 59.1% respectively at P_{min}=2 bar, x=0.85 and DF=0.3. The highest exergy efficiency with MKCS2 because MKCS2 uses two heat exchangers to exploit the heat rejected.

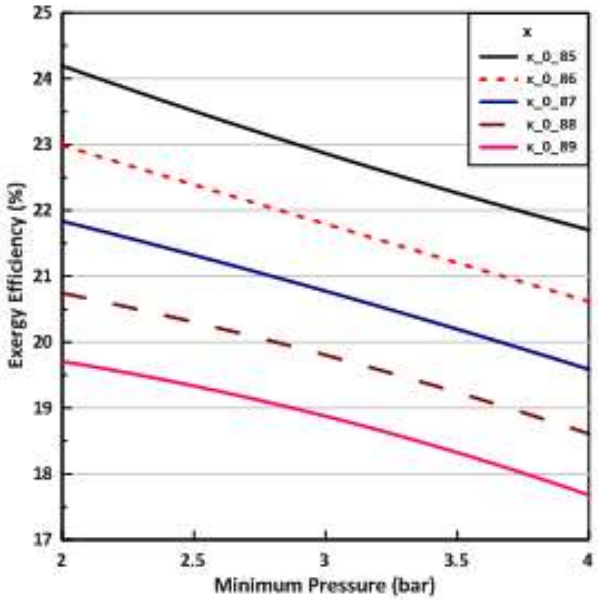

Figure (5.45) Effect of Minimum Pressure on Exergy Efficiency for SKCS at P_{max}=35 bar and DF=0.3

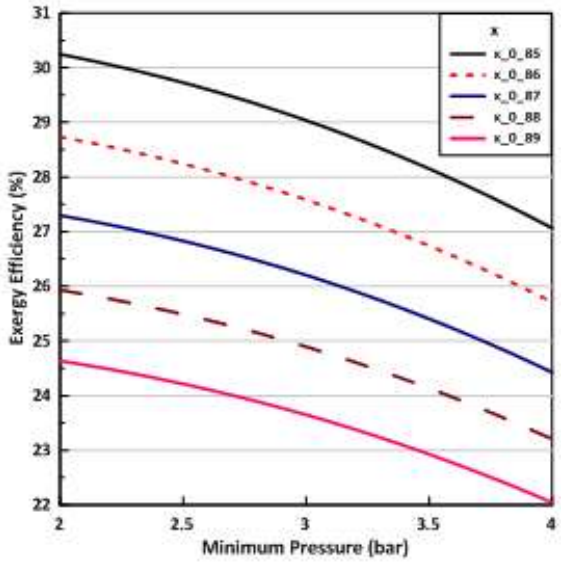

Figure (5.46) Effect of Minimum Pressure on Exergy Efficiency for MKCS1 at P_{max}=35 bar and DF=0.3

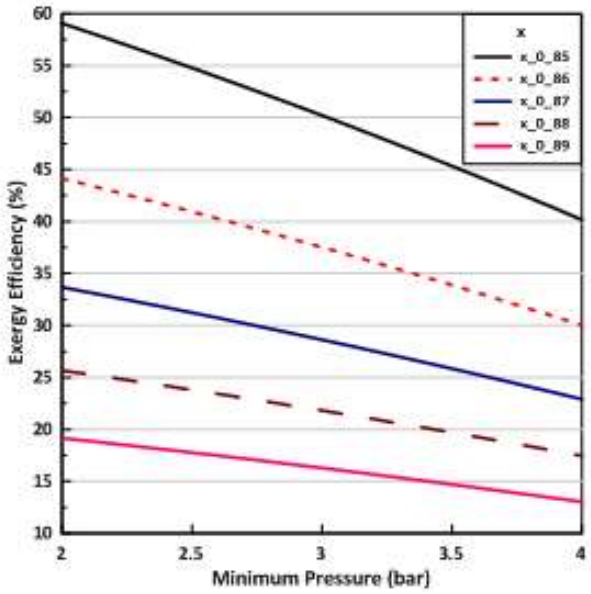

Figure (5.47) Effect of Minimum Pressure on Exergy Efficiency for MKCS2 at P_{max}=35 bar and DF=0.3

5.6.7 -Exergy destruction for SKCS, MKCS1 and MKCS2

This section is divided into two parts. First part is studying the total exergy destruction in each cycle, while the second part is studying the exergy destruction in each component for each cycle individually.

5.6.7.1 Effect of ammonia mass fraction

Figs (5.48-5.50) show the effect of the ammonia mass fraction on the exergy destruction for SKCS, MKCS1 and MKCS2 at constant maximum pressure and different minimum pressure with constant dryness fraction. All the figures for the three cycles have same trend. It is noticed that when the ammonia mass fraction increases the exergy destruction (loses) increases due to increase the mass flow rate. This lead to increase the speed of the working fluid inside the HRVG that means the working fluid doesn't gain more heat from the HRVG. When the mass flow rate increases the ammonia mass fraction increases and the boiling temperature of the working fluid decreases which means it needs less heat for evaporation. The highest exergy

destruction occurs at x=0.89 because at this ammonia mass fraction has highest mass flow rate. The exergy destruction for SKCS, MKCS1 and MKCS2 are 0.74 kW, 0.68 kW and 0.61 kW respectively. The reduction ratio between SKCS and MKCS1 is 8.12%, the reduction ratio between SKCS and MKCS2 is 17.6%.

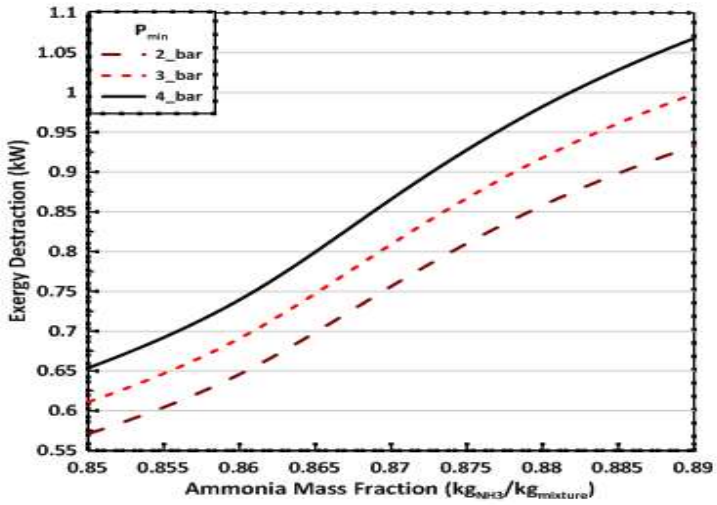

Figure (5.48) Effect of Ammonia Mass Fraction on Exergy Destruction for SKCS at P_{max}=35 bar and DF=0.3

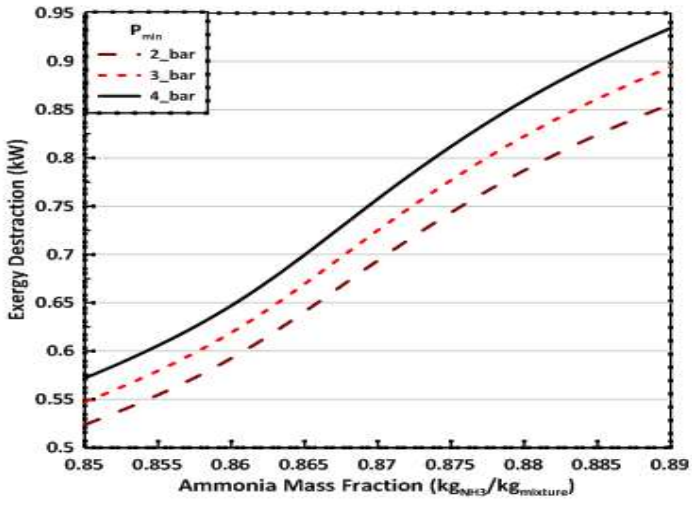

Figure (5.49) Effect of Ammonia Mass Fraction on Exergy Destruction for MKCS1 at P_{max}=35 bar and DF=0.3

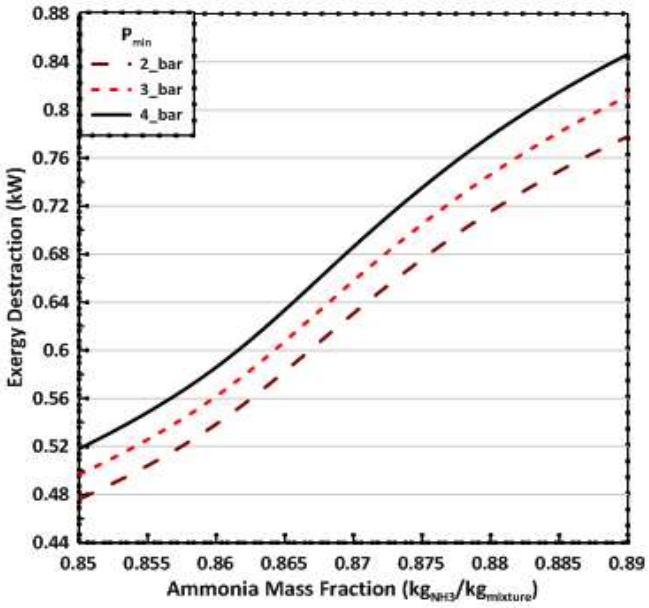

Figure (5.50) Effect of Ammonia Mass Fraction on Exergy Destruction for MKCS2 at P_{max}=35 bar and DF=0.3

5.6.7.2 Effect of Maximum pressure

Figs (5.51-5.53) show the effect of maximum pressure on the exergy destruction in the three cycles. It is noticed when the maximum pressure increases the exergy destruction increases since the net power decreases as mentioned before. The exergy destruction in SKCS is larger than the exergy destruction in the other two cycles because it has no recovery heat, most of the heat is rejected to environment as loses. The ratio of reduction of the exergy destruction from SKCS to MKCS1 is 9.17% and the ratio of reduction of the exergy destruction from SKCS to MKCS2 is 19.17% at P_{min}=3 bar. But the reduction ratio at P_{min}=2 bar, from SKCS to MKCS1 is 8.93%, the reduction ratio from SKCS to MKCS2 is 16.07%.

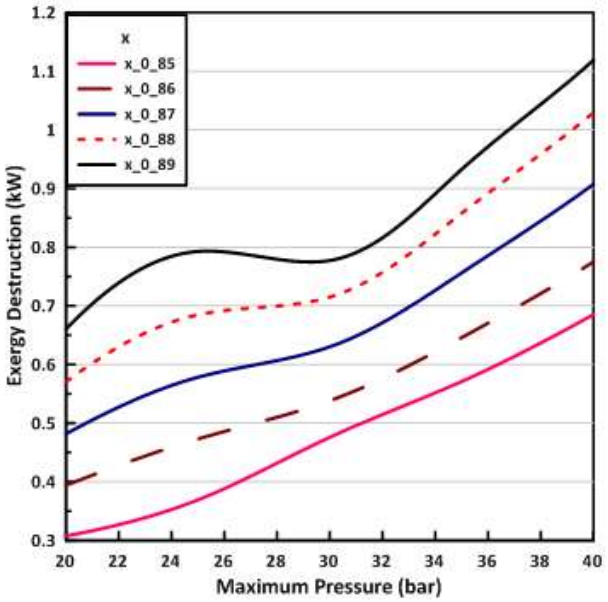

Figure (5.51) Effect of Maximum Pressure on Exergy Destruction for SKCS at P_{min}=2 bar and DF=0.3

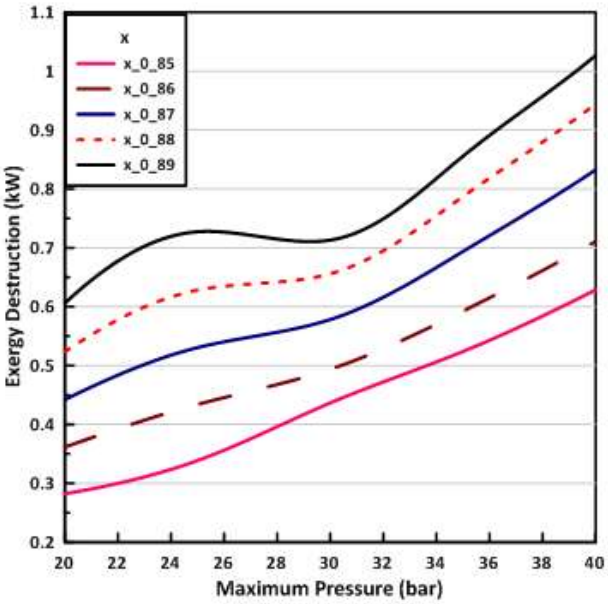

Figure (5.52) Effect of Maximum Pressure on Exergy Destruction for MKCS1 at P_{min}=2 bar and DF=0.3

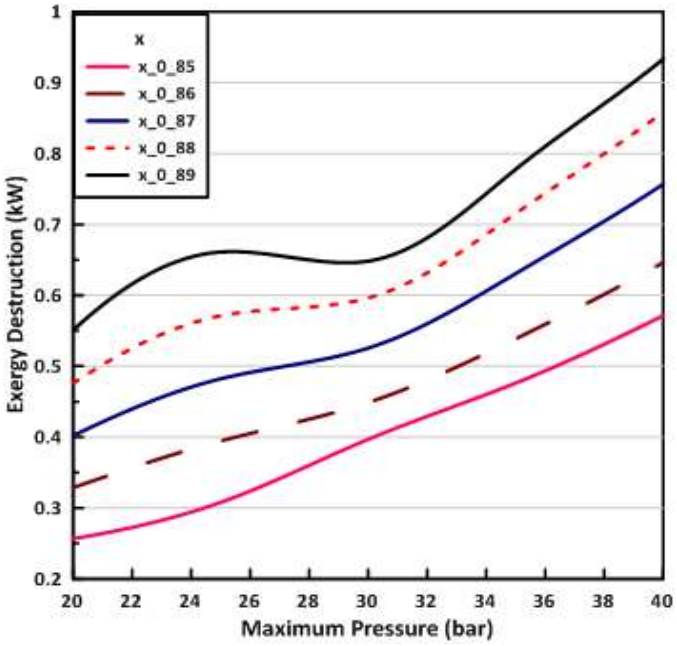

Figure (5.53) Effect of Maximum Pressure on Exergy Destruction for MKCS2 at P_{min}=2 bar and DF=0.3

5.6.7.3 Effect of minimum pressure

Figs (5.54-5.56) show the effect of minimum pressure on the exergy destruction with different ammonia mass fraction and constant maximum pressure and dryness fraction. When the minimum pressure increases the exergy destruction increases because with low minimum pressure the net power increases the exergy destruction decreases. It is found from the figures the highest exergy destruction at P_{min}=4 bar and the lowest exergy destruction at P_{min}=2 bar. That is a good indication to choose the minimum pressure is 2 bar. It is seen very clear the exergy destruction increases with the increase of the ammonia mass fraction as mentioned before.

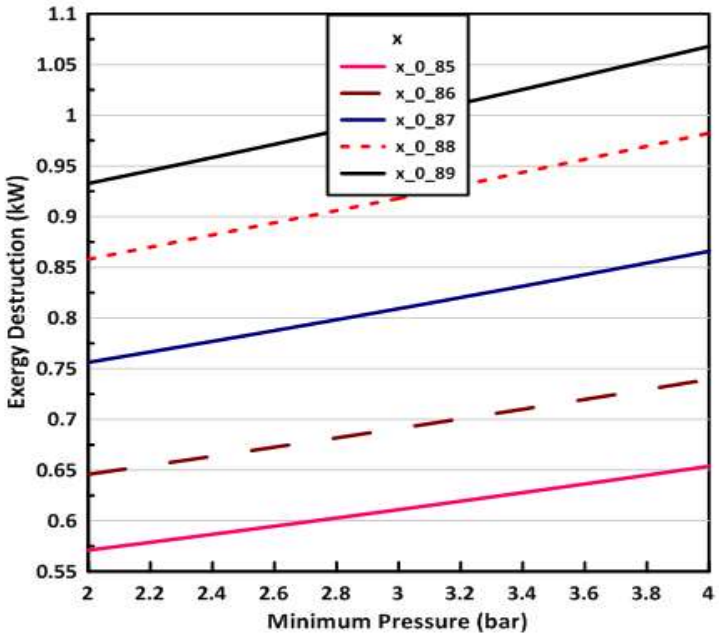

Figure (5.54) Effect of Minimum Pressure on Exergy Destruction for SKCS at P_{max}=35 bar and DF=0.3

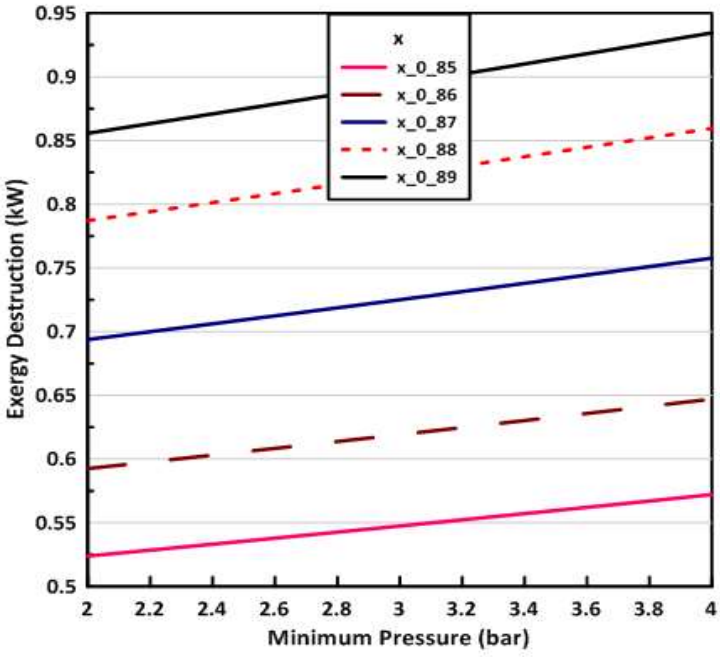

Figure (5.55) Effect of Minimum Pressure on Exergy Destruction for MKCS1 at P_{max}=35 bar and DF=0.3

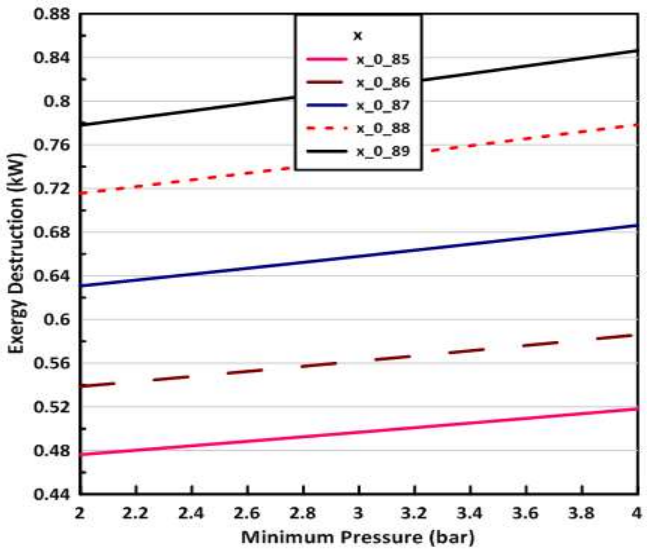

Figure (5.56) Effect of Minimum Pressure on Exergy Destruction for MKCS2 at P_{max}=35 bar and DF=0.3

5.6.8 Exergy Destruction in each Component

Fig (5.57) shows the exergy destruct in each component of the simple Kalina cycle system (SKCS). It is found that the highest exergy destruction is in the HRVG since the exergy destruction depends on the amount of the mass flow rate of the working fluid, ammonia mass fraction and the separator temperature. If the working fluid has low ammonia mass fraction it will absorb more heat from the HRVG then there is less exergy destruction, but if the working fluid has high ammonia concentration it will absorb less heat from the HRVG then there is more exergy destruction since when the ammonia mass fraction increases in the working fluid the boiling temperature of the working fluid will decrease that leads to more exergy destruction. The exergy destruction increases with the increase of the mass flow rate. The exergy destruction in SKCS, MKCS1 and MKCS2 in HRVG is 38%, 46% and 49% respectively as shown in figs (5.57-5.59). The other components such as the condenser in each cycle has 13%, 18% and 15% for SKCS, MKCS1 and MKCS2 respectively. The mass flow rate for SKCS, MKCS1 and MKCS2 0.002873 kg/s, 0.003995 kg/s and 0.006253 kg/s

respectively at P_{max}=35 bar, P_{min}=2 bar, DF=0.3 and x=0.85. When the mass flow rate gets large the exergy destruction also gets large.

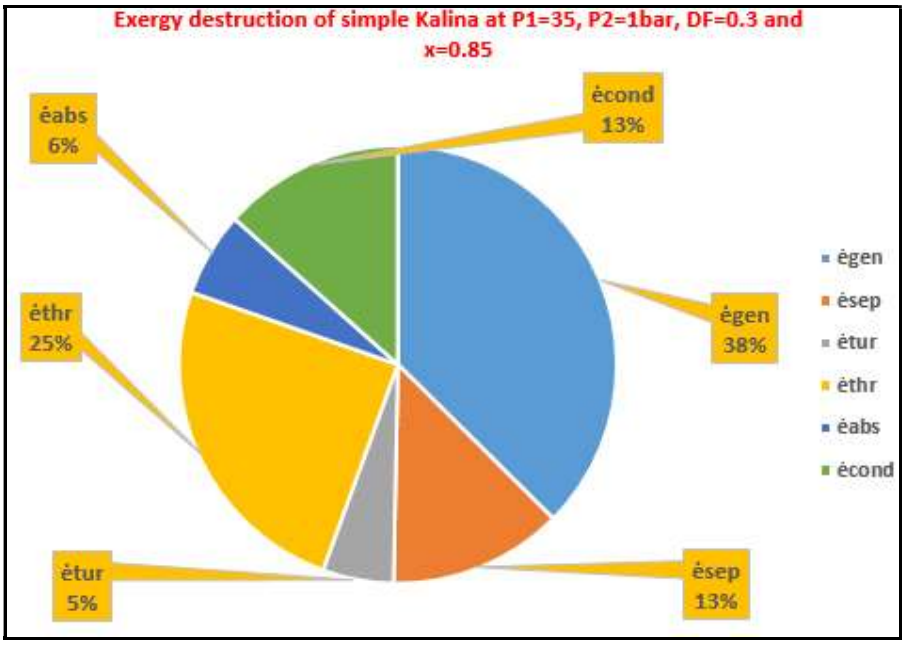

Figure (5-57) Exergy Destruction for SKCS

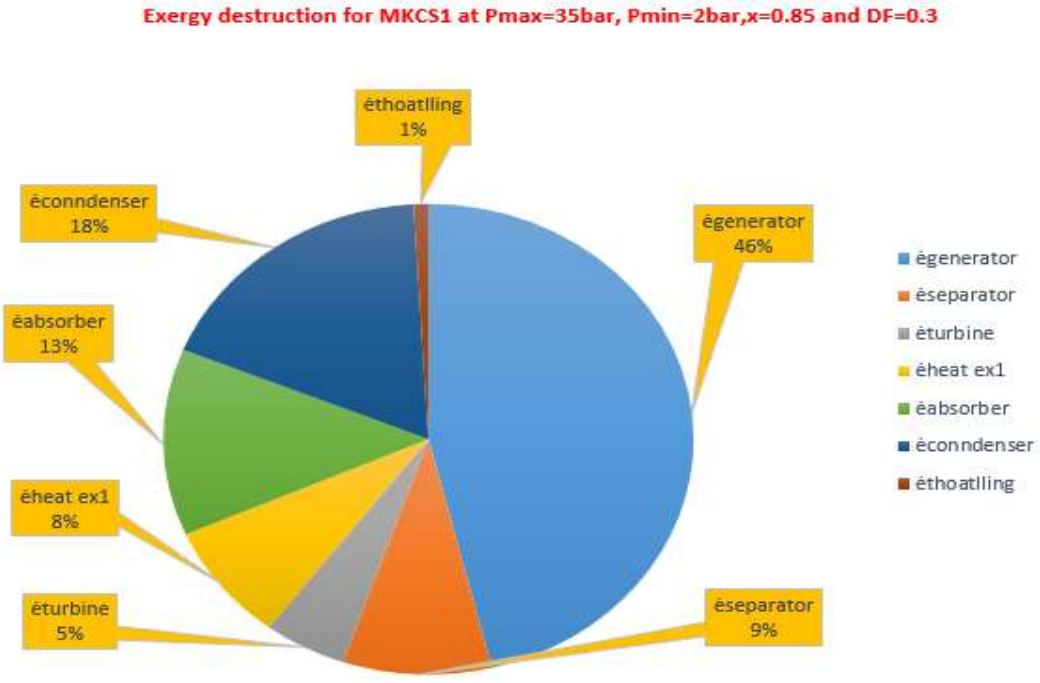

Figure (5-58) Exergy Destruction for MKCS1

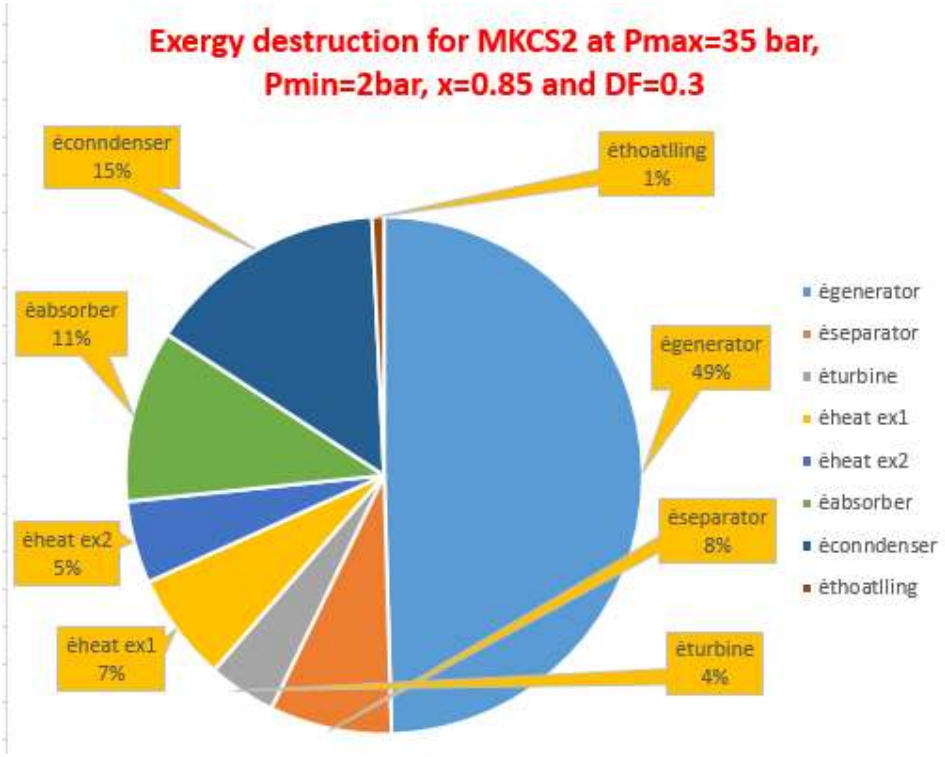

Figure (5-59) Exergy Destruction for MKCS2

5.6.9 The selection of the best conditions

After the theoretical analysis for the three cycles SKCS, MKCS1 and MKCS2 and studying the effect of different parameters on their performance, fig (5.60) shows the thermal efficiency in the three cycles. It is seen clearly when ammonia mass fraction increases the thermal efficiency decreases, but the maximum thermal efficiency for MKCS2 is 23.4% at x=0.85. Fig (5.61) shows the net power in the three cycles. When the ammonia mass flow rate increases the net power increases. It is found that the maximum net power at x=0.89 for the three cycles. Fig (5.62) shows the exergy efficiency for the three cycles. The maximum exergy efficiency at x=0.85. The conditions which are selected according to this work is P_{max}=35 bar, P_{min}=2 bar, DF=0.3 and x=0.85.

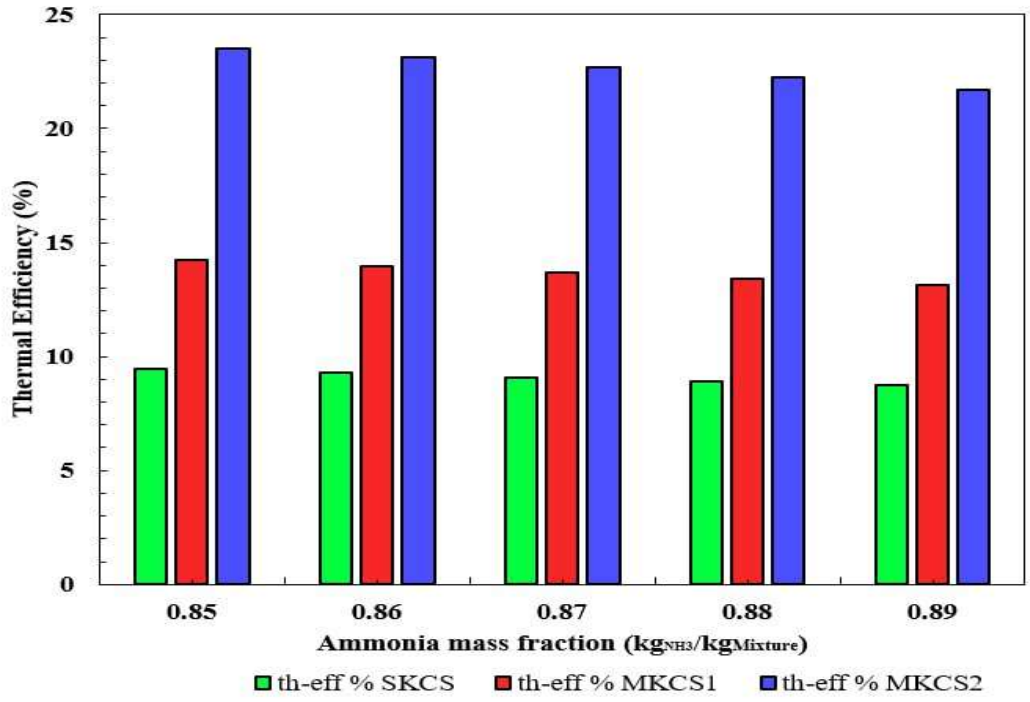

Figure (5.60) Thermal Efficiency

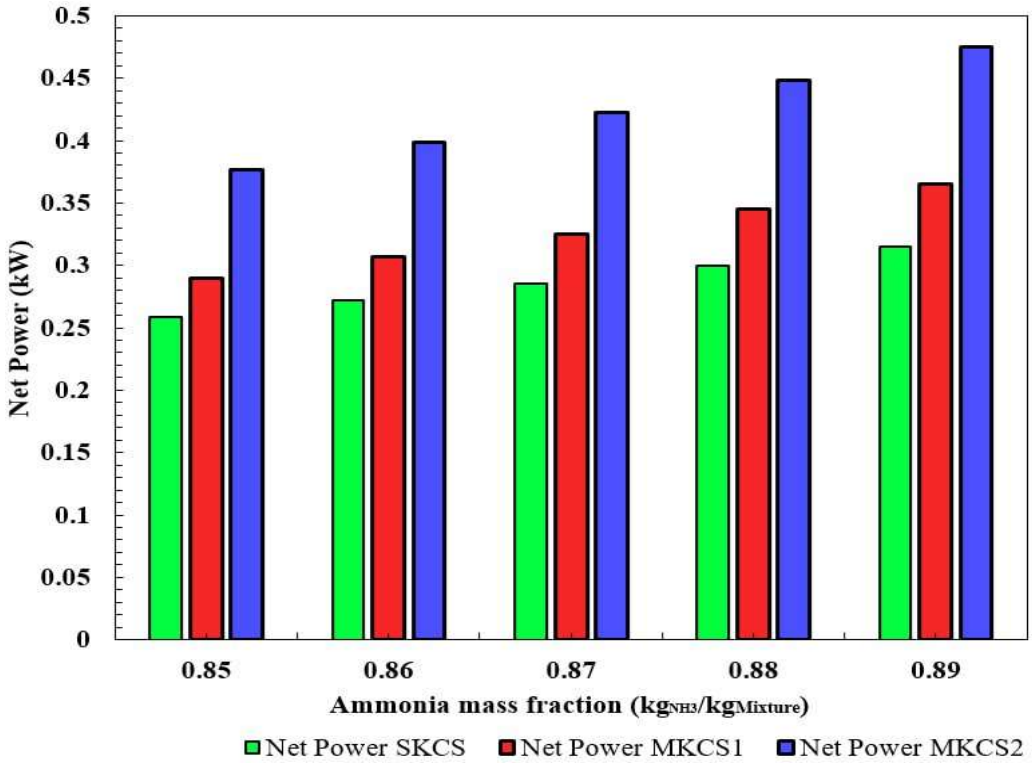

Figure (5.61) Net Power

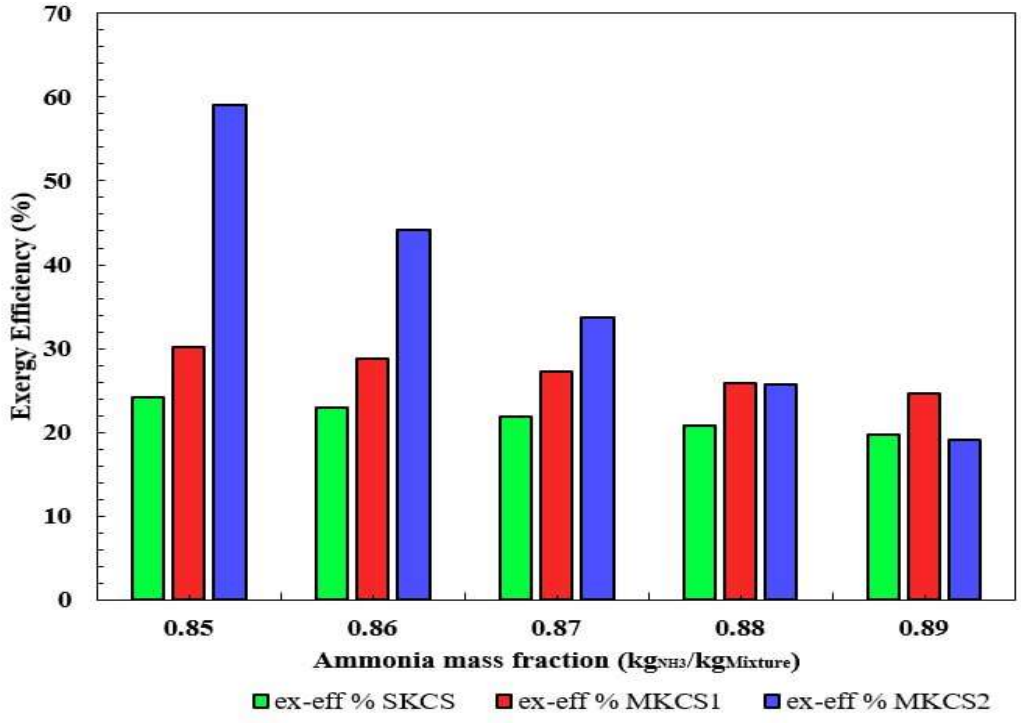

Figure (5.62) Exergy Efficiency

5.7 The Experimental Study Results

In this section the results of the experimental investigation are presented and discussed. For ease of discussion the results are divided into three parts which are:

1- The effect of ammonia mass fraction on the performance.
2- The effect of maximum pressure on the performance.
3- The effect of minimum pressure on the performance.

The performance includes the thermal efficiency, net power, exergy efficiency and exergy destruction during the modified cycle (MKCSE). The maximum pressure is varied from 20 bar to 40 bar with 5bar step, minimum pressure is varied from 2 bar, 3 bar and 4 bar, ammonia mass fraction is varied from 0.85 to o.89 with 0.01 step while the dryness fraction (DF) at separator inlet is kept constant at 0.3. The thermal source which supplied

heat to the system is electrical heater, the power of the electrical source between 1000W-4000W.

5.7.1 Effect of ammonia mass fraction

5.7.1.1 - Thermal Efficiency

Figs (5.63-5.65) show the relationship between the ammonia mass fraction and the thermal efficiency with different maximum pressures at constant minimum pressure and dryness fraction. All figures show same trend for all cases. When the ammonia mass fraction increases the efficiency decreases at constant maximum pressure because of the increase of the mass flow rate. The highest thermal efficiency is 12.9% at P_{max}=35 bar, P_{min}=2 bar, DF=0.3 and x=0.85. The lowest thermal efficiency is 6.8% at P_{max}=20 bar, P_{min}=4 bar, DF=0.3 and x=0.89 because at these conditions high mass flow rate and high minimum pressure. The results agree with the theoretical findings presented previously.

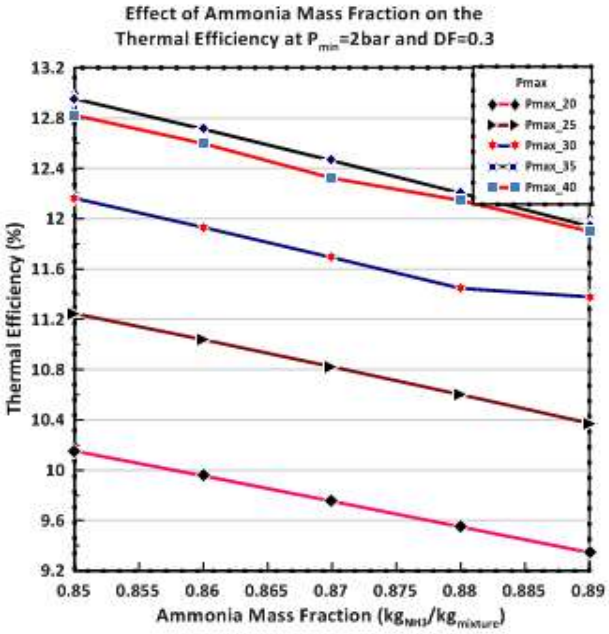

Figure (5.63) Effect of Ammonia Mass Fraction on Thermal Efficiency for MKCSE at P_{min}=2 bar and DF=0.3

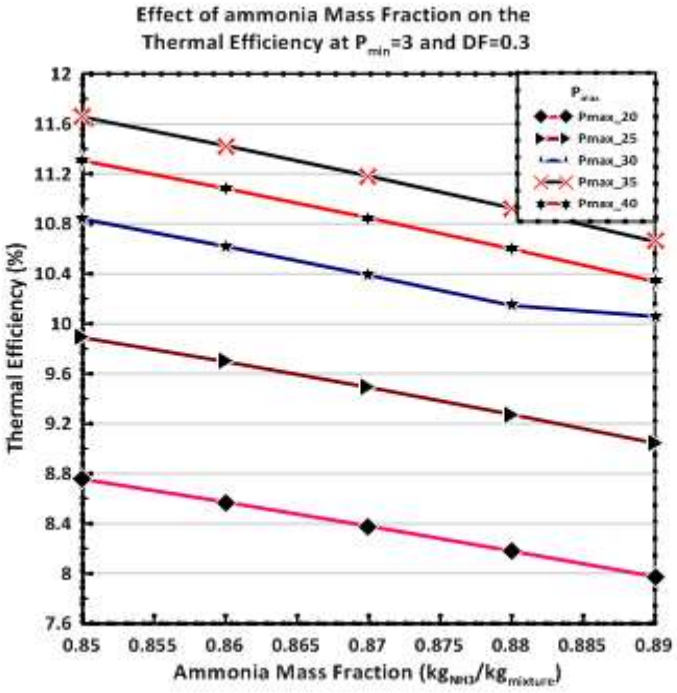

Figure (5.64) Effect of Ammonia Mass Fraction on Thermal Efficiency for MKCSE at P_{min}=3 bar and DF=0.3

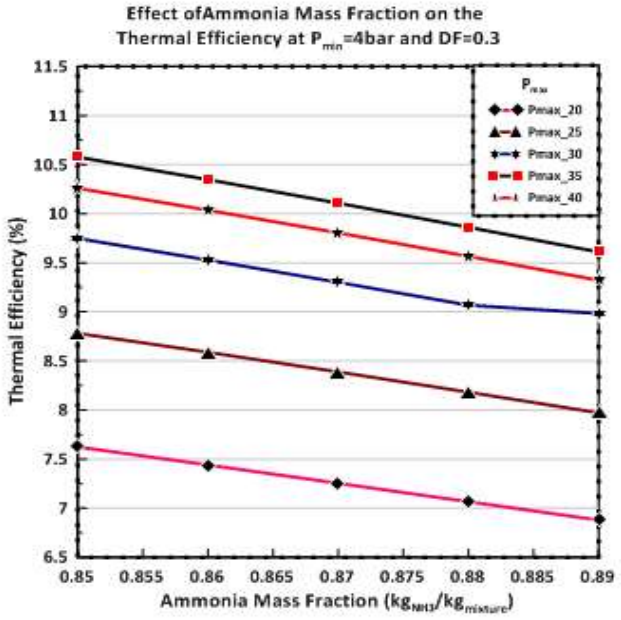

Figure (5.65) Effect of Ammonia Mass Fraction on Thermal Efficiency for MKCSE at P_{min}=4 bar and DF=0.3

5.7.1.2-Net Power

Figs (5.66-5.68) display the effect of the ammonia mass fraction on the net power. The highest value of the net power is 0.367 kW at x=0.89 at turbine inlet, P_{max}=20 bar and DF=0.3 at separator inlet. When the ammonia mass fraction increases the net power increases. Since the increase in ammonia mass fraction increases the vapor mass flow rate through the turbine, which increases the power output. The lowest value of the net power is obtained at x=0.85 because in this ammonia mass fraction has low mass flow rate as mentioned in section 5.2.1.

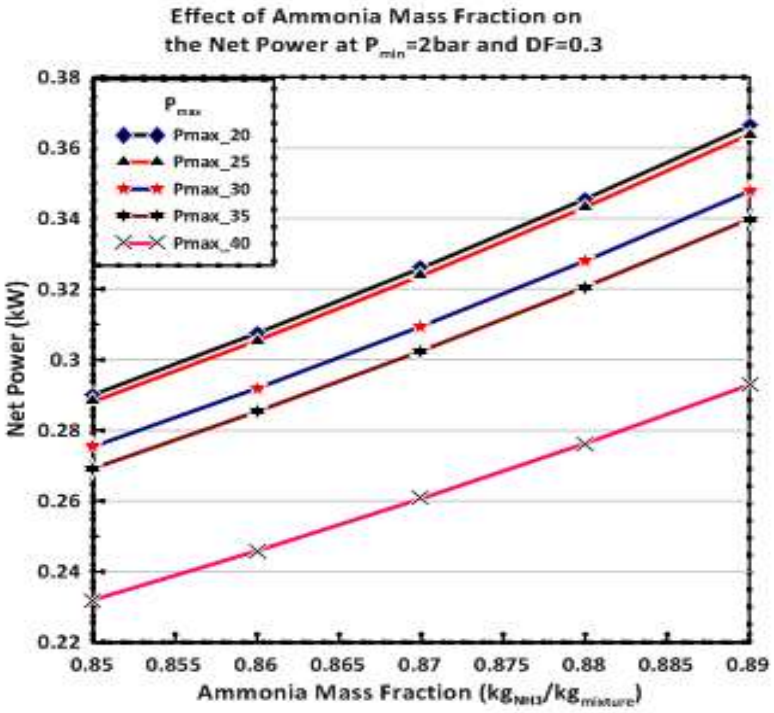

Figure (5.66) Effect of Ammonia Mass Fraction on Net Power for MKCSE at P_{min}=2 bar and DF=0.3

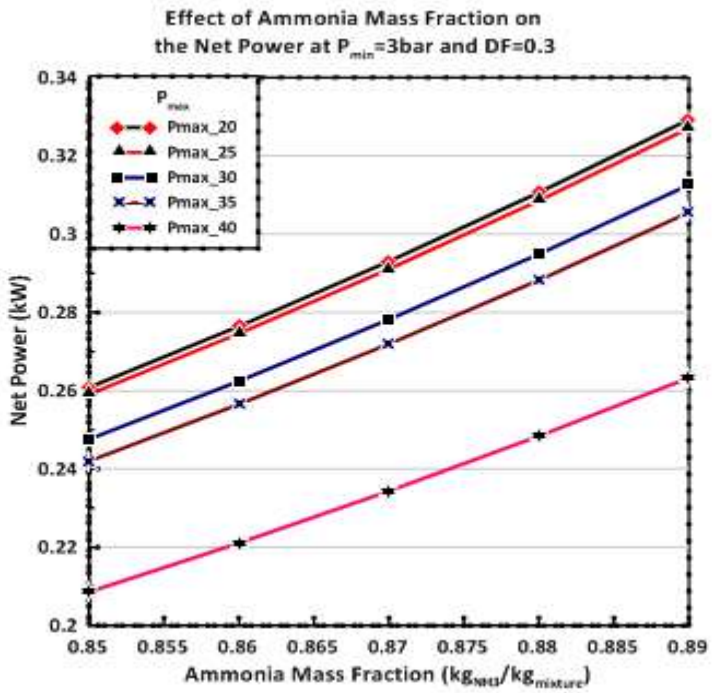

Figure (5.67) Effect of Ammonia Mass Fraction on Net Power for MKCSE at P_{min}=3 bar and DF=0.3

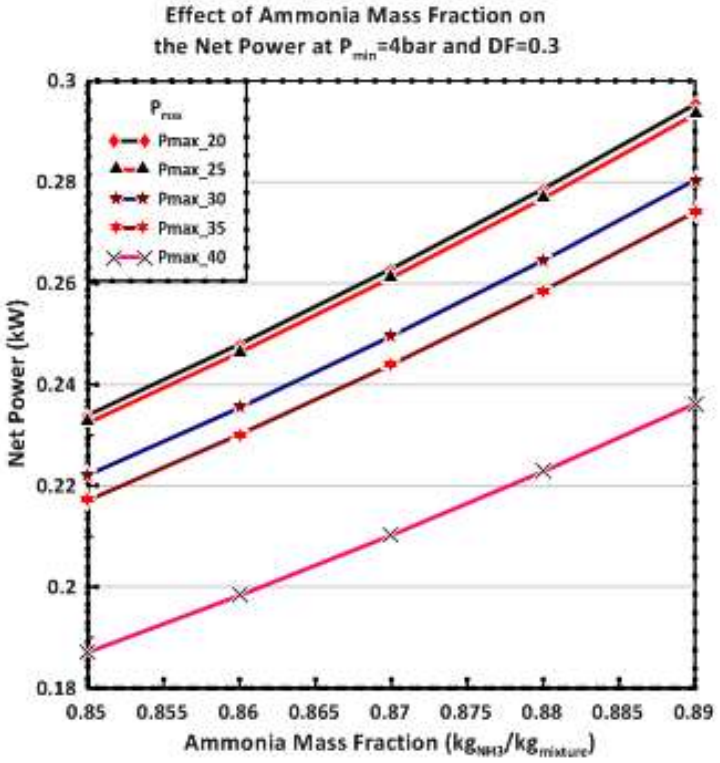

Figure (5.68) Effect of Ammonia Mass Fraction on Net Power for MKCSE at P_{min}=4 bar and DF=0.3

5.7.1.3-Exergy Efficiency

Figs (5.69-5.71) display the relationship between the ammonia mass fraction and the exergy efficiency. When the ammonia mass fraction increases the exergy efficiency drops due to the increase in mass flow rate same as mentioned before. Hence the exergy destraction increases that's lead to drop the exergy efficiency. This is the same behavior as the thermal efficiency. The highest value of exergy efficiency is 28.5% at P_{max}=35 bar, P_{min}=2 bar and DF=0.3. It is noticed that the minimum value of exergy efficiency is 15% at P_{max}=20 bar, P_{min}=4 bar and x=0.89.

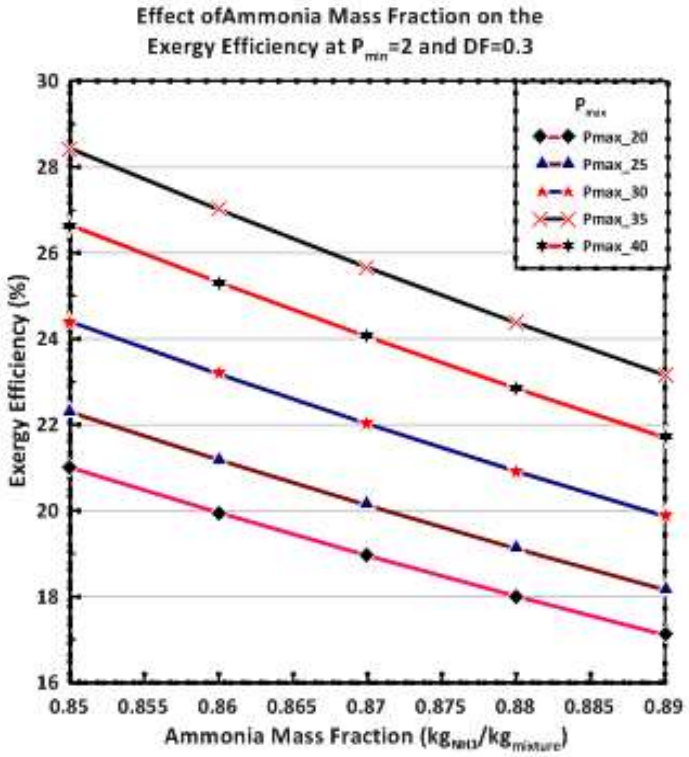

Figure (5.69) Effect of Ammonia Mass Fraction on Exergy Efficiency for MKCSE at P_{min}=2 bar and DF=0.3

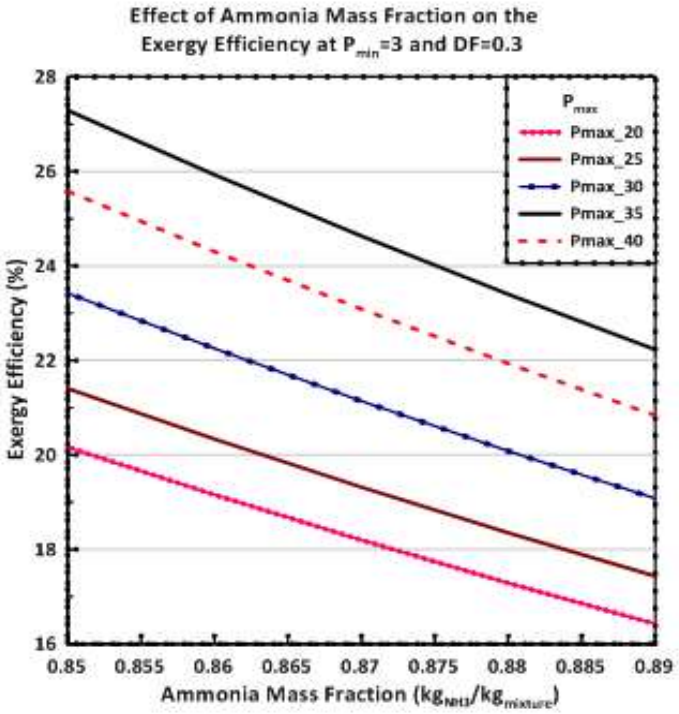

Figure (5.70) Effect of Ammonia Mass Fraction on Exergy Efficiency for MKCSE at P_{min}=3 bar and DF=0.3

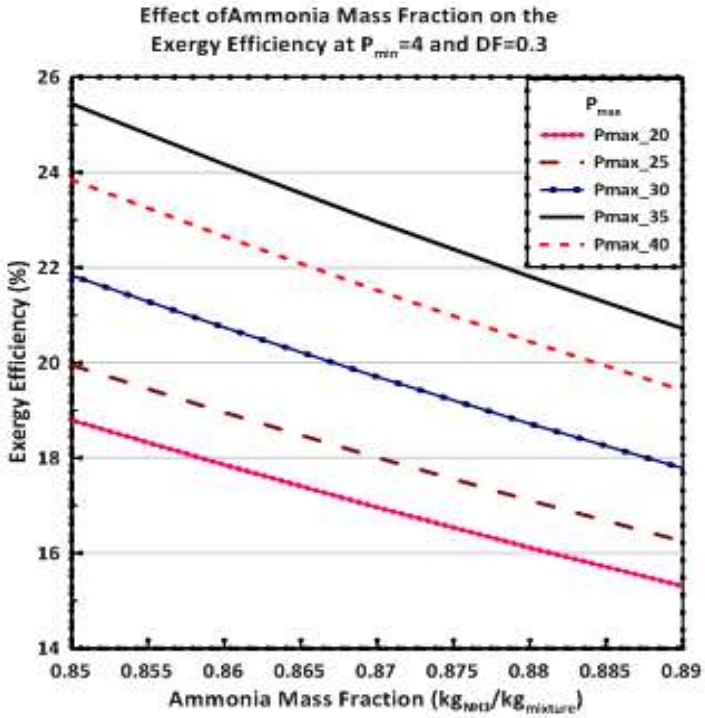

Figure (5.71) Effect of Ammonia Mass Fraction on Exergy Efficiency for MKCSE at P_{min}=4 bar and DF=0.3

5.7.2 The Effect of Maximum pressure on the Performance

5.7.2.1 Thermal efficiency

Figs (5.72-5.74) display the relationship between the maximum pressure and thermal efficiency for different ammonia mass fraction. It is seen when the maximum pressure increases the thermal efficiency increases sharply till P_{max}=35 bar, after that when the maximum pressure increases the thermal efficiency decreases. Actually there are two effective factors the evaporation heat (h_{fg}) and sensible heat. When the maximum pressure increases the evaporation heat (h_{fg}) decreases, while the sensible heat increases. The sensible heat factor is more effective from the other factor. When the mass flow rate decreases that means the speed of the working fluid decreases then the working fluid absorbs more heat that leads to increase the temperature in the separator also maximum pressure increases as consequently. It is found that the highest thermal efficiency is 12.9% at x=0.85 at turbine inlet and P_{min}=2 bar.

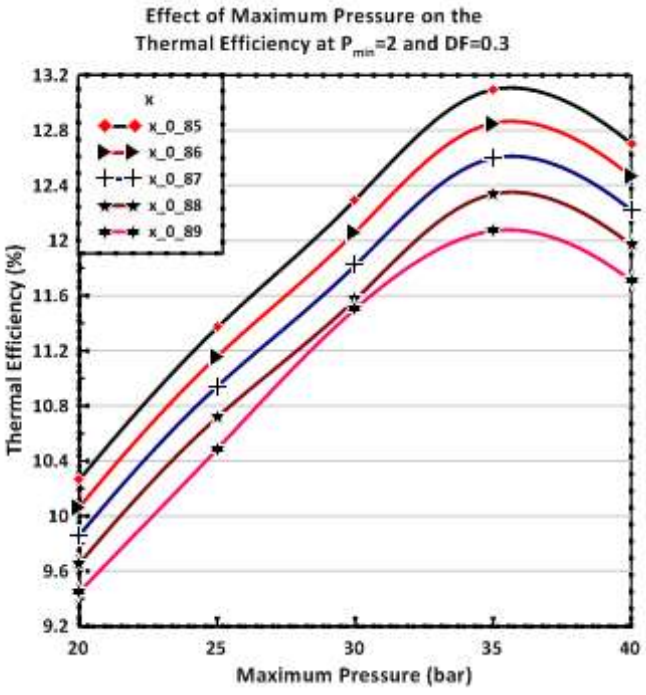

Figure (5.72) Effect of Maximum Pressure on Thermal Efficiency for MKCSE at P_{min}=2 bar and DF=0.3

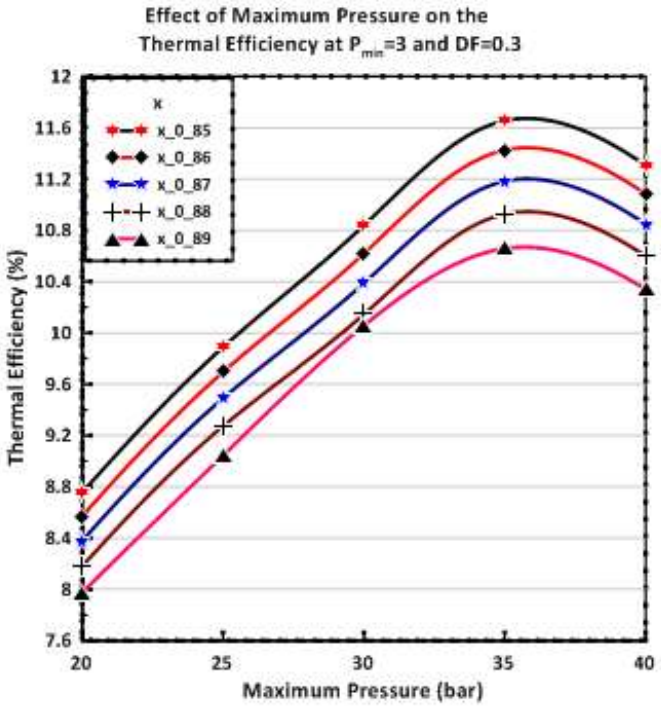

Figure (5.73) Effect of Maximum Pressure on Thermal Efficiency for MKCSE at P_{min}=3 bar and DF=0.3

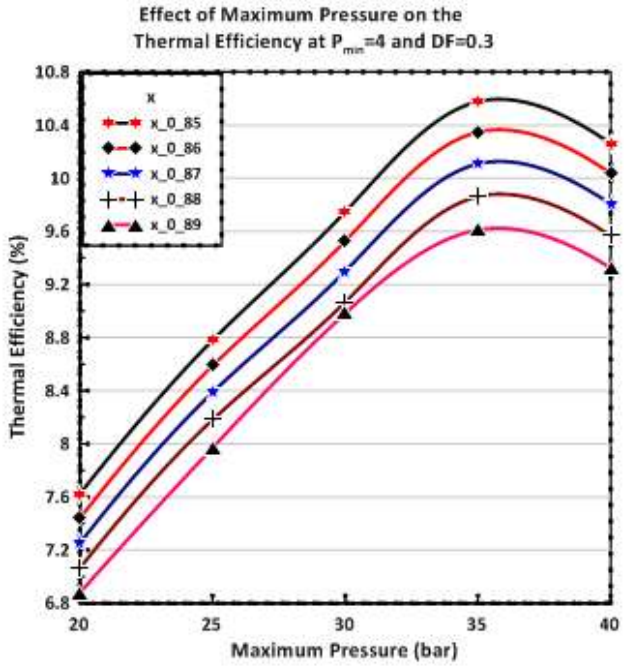

Figure (5.74) Effect of Maximum Pressure on Thermal Efficiency for MKCSE at P_{min}=4 bar and DF=0.3

5.7.2.2 -Net Power

Figs (5.75-5.77) show the effect of the maximum pressure on the net power with different ammonia mass fraction. All behaviors are same for all figures. The values of the net power at 2 bar, 3 bar and 4 bar are 0.37 kW, 0.33 kW and 0.295 kW respectively. To increase the maximum pressure, have to increase the temperature of the working fluid in the separator, to increase the temperature must decrease the mass flow rate which comes from the pump same as mentioned before. So when the maximum pressure increases the net power decreases because of the decrease of the mass flow rate. All the figures display the best net power at maximum pressure 20 bar because it has high mass flow rate at this maximum pressure. As the maximum pressure increases the vapor mass flow rate decreases due to decrease in total mass flow rate which reduces turbine output.

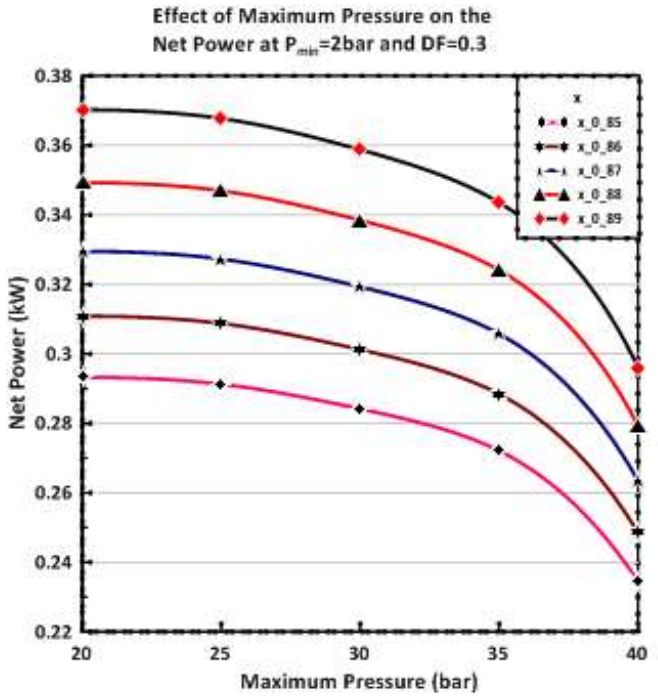

Figure (5.75) Effect of Maximum Pressure on Net Power for MKCSE at P_{min}=2 bar and DF=0.3

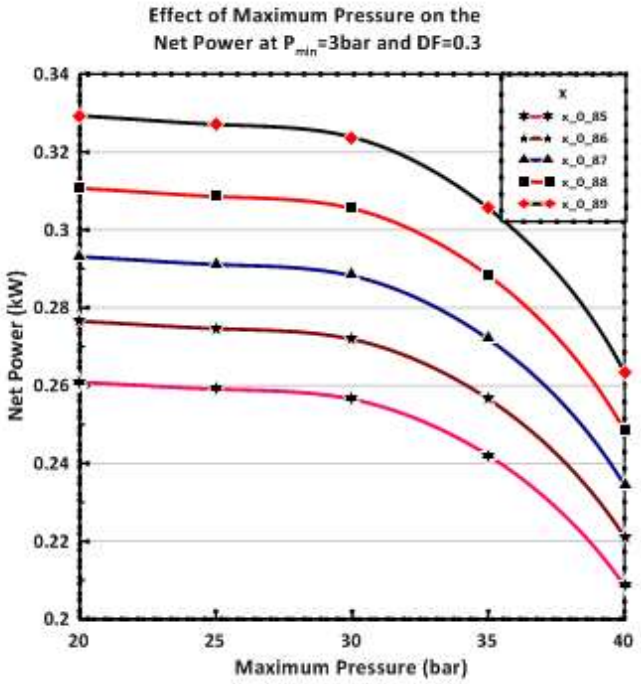

Figure (5.76) Effect of Maximum Pressure on Net Power for MKCSE at P_{min}=3 bar and DF=0.3

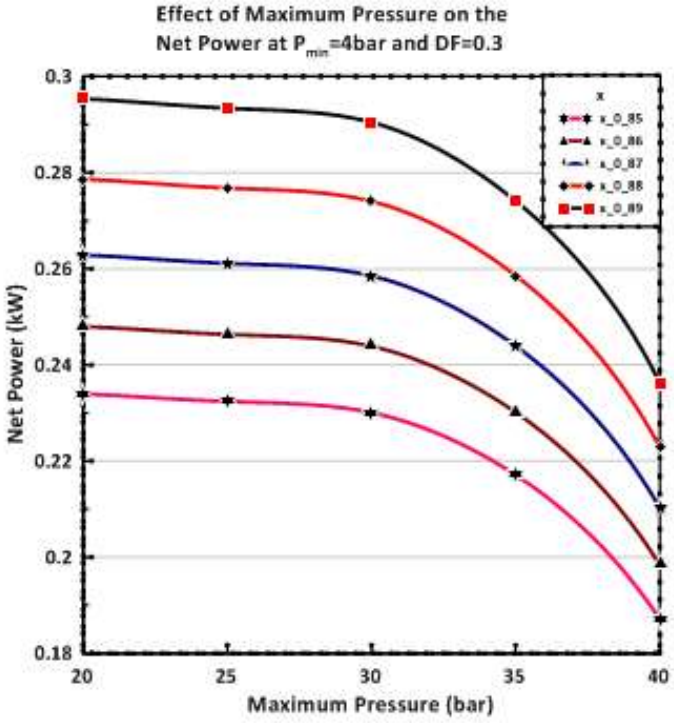

Figure (5.77) Effect of Maximum Pressure on Net Power for MKCSE at P_{min}=4 bar and DF=0.3

5.7.2.3 -Exergy Efficiency

Figs (5.78-5.80) display the relationship between maximum pressure and exergy efficiency. When maximum pressure rises the exergy efficiency increases because the increase of the mass flow rate, then the working fluid takes time to absorb more heat from HRVG. The best values of the exergy efficiency at P_{max}=35 bar. The exergy efficiency is 28.4%, 27.35% and 25.4% at 2 bar, 3 bar and 4 bar respectively. The trend all of the figures as shown below is same. The exergy efficiency drops after P_{max}=35 bar because the net power drops due to that decrease of the mass flow rate. This is the same behavior as the thermal efficiency. It is due to less heat absorbed in the HRVG and less exergy destruction.

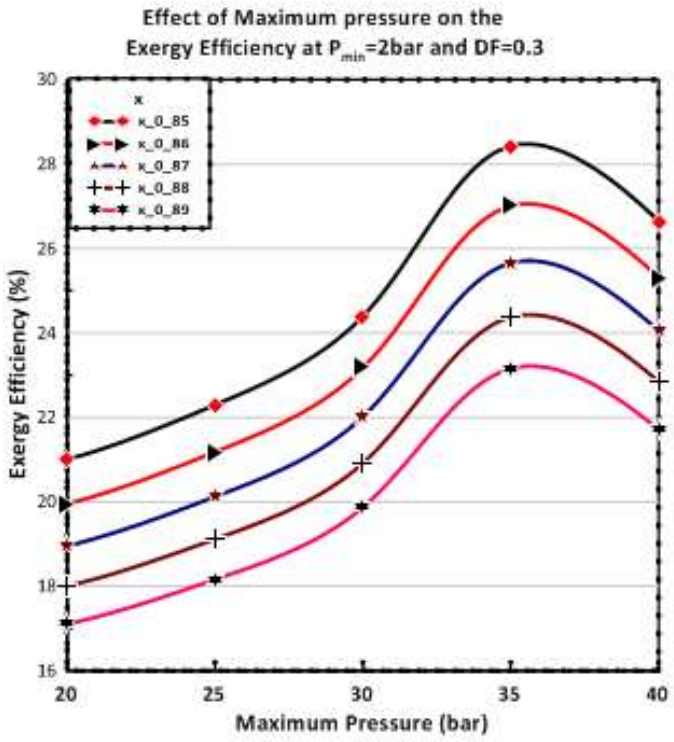

Figure (5.78) Effect of Maximum Pressure on Exergy Efficiency for MKCSE at P_{min}=2 bar and DF=0.3

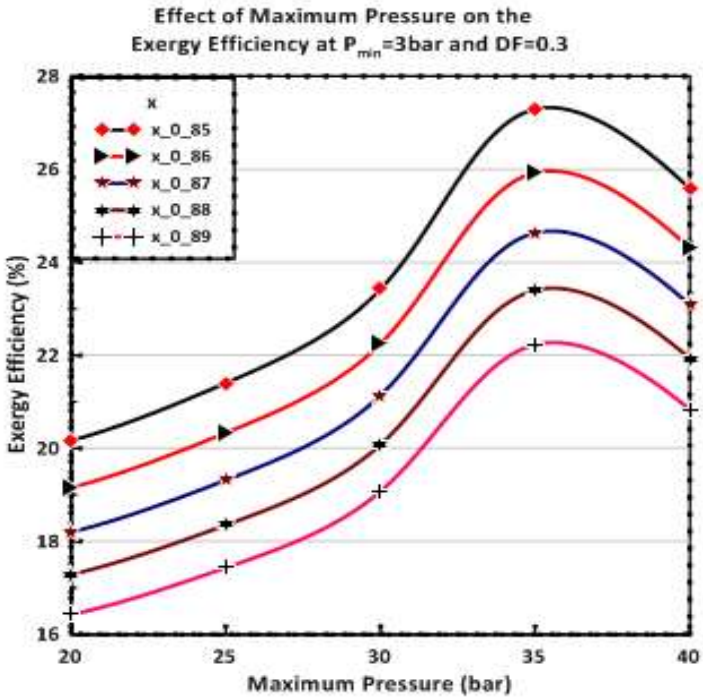

Figure (5.79) Effect of Maximum Pressure on Exergy Efficiency for MKCSE at P_{min}=3 bar and DF=0.3

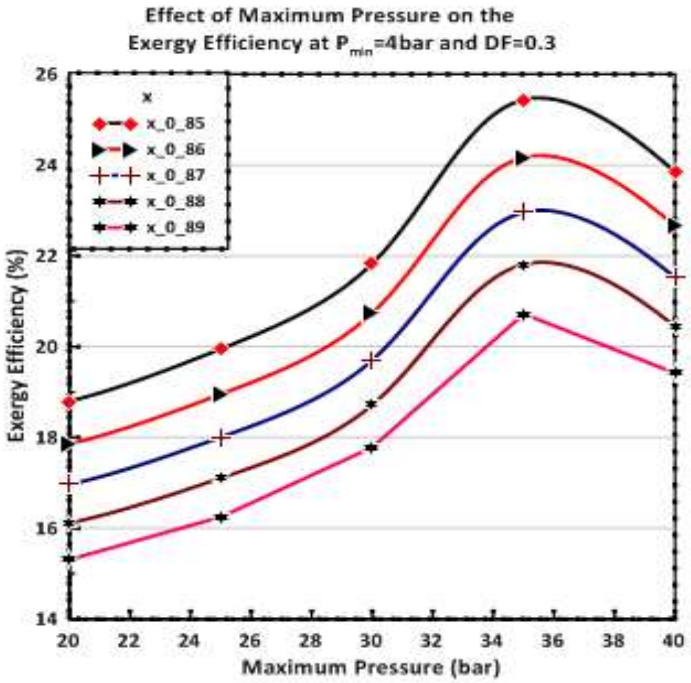

Figure (5.80) Effect of Maximum Pressure on Exergy Efficiency for MKCSE at P_{min}=4 bar and DF=0.3

5.7.3 Effect Minimum Pressure on the Performance

5.7.3.1 *Thermal Efficiency*

Figs (5.81) and (5.82) show the effect of the minimum pressure on the thermal efficiency at constant maximum pressure and dryness fraction at separator inlet.The pressure in the separator is the maximum pressure and the pressure in the mixer is the minimum pressure. It is noticed when the minimum pressure decreases the cycle efficiency increases because the change of enthalpy across the turbine increases although the mass flow rate decreases. It is clear the highest values of thermal efficiency at low pressure is 2 bar while the lowest values of thermal efficiency at minimum pressure is 4 bar. Thermal efficiency is 10.2% at x=0.85 at P_{min}=2 bar while thermal efficiency is 7.6%. It is seen the thermal efficiency drops from 10.2% to 7.6% because the minimum pressure increases.

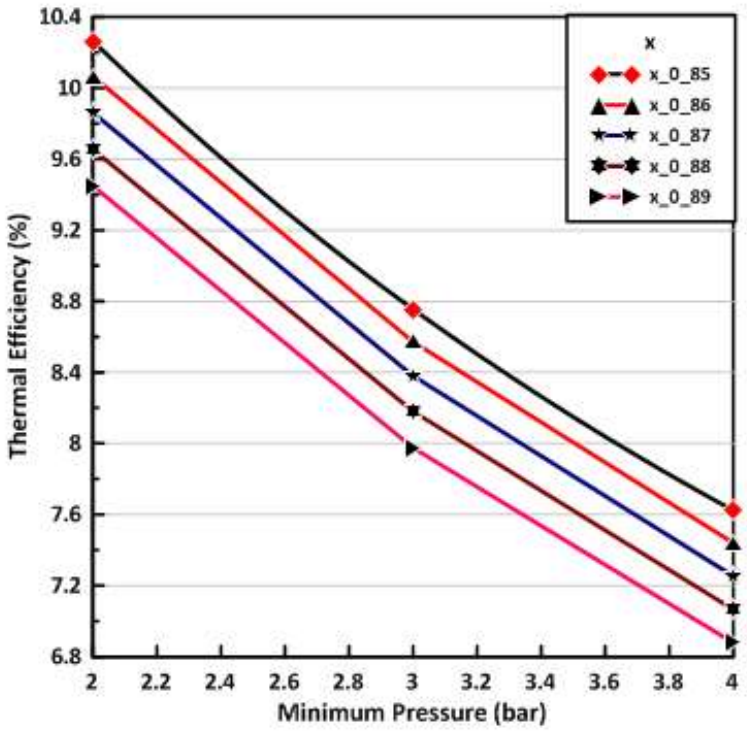

Figure (5.81) Effect of Minimum Pressure on Thermal Efficiency for MKCSE at P_{max}=20 bar and DF=0.3

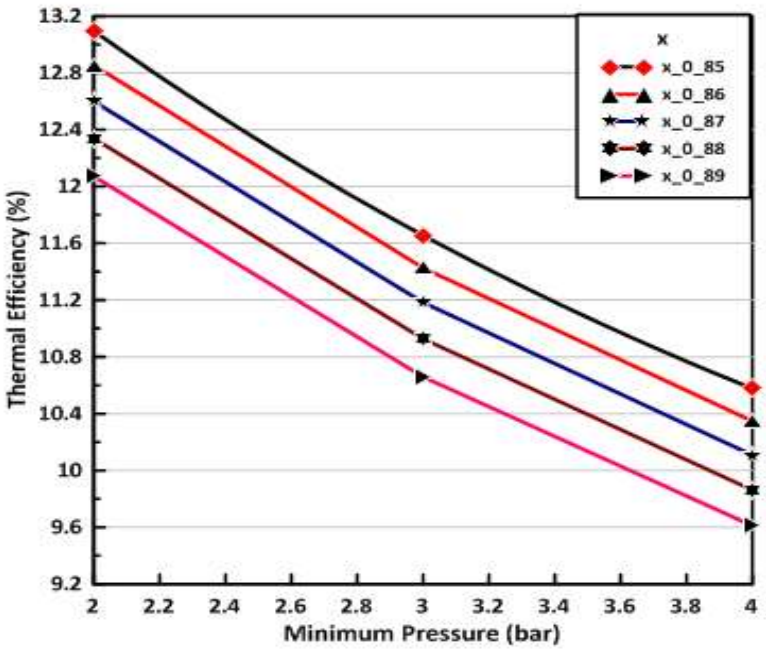

Figure (5-82) Effect of Minimum Pressure on Thermal Efficiency for MKCSE at P_{max}=35 bar and DF=0.3

5.7.3.2 Net Power

Fig (5.83) and fig (5.84) show the relationship between minimum pressure with the net power for different ammonia mass fraction at constant maximum pressure and dryness fraction at separator inlet. It is shown that when the low pressure increases the net power decreases due to decrease of the enthalpy change across the turbine. The highest value of the net power at P_{min}=2 bar because it has high enthalpy change. The lowest value of the net power at P_{min}=4 bar because it has low enthalpy change. The value of the net power is 0.364 kW at x=0.89 and P_{min}=2 bar, but at same ammonia mass flow rate and P_{min}=4 bar the net power is 0.294 kW this drop in the net power accours because the increase of the minimum pressure.

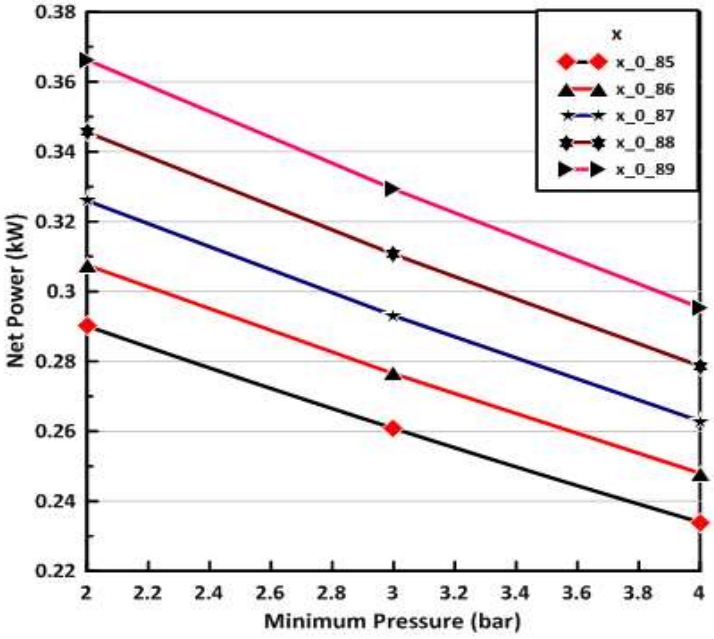

Figure (5.83) Effect of Ammonia Mass Fraction on Net Power for MKCSE with Different Minimum Pressure at P_{max}=20 bar and DF=0.3

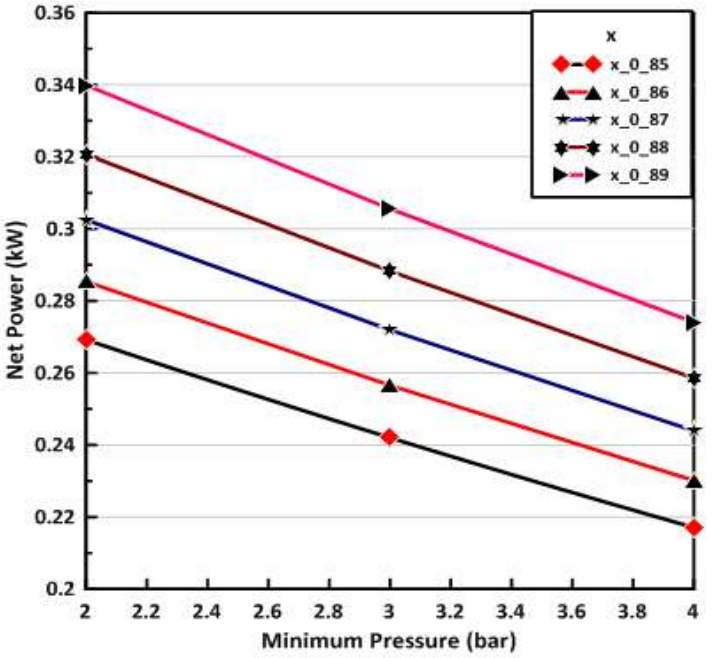

Figure (5-84) Effect of Ammonia Mass Fraction on Net Power for MKCSE with Different Minimum Pressure at P_{max}=35 bar and DF=0.3

5.7.3.3 -Exergy Efficiency

Figs (5.85) and (5.86) show the effect of minimum pressure on exergy efficiency of MKCSE for different ammonia mass fraction at constant maximum pressure. It is found that the highest exergy efficiency is obtained at low pressure 2 bar, high pressure 35 bar at x=0.85, which is 28 .5%. When the minimum pressure increases exergy efficiency decreases which is the same behavior as the cycle thermal efficiency. It is also shown that the exergy efficiency decreases as ammonia mass fraction increases for all minimum pressure since less work is done and more exergy is destructed. It is also shown that the exergy efficiency increases as low pressure decreases since high work is done and less exergy destructed.

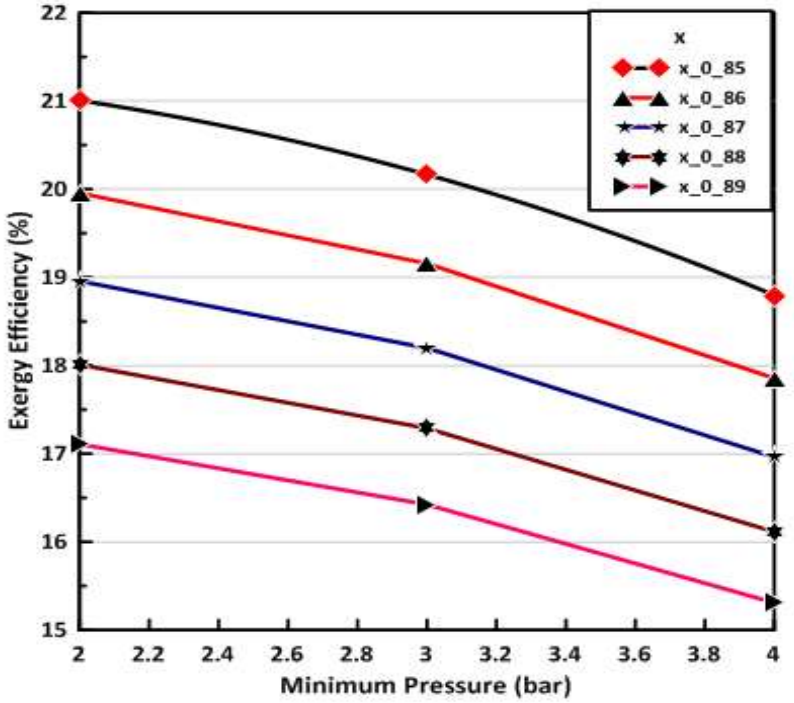

Figure (5.85) Effect of Ammonia Mass Fraction on Exergy Efficiency for MKCSE with Different Minimum Pressure at P_{max}=20 bar and DF=0.3

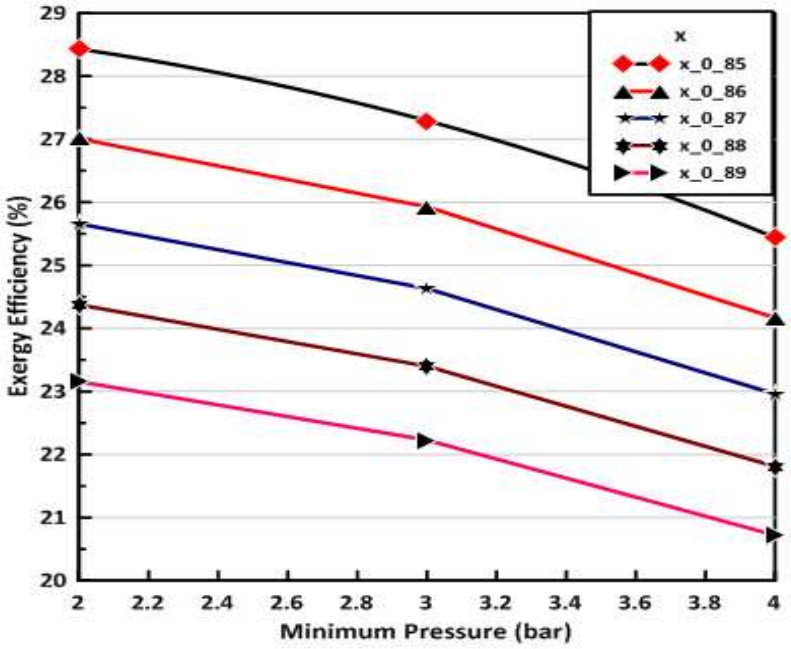

Figure (5.86) Effect of Ammonia Mass Fraction on Exergy Efficiency for MKCSE with Different Minimum Pressure at P_{max}=35 bar and DF=0.3

5.8 Exergy Destruction in MKCSE

5.8.1 - Exergy destruction in each component in MKCSE

Fig (5.87) shows the exergy destruction in each component. It is noticed that the highest exergy destruction is in the heat recovery vapor generator (HRVG) which is about 47% because the high mass flow rate which pass through the HRVG that lead to more loses in the HRVG and also heat transfer devices produce more exergy destruction. It may be due to the higher temperature at which is heat is exchanged. The second component which has more loses is the condenser has 17% from the exergy destruction. The hot working fluid should be cooled in the condenser that is loses. The other loses are in the absorber, separator and heat exchanger are 13%, 9% and 8% respectively. The exergy destruction in the throttling valve is 1% because the temperature doesn't drop too much.

5.8.2 – Cycle Exergy Destruction in All Cycle with Different Conditions

Figs (5.88) and (5.89) show the effect of ammonia mass fraction on exergy destruction in the MKCSE cycle for different minimum pressure at maximum pressure. The dryness fraction is kept constant in both figures at 0.3. It is seen that the exergy destruction increases with the increasing ammonia mass fraction in the solution due to the increase in the circulate rate throughout the cycle. The exergy destruction in P_{max}=35 bar and x=0.89 is larger than the exergy destruction at P_{max}=20 bar and x=0.89 because the net power at P_{max}=20 bar is higher than the net power at P_{max}=35 bar. As mention in section 5.2.2 when the maximum pressure increases the mass flow rate decreases.

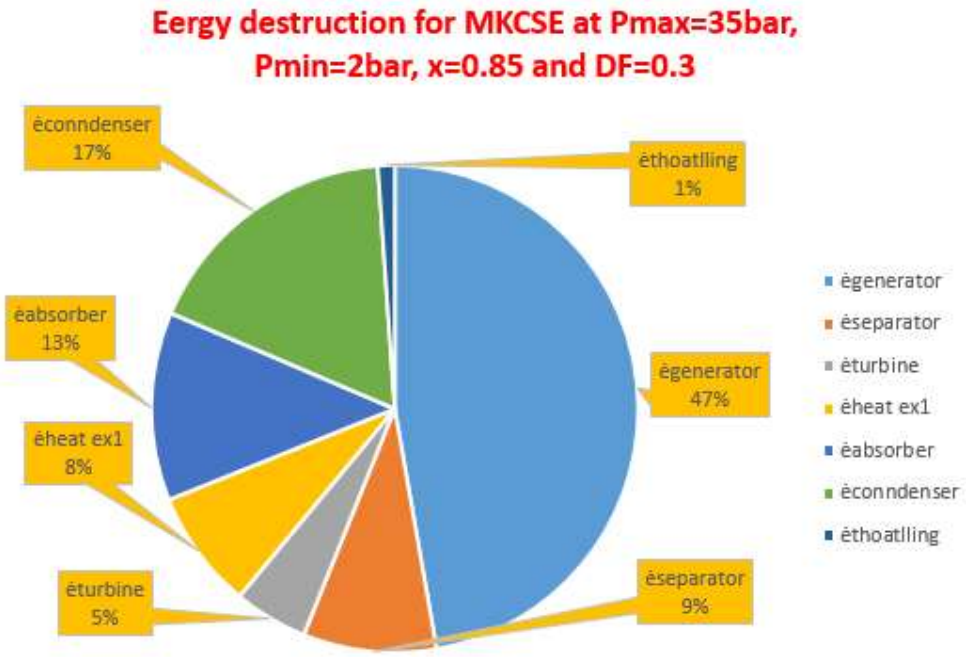

Figure (5.87) Exergy Destruction in MKCSE at P_{max}=35 bar, P_{min}=2 bar, X=0.85 and DF=0.3

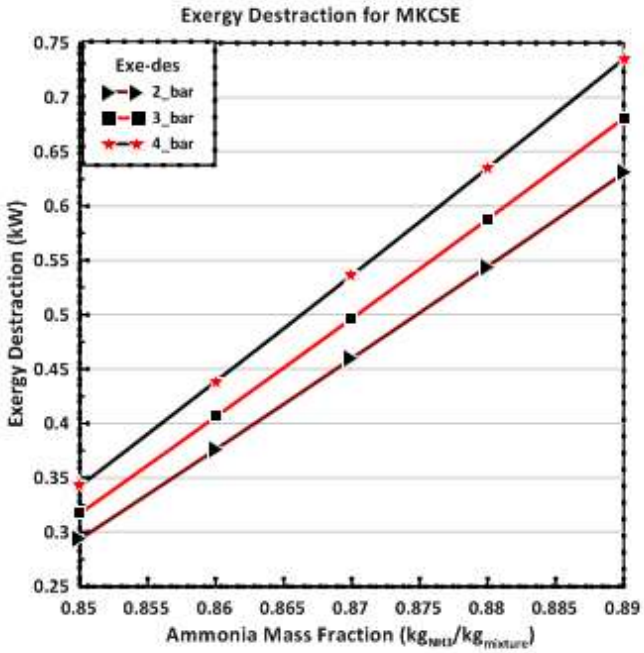

Figure (5-88) Exergy Destruction for MKCSE at P_{max}=20 bar and DF=0.3

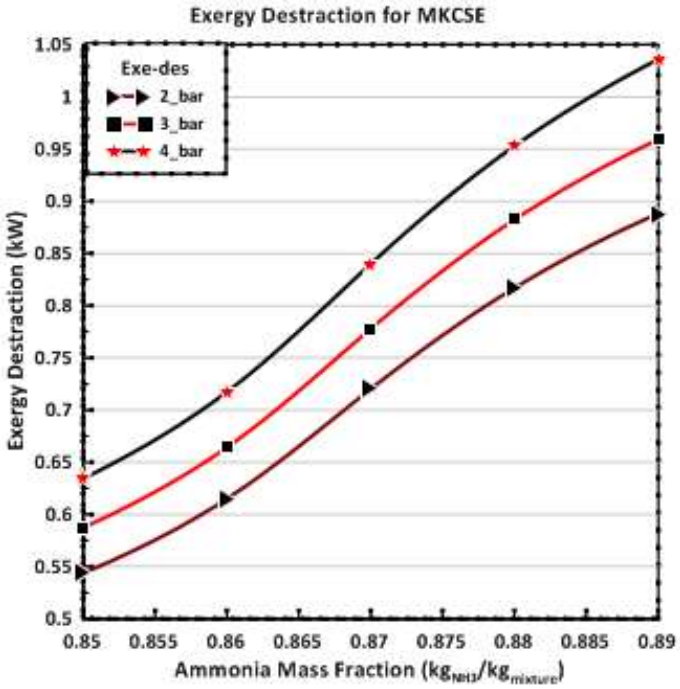

Figure (5-89) Exergy Destruction for MKCSE at P_{max}=35 bar and DF=0.3

5.9 Optimizing Operating Conditions

5.9.1 Thermal Efficiency

Figs (5.90-5.93) display the relationship between the thermal efficiency, maximum pressure and ammonia mass fraction at P_{min} = 3 bar and 2 bar for MKCS1 and MKCSE. It is noticed that the best operating conditions to obtain maximum thermal efficiency are x=0.85, P_{min}=2 bar and P_{max}=35 bar for both cycles. Also it is very clear that the thermal efficiency decreases with increasing the minimum pressure. For MKCS1 it is dropped from 11.2% to 9.5%, and for MKCSE it is dropped from 10.3% to 8.7%. The deviation between of them in each minimum pressure 2 bar and 3 bar is 8.04% and 7.98% respectively.

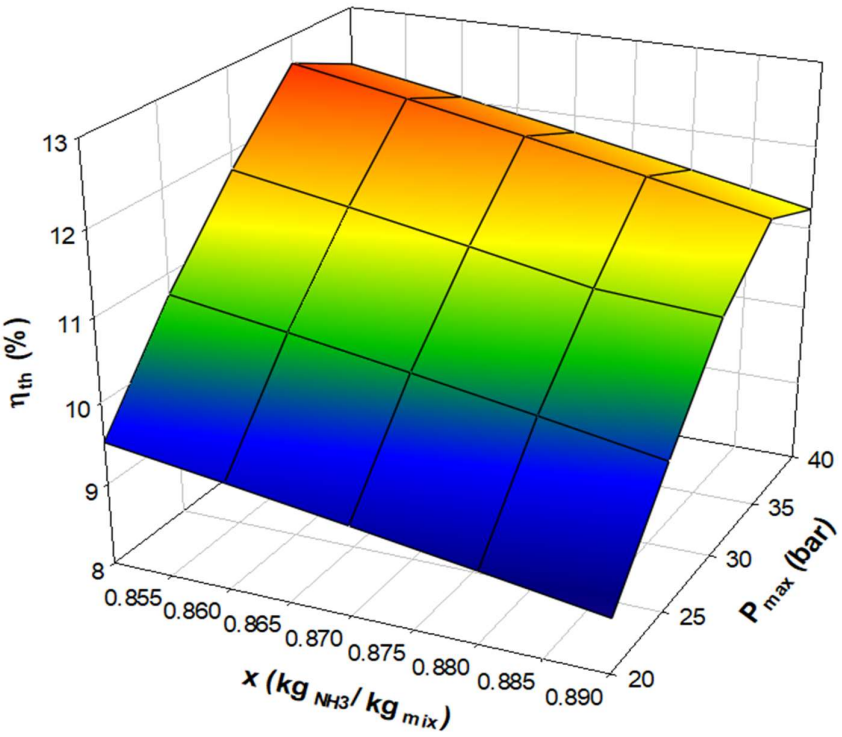

Figure (5.90) Thermal Efficiency for MKCS1 at P_{min}=3 and DF=0.3

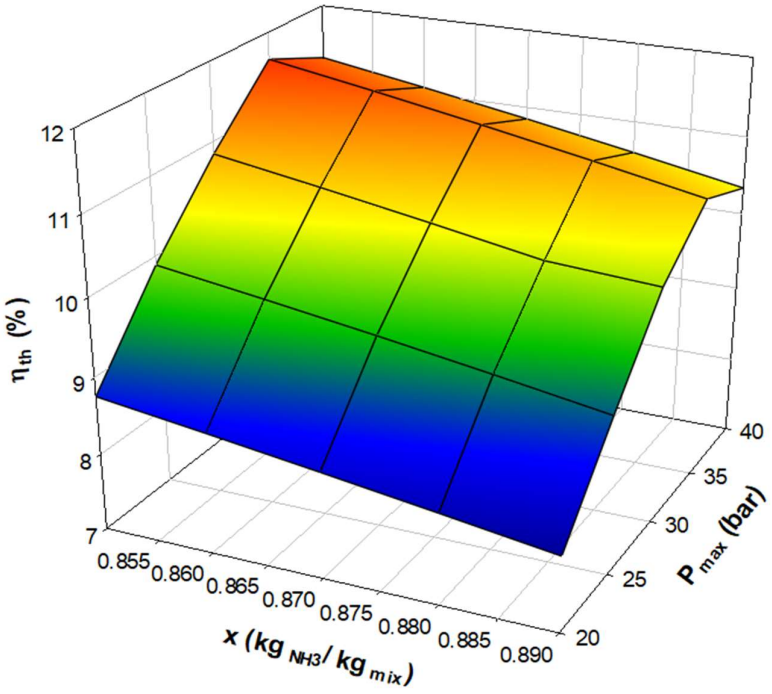

Figure (5.91) Thermal Efficiency for MKCSE at P_{min}=3 and DF=0.3

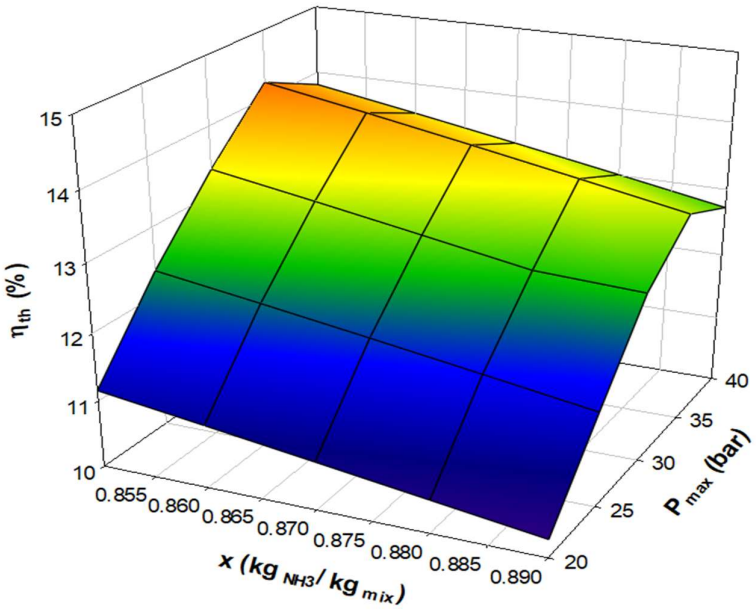

Figure (5.92) Thermal Efficiency for MKCS1 at P_{min}=2 and DF=0.3

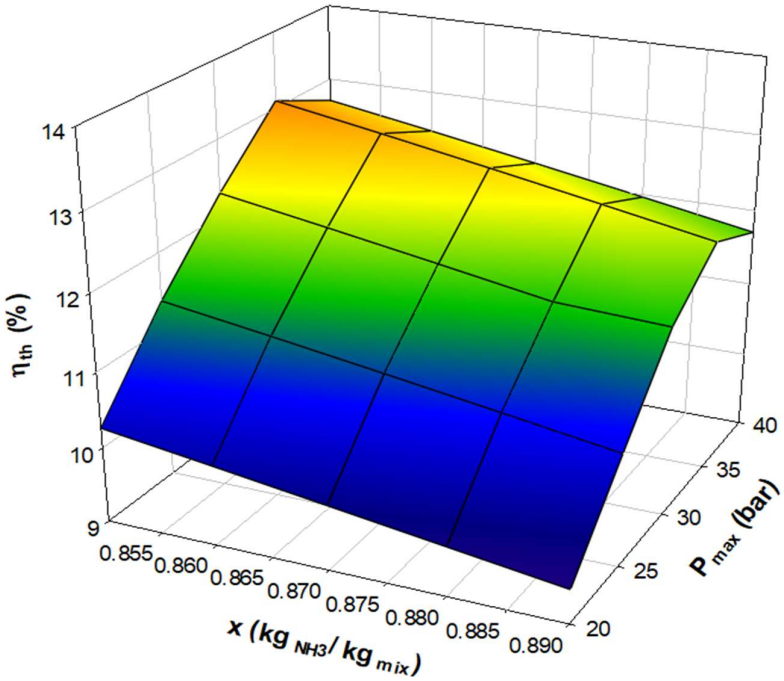

Figure (5.93) Thermal Efficiency for MKCSE at P_{min}=2 and DF=0.3

5.9.2 - Net Power

Figs (5.94-5.97) illustrate the relationship between the net power and ammonia mass fraction and maximum pressure for P_{min} equal 3 and 2 bar with constant DF=0.3 at separator inlet. All the figures have same behavior. When the minimum pressure decreases the net power increases. It is very clear the best condition for net power at x=0.89 because at this condition it has large mass flow rate. It is clear that the effect of the maximum pressure on the net power when the maximum pressure increases the net power decreases. The highest value of net power is obtained at P_{max}=20 bar, x=0.89 and P_{min}=2 bar for both experimental and theoretical. The net power in experimental work is 0.37 kW and the net power in theoretical work is 0.39 kW. The difference between of them is 5.13%.

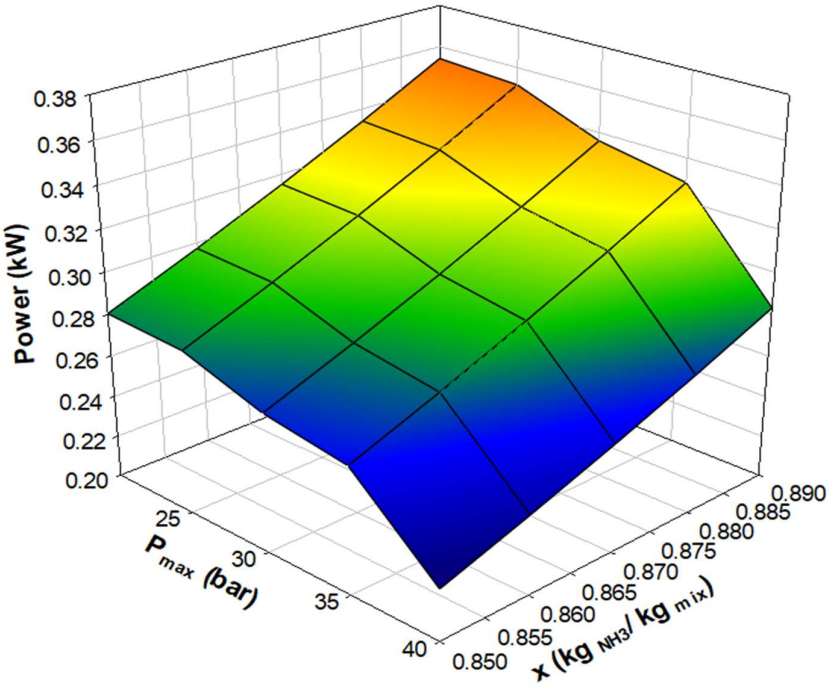

Figure (5.94) Net Power for MKCS1 at P_{min}=3 and DF=0.3

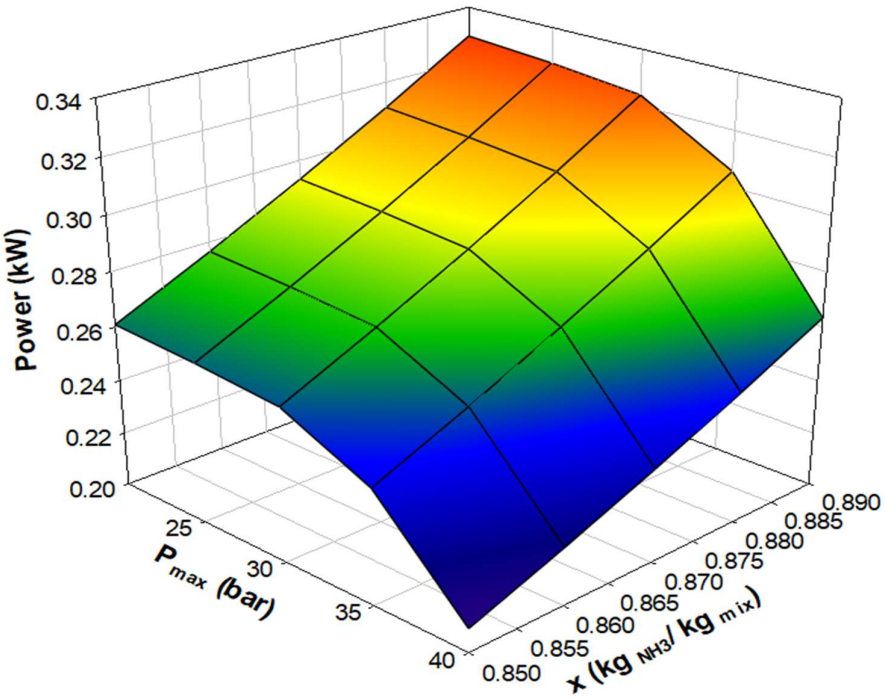

Figure (5.95) Net Power for MKCSE at P_{min}=3 and DF=0.3

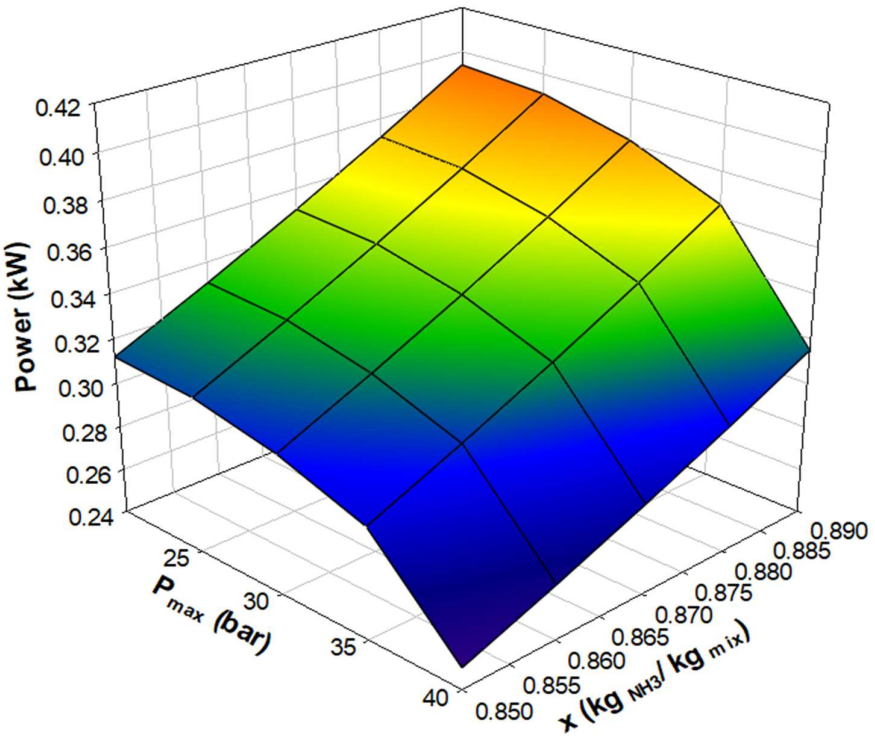

Figure (5.96) Net Power for MKCS1 at P_{min}=2 and DF=0.3

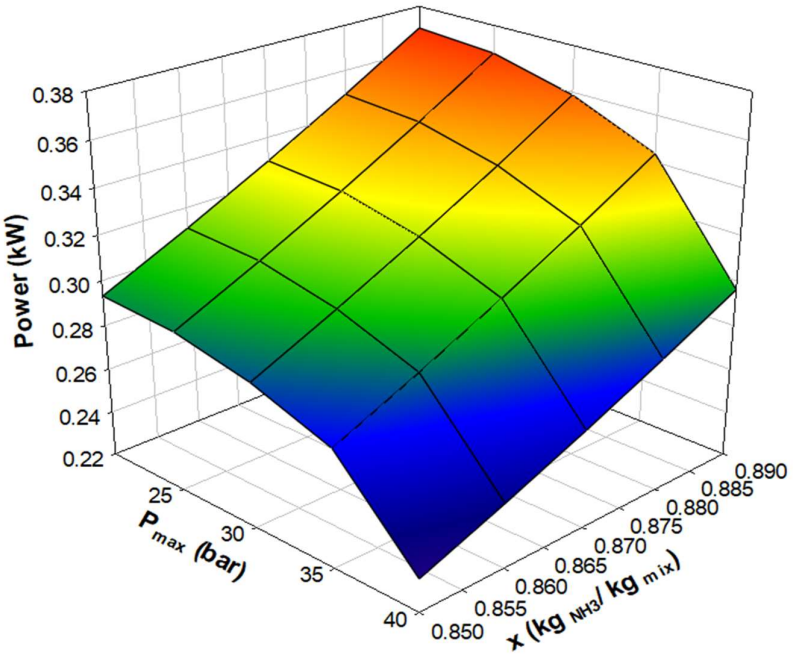

Figure (5.97) Net Power for MKCSE at P_{min}=2 and DF=0.3

5.9.3 -Exergy Efficiency

Figs (5.98-5.101) show the effect of both maximum pressure and ammonia mass fraction on the exergy efficiency for MKCS1 and MKCSE at P_{min}=2 bar and P_{min}=3 bar for constant DF=0.3. It is seen that when the minimum pressure decreases the exergy efficiency increases. The exergy efficiency for MKCS1 is dropped from 30.24% to 28.43% while the exergy efficiency for MKCSE is dropped from 29.23% to 27.29%. The highest exergy efficiency is obtained at P_{max}=35bar, P_{min}=2 bar and x=0.85 for both cycles which are 38% and 28.5% for MKCS1 and MKCSE respectively. The deviation between the experimental work and theoretical work is 5.99% and 6.64%for P_{min}=2 bar and P_{min}=3 bar respectively. The effect of maximum pressure on the performance is the thermal and exergy efficiencies increase, but the net power decreases same as mentioned before.

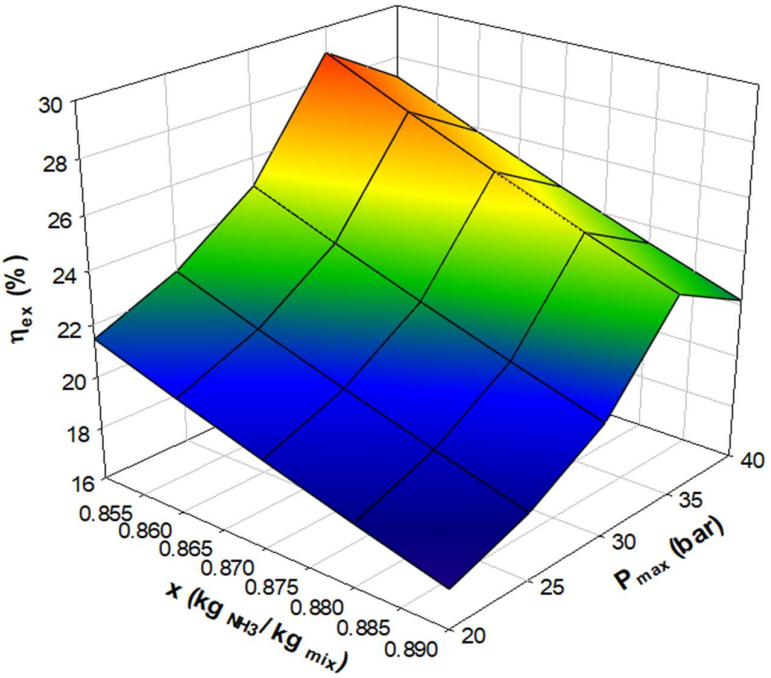

Figure (5.98) Exergy Efficiency for MKCS1 at P_{min}=3 and DF=0.3

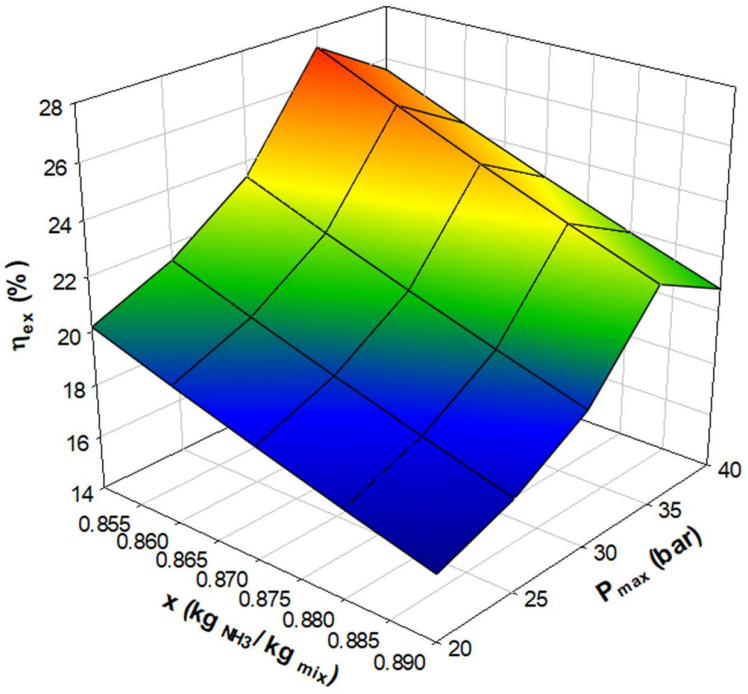

Figure (5.99) Exergy Efficiency for MKCSE at P_{min}=3 and DF=0.3

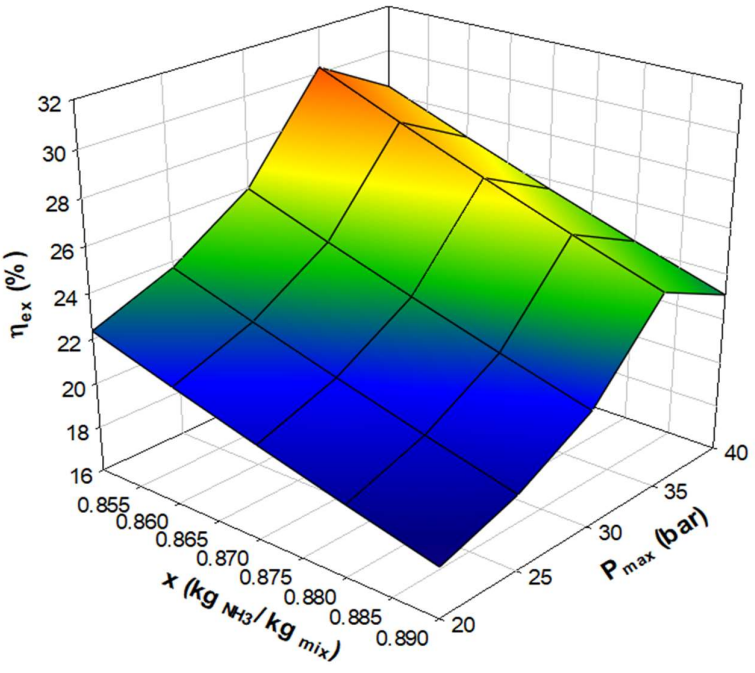

Figure (5.100) Exergy Efficiency for MKCS1 at P_{min}=2 bar and DF=0.3

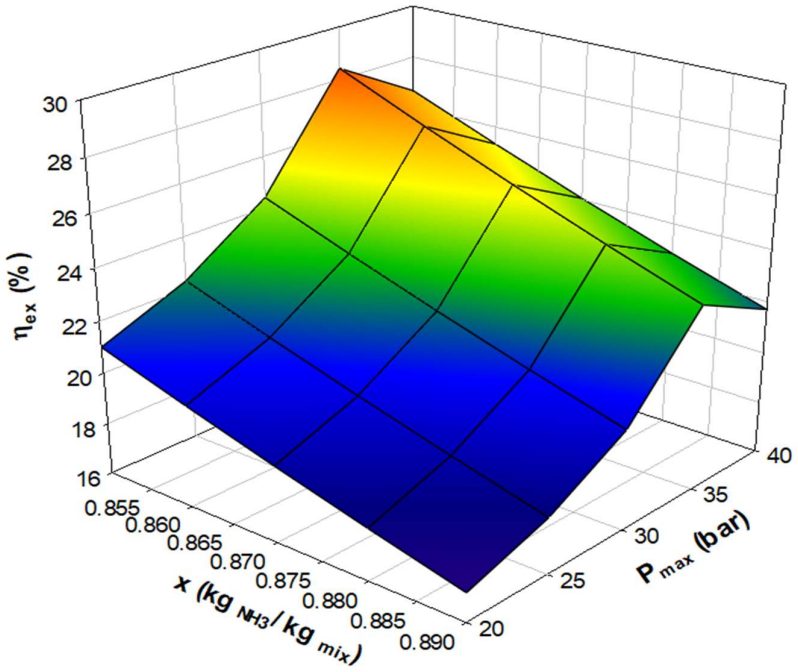

Figure (5.101) Exergy Efficiency for MKCSE at P_{min}=2 bar and DF=0.3

5.10 Comparison between Theoretical and Experimental Cycles Performance

5.10.1 Thermal Efficiency

5.10.1.1 The Effect of the Maximum Pressure

Fig (5.102) shows the effect of the maximum pressure on the thermal efficiency for two cycles MKCS1 and MKCSE with different of ammonia mass fraction with constant minimum pressure and dryness fraction at separator inlet. The trend is same for both of them. When the maximum pressure increases the thermal efficiency increases. The value of maximum thermal efficiency for theoretical and experimental are 14.23% and 13.09% respectively. The deviation between the theoretical and experimental results at P_{min}=2 bar and P_{max}=35 bar is 8.01% which is due to experimental error.

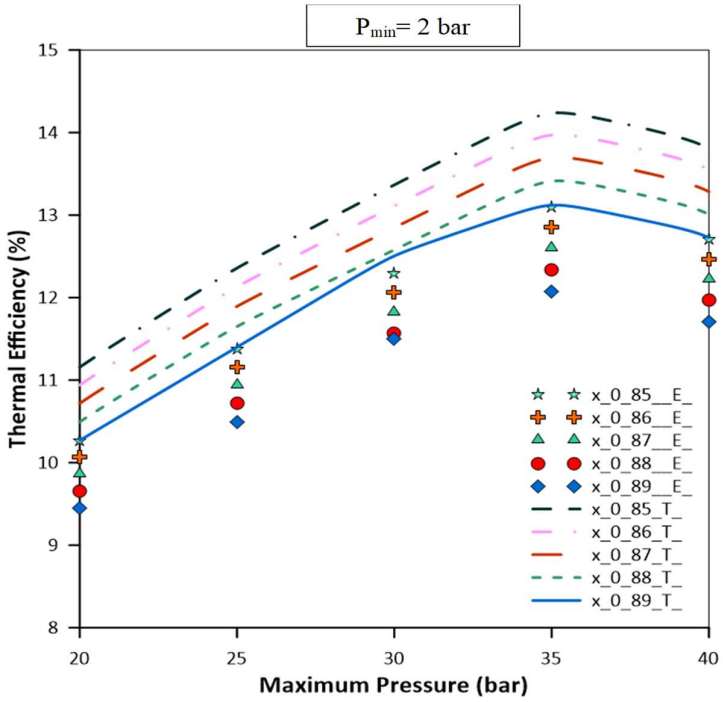

Figure (5.102) Comparison Theoretically and Experimentally the Effect of Maximum Pressure On the Thermal Efficiency at P_{min}=2 bar and DF=0.3 with Different Ammonia Mass Fraction

5.10.1.2 The Effect of the Ammonia Mass Fraction

. Fig (5.103)) demonstrates the effect of the ammonia mass fraction on the thermal efficiency of the two cycles MKCS1 and MKCSE with different maximum pressure and constant minimum pressure and DF at separator inlet. When the ammonia mass fraction increases the thermal efficiency decreases. The deviation between thermal efficiency of MKCS1 and MKCSE at P_{max}=35 bar is 8.02%, 7.95% and 7.86% for 2 bar, 3 bar and 4 bar respectively.

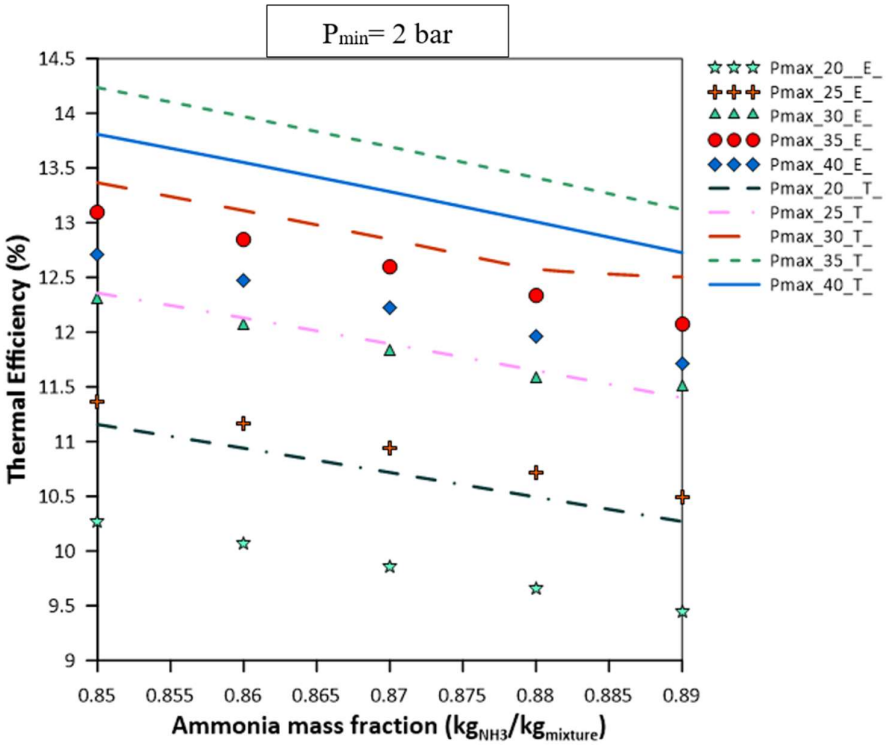

Figure (5.103)) Comparison Theoretically and Experimentally the Effect of Ammonia Mass Fraction on the Thermal Efficiency at P_{min}=2 bar and DF=0.3 with Different Maximum Pressure

5.10.1.3 The effect of the minimum pressure

Fig (5.104) displays the comparison between the experimental and theoretical work. The effect of the minimum pressure on the thermal efficiency of the two cycles MKCS1 and MKCSE with different of ammonia mass fraction. The deviation between the two cycles at x=0.85 and P_{max}=35 bar is 8.01%.

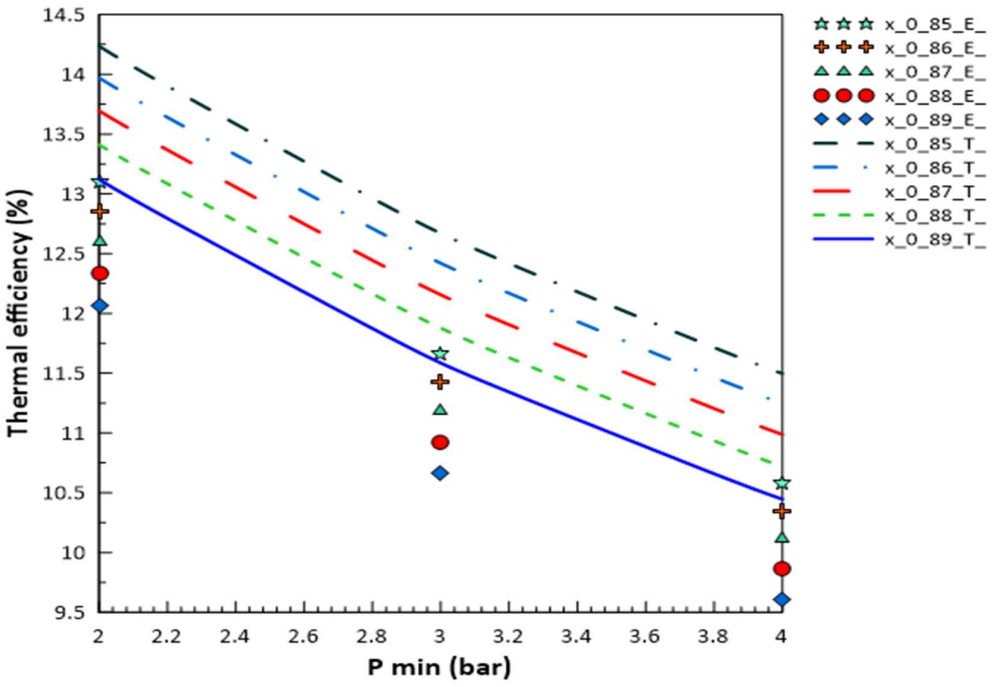

Figure (5.104) Comparison Theoretically and Experimentally the Effect of Minimum Pressure on the Thermal Efficiency at P_{max}=35 bar and DF=0.3 with Ammonia Mass Fraction

5.10.2 Net Power

5.10.2.1 The Effect of the Maximum Pressure

Fig (5.105) illustrates the effect of maximum pressure on the net power for MKCS1 and the net power for MKCSE. The deviation between of the net power for two cycles MKCS1 and MKCSE at x=0.89 and DF=0.3 are 5.99% for 2 bar.

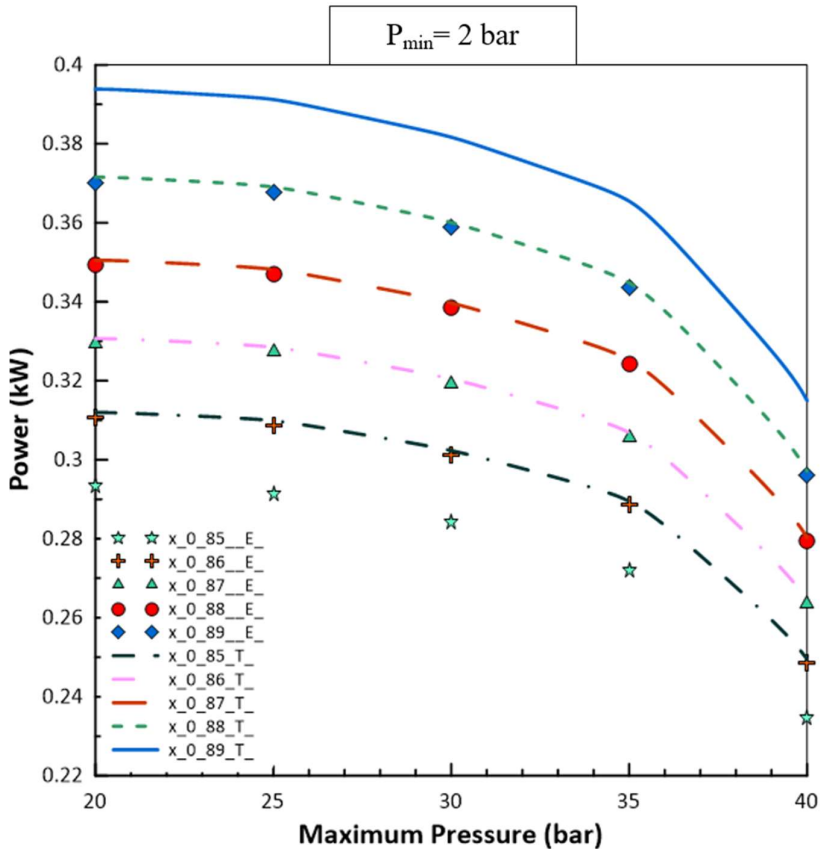

Figure (5.105) Comparison Theoretically and Experimentally the Effect on the Net Power At P_{min}=2 bar and DF=0.3 with Different Ammonia Mass Fraction

5.10.2.2 The Effect of the Ammonia Mass Fraction

Fig (5.106) shows the effect of ammonia mass fraction on the net power for two cycles MKCS1 and MKCSE at P_{max}=35 bar, x=0.85 and DF=0.3 at separator inlet. The deviation between of the net power for two cycles MKCS1 and MKCSE at x=0.85 and DF=0.3 are 7.05% for 2 bar.

5.10.2.3- The Effect of the Minimum Pressure

Fig (5.107) shows the effect of minimum pressure on net power for MKCS1 and MKCSE at P_{min}=2 bar, x=0.89 and DF=0.3. The deviation between of the net power for two cycles MKCS1 and MKCSE at x=0.85 and DF=0.3 are 7.1% for 2 bar.

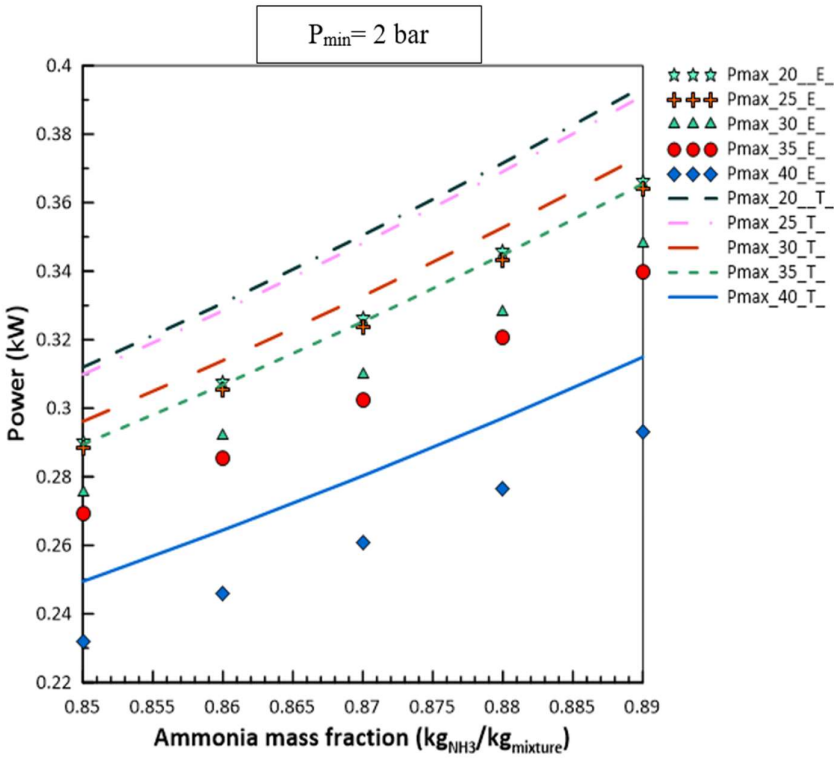

Figure (5.106) Comparison Theoretically and Experimentally the Effect of Ammonia Mass Fraction on the Net Power At P_{min}=2 bar and DF=0.3 with Different Maximum Pressure

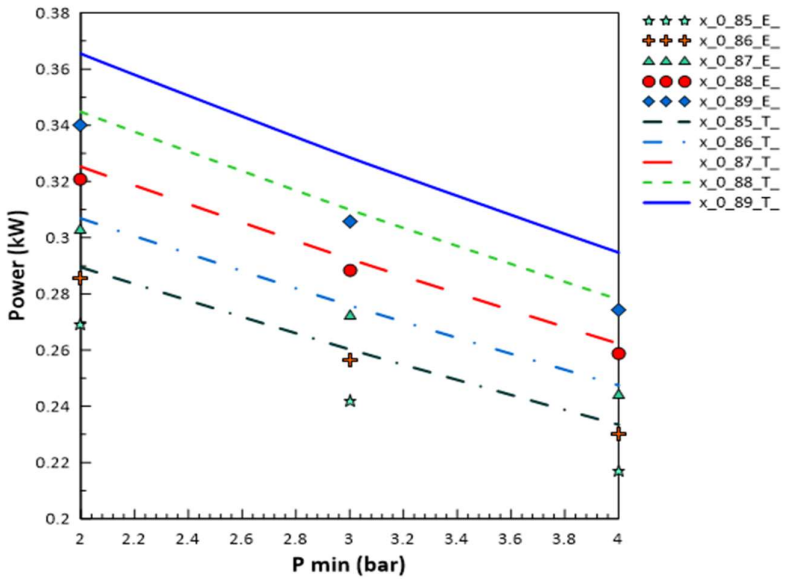

Figure (5.107) Comparison Theoretically and Experimentally the Effect of Ammonia Mass Fraction on the Net Power At P_{max}=35 bar and DF=0.3

5.10.3 Exergy Efficiency

5.10.3.1-The Effect of the Maximum Pressure

Fig (5.108) explains the effect of maximum pressure on the exergy efficiency for MKCS1 and the exergy efficiency for MKCSE at P_{max}=35, x=0.85 and DF=0.3. The deviation between of theoretical and experimental result is 6.01%.

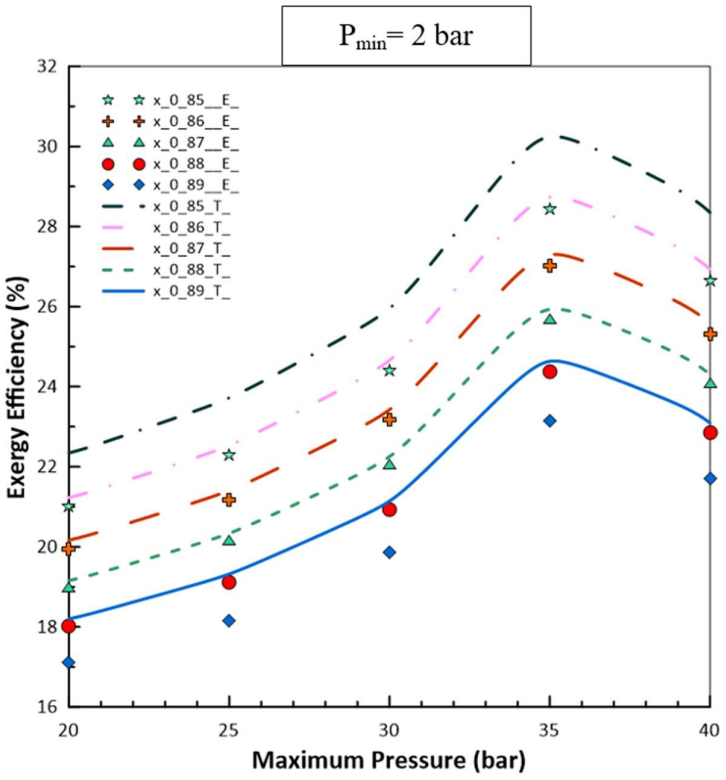

Figure (5.108) Comparison Theoretically and Experimentally the Effect of Maximum Pressure on the Exergy Efficiency at P_{min}=2 bar and DF=0.3 with Different Ammonia Mass Fraction

5.10.3.2 -The Effect of the Ammonia Mass Fraction

Fig (5.109) shows the effect of ammonia mass fraction on the exergy efficiency for two cycles MKCS1 and MKCSE. The deviation between the theoretical and experimental at P_{max}=35 bar, x=0.85 and DF=0.3 is 5.99%.

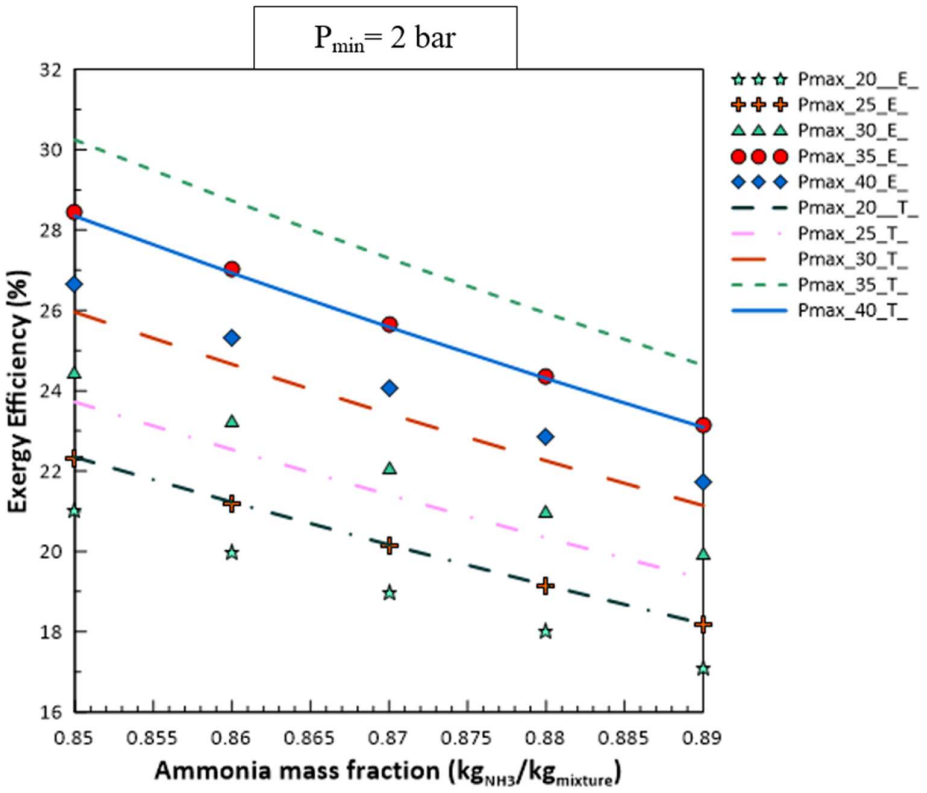

Figure (5.109) Comparison Theoretically and Experimentally the Effect of Ammonia Mass Fraction on the Exergy Efficiency at P_{min}=2 bar and DF=0.3 with Different Maximum Pressure

5.10.3.3-The Effect of the Minimum Pressure

Fig (5.110) shows the effect of ammonia mass fraction on the exergy efficiency for MKCS1 and MKCSE. The differences between the theoretical results and experimental at P_{min}=2 bar, P_{max}=35 bar, x=0.89 and DF=0.3 is 7.65%.

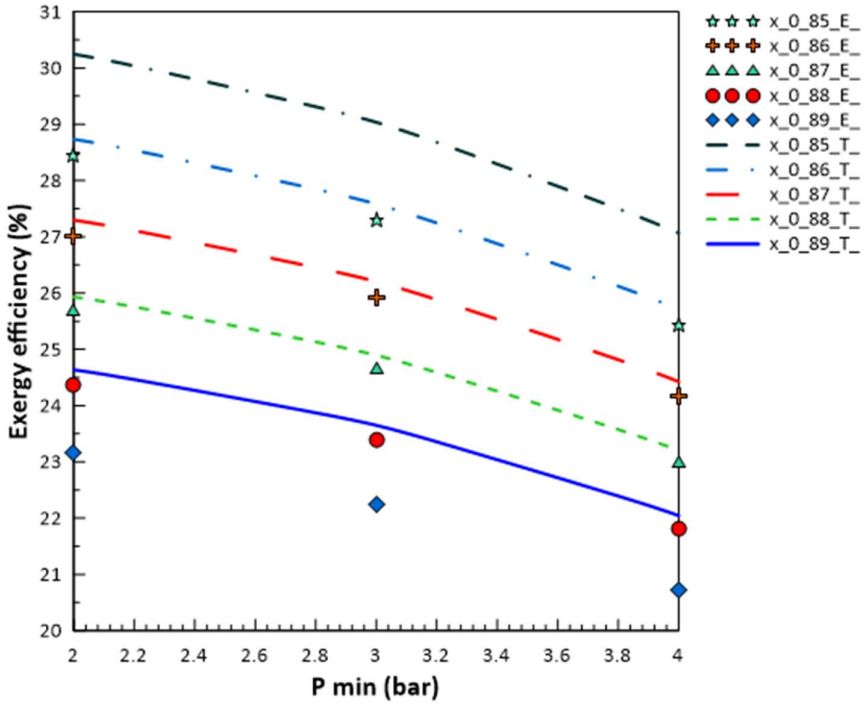

Figure (5.110) Comparison Theoretically and Experimentally the Effect of Ammonia Mass Fraction on the Exergy Efficiency at P_{max}=35 bar and DF=0.3 with Different Minimum Pressure

5.10.4 Exergy Destruction

Fig (5.111) shows the exergy destruction in both cycles MKCS1 and MKCSE. It shows the exergy destruction for different ammonia mass fractions at maximum pressure 35 bar with constant minimum pressure P_{min}=2 bar and dryness fraction DF=0.3. The exergy destruction in the theoretical cycle is less than that in the experimental cycle due to the assumptions used in the theoretical analysis. The difference between the theoretical and experimental cycles may be attributed to accuracy in manufacturing the cycle components, the difference in sizes, the accuracy of measuring devices and due to human errors. There are a lot of loses in experimental work that is why it has largest amount of exergy destruction. As mentioned before when the maximum pressure increases the exergy destruction increases. Also when ammonia mass fraction increases the

exergy destruction increases. All Figures show the effect of ammonia mass fraction on the lowest exergy destruction for MKCS1 and MKCSE at P_{min}=2 bar, x=0.85 and DF=0.3 are 0.66 kW and 0.94 kW respectively. The highest exergy destruction occurs at x=0.89 for MKCS1 and MKCSE which are 1.1 kW and 1.4 kW respectively.

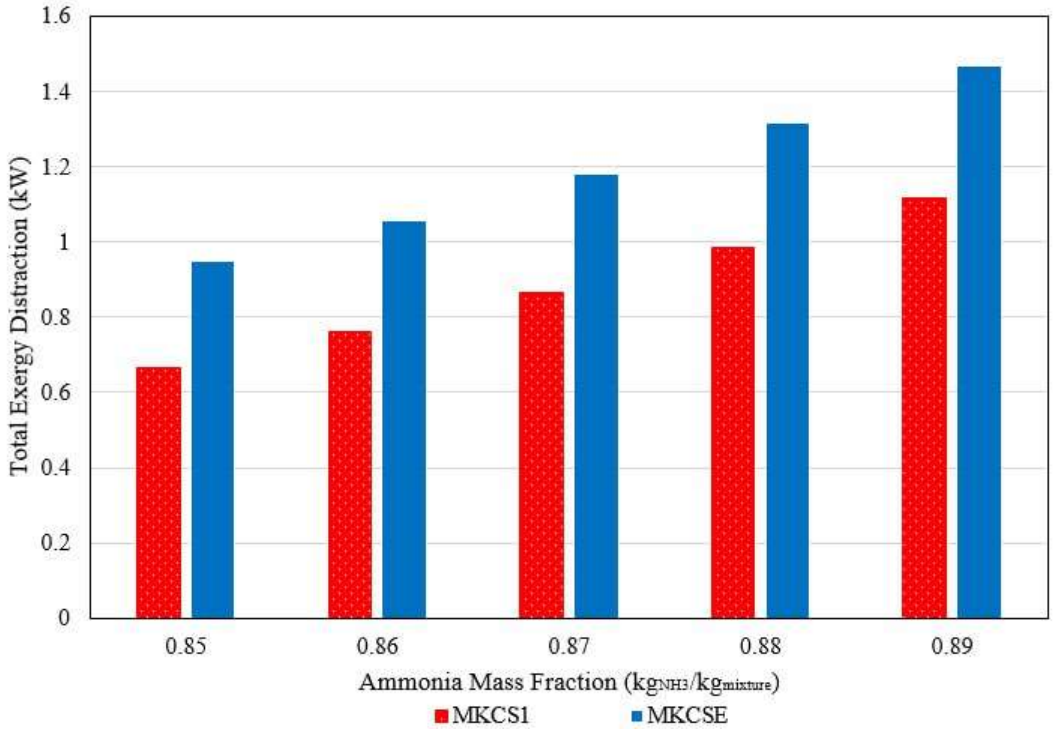

Figure (5.111) Exergy Destruction in Each Cycle at P_{max}=35 bar, P_{min}=2 bar and DF=0.3

5.11 Economic Feasibility

Kalina cycle system is a good solution to produce electricity from low temperature heat sources such as waste heat. Therefore the use of KCS helps to reduce the fossil fuels consumption and reduce harmful emission of greenhouse gases (GHG) globally by producing useful power from heat which is otherwise rejected to environment. The calculation of equivalent fuel saving and equivalent CO_2 emission reduction is based on MKCS2

cycle, which gave maximum power production. This calculation is based on the following assumptions:

1- Assume the fuel is diesel fuel with a chemical formula of ($C_{16}H_{34}$), with lower calorific value of 44000 kJ/kg.
2- The thermal efficiency for conversion from thermal energy to electricity energy is 25%.
3- The fuel air mixture is stoichiometric.

For MKCS2 the net output power is 0.41 kW at P_{max}=20 bar and x=0.89.

To find $\dot{Q}_{in}$ (heat input in HRVG) from equ. (5.7), this value represents the total required thermal energy.

$$(\eta_{conv})_{th} = \frac{\dot{W}_{net}}{\dot{Q}_{in}} \quad (5.7)$$

$$\dot{Q}_{in} = \frac{0.41}{0.25} = 1.64 \text{ kW}$$

To find fuel mass flow rate $\dot{m}_f$ from equ. (5.8)

$$\dot{Q}_{in} = \dot{m}_f * LCV \quad (5.8)$$

$$\dot{m}_f = \frac{\dot{W}_{net}}{(\eta_{conv})_{th} * LCV} \quad (5.9)$$

$$\dot{m}_f = \frac{0.41}{0.25 * 44000} = 3.7273 * 10^{-5} \ \frac{kg}{s}$$

The fuel saving per unit electricity power $\frac{\dot{m}_f}{(kW)_{elec}}$ is calculated as follows.

The fuel saving per unit electricity power=$3.7273*10^{-5}/0.41$

$=9.091*10^{-5} \ \frac{kg/s}{kW_{elec}}$

The reduction of CO_2 emission per unit electrical power $\frac{\dot{m}_f}{(kW)_{elec}}$. It is obtained as follows

From chemical reaction equation

$C_{16}H_{34}+24.5(O_2+3.76N_2) \rightarrow 16\ CO_2+ 17\ H_2O+ 92.12\ N_2$

Form the above stoichiometric reaction equation it is found that each 1kg of fuel produces 3.115 kg CO_2. Therefore the fuel consumption rate of $3.73*10^{-5}$ kg/s produces $0.0116*10^{-2}$ kg/s CO_2. The carbon dioxide produced per unit electrical power generated is $0.0283*10^{-2}\ \frac{kg/_s}{kW_{elec}}$.

Where

LCV is Lower calorific value (kJ/kg)

$(\eta_{conv})_{th}$ is Thermal efficiency for convention

Chapter Six

Conclusions and Suggestions for Future Work

Chapter Six: Conclusions and Suggestions for Future Work

6.1 Conclusions

After the analysis of the theoretical and experimental results, the following conclusions are drawn

1- The effect of the dryness fraction on the performance of different versions of Kalina cycles. When dryness fraction increases, the thermal efficiency increases, the net power increases.

2-When the ammonia mass fraction increases, the thermal efficiency decreases, the net power increases, the exergy efficiency decreases and the exergy destruction increases for all cycles.

3- The effect of maximum pressure on the performance of SKCS, MKCS1 and MKCS2 with different ammonia mass fraction and constant minimum pressure and dryness fraction. When maximum pressure increases, thermal efficiency increases till P_{max}=35 bar after that the thermal efficiency drops, the net power drops, exergy efficiency and exergy destruction increase.

4- When the minimum pressure increases, the thermal efficiency, net power and exergy efficiency increase, and exergy destruction drops.

5-The highest exergy destruction occurs in the HRVG. The exergy destruction increases with the increase of the mass flow rate. The exergy destruction for SKCS, MKCS1 and MKCS2 in HRVG is 36%, 46% and 49% respectively. The exergy destruction in the condenser in each cycle is 13%, 18% and 15% for SKCS, MKCS1 and MKCS2 respectively. The exergy destruction in the throttling valve in SKCS, MKCS1 and MKCS2 are 24%, 8% and7% respectively.

6- The best operating conditions are x=0.85, P_{max}=35 bar, P_{min}=2 bar and DF=0.3. The value of the maximum thermal efficiencies for SKCS, MKCS1 and MKCS2 are 9.44%, 14.23% and 23.53% respectively.

7- The optimum operating conditions are found at P_{max}=30.8 bar and x=0.88 for SKCS. The optimum thermal efficiency and optimum net power are 8.8% and 0.33 kW respectively. It is noticed that the optimum operating conditions at x=0.88 and P_{max}=33.5 bar for MKCS1, the optimum value of the thermal efficiency and net power are 13.5% and 0.354 kW. It is found that the value of the optimum P_{max} and x are 34 bar and 0.88 respectively for MKCS2. The value of the optimum thermal efficiency and net power are 21.8% and 0.462 kW respectively.

8- The maximum cycle efficiency is 13.1% at operating conditions P_{max}=35 bar, x=0.85, P_{min}=2 bar and DF=0.3 at separator inlet. The difference between of them is 7.94%.

9- The maximum net power is obtained at P_{max}=20 bar, x=0.89 and DF=0.3 which is 0.37 kW. The deviation between the efficiency of MKCSE is 6.1%.

10- The highest value of exergy efficiency for theoritical and experimental is 30.24% and 28.43% at P_{max}=35 bar, P_{min}=2 bar, DF=0.3 and x=0.89. The deviation between the experimental and theoretical is 5.99%.

11- The exergy destruction, in the heat recovery vapor generator (HRVG) is 40%, while the exergy destruction in other components are condenser, absorber, separator, heat exchanger, pump and the throttling valve are 13%, 9%, 7%, 6%, 1% and 1% respectively in the MKCSE.

12- Thermal efficiency is decreased with an increase of the minimum pressure from 2 bar to 3 bar for MKCSE to be dropped from 10.3% to 8.7%.

13- When the minimum pressure increases from 2 bar to 3 bar and x=0.89, the net power drops in MKCSE from 0.37 kW to 0.32 kW.

14- When the maximum pressure increases, the thermal efficiency increases sharply till P_{max}=35 bar, after that when the maximum pressure increases, the thermal efficiency decreases.

15- When the minimum pressure increases, the exergy efficiency decreases for MKCSE is dropped from 28% to 27%.

6.2 Suggestions for Future Work

1. Studying the effect of super heat conditions at turbine inlet by adding heat exchanger before the turbine.
2. Studying the cycle performance, as a bottoming cycle, integrated with the topping cycle of a solar system or a gas turbine system.
3. Studying the effect of working fluid type on cycle performance.
4. Studying the effect of the reheating system of vapor.
5. Expliot the heat rejected in the condenser to be used for heating.
6. Studying the effect of adding a heat exchanger between the throttling valve and the pump.
7. Using the working fluid which comes from the pump to cool the mixer instead of the cooling mixer system which is used in the present work.

References

REFERENCES

[1] G. Wall. C.-C. Chuang. M. Ishida. R. A. R. Von Spakovsky. And Geskin. Eds, “Exergy Study of the Kalina Cycle." ASME.

[2] Srinivas, Tangellapalli, N. Shankar Ganesh, and Raman Shankar. Flexible Kalina Cycle Systems. Apple Academic Press, 2019.

[3] P. Bombarda, C. M. Invernizzi, and C. Pietra, "Heat recovery from Diesel engines: A thermodynamic comparison between Kalina and ORC cycle," Appl. Therm. Eng., Vol.30, no. 2-3, pp. 212-219, Feb. 2010.

[4] Nihaj A.N.M. and Uddin S., "A Review of Kalina Cycle" Int. Jour. Of Smart Energy Technology and Environmental Engineering. (2020). Volume 1, Issue 1, pp. (77-107).

[5] Ibrahim M. B. and Kovach R. M., "A Kalina Cycle Application for Power Generation". Energy (1993), volume 18, no. 9, pp. 961-969.

[6] kalina A. I., "Combined-Cycle System with novel bottoming cycle" J. Eng. Gas Turbine Power (Oct. 1984), Vol. 106, no 4,pp. (737-742).

[7] kalina A. I.," Combined cycle and Waste Heat Recovery Power System Based on a Novel Thermodynamic Energy Cycle Utilizing Low-Temperature Heat for Power Generation". (1983) Joint Power Generation Con., pp. (1-5).

[8] Kumar A. Ch., Kandpal H., and Kapoor T. "Design and analysis of Kalina cycle for waste heat recovery from 4 stroke multi-cylinders" Int. Res. Jou. Of Eng. And Tech. (IRJET) 2018 Vol.05 pp 2463-2468.

[9] Chen Y., Guo Z., Wu J., Zhang Z. and Hua J. "Energy and Exergy analysis of integrated system of ammonia-water Kalina-Rankine cycle." Energy (2015), pp. 1-10.

[10] Zhang Z., Guo Z., Chen Y., Wu J. and Hua J., "Power generation and heating performances of integrated system of ammonia-water Kalina-Rankine cycle". Energy Conversion and Management. (2015), Vol. 92, pp. 517-522.

[11] Deepak and Gupta, "Thermal Performance of Geothermal Power Plant with KCS". Int. Jour. Of Ther. Tech. (2014), Vol. 4, No.2, pp. 61-64.

[12] Congcong Z., Yu Z., Lei Z., Linlin L., Jian D. and Shengqiang S. "A novel pinch-based mothod for process integration and optimization of Kalina cycle". Energy Con. and management. (2020), Vol. 209, issue 112630, pp. (1-9).

[13] Ulirk Larsen, Tuong-Van Nguyen, Thomas K. and Fredrik H., "System analysis and optimization of a Kalina split-cycle for waste heat recovery on large marine diesel engines", Energy. (2014), Vol. 64, pp. 484-494.

[14] Eller, T., Heberle, F., Bruggeman and D., "Techno-economic analysis of novel working fluid pairs for the Kalina cycle". Energy Procedia. (2017), Vol. 129, pp. 113-120.

[15] Modi A., Ryhl M., Andreasen J. G. and Haglind F., "Thermodynamic optimization of a Kalina cycle for a central receiver concentrating solar power plant". Energy Conversion and Management. (2016), Vol. 115, pp. 276-287.

[16] Knudsen T., Clausen L., Haglind and Modi A., "Energy and Exergy analysis of the Kalina cycle for use in concentrated solar power plants with direct steam generation". Energy Procedia. (2014), Vol, 57, pp. 361-370.

[17] Revz M. and Engelhard M., "The New Generation Kalina Cycle". Energy Enhanced Geothermal Innovative Network for Europe. M+W Zander, Strasbourg, France September 14 2006, pp. (1-18).

[18] Zhao P., Wang J. and Dai Y., "Thermodynamic analysis of an integrated energy system based on compressed air energy storage (CAES) system and Kalina cycle". Energy Con. and management. (2015), Vol. 98, pp. 161-172.

[19] Long R., Kuang Z., Zhichun B., and Wei L. "Exergy analysis and performance optimization of Kalina cycle system 11 (KCS-) for low grade waste heat recovery" Energy Procedia. (2019), Vol. 158, pp. 1354-1359.

[20] Ahmed M. and Karimi M., A., "Thermodynamic Analyses of Kalina Cycle". Int. Jor. Of Sci. and Res. (IJSR). (2016), Vol. 5 Issue 3, pp. 2244-2249.

[21] Adi L., P., Muhammad T., F., S., Aziz M., "Adoption of Kalina cycle as a bottoming cycle in Wayang Windu geothermal power plant". Energy Procedia. (2017), Vol. 142, pp. 1147-1152.

[22]Sayed Y. and Tribus M., "Theoretical comparison of the Rankine and Kalina cycles". 1985ASME. Publication AES-Vol. 1, pp. (97-102)

[23] Milenko B. J., Srbislav and Genic N., "Application of modified Kalina cycle in biomass chp plants" Int. Jour. Of Energy Research. (2020), vol 44, issue 11, pp. (8754-8768).

[24] Wei G., Meng J., Du X. and Yang X., "Performance analysis on a hot dry rock geothermal resource power generation system based on Kalina cycle" Energy Procedia. (2015), Vol. 75, pp. 937-945.

[25] Nasruddin, R. Usvika, M. Rifaldi, and A. Noor, "Energy and exergy analyses of Kalina cycle system (KCS) 34 with mass fraction ammonia-water mixture variation," J. Mech. Sci. Technol. (2009), Vol. 23, pp. 1871-1876.

[26] Modi A. and Haglind F. "Thermodynamic optimization and analysis of four Kalina Cycle layouts for high temperature applications" Applied Thermal Engineering 76 (2015) 196-205.

[27] Parvathy D. S. and Varghese J., “Energy Analysis of a Kalina Cycle with Double Turbine and Reheating”. Materials Today: Proceedings. (2021), Vol. 636, pp. (1-7)

[28] Diniz M. P. A. and Raul F. P. A., "KCS34 evaluation for WHR in cement industry". Int. Jour. Of Advanced Eng. Res. And Sci (IJAERS) (2018), vol. 5, issue 11, pp. (190-196)

[29] M. Ishida and K. Kawammura, "Energy and Exergy Analysis of a Chemical Process System Distributed Parameters Based on the Enthalpy-Direction Factor Diagram," Ind. Eng. Chem. Process Des. Dev., vol. 21, no. 4, pp. 690-695, Oct. 1982.

[30] W. Qu, H. Hong, B. Su, S. Tang, and H. Jin, "A concentrating photovoltaic/Kalina cycle coupled with absorption chiller," Appl. Energy, Vol. 224, pp. 481-493, Aug. 2014.

[31] Hoon K., K., Jong H., K., Ho C. and H., "Exergy Analysis of Kalina .and Kalina Flash Cycle by Renewable Energy". Appl. Sci. (2020), Vol. 10, issue, pp. 1-16.

[32] Lee, H. Y.; Park, S.H.; Kim. "Comparative analysis of thermodynamic performance and optimization of Organic flash Cycle (OFC) and Organic Rankine Cycle (ORC)". Appl. Therm. Eng. (2016), Vol. 100, pp. 680-690.

[33] Gharde P., R. and Sali N. and V., "Design of Kalina Cycle for Waste Heat Recovery from 1196 CC Multi-Cylinder Petrol Engine". (2015). Int. Jour. Of Advance Research in Sci. and Engi. IJARSE, Vol. No. 4, Issue 03, pp. (75-84).

[34] Uehara H., Ikegami Y., Fufugawa H. and Uto M., ""Performance Analysis of OTEC System Using Kalina Cycle-Thermodynamic Characteristics of Cycle". Trans. Of the Jap. Soci. Of Mech. Engineers Series B. (1994), vol. 60, issue 578, pp. (3519-3525) ci.nii.ac.jp.

[35] Jonsson M. and Yan J., "Ammonia-water bottoming cycle: a comparison between gas diesel engines as prime movers". Energy. (2001), vol. 26, issue 1, pp. (31-44).

[36] Dhahad A. H., Hussen H., M., Nguyen P., T. and Ghaebi H., "Thermodynamic and thermoeconomic analysis of innovative integration of Kalina and absorption refrigeration cycles for simultaneously cooling and power generation". Energy Con. and Manag. (2020), Vol. 203, pp. 1-16.

[37] Z. Liu, N. Xie, and S. Yang, "Thermodynamic and parametric analyses of coupled LiBr/H_2O absorption chiller/Kalina cycle for cascade utilization of low-grade waste heat," Ener. Convers. Manag. Vol. 205, p. 112370, 2020.

[38] Zhang S., Chen Y., Wu J. and Zhu Z., "Thermodynamic analysis on a modified Kalina cycle with parallel cogeneration power and refrigeration" Energy Conversion Management. (2018), Vol. 163, pp. 1-12.

[39] Demirkaya G., Vasquez R., P., Fontalvo A., Bula A., Yogi D. and G."Experimental and Theoretical Analysis of the Goswamy Cycle Operating at Low Temperature Heat Sources.". Journal of Energy Resources Technology. July 2018, Vol. 140, pp. 1-13.

[40] Abam F., Briggs T., Die O., Ekwe E., Ujuatuonu K., Isaac J. and Ndukwu M. "Thermodynamic of economic analysis of Kalina system with integrated lithum-bromide-absorption cycle for power and cooling production". Energy Reports. (2020), Vol. 6, pp. 1992-2005.

[41] Shankar and Srinivas, "Option in Kalina Cycle Systems". Energy Procedia. (2016), Vol. 90, pp. 260-266.

[42] Kumar N. P., Wanve S., Maheshwari A. and Kumer M., "Kalina Cycle (waste heat recovery applications)-A Review". Int. Jor. Of Advanced in Man., Tech. and Eng. Sci. Vol. 8, Issue 111, march/2018, pp. 1369-1376.

[43] Hettiarachchi H. D. M., Golubovic M., Worek W. M. and Ikegami Y., "The performance of Kalina cycle system 11 (KCS 11) with Low Temperature Heat Resource". J. En. Res. Tech. (2007), vol. 129, issue 3, pp. (243-2470).

[44] Khankari G., Munda J., Karmakar S., "Power Generation from Condenser Waste Heat in Coal-Fired Thermal Power Plant Using Kalina Cycle". Energy Procedia. (2016), Vol 90, pp. 613-624.

[45] Ogriseck S., "Integration of Kalina Cycle in a combined Heat and Power Plant, A Case Study". Applied Thermal engineering. (2009), vol. 29, issue 14-15, pp. 2843-2848.

[46] Zheng, D., Chen, B., Q., Y., and Jin, H., "Thermodynamic analysis of a novel absorption power/cooling combined-cycle". Applied Energy, 2006, 83(4), pp. 311-323.

[47] E. D. Rogdakis, "Thermodynamic analysis parametric study and optimum operation of the Kalina cycle," Int. J. Energy Res. (1996), vol. 20, no. 4, pp. 359-370.

[48] Wall G., Chin C. and Ishida M., R. A. Bajura. "Exergy study of the Kalina cycle". Energy System: Analysis of Industrial Processes. (1989), vol. 10, issue 3, pp. (73-77).

[49] Takeshita, K., Amano, Y., and Hashizume, T., "Experimental study of advanced cogeneration system with ammonia-water mixture cycles at bottoming" Energy, 2005, vol. 30(2-4), pp. 247-260.

[50] Nasruddin, Monasari R., Rizky B., Iiham M., Satrio A. and Surachman A., "Thermodynamic analysis and multi objective optimization of Kalina and absorption cycle for power and cooling driven by Iahenddong geothermal source". Earth and Environmental Science. (2017), Vol. 105, pp. 1-6.

[51] Lorincz, J., Bule I., and Kapov, M.," Performance analyses of renewable and fuel power supply systems for different base station sites ", Energies Journal, Vol. 7, pp 7816–7846, 2014.

[52] Balaras CA., Grossman G., Henning H-M., Infante Ferreira CA., Podesser E. and Wang L.,"Solar air conditioning in europe an overview", Renewable and Sustainable Energy Reviews, Vol. 11, pp 299–314, 2007.

[53] Eller, T., Heberle, F., Bruggeman, D., "Second law analysis of novel working fluid pairs for waste heat recovery by the Kalina cycle".App.Energy 2017, 119, 188-198.

[54] Y. M. Park and R. E. Sonntag, "A preliminary study of the Kalina power cycle in connection with combined cycle system, " Int. J. Energy Res., vol. 14, no. 2, pp. 153-162, 1990.

[55] Murugan R. S. and Subbarao P. M. V., "Thermodynamic analysis of Rankine and Kalina combined Cycle". Int. Jour. Of Thermodynamics. (2008), vol. 11, issue 3, pp. (133-141).

[56] Wang J., Dai Y., L. G.-A., "Energy, and undefined 2009, "Exergy analyses and parametric optimizations for different cogeneration power plants in cement industry". Applied Energy. (2009), vol. 86, issue 6, pp. (941-948).

[57] Rumminger M. D., Dibble R. W., Lutz A. E. and Yoshimura A. S., "An integrated analysis of Kalina cycle in combined cycles". Intersociety Energy Conversion Engineering Conference, 1994, pp. 974-979.

[58] H. Leibowitz, H. M. - Transactions, and undefined 1999, "Design of a 2 MW Kalina cycle binary module for installation in Husavik, Iceland,"…The Geotherm. Resour. Counc. Volume 1, Issue 1, pp. (77-107).

[59] Valdimarsson P. S. Ing, and L. Eliasson, "Factor influencing the economics of the Kalina power cycle and situations of superior performance,"2003, pp. (32-40).

[60] Mlcak H., "Kalina cycle concepts for low temperature geothermal". Trans. Geothermal. Resos Council. (2002), vol. 26, issue 26, pp. (707-713).

[61] Amano, Y., Takeshite, K., Hashizuma, T., Akiba, M., Usui, A., and Tanzawn, Y., "Experimental results of an ammonia-water mixture turbine system". In Proceedings of Int. Joint Power Generation Conf.; New Orleans, LA, USA, (2004), pp. 69-75.

[62] Amano, Y., Suzuki, T., Akaiba, M., Tanzawa, Y., and Usui, A., "A hybrid power generation and refrigeration cycle with NH_3-H_2O mixture". In Proceedings of Int. Joint Po. Gen. Conf., Miami, FL, USA, pp. 23-26.

[63] Borgert J. A. and J. A. V., "Exergoeconomic optimization of a Kalina cycle for power generation," Int. J. Exergy. (2004), Vol. 1, no. 1, pp. 18-28.

[64] Lin D., Zhu Q., Li X., "Thermodynamic comparative analysis between (organic) Rankine cycle and Kalina cycle". Energy Procedia. (2015), Vol. 75, pp. 1618-1623.

[65] X. Zhang, M. He, and Y. Zhang, "A review of research on the Kalina Cycle," Renewable and Sustainable Energy Reviews. (2012), Vol. 16, no. 7, pp. 5309-5318.

[66] M. Conde, “Thermo-physical Properties of (NH_3+H_2O) Mixtures for the industrial design of absorption refrigeration equipment”, Manuel code engineering, (Zurich, Switzerland), 2006.

[67] Shi, Liang, et al. "Absorption of CO_2-NH_3-H_2O mixture in mini-channel heat exchangers." Proceedings 12th IEA Heat Pump Conference. Stitching HPC 2017.

[68] Miyatake O. Laminar-flow heat transfer to a fluid flowing axially between cylinders with a uniform wall heat flux. Int. J. Heat Mass Transfer. 1991;34: 322–327.

[69] Nefs CWM. Experimental validation of a mini-channel multi-tube ammonia-water absorption/desorption model. Delft University of Technology. Master thesis; 2013.

[70] J. P. Holman, “Experimental Methods for Engineers”, 8th Edition, Mcgraw-hill Series in Mechanical Engineering, 2021.

[71] Ganesh N. S. "Development of Thermo-physical Properties of Aqua ammonia for Kalina Cycle System" Int. J. Materials and Product Technology, Vol. 55, Nos. 1/2/3, 2017, pp:113-141.

[72] S. A. Bell, "A beginner's guide to uncertainty of measurement," 2001.

[73] Heat Transfer to Water Boiling Under Pressure Transaction of ASME, vol. 70, 1948, pp: 369-384.

[74] Babaelahi M., Mofidipour E. and Rafat E., “Design dynamic analysis and control-based exergetic optimization for solar-driven Kalina power plant”. Energy. (2019), vol. 187, no. 115977, pp. (1-12).

[75] Incropera, F. P., DeWitt, D. P., Bergman, T. L., & Lavine, A. S. “Fundamentals of heat and mass transfer”. Vol. 6. New York: Wiley, 1996.

APPENDICES

APPENDIX (A)

Design the condenser

EES Code for Condenser Design

"!This example uses the Compact Heat Exchanger library to calculate the heat transfer rate between air and an fluid solution in a cross-flow finned-tube heat exchanger ."

$UnitSystem SI Mass J K Pa

```
L=2.4[inch]*convert(inch,m)                    "length"
HX$='fc_tubes_sCF-775-58T'                     "core geometry"

Call CHX_geom_finned_tube(HX$: D_o, fin_pitch, D_h, fin_thk, sigma, alpha,
A_fin\A)
                                               "geometry parameters"

"Air-side calculations"
{T_C_out=T_H_in}                               "initial guess for T_C_in"
T_C_bar=(T_C_in+T_C_out)/2                     "average temperature on air-
side"

A_fr=W*H                                       "frontal area"
rho_C=Density(Air,T=T_C_in,P=Po#)              "density of air"
m_dot_C=V_dot_C*rho_C                          "mass flow rate of air"
Call CHX_h_finned_tube(HX$, m_dot_C, A_fr, 'Air',T_C_bar,Po#:h_C)
                                               "heat transfer coefficient on air-
side"
Vol=W*H*L                                      "total heat exchanger volume"
A_C=Vol*alpha                                  "total air-side surface area"
R_C=1/(h_C*A_C)                                "air-side resistance"

Call CHX_DELTAp_finned_tube(HX$, m_dot_C, A_fr,L, 'Air', T_C_in, T_C_out,
Po#: DELTAP_C)
                                               "pressure drop on air-side"

"Tube-side calculations"
{T_H_out=T_C_in}                               "initial guess for T_H_out"
T_H_bar=(T_H_in+T_H_out)/2                     "average temperature on liquid-
side"

W_tube=0.0445 [m]                              "horizontal distance between
tubes"
H_tube=0.005 [m]                               "vertical distance between
tubes"
th_tube=0.065 [inch]*convert(inch,m)           "tube wall thickness"
```

```
N_tube_h=floor(L/W_tube)                    "number of tubes horizontally"
N_tube_v=floor(H/H_tube)                    "number of tubes vertically"
L_tube=W*N_tube_h                           "length of one tube"
D_i=D_o-2*th_tube                           "inner tube diameter"
rho_H=800                                   "density of NH3H2O"
m_dot_H=V_dot_H*rho_H                       "mass flow rate of NH3H2O"
call PipeFlow('EG',T_H_bar,Conc_H,m_dot_H/N_tube_v,D_i,L_tube,0[-]:h_H_T, h_H_H ,&
    DELTAP_H_tube, Nusselt_H_T, f_H, Re_H)"correlations for internal flow in a circular tube"

u_H=V_dot_H/(N_tube_v*pi*D_i^2/4)           "velocity of NH3H2O"
K_total=K_Sharp_Edged_Pipe_Exit('turbulent')+K_Sharp_Edged_Pipe_Inlet(D_i)&
    +(N_tube_h-1)*K_ReturnBend(0 [-])       "total minor loss coefficient"
DELTAP_H=DELTAP_H_tube+K_total*rho_H*u_H^2/2
    "total liquid-side pressure loss"
A_H=N_tube_v*pi*D_i*L_tube                  "total liquid-side surface area"
R_H=1/(h_H_T*A_H)                           "liquid-side resistance"

"Fouling"
FF_H=FoulingFactor('Ethylene glycol solution') "liquid-side fouling factor"
R_foul=FF_H/A_H                             "fouling resistance"

"Heat Exchanger Calculation"
R_total=R_C+R_foul+R_H                      "total resistance"
UA=1/R_total                                "conductance"
c_C=cP(Air,T=T_C_bar)                       "specific heat capacity of air"
C_dot_C=c_C*m_dot_C                         "capacitance rate of air"
c_H=cP(EG,T=T_H_bar,C=Conc_H)               "specific heat capacity of NH3H2O"
C_dot_H=c_H*m_dot_H                         "capacitance rate of NH3H2O"
C_dot_min=MIN(C_dot_C,C_dot_H)              "minimum capacitance rate"
NTU=UA/C_dot_min                            "number of transfer units"
eff=HX('crossflow_both_unmixed', NTU, C_dot_C, C_dot_H, 'epsilon')
                                            "effectiveness"
Q_dot_max=C_dot_min*(T_H_in-T_C_in)         "maximum possible rate of heat transfer"
Q_dot=Q_dot_max*eff                         "actual rate of heat transfer"
T_C_out=T_C_in+Q_dot/C_dot_C                "energy balance on air"
T_H_out=T_H_in-Q_dot/C_dot_H                "energy balance on NH3H2O"
```

Design Results

alpha=3285 [m^2/m^3]

A_C=6.711 [m^2]

A_fin\A=0.95 [-]

A_fr=0.1987 [m^2]

A_H=1.729 [m^2]

Conc_H=47 [%]

c_C=1004 [J/kg-K]

C_dot_C=1092 [W/K]

C_dot_H=19.29 [W/K]

C_dot_min=19.29 [W/K]

c_H=3823 [J/kg-K]

DELTAP_C=63.47 [Pa]

DELTAP_H=0.07048 [Pa]

DELTAP_H_tube=0.07027 [Pa]

D_h=0.00348 [m]

D_i=0.01387 [m]

D_o=0.01717 [m]

eff=0.9997 [-]

FF_H=0.000352 [K-m^2/W]

fin_pitch=305 [1/m]

fin_thk=0.0004064 [m]

f_H=16.21 [-]

H=0.3556 [m]

HX$='fc_tubes_scf-775-58t'

h_C=92.11 [W/m^2-K]

h_H_H=166.1 [W/m^2-K]

h_H_T=138.7 [W/m^2-K]

H_tube=0.005 [m]

K_total=1.5 [-]

L=0.06096 [m]

L_tube=0.5588 [m]

m_dot_C=1.087 [kg/s]

m_dot_H=0.005047 [kg/s]

NTU=8.542 [-]

Nusselt_H_T=3.821 [-]

N_tube_h=1 [-]

N_tube_v=71 [-]

Q_dot=270 [W]

Q_dot_max=270.1 [W]

Re_H=3.957 [-]

rho_C=1.212 [kg/m^3]

rho_H=800 [kg/m^3]

R_C=0.001618 [K/W]

R_foul=0.0002036 [K/W]

R_H=0.004392 [K/W]

R_total=0.006213 [K/W]

sigma=0.481 [-]

th_tube=0.001651 [m]

T_C_bar=291.3 [K]

T_C_in=291.2 [K]

T_C_out=291.4 [K]

T_H_bar=298.2 [K]

T_H_in=312.2 [K]

T_H_out=291.2 [K]

UA=162 [W/K]

u_H=0.0005883 [m/s]

Vol=0.01211 [m^3]

V_dot_C=0.8967 [m^3/s]

V_dot_H=0.000003309 [m^3/s]

V_dot_H_gpm=0.05 [gal/min]

APPENDIX

(B)

Calculation of mass of working fluid

The size of the separator=$\pi * r_{sep}^2 * l_{sep}$=9*10^{-3}m^3

The size of the mixer=$\pi * r_{mix}^2 * l_{mix}$=9*10^{-3}m^3

Separator and mixer has same dimensions and same size

The size of the condenser=$a * b * l_c * n$=1.35*10^{-3}m^3

a=3.5*10^{-3}mm, b=41.5mm, l_c=580mm and n=16

There are many pipes have different lengths and different diameters

The size of pipes which connected the HE, mixer and the tank =$\pi * r_p^2 * l_p$=1.5*10^{-3}m^3

The size of the HRVG=$\pi * r_{SG}^2 * l_{SG}$=2.31*10^{-3}m^3

Other plastic pipes= $\pi * r_1^2 * l_1 + \pi * r_2^2 * l_2$=1.92*10^{-4}m^3

The size of the main tank is 3*10^{-2} m^3

The total volume= 19.35 litters

The total mass which is used it at first is 20kg and then it increases with ammonia mass fraction increases for example at x=0.44, the mass of ammonia is 8.8kg and the mass of water is 11.2kg. At x=0.45 the total mass will be 20.364kg, the mass of ammonia is 9.164kg, while the mass of water still same 11.2kg. In this calculation is accounted half size of mixer and half size of separator and at least 5litters in the main tank.

Where

r_{sep} radius of the separator

r_{mix} radius of the mixer

l_{sep} length of the separator (cm)

l_{mix} length of the mixer (cm)

a, b, l_c and n are the width, height of the cross section of tube of the condenser, length and number of turns of the condenser tube.

r_p and l_p are the radius and length of the pipes which connected the heat exchanger and mixer.

r_{SG} and l_{SG} are the radius and length of the steam generator.

r_1, l_1, r_2 and l_2 the radius and the length of the two plastic pipes.

APPENDIX

(C)

Calibration Certifications

COSQC
Central Organization For Standardization and Quality
Calibrated
Cert. No : IRE/287
Date : 8-11-2022
Due to (if applicable) :

C.O.S.Q.C IRAQ

Calibration Certificate

Central Organization for Standardization and Quality Control (COSQC)
Metrology Department/Mass & Pressure Section/Pressure Lab.
P.O. Box13032 Algeria street, Baghdad ,Tel:7765180 E-Mail : cosqc@cosqc.gov.iq

Certificate No: PRE/ 287 /2022

QF-7.8-01-C **Date of issue: 8/ 11 /2022**

Customer			
Name:	جامعة بابل/كلية الهندسة/شعبة الدراسات العليا		
Address:	بابل		
Item under calibration			
Description:	Pressure gauge		
Manufacturer:	P-NEU TEC		
Model:	Bourdon Tube		
Serial number:	138-1		
Other identification:	Range = 60 bar	d = 1 bar	
Date of reception:	3/11/2022	Oredr No.= 138	
Condition of reception:	As found		
Standard(s) used in the calibration			
Description:	Digital Pressure Gauge		
Manufacturer:	GE Druck		
Model:	DPI104		
Serial number:	5287298		
Other identification:	Range = 700 bar	d = 0.01 bar	

Calibration information	
Date of calibration:	8 /11 /2022
Place of calibration:	Pressure Lab
Method(s) of calibration:	Calibration method are based on (QF-7.8-01-C) according to DKD-R 6-1:2014
Calibrated quantity:	Pressure
Results of calibration:	Attached a complete result in Annex 1 of this certificate
Measurement uncertainty:	The reported expanded uncertainty is DKD-R 6-1:2014 and the standard Uncertainty multiplied by coverage factor k=2 to give confidence level of 95% .
Metrological traceability:	The traceability of measurement to the SI units issued by the National Standard maintained at centeral organization for standardization and quality control through calibration certificat issued of certificate NO.= REF/PRE/033/2022
Environmental conditions of calibration:	Temp.(23°C) R.H(41%)
Observations, opinions or Recommendations:	**The resulte are within the tolerance according to DKD-R 6-1:2014 & decision rule**

COSQC

Approved by:
Saif Ali
Head of Mass & Pressure Section
8/ 11 /2022

page 1 of 2

This certificate is issued in accordance with the laboratory accrediation requirements.It provides tracibility of measurement to recognized national standards,and to the units of measurement realized at the COSQC or other recognized national standards laboratories.This certificate may not be reproduced other than in full by photographic process.This certificate refers only to the particular item submitted for calibration

Calibration Certificate

Central Organization for Standardization and Quality Control (COSQC)
Metrology Department/Mass & Pressure Section /Pressure Lab.

P.O. Box13032 Al jadria street, Baghdad ,Tel:7765180
E-Mail : cosqc@cosqc.gov.iq

Certificate No: PRE/ 287 /2022
Date of issue: 8/ 11 /2022

QF-7.8-01-C

Annex 1/ Results

Pressure Standard	Reading from calibration		Mean value	Deviation (M-Pstand.)	Expanded Uncertainty	Error span	
	M1(up)	M2(down)	bar	bar	±bar	(Dev.+Uexp)	(Dev.-Uexp)
bar	bar	bar				bar	bar
0	0.0	0.0	0.00	0.00	0.15	PASS	PASS
10	10.3	10.5	10.40	0.40	0.19	PASS	PASS
20	20.5	20.8	20.65	0.65	0.23	PASS	PASS
35	35.7	35.7	35.70	0.70	0.15	PASS	PASS
37	37.8	37.8	37.80	0.80	0.15	PASS	PASS
40	40.7	40.7	40.70	0.70	0.15	PASS	PASS

Tolerance =± 1.00 bar

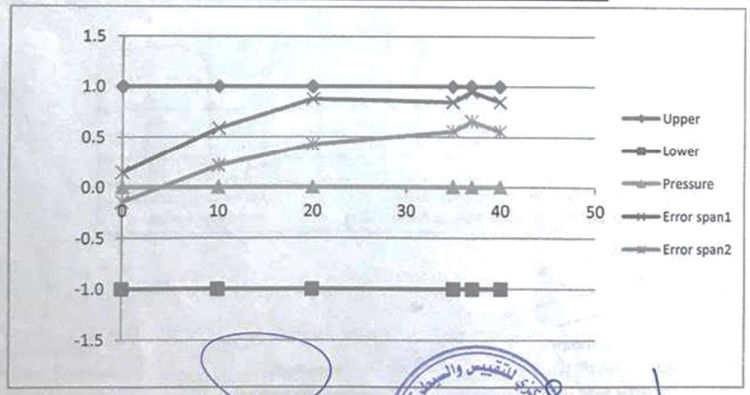

Calibrated by:
Mustafa Faisal
8/ 11 /2022

Revisid by :
Nabeel Lateef
8/ 11 /2022

COSQC

Approved by:
Saif Ali
Head of Maas & Pressure Section
8/ 11 /2022

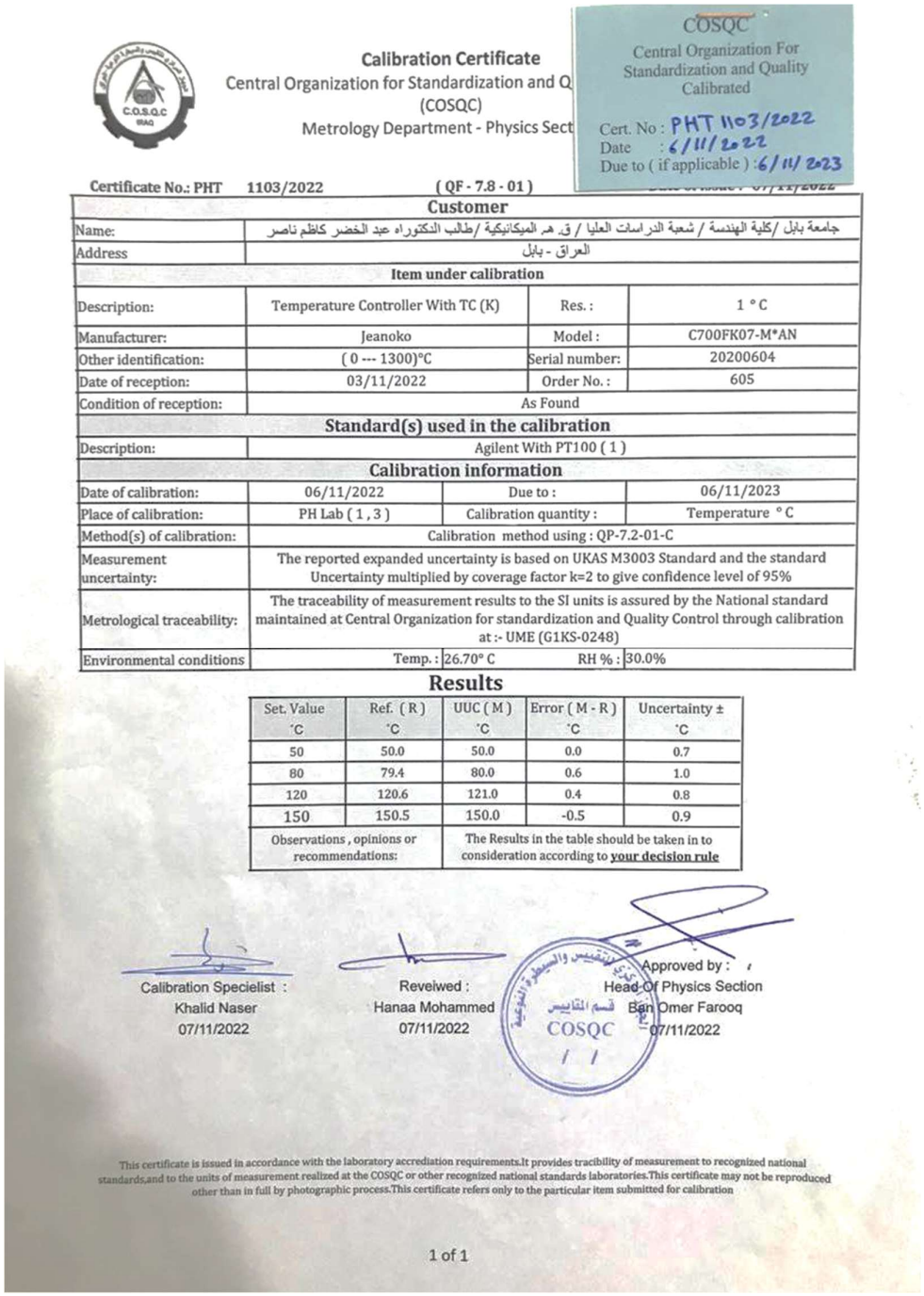

Calibration Certificate
Central Organization for Standardization and Q
(COSQC)
Metrology Department - Physics Sect

COSQC
Central Organization For Standardization and Quality
Calibrated
Cert. No : PHT 1103/2022
Date : 6/11/2022
Due to (if applicable) : 6/11/2023

Certificate No.: PHT 1103/2022 (QF - 7.8 - 01)

Customer			
Name:	جامعة بابل /كلية الهندسة / شعبة الدراسات العليا / ق. هـ الميكانيكية /طالب الدكتوراه عبد الخضر كاظم ناصر		
Address	العراق - بابل		
Item under calibration			
Description:	Temperature Controller With TC (K)	Res. :	1 °C
Manufacturer:	Jeanoko	Model :	C700FK07-M*AN
Other identification:	(0 --- 1300)°C	Serial number:	20200604
Date of reception:	03/11/2022	Order No. :	605
Condition of reception:	As Found		
Standard(s) used in the calibration			
Description:	Agilent With PT100 (1)		
Calibration information			
Date of calibration:	06/11/2022	Due to :	06/11/2023
Place of calibration:	PH Lab (1 , 3)	Calibration quantity :	Temperature °C
Method(s) of calibration:	Calibration method using : QP-7.2-01-C		
Measurement uncertainty:	The reported expanded uncertainty is based on UKAS M3003 Standard and the standard Uncertainty multiplied by coverage factor k=2 to give confidence level of 95%		
Metrological traceability:	The traceability of measurement results to the SI units is assured by the National standard maintained at Central Organization for standardization and Quality Control through calibration at :- UME (G1KS-0248)		
Environmental conditions	Temp. : 26.70° C	RH % :	30.0%

Results

Set. Value °C	Ref. (R) °C	UUC (M) °C	Error (M - R) °C	Uncertainty ± °C
50	50.0	50.0	0.0	0.7
80	79.4	80.0	0.6	1.0
120	120.6	121.0	0.4	0.8
150	150.5	150.0	-0.5	0.9
Observations , opinions or recommendations:		The Results in the table should be taken in to consideration according to **your decision rule**		

Calibration Specielist :
Khalid Naser
07/11/2022

Reveiwed :
Hanaa Mohammed
07/11/2022

Approved by :
Head Of Physics Section
Ban Omer Farooq
07/11/2022

COSQC

This certificate is issued in accordance with the laboratory accrediation requirements.It provides tracibility of measurement to recognized national standards,and to the units of measurement realized at the COSQC or other recognized national standards laboratories.This certificate may not be reproduced other than in full by photographic process.This certificate refers only to the particular item submitted for calibration

1 of 1

APPENDIX

(E)

Published Articles

Certificate

OF PARTICIPATION

THIS CERTIFICATE IS PROUDLY PRESENTED TO

Abdulkhodor Kathum Nassir

For successful participation in the 1st International Conference on Advances in Engineering Science and Technology (AEST-2021), Iraq, with the STEPS Ltd, and Liverpool John Moores University, UK that was held online on 26-27th April 2021.

Prof. Dr. Jasim M.Salman
On behalf of the University of Babylon
Signature

R. S. Mohammed
On behalf of the Academic Steps Ltd
Signature

University of AlKafeel

Acceptance Letter

Author :Abdulkhodor Kathum Nassir [1] ,Haroun A. K. Shahad [2]
Affiliation : [1,2] Department of Mechanical Engineering University of Babylon, Babylon-Iraq
Email : abdul.hussain@student.uobabylon.edu.iq

Dear (author) We are pleased to inform you that your manuscript,
Kalina Cycle System (a State of the Art)
after being peer- reviewed , has been accepted for participating in the

4th INTERNATIONAL SCIENTIFIC CONFERENCE OF ALKAFEEL UNIVERSITY , ISCKU 2022

in Al-Najaf Al-Ashraf, Iraq ,December 20th -21st , 2022 . Given that your manuscript will be published after passing the conference Scopus-indexed journals requirements.

With Best Regards

N. ALDAHA

Prof. Dr. N. Al-Dahan
Rector of Alkafeel University

AIP Publishing Scientific.Net Scopus

University of AlKafeel

Acceptance Letter

Authors : Abdulkhodor Kathum Nassir [1], Haroun A. K. Shahad [2]
Affiliation :[1,2] Department of Mechanical Engineering University of Babylon-Babylon-Iraq
Email of Corresponding Auther : abdul.hussain@student.uobabylon.edu.iq

Dear (author) We are pleased to inform you that your manuscript,
Thermodynamic Analysis of Ammonia Mass Fraction Effect on Simple Kalina Cycle System Performance
after being peer- reviewed , has been accepted for participating in the

4th INTERNATIONAL SCIENTIFIC CONFERENCE OF ALKAFEEL UNIVERSITY , ISCKU 2022

in Al-Najaf Al-Ashraf, Iraq ,December 20th -21st , 2022 . Given that your manuscript will be published after passing the conference Scopus-indexed journals requirements.

With Best Regards

Prof. Dr. N. Al-Dahan
Rector of Alkafeel University

Scopus AIP Publishing

Kalina Cycle System (a State of the Art)

Abdulkhodor Kathum Nassir [a)] and Haroun A. K. Shahad [b)]

Department of Mechanical Engineering University of Babylon, Babylon-Iraq

[a)]Corresponding author : abdul.hussain@student.uobabylon.edu.iq
[b)]hakshahad@yahoo.com

Abstract. This work is a historical review of Kalina System Cycle (KSC) development during last decades. This review shows that a family of KCS was developed for the conversion of low grade energy into useful power or for cooling and heating purposes, which is otherwise rejected to the environment. These low grade energy sources include solar energy, geothermal energy, waste heat energy, etc. The successful operation of KCS requires special type of working fluid. This working fluid is a solution of two liquids, one is refrigerant with low boiling temperature while the other is absorbent with high boiling temperature. The important characteristics of working fluid include constancy, green impact, security, compatibility, toxicity, low cost and latent heat. This review shows that there is a good potential of using KCS to generate useful power when using the right workin fluid.

Keywords: Waste Heat, Kalina Cycle System, Aqua-Ammonia, Exhaust Heat Recovery.

INTRODUCTION

The request for power is in rising with the increasing population, while the conventional resources such as fossil fuel are insufficient and decreasing. In this case, it is required to find other source of heat to meet population requirements. Other types of heat sources are wind, geothermal, solar, waste heat and so on, but some of these energy are it low grade such as waste heat, solar and geothermal. Energy mass is small or very small and can't be transformed to work. Special technologies are needed to change low-grade energy sources into useful power. Low grade energy is the energy available at low temp, and cannot be converted into useful work unless special technologies are devised. Temps of low grade energy sources range from atmosphere temp to about 400°C. The first technology used was Organic Rankine Cycle (ORC), which usages low bubble temp organic mixtures to recuperate part of energy from low grade sources. Another technology was suggested by Alexander I. Kalina in 1980. KC technology uses in power plant. It consists of many components such as turbine, heat exchangers, pump, expansion valve, etc [1]. It same the other cycles for constructing a conventional steam power plant. Most of the studying displayed that KC technology can a reach to better performance than performance of ORC [2, 3 & 4]. studied numerically performance of composition-adjustable Kalina cycle. The results showed that the composition-adjustable Kalina cycle system could achieved higher thermal efficiency than normal KCS at same conditions. The optimized ammonia mass fraction based on the thermal efficiency is in the range of 6.12-9.24% [5].

The working fluid is a binary fluid consists of two types of fluids with different boiling and dew points temperatures. Aqua ammonia mixture is very important in Kalina cycle system. The concentration of the working fluid is not constant though out the cycle. Kumar, et. al. **[6]** indicated that the Kalina cycle technique is important

Thermodynamic Analysis of Ammonia Mass Fraction Effect on Simple Kalina Cycle System Performance

Abdulkhodor Kathum Nassir [a] and Haroun A. K. Shahad [b]

Department of Mechanical Engineering University of Babylon-Babylon-Iraq,

[a] Corresponding author: abdul.hussain@student.uobabylon.edu.iq
[b] hakshahad@yahoo.com

Abstract. This work studied the effect of ammonia mass fraction on Kalina cycle system performance with NH_3-H_2O as working fluid. The mass fractions used in this theoretical study are 0.85, 0.86, 0.87, 0.88 and 0.89. The inlet turbine temperature is 160°C. The maximum pressure varies from 35 bar to 50 bar with step 5 bar and minimum pressure are 1, 2, 3 and 4 bar. The dryness fraction at separator entrance is 0.3. The waste heat of combustion products from boiler is used as the source of energy. The temperature of this combustion products is 175°C. The results showed that the highest thermal efficiency and exergy efficiency are about 9.6% and 56% respectively at x=0.85, P_{max}=50 bar and P_{min} = 2 bar. While the network is 0.139 kW at the same conditions. The highest exergy destruction is found in the vapour generator is 52% compare with other components at ammonia mass fraction x=0.89, maximum pressure P_{max} =35 bar and minimum pressure P_{min} =2 bar and dryness fraction DF=0.3. The highest exergy destruction is found at heat recovery vapour generator is 0.62 kW at P_{max} =35bar, P_{min} =2bar and x=0.85.

Keywords: Waste Heat, Separator, KalinaTechnology System, Aqua-Ammonia, Heat Recovery.

List of Symbols

$\dot{E}_d$–The exergy destruction [kW].
$\dot{Q}$–Heat [kW]
cp_{exh} –The specific heat of exhaust gas [kJ/kg. K]
v_f –The specific volume of the working solution [m^3/kg]
P- pressure [bar]
T-temperature [°C].
x – ammonia (NH_3) concentration [$kg_{NH3}/kg_{mixture}$]
h – specific enthalpy [kJ/kg]
s- specific entropy [kJ/kg. K]
$\dot{m}$ – mass flow rate [kg/s]
Cw- specific heat of water [kJ/kg. K]
$\dot{W}$ – power [kW].

International Journal of Heat and Technology
Vol. 40, No. 6, December, 2022, pp. 1454-1461
Journal homepage: http://iieta.org/journals/ijht

Energy and Exergy Performance Analysis of Different Kalina Cycle Configurations

Abdulkhodor Kathum Nassir*, Haroun A.K. Shahad

College of Engineering, Mechanical Engineering Department, University of Babylon, Babylon City 51001, Hilla, Iraq

Corresponding Author Email: abdul.hussain@student.uobabylon.edu.iq

https://doi.org/10.18280/ijht.400613

Received: 4 December 2022
Accepted: 23 December 2022

Keywords:
waste heat, modified Kalina cycle system, aqua-ammonia, exhaust heat recovery

ABSTRACT

The main challenge of using Kalina cycle system (KCS) is to make use of waste heat to produce electrical power or cooling effect. Thus reducing fossil fuel consumption and pollutants emission. This study is concerned with a theoretical performance analysis of different configures of Kalina cycle. Three configurations are studied which are a simple Kalina cycle and two modifications of the simple cycle (MKCS1) and (MKCS2). A binary fluid of ammonia and water (NH_3-H_2O) is used as the working fluid. The varying operating parameters include ammonia mass fraction at turbine inlet and maximum cycle pressure. The dryness fraction at separator inlet is assumed constant and equal 0.3 and the minimum cycle is also assumed constant at 3bar. The results show that the maximum thermal efficiency for KCS, MKCS1 and MKCS2 are 8.64%, 12.7% and 18.85% respectively at the same conditions maximum pressure (Pmax)=35bar, minimum pressure (Pmin)=3bar, dryness fraction (DF)=0.3, ammonia mass fraction (x)=0.85 and the temperature at turbine inlet is 160°C. The maximum exergy efficiency for KCS, MKCS1 and MKCS2 are 34.21%, 51.92% and 75.34% respectively at the conditions Pmax=40bar, x=0.85, DF=0.3 and Pmin=3bar. The maximum net output power for KCS is 0.21kW at Pmax=15bar and x=0.85, the maximum net output power for MKCS1 and MKCS2 0.28kW and 0.41kW respectively at Pmax=30bar and x=0.89. This is equivalent to a reduction in the diesel fuel consumption by about $9.1*10^{-5}$ kgf/kWelec. Also it reduction the pollution especially CO_2 about $2.91*10^{-4}$ $kgCO_2/kW_{elec}$.

1. INTRODUCTION

The demand of energy is increasing worldwide which requires large fossil fuel consumption. This means more pollutants emission. Therefore, the need for new clean and sustainable energy resources become urgent. These resources includes, solar energy, wind energy, bioenergy, waste heat, geothermal … etc. However, these resources are of low grade type since it is available at low temperatures. Therefore, new technologies are needed to make use of these resources. One of these technologies is Kalina cycle system. Hossain et al. [1] improved Kalina Cycle System-12 (KCS-12) by adding a multi-phase expander in two positions. The first position of the multi-phase expander is after the separator and this cycle is named KC-12A. The second position of the multi-phase expander is before the separator and this named KCS-12B. The results show that the net power and efficiency of KC-12Aas compared with KCS-12 increased by 3.23% and 3.68% respectively, while it was 3.94% and 4.04% respectively for KC-12B. It was found the maximum power output for KC-12B is obtained at 15.217MPa and 0.8 ammonia mass fraction. Kaczmarczyk et al. [2] studied and compared between Kalina cycle and Organic used geothermal resources. The flow rate of geothermal water is assumed from 120 m^3/h to 550 m^3/h and the temperature of water is not exceed 86°C. The results showed that the gross power obtain from Kalina cycle is larger than power obtained from ORC about 40%, but both of them have same thermal efficiency around 6.49%. Cruz and Manuel [3] studied the improvement of Kalina Technology and potential of using for the global electricity productions. When the maximum temperature is (116°C) for the heat source, the working fluid leaves the HRVG at wet vapor. (KCS 1-2) consists of eight heat exchangers, two pumps, separator, expansion valve and turbine. It used the waste heat (exhaust gases) in the factory of cement. ORC and KCS cogeneration cycle is operated on exhaust gases and cinder cooler exhaust gasses in cement factory. Kaczmarczyk et al. [4] studied and analyzed two cycles (Organic Rankine and Kalina Technology) to produce electricity from geothermal resources. The temperature of the water of geothermal is 82°C and a peak flow rate of 51.22kg/s. The results show that, when ORC was used the total power and total energy are about 0.24 MW and 940 MWh respectively. When KCS was used the total power and total energy increase to 0.43MW and 1730 MWh respectively. Özahi and Toziu [5] studied and analyzed KCS which is operated by waste heat from power plant in Turkey. It used to recover the heat from the power plant to generate 0.9546MW with thermal efficiency of 24.15%. Meng et al. [6] studied and investigated organic Rankine cycle ORC. It is found that the ORC operates with low temperature and heat sources, as low as 80°C. The steam is a working fluid with normal RC, it needs high temperature of the heat sources above 360°C. Li and Dai [7] studied the use of working fluid pair which consists of 86% NH_3 and 14% H_2O and obtained better performance (thermal efficiency and output power) plants as compare as to normal RC. Dhahad et al. [8] presented a new cycle which consists of Kalina Cycle and the absorption refrigeration cycle. The system works with low-temperature and the source of the heat was waste heat source. The results showed that the system is suitable for cooling rather than for

IIETA International Information and Engineering Technology Association
Advancing the World of Information and Engineering

International Journal of Heat and Technology
Vol. 40, No. 5, October, 2022, pp. 1186-1195
Journal homepage: http://iieta.org/journals/ijht

Effect of Operating Conditions on Modified Kalina Cycle Performance

Abdulkhodor Kathum Nassir*, Haroun A.K. Shahad

College of Engineering, Mechanical Engineering Department, University of Babylon, Babylon City 51001, Hilla, Iraq

Corresponding Author Email: abdul.hussain@student.uobabylon.edu.iq

https://doi.org/10.18280/ijht.400509

Received: 15 September 2022
Accepted: 20 October 2022

Keywords:
dryness fraction, mass of concentration, waste heat, aqua-ammonia, exhaust heat recovery

ABSTRACT

Simple Kalina cycle system (SKCS) is used for low temperature, intermediate temperature and high temperature heat recoveries. However, its efficiency is rather low. Therefore, a modification is suggested to improve its efficiency. In this work a computer program is developed to predict the energy-exergy performance of a modified Kalina Cycle System (MKCS) using aqua ammonia solution. It consists of heat recovery vapor generator (HRVG), condenser, heat exchanger, separator, turbine, throttling valve, absorber and pump. The modification is implemented by introducing a heat exchanger (HE) between the separator and expansion valve. This HE is used to reheat the work solution which comes from the pump by the high temperature hot weak solution which comes from the separator. The effect of many operating conditions such as dryness fraction (DF) at separator inlet, low pressure and ammonia (NH3) mass fraction with constant high pressure on cycle performance is studied. The results show that the modified cycle efficiency is higher than

Experimental Investigation of a Regeneration Kalina Cycle for Electrical Power Generation Using Waste Heat

Abdulkhodor Kathum Nassir [1,*] Haroun A. K. Shahad[2]

[1,2] College of Engineering- Mechanical Engineering Department- University of Babylon- Babylon City– Hilla– Iraq.

*Corresponding Author Email: abdul.hussain@student.uobabylon.edu.iq

ABSTRACT

Kalina cycle is a thermodynamic power cycle uses any waste heat source (low temperature source) to generate electrical power or cooling. Many versions of Kalina cycle exist. In this paper a regeneration Kalina version is designed and constructed. The cycle consists of the following main components: heat recovery vapor generator (HRVG), separator, turbine, condenser, throttling valve, mixer (absorber), heat exchanger and pump. The heat exchanger is used to heat the working fluid coming from the pump before entering the HRVG by the hot saturated liquid (weak solution) coming from the separator. The cycle uses aqua ammonia mixture as the working fluid with different ammonia concentrations. The effect of many operating conditions on cycle performance is studied such as ammonia (NH_3) mass fraction (range from 0.85-0.89), low pressure (range from 2-4 bar), and maximum pressure (range from 20-40 bar). The dryness fraction (DF) at separator entrance is kept at 0.3. The results show that the highest thermal efficiency obtained is 12.9% at P_{max}=35bar, P_{min}=2bar, and x=0.85. The highest value of the net power is 0.367kW at x=0.89 at turbine inlet pressure of , P_{max}=20 bar. The highest value of exergy efficiency is 28.5% at P_{max}=35bar, P_{min}=2 bar. It is noticed that the highest exergy destruction is in the heat recovery vapor generator (HRVG) which is about 48% due to high temperature heat exchange process and low mass flow rate. The exergy destruction is larger at P_{max}=35 and x=0.89 than the exergy destruction at P_{max}=20 bar and x=0.89.

Keywords: Kalina cycle, waste heat source, aqua-ammonia, heat recovery vapor generator, exergy efficiency.

1- Introduction

Nowadays, as energy need and fossil fuel consumption increase, pollution is increasing also. Due to the limited conventional energy resources, many researches have been carried out to develope new energy resources and to reduce pollution and cost. Kalina cycle recovers heat from low grad energy sources and converts it to useful work and to generate electrical power. This application helps to reduce fossil fuel consumption which leads to reduction in pollutants emission. **Horta et al. (2021) [1]** studied and compared the performance of two versions of Kalina cycle, (Kalina cycle system (KCS1) and kalian cycle system (KCS34). Both of them were performed for cogeneration of electricity from waste heat recovery in the cement industry. The optimization results showed that, the efficiency of the cycle of the KCS1 and KCS34 was 22.9%, 21.9% respectively. The exergy efficiency for KCS1 and KCS34 was 55.8%, 53.2% respectively. **Parvathy nd Varghese (2021) [2]** studied the effect of two turbines on the

الخلاصة

تم في هذا البحث دراسة نظرية وعملية لتحليل الطاقة والمتاحية لأنواع مختلفة من دورة كالينا. دورة كالينا دورة حرارية تستخدم لأنتاج الطاقة الكهربائية والتبريد . حيث أُستخدمت دورة كالينا البسيطة والمحسنة . اما مائع العمل هو خليط من الامونيا والماء. المصدر الخارجي للطاقة هو غازات العادم من مرجل بخاري موجود في جامعة بابل/كلية الهندسة الميكانيكية/مختبرالموائع . حيث تم قياس درجة حرارة الغازات العادمة بواسطة مزدوج حراري وحساب التصريف اللكتلي بواسطة معادلة الأحتراق القياسية وكانت 175 مئوية و122.3 كغم بالساعة. تم في هذه الدراسة تحسين وتطوير دورة كالينا البسيطة الى دورة كالينا المحسنة الأولى وذلك بإضافة مبادل حراري بين الفرازة والمضخة لكي يقوم باسترداد جزء من الحرارة التي سوف تطرح الى المحيط. وبعدها تم تطوير دورة كالينا المحسنة الأولى الى دورة كالينا المحسنة الثانية وذلك بإضافة مبادل حراري ثاني بين العنفة والمضخة لأسترداد جزء من الحرارة التي ستطرح الى المحيط.

وتنقسم هذه الدراسة الى قسمين نظري وعملي. القسم النظري يدرس تأثير تغيير العوامل مثل الضغوط والتراكيز على أداء الدورات الثلاث واما العملي يدرس تأثير نفس العوامل على أداء دورة كالينا المحسنة الأولى ويقارن بين النتائج النظرية والعملية.

حيث تم دراسة تأثير المتغيرات التالية وهي الضغط الأعظم والضغط الأدنى ونسبة تركيزالأمونيا ونسبة الجفاف على أداء دورة كالينا (الكفاءة الحرارية والطاقة الصافية وكفاءة القانون الثاني والخسائرللدورة كاملة ولكل جزء من أجزاء الدورة). يُدرس تأثير المتغيرات مثل الضغط الأعظم من 20 بار الى 40 بار لكل خطوة 5بار. والضغط االأدنى 2بار, 3بار, 4بار واما نسبة تركيز الأمونيا من 0.85 الى 0.89 لكل خطوة 0.01 وكذلك نسبة الجفاف 0.2, 0.3 0.4 .

العلاقة بين نسبة تركيز الامونيا والتدفق الكتلي علاقة طردية أي كلما زاد تركيز الامونيا زاد التدفق الكتلي وبالعكس. العلاقه بين الضغط الأعلى في الدورة والتدفق الكتلي عكسية كلما قل التدفق الكتلي ازداد الضغط الأعلى في الدوره.

في البداية دُرس تأثير نسبة الجفاف نظرياً على أداء الدورات الثلاث وكان السلوك متشابهاً في الدورات الثلاث. كلما زادت نسبة الجفاف زادت الكفاءة الحراريه الى 0.3 وبعدها كلما زادت نسبة الجفاف قلت الكفاءة الحارية. وعلى هذا الأساس أُعتمدت قيمة نسبة الجفاف هي 0.3 وكانت قيمة الكفاءة الحرارية لدورة كالينا البسيطة ودورة كالينا المحسنة الأولى ودورة كالينا المحسنة الثانية هي 9.44%, 14.23%, 23.53% على التوالي. ومن ثم تم دراسة تأثير نسة الجفاف على صافي القدرة

وكانت النتيجة كلما زادت نسبة الجفاف قلت القدرة الصافية وكانت قيمة القدرة الصافية للدورات الثلاث هي 0.26 كيلوواط, 0.29 كيلوواط, 0.38كيلوواط على التوالي. وكانت قيمة كفاءة القانون الثاني هي 24.2%, 30.2%, 59.06% على التوالي.

وتم دراسة تأثير تغيير تركيز الامونيا على أداء الدورات الثلاثة وكانت النتائج كالآتي:-

1-كلما ازاد تركيز الامونيا قلت الكفاءة الحرارية وذلك بسبب زيادة التدفق الكتلي. مثلا الكفاءة عند تركيز 0.86 اقل من الكفاءة الحرارية عند تركيز0.85 لان التدفق الكتلي عند 0.86 هو0.009521 كغم/ثا بينما التدفق الكتلي للتركيز0.85 هو 0.009324 كغم/ثا. الكفاءة الحرارية عند تركيز 0.86 هي 12.9% وعند تركيز 0.85 هي 13.1%. كلما زاد تركيز الامونيا تقل كفاءة القانون الثاني لنفس السبب. كفاءة القانون الثاني عند تركيز امونيا 0.86 هي 26% وعند تركيز 0.85 هي 28.5%.

2-كلما زاد تركيز الامونيا زادت القدرة الصافية فمثلاً القدرة الصافية عند تركيز امونيا 0.86 هي 0.31 كيلوواط وعند تركيز امونيا0.85 هي 0.29 كيلوواط. وكذلك كلما زاد تركيز الامونيا زادت الخسائر بسبب زيادة تركيز الامونيا التي لاتحتاج الى حرارة عالية لتسخينها لذلك تذهب بقية طاقة المرجل الى خسائر.

وتم أيضا دراسة تأثير الضغط الأعلى على أداء الدورات الثلاثه

1-كلما زاد الضغط الآعلى زادت الكفاءة الحرارية الى ضغط35 بار وبعدها كلما زاد الضغط تقل الكفاءة, الكفاءة الحرارية تعتمد على القدرة الصافية والحرارة التي ياخذها مائع العمل من المرجل, ان تغير المحتوى الحراري عبر العنفة والمرجل يزداد ولكن يزداد عبر المرجل اكبر من زيادته عبر العنفه اضف الى ذلك نقصان التدفق الكتلي وهذا هو العامل المهم في نقصان الكفاءة الحراريه. وايضاً كلما زاد الضغط الأعلى تقل القدرة الصافيه فمثلاً القدرة عند ضغط 20 بارهي 0.394 كيلوواط اما عند ضغط 25 بار هي 0.391 كيلوواط. وكلما زاد الضغط الأعلى قلت كفاءة القانون الثاني وهي نفس سلوك الكفاءة الحرارية وكذلك كلما زاد الضغط الأعلى زادت الخسائر.

وكذلك تمت دراسة تأثير الضغط الأدنى على أداء الدورات الثلاث كلما زاد الضغط االادنى قلت الكفاءة الحرارية وقلت القدرة الصافية وكذلك تقل كفاءة القانون الثاني وتزداد الخسائر لذلك احسن ظروف هي عند ضغط ادنى 2 بار.

تمت دراسة الخسائر في الدورات الثلاث ووجد بان اكثر الدورات خسائر هي دورة كالينا البسيطة 0.81 كيلوواط ويليها دورة كالينا المحسنة الأولى 0.667 كيلوواط ويليها دورة كالينا المحسنة الثانية 0.261 كيلوواط. وتكون دورة كالينا المحسنة الثانية هي اقل خسائر لانها تحتوي على مبادلين

حراريين لاسترداد الطاقة المهدورة بينما دورة كالينا المحسنة الأولى تحتوي على مبادل حراري واحد واما دورة كالينا البسيطه تطرح الكثير من الطاقة الى المحيط.

ومن خلال ماتقدم من دراسة نظرية على الدورات الثلاث هي دورة كالينا البسيطة ودورة كالينا المحسنة الأولى ودورة كالينا المحسنة الثانية. وجد بان اعلى كفاءة حرارية وقدرة وكفاءة القانون الثاني واقل خسائر هي دورة كالينا المحسنة الثانية. وكذلك احسن الظروف هي ضغط اعلى 35 بار وضغط ادنى 2 بار ونسبة جفاف 0.3 وتركيز الامونيا 0.85.

وكذلك تمت دراسة عملية على دورة كالينا المحسنة الأولى وتنفيذها عمليا وتمت دراسة تاثير الضغط الأعلى والضغط الأدنى و تركيزالامونيا على أداء دورة كالينا المحسنة الأولى عمليا وكانت النتائج هي نفس السلوك ونفس التاثير على أداء الدورة عند الدراسة النظرية. اما بالنسبة الى بناء وتصميم الدورة معقد جداً لذلك تم بناءها وتصميمها في االاسواق المحلية لذلك تغير مصدر الطاقة الخارجي من غازات عادم المرجل الى مصدركهربائي وذلك بعمل مقاومة حرارية تلف حول انبوبة مصنوعة من الالمنيوم بطول 1.5 متر وقطر داخلي14 ملم وقطرخارجي16 ملم وبسمك 1 ملم. وكذلك حتى نضمن عمل الدورة بانتظام وكذلك تشغيل المرجل باوقات قليلة فقط عند أداء التجارب وكذلك تشغيل المرجل يؤدي للكثير من الانبعاثات والضوضاء وكذلك بناء الدورة يحتاج الى إمكانيات مادية وعملية والجامعة تفتقر اليها لذلك تم بناءها في الأسواق المحلية

مقارنة الدراسة النظرية والعملية بالظروف ضغط اعلى 35 بار وضغط ادنى 2بار ونسبة تركيز 0.85 ونسبة جفاف 0.3 وتم مقارنة أداء دورة كالينا المحسنة نظريا وعمليا. بالنسبة الى الكفاءة الحرارية نظريا هي 14.23% واما عمليا هي 13.09% ونسبة الخطا بينهما 8.01%. اما بالنسبة الى القدرة الصافية نظريا 0.289 كيلوواط اما عمليا 0.272 كيلوواط ونسبة الخطا بينهما5.88%. اما بالنسبة الى كفاءة القانون الثاني نظريا 30.24% اما عمليا 28.43% واما نسبة الخطا بينهما 5.99%. اما بالنسبة للخسائر نظريا 0.5239 كيلوواط اما عمليا فتكون الخسائر اكبر 0.581 كيلوواط اما نسبة الخطا 10.899%.

وتم دراسة جدوى اقتصادية وذلك من خلال حساب القدرة الصافية التي حصلنا عليها وبنفس الظروف التي تمت بها المقارنة وكانت القدرة الصافية 0.272 كيلوواط ومعدل الجريان الكتلي 0.009324 كغم/ثا. من خلال الحسابات وجد ان الحصول على قدرة صافية 0.272 كيلواط يجب ان نحرق كمية من الوقود 858 كغم سنويا. اما بالنسبة للانبعاثات لكل كيلو غرام من الوقود ينبعث 3.155 كغم من ثاني أوكسيد الكاربون وبالتالي استخدام دورة كالينا المحسنة الأولى عمليا يقلل انبعاثات ثاني أوكسيد

الكاربون 2672 كليوغرام سنويا. وعند استخدام دورة كالينا المحسنة الثانية وعند نفس الظروف وكانت القدرة الصافية 0.585 كيلوواط ولاجل الحصول على مثل هذه القدرة الصافيه يجب ان نحصل على طاقه من حرق الوقود ومقدارها 2.34 كيلوواط وكمية الوقود الذي يجب حرقه 1844.9كيلوغرام سنويا ويقلل 5820.5 كيلوغرام سنويا من انبعاثات ثاني أوكسيد الكاربون.

جمهورية العراق
وزارة التعليم العالي و البحث العلمي
جامعة بابل/كلية الهندسة
قسم الهندسة الميكانيكية

تحليل الطاقة والمتاحية لتشكيلات مختلفة من دورة كالينا

أطروحة
مقدمة إلى كلية الهندسة – جامعة بابل وهي جزء من متطلبات نيل شهادة الدكتوراه في علوم الهندسة الميكانيكية/ قدرة

من قبل

عبد الخضر كاظم ناصر حسين

باشراف

الاستاذ الدكتور هارون عبد الكاظم شهد

1445هـ 2023 م